60805

A WORLD BANK STUDY

Assessment of the Impacts of Climate Change on Mountain Hydrology

DEVELOPMENT OF A METHODOLOGY THROUGH A CASE STUDY IN THE ANDES OF PERU

Walter Vergara, Alejandro Deeb, Irene Leino, Akio Kitoh, Marisa Escobar

THE WORLD BANK

Assessment of the Impacts of Climate Change on Mountain Hydrology

Development of a Methodology through a Case Study in the Andes of Peru

Walter Vergara
Alejandro Deeb
Irene Leino
Akio Kitoh
Marisa Escobar

ESMAP
Energy Sector Management Assistance Program

THE WORLD BANK
Washington, D.C.

Contents

Tables

Figures

Foreword

Climate change is beginning to have effects on resource availability in ways that need to be anticipated when planning for the future. In particular, changes in rainfall patterns and temperature may impact the intensity or schedule of water availability, which could affect activities such as irrigation and energy production from hydropower plants. These changes have the potential to impact the energy and other sectors, such as agriculture, and could have broader economic effects.

However, anticipating the impacts of climate change is a new frontier. There are few examples of predictions of the impact of climate change on resource availability and even fewer examples of the applications of such predictions to planning for sustainable economic development. Developing methodologies to assess the climate impacts and translating them into anticipated impacts on the energy, agricultural and other sectors will be increasingly important in the future as governments and the private sector aim to increase the resilience of their activities to the impacts of climate change.

This report presents a summary of the efforts of a Bank energy and climate change team to develop methodological tools for the assessment of climate impacts on surface hydrology in the Peruvian Andes. The importance of analyzing the potential climate impacts on hydrology in Peru arises in part from concerns about the retreat of tropical glaciers, the drying of unique Andean wetland ecosystems, as well as increased weather variability and weather extremes, all of which will affect water regulation. The study, together with a recently published report by the World Bank, *Peru: Overcoming the Barriers to Hydropower,* is intended to inform plans for energy development in Peru and enable the consideration of the consequences of climate change for such development.

While the report provides some insights into how hydrology may behave under future climate scenarios in Peru, the main purpose is to contribute to the methodological approaches to anticipate impacts from climate change in the Andes Region and other mountain ranges. Developing a methodology is a first step toward improving our ability to predict hydrological conditions in the future. In turn, these predictions could be used to make planning more robust to uncertainty with respect to climate change impacts. Ultimately, such insights could inform and enrich economic and energy planning, thereby permitting the integration of the consideration of climate change impacts into the planning process.

Phillipe Benoit
Energy Sector Manager
Latin America and the Caribbean Region

Acknowledgments

Executive Summary

Climate change is expected to result in larger temperature increases (anomalies) at high altitudes compared with surrounding lowlands. In the Andes, this may lead to the accelerated retreat of tropical glaciers, the drying of unique neotropical high-mountain wetland ecosystems locally known as *páramos* or *bofedales*, as well as increased weather variability and weather extremes, all of which will affect water regulation. In turn, these impacts may affect ecosystem integrity and the economics of power and water supply in the region. Peru is one of the countries that could be affected by these changes: it relies on its mountain basins for the provision of over 50 percent of its power, and discharges from upper basins feed water supply and agricultural systems.

The objective of the study is to develop a methodology to assess the net impacts of climate change on the hydrological response in mountainous regions. This is done through a case study in the Peruvian Andes. Having access to an effective methodology would allow planners and policy makers to better plan for adaptation measures to address the consequences of climate change on the power and water sectors.

In order to assess future climate change impacts on surface hydrology in mountainous areas in Peru, three analyses were conducted: (i) a climate analysis to define future climate scenarios; (ii) a mountain hydrology analysis to complement existing tools with elements that incorporate the dynamic behavior of glaciers and páramos; and (iii) the application of the methodology at a watershed level. As part of the climate analysis, the study reviewed different methods to produce future climate change scenarios and tested these by making projections of the future climate conditions at national and basin levels in Peru.

Climate Analysis

Four approaches were used as part of the climate analysis:

- ■ **Deployment of a high-resolution Global Circulation Model (GCM).** The GCM of the Meteorological Research Institute of Japan (MRI) was used. Data were generated by running the MRI-AGCM3.1 model in a supercomputer called the Earth Simulator-2. For this application, only a few climate variables were downloaded and analyzed, including temperature, rainfall, soil moisture and evaporation at a very high resolution (20 km), capturing the intensity and frequency of extreme weather events.[1] Achieving such a high resolution in GCM is unique in global climate change studies. The challenge of this tool is that the available computing power is insufficient to enable multiple emissions scenario runs. Therefore, the application of the high-resolution GCM was limited to a single run. To address this limitation and strengthen the robustness of the projections made at a 20-km resolution, the same GCM was run at lower resolutions (60 km and lower). These results were compared with the 20-km version.

- ■ **Ensemble of GCMs.** Since GCMs used for projecting the changing climate are imprecise representations of the earth's climate system, all of them are deemed to have "model errors." Therefore, an often recommended practice is to use the

results of multiple GCMs in future climate projections. This study used combined output from 16 GCMs presented in the Fourth Assessment Report of the Intergovernmental Panel on Climate Change (IPCC). These were used in this study to project the potential range of precipitation and temperature changes that might be anticipated at a basin level.

- **Subgrid Orography Dynamic Model**. The use of the Subgrid Orography Dynamic Model has shown that downscaling could greatly improve the simulation of snowfall, temperature and precipitation in mountainous regions. In this study, the subgrid scheme was used to downscale outputs from the Community Climate System Model (CCSM). The CCSM is a GCM developed by the National Center for Atmospheric Research of the United States.

- **Rainfall trend analysis.** In order to further strengthen the robustness of the projections, the analysis used statistical analysis of observed meteorological data for over 20 years to verify the modeled GCM projections with local linear future projections.

Table ES 1 summarizes the different approaches pursued in the study, outlining the final role played by each individual approach in the analysis.

Table ES 1. Summary of approaches used in the climate analysis

Climate analysis	Strengths	Limitations	Observations
Use of the MRI-AGCM3.1 at the Earth Simulator	High resolution. Ideal to visualize climate extremes. In conjunction with GRiverT, it can resolve hydrological impacts at large basin scale (+100,000 km^2).	Large computing requirements limit the use to one or two emissions scenarios. Simulation of current climate in mountain regions is still uneven.	Best use in the context of regional rather than basin level. Used in the study to project future climate nationwide and visualize weather extremes.
Ensemble of 1 6 GCM	Combination of outputs from different models has the potential to define the range of uncertainty. Combination of results can provide upper and lower levels for future climate variables at a basin level.	Results show large variance among models. Unless weighted, ensembles combine the projections of poor and good fits.	Used in the study to set the upper and lower envelopes for precipitation. Adequate if the final objective is to minimize the maximum loss.
Subgrid Orography Dynamic Model	Able to model elevations in complex terrains. Very high resolution can potentially resolve basins in mountain areas.	Does not treat rain shadows. The influence of slope and aspect on surface processes is neglected.	Highlighted as a tool with potential basin-level application once the limitations are addressed.
Rainfall Trend Analysis	Not a modeling technique but uses current climate as basis for projections.	Requires the existence of adequate weather records for a period of 20 years or more. Only addresses potential changes in mean values. Assumes that past linear trends will not change in the near future. Use of current trends may be misleading if emerging parameters such as climate drivers are in play in the immediate future.	The analysis used statistical methods on observed climate data for over 20 years to verify the modeled GCM projections with local linear future projections.

Source: Authors.

Hydrology Analysis

The Water Evaluation and Planning Model (WEAP) was used to estimate hydrological responses to climate change. However, before the outputs from the climate analysis could be used as inputs for the hydrology analysis, WEAP had to be adapted to handle the region's specific conditions. Glacier and páramo modules were developed to complement an existing and flexible water resources management tool to integrate climate impacts in the hydrological response in mountainous regions. The glacier module allows the model to reflect the dynamic behavior of glaciers and estimate their net contribution to runoff. The páramo module does the same with high mountain wetlands. WEAP was selected for its flexibility to integrate the addition of glacier and páramo modules.[2]

Although the purpose of this study is to develop a useful methodology, and not necessarily to produce an assessment of the impacts of climate change at a basin level, this report nonetheless also discusses how hydrology might be impacted by the projected consequences of climate change. The analysis includes an estimate of increases in temperature, changes in precipitation, and rate of glacier retreat.

Results of the Case Study Analysis

The model was first calibrated in sub-basins that do not have glacier coverage to check the existing rainfall-runoff routines. Based on the initial findings of the calibration in nonglaciated river basins, the model was applied to the Santa and Mantaro-Rímac Basins. The modeling period for calibration was 1970–1984, and the 1985–1998 period was used for validation.

In the Santa Basin, the analysis projects lower mean runoffs by mid-century, including decreased year-round monthly runoffs at the La Balsa station, the diversion point for Cañón del Pato, an important power generation facility. The mean reduction is projected to be 21 percent by 2050–2059 compared with the present. Similarly, average flows at the Condocerro station, in the lower part of the Santa River Basin, are projected to decrease by six percent. The minimum flows at this station are projected to decrease by 18 percent.

The Mantaro-Rímac Basins are more complex to simulate given the high level of man-made infrastructure for water storage and runoff regulation, including dams and channels. Nevertheless, some interesting results were obtained. The expected response to future climate conditions in the Mantaro Basin indicates a shift in the distribution of runoffs as well as a reduction in peak flows. Overall, discharges at key points in the basin seem to decrease. Conversely, at Rímac, projected conditions indicate no significant changes and at the most suggest the possibility for a slight reduction during the dry season. The results of the simulation of the glacier evolution in the Santa and Mantaro-Rímac River systems were also consistent with historical records.

Conclusion

On the basis of the results obtained, **it seems that the combination of the climate and hydrology analysis can simulate current conditions at a regional and basin level and project future hydrological conditions**. The methods employed could be of use to predict future impacts of climate change on hydrology for other mountain basins in the Andes.

Notes

1. The Fourth Assessment Report (AR4) of the Intergovernmental Panel on Climate Change (IPCC) uses a dataset of 24 global coupled atmosphere-ocean general circulation models (AOGCM, or GCM for short) to project future climate under various scenarios. The use of numerous models is intended to reduce errors and uncertainty. However, most of these models have a very coarse resolution (100–400 km) and this has an undesirable impact on results, particularly as it relates to extreme weather events. This is because global warming would result not only in changes in mean climate conditions but also in increases in the amplitude and frequency of extreme events that would not be captured in a meaningful way with coarse resolutions. Changes in extremes are more important for assessing adaptation strategies to climate changes.

2. Although the páramo module was developed as part of this study, it was not used in the case studies because no extensive páramo landscapes could be characterized in the three river basins used in the study. However, efforts are underway to apply the technique in Colombia.

Acronyms and Abbreviations

AMIP	Atmospheric Model Intercomparison Project
AOGCM	Atmosphere-ocean General Circulation Model
AR4	The Fourth Assessment Report of Intergovernmental Panel on Climate Change
CAM3	Community Climate System Model
CCSM	Community Climate System Model
CCSR	Center for Climate System Research (of the University of Tokyo)
CDD	Consecutive Dry Days
CLM	Community Land Model
CMIP	Coupled Model Intercomparison Project
COES	*Comité de Operación Económica del Sistema Interconectado Nacional*
DDF	Degree-Day Factor
GCM	General Circulation Model
GIS	Geographic Information System
IPCC	Intergovernmental Panel on Climate Change
IRD	*Institut de Recherche pour le Développement*
JMA	Japan Meteorological Agency
MRI	Meteorological Research Institute (of Japan)
MRI-AGCM3.1	A high-resolution GCM by MRI of Japan
NIES	National Institute for Environmental Sciences (of Japan)
PNNL	Pacific Northwest National Laboratory
PRAA	Regional Adaptation to Glacier Retreat Project
RCM	Regional Circulation Model
RMSE	Root Mean Square Error
RX5D	Maximum 5-day Precipitation Total in Millimeters
SDII	Simple Daily Intensity Index
SEI	Stockholm Environmental Institute
SENAMHI	*Servicio Nacional de Meteorología e Hidrología del Perú*
SRES	Special Report on Emissions Scenarios
SWI	Soil Wetness Index
UNFCCC	United Nations Framework Convention on Climate Change
WCRP	World Climate Research Program
WEAP	Water Evaluation and Planning Tool

Introduction

Objective of the Study

The objective of the study is to develop a methodology to assess the net impacts of climate change on hydrological response in mountainous regions. This is done through a case study in the Peruvian Andes. Having access to an effective methodology would allow planners and policy makers to better plan for adaptation measures to address the consequences of climate change on the power and water sectors.

Methodology

In order to assess future climate change impacts on surface hydrology in mountainous areas in Peru, three analyses were conducted: (i) climate analysis to help define future climate scenarios; (ii) a mountain hydrology analysis to complement existing tools with elements that incorporate the dynamic behavior of glaciers and *páramos* (neotropical high mountain wetlands); and (iii) the application of the hydrology model at a basin level. For the climate analysis, the study examined different methods to produce future climate change scenarios and tested these by making projections of the future climate conditions at national and basin levels in Peru. The analysis was conducted at three basins in Peru as test objects. Finally, the study developed criteria to judge the adequacy of the projections made.

Climate Analysis

The climate analysis reviewed four approaches to define projected future climate conditions that could be used as inputs in a river basin hydrological model:

- **Use of high-resolution GCM**. Data from the MRI-AGCM3.1, provided by MRI of Japan, at a resolution of 20 km by 20 km covering Peru, were used to analyze three time periods: recent past (1979–2000), near future (2015–2039) and end of century (2075–2099).
- **Use of ensemble GCM outputs.** Data from an ensemble of results from 16 GCMs were available from the IPCC. These data were used to identify two future scenarios that were representative of the range of anticipated changes in temperature and precipitation at a local basin scale.
- **Use of Subgrid Orography Dynamic Model**. An advanced downscaling routine was applied to the outputs of the Community Climate System Model (CCSM) GCM from the US National Center for Atmospheric Research. The downscaled results (at a resolution of 5 km) were the basis for developing future climate scenarios.

- ■ **Rainfall trend analysis.** Complementing the use of GCMs**,** a rainfall trend analysis was conducted. A trend analysis takes historical trends from the past and projects them into the future. This provides an observational basis by which to analyze recent climate behavior, useful information related to trends (increasing, neutral or decreasing) of key climate variables of interest, and statistics by which to judge the adequacy of GCMs in simulating local conditions.

To judge the skill of the different approaches in reproducing the observed climate, the outputs of the GCMs were compared with observations at local weather stations and with the results from the trend analysis.

Hydrology Analysis

The hydrological work sought to translate the projected climate conditions into expected future river discharges at selected points. An overall picture of the changes in runoffs in Peru was drawn with the help of the GRiverT routine, a direct application of the high-resolution MRI-AGCM3.1 that calculates the aggregated runoff in large basins. In addition, a rainfall runoff model was chosen to assess the changes at the river basin level. The WEAP model, developed by the Stockholm Environmental Institute (SEI), was used for this task and modified to properly simulate the dynamic hydrological behavior in high mountain conditions.[1] The WEAP model was complemented with modules to simulate the dynamic response of ice caps (glaciers) and high mountain wetlands (páramos) to changes in temperature and precipitation associated with global warming. The development and validation of these modules is by itself an important contribution to help bridge an existing knowledge gap in understanding the impacts of climate change on mountain hydrology.

Structure of the Report

After a brief introduction and context, Chapter 3 describes results for the climate projections (climate analysis). Chapter 4 presents the hydrological model (WEAP) and describes how it was modified to account for the complexity of mountain hydrological systems (hydrology analysis). In Chapter 5 the results of the climate analysis are fed into the upgraded hydrological model to test the hydrology tool at a river basin level. Finally, Chapter 6 presents the main results from the hydrology analysis. This includes both the countrywide assessment of changes in runoffs, made by using the MRI-AGCM3.1, and the river basin-level analysis made with the help of the WEAP model.

River Basins Used as Case Studies

The hydrology tool was tested at three river basins in Peru: the Santa, Rímac and Mantaro River Basins. The basins were selected on the basis of their perceived vulnerability to climate impacts and their economic relevance. The basins were also selected based on their characteristics, including the important role of glaciers in the Santa Basin, Mantaro's size and distinct regions, and Rímac's typical steep, dry coastal basin. The basins are also home to large populations, provide water to urban centers, and are major producers of agricultural products. The country's main hydropower plants are located in these river basins. These plants provided over 43 percent of hydropower production in

Figure 1.1. Components of the methodology to address the hydrological response to climate change in mountain regions
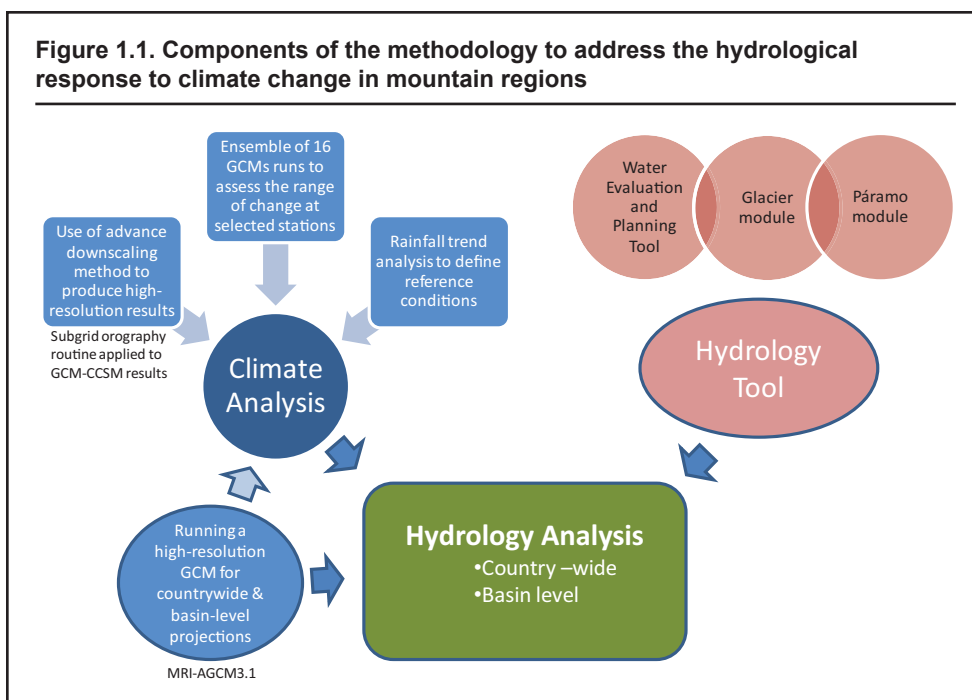
Source: Figure generated for this study.

Peru in 2009 (COES 2009). According to estimates by the *Comité de Operación Económica del Sistema Interconectado Nacional* (COES), the future hydropower potential in these basins is also significant. It is estimated that these three river basins would total 42 percent of new hydropower capacity and 47 percent of added hydro generation in the future.

While applying and testing the models in the selected basins provides useful insight, the results cannot be generalized directly to other basins. The basins are briefly described below.

Santa River

The Santa River Basin has a total area of about 12,200 km^2, making it the second largest and most regularly flowing Peruvian river to reach the Pacific Ocean. The Santa River is fed by the glaciers of the Cordillera Blanca, which define the basin's eastern boundary. The Cordillera Blanca contains the world's largest concentration of tropical glaciers, most of which flow westward toward the Pacific Ocean along the Santa River (Mark et al. 2010). The river flows north along a central valley guarded by the cordilleras on both sides, known as the Callejón del Huaylas. The river basin is home to the Cañón del Pato hydropower plant, the second largest in the country. On the coastal delta the Santa River feeds the Chavimochic irrigation district, which provides water to the Chao, Virú, Moche and Chicama valleys. Nearly one million people live in the basin. Figure 1.2 below offers a schematic representation of the Santa River Basin and its hydrological representation in WEAP.

Figure 1.2. Schematic of Santa River
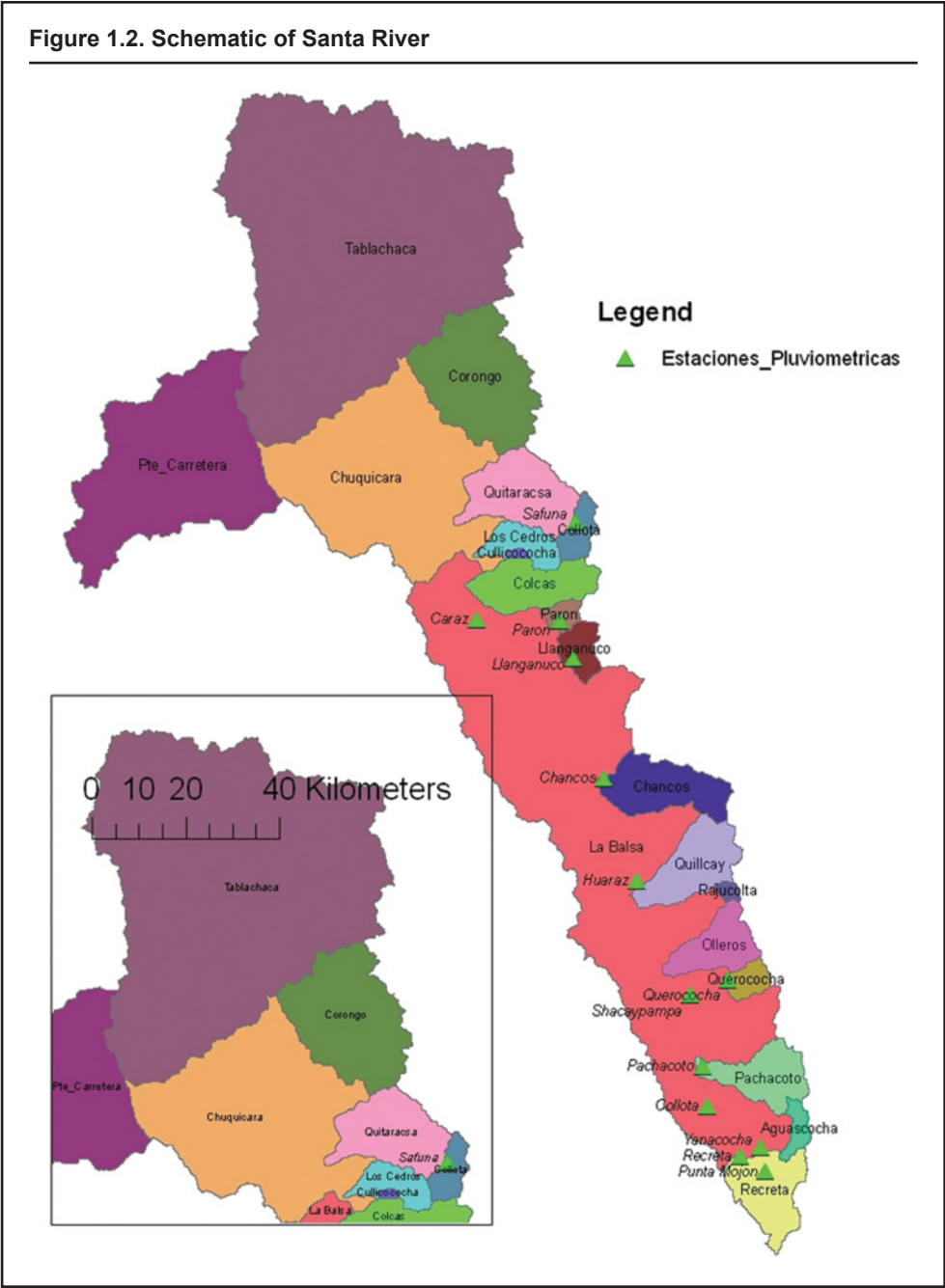
Source: Figure generated for this study by Escobar et al. 2008.

Mantaro River

The Mantaro River Basin covers an area of 34,550 km^2 and is divided in 23 subcatchment areas. The basin has great socioeconomic relevance in Peru. Located in the center of the country, it houses several important cities and is the most densely populated basin in the *sierra* with over 700,000 inhabitants. It contains hydropower plants that supply over 34 percent of the energy required by the national interconnected grid. It is also the food basket for Lima. Its agricultural production not only feeds the major urban centers, but it is also a major exporter of nontraditional products. Precipitation is one of the most important climatological variables in the Mantaro Basin due to its important role in the country's agriculture, energy generation and potable water supply sectors. There are nearly 340,000 hectares of agricultural land in the basin area. Over 70 percent of this land is not irrigated and therefore depends heavily on precipitation. This makes droughts the major climate hazard to agriculture in the region (IGP 2005a; Martínez et al. 2006).

Rímac River

The Rímac River, located in western Peru, is part of the Pacific Basin and has a length of 160 km. The river begins in the highlands of Huarochirí Province in the Lima region at an elevation of 5,706 meters above sea level, fed initially by glaciated subcatchments. Its mouth is located in Callao. The Rímac Basin is the most important source of potable water for the Lima and Callao Metropolitan Area, serving a population of over seven million people. This basin's very large slope (over 3.5 percent) makes its hydraulic behavior mostly critical and supercritical, with great capacity to transport sediments and large boulders. It also makes the basin attractive for hydropower development. Precipitation in the Rímac Basin ranges from values close to 800 mm/year in the high mountains to close to zero (less than 2 mm/year) on the Pacific coast. The Rímac Basin is also listed as a basin that is highly vulnerable to the impacts of climate change.

Because there is a major water transfer from the Mantaro River to the Rímac River Basin, it was decided after the analysis was started that the simulation runs should include both basins (the Mantaro-Rímac system).

Notes

1. The WEAP model can evaluate the hydrological feasibility of water management options related to the storage, distribution, use and conservation of regional water supplies (Sieber et al. 2004; Yates et al. 2004). WEAP is a microcomputer tool for integrated water resources planning. It provides a comprehensive, flexible, user-friendly framework for policy analysis. WEAP is distinguished by its integrated approach to simulating water resources systems and by its policy orientation.

Figure 1.3. Location of the Rímac and Mantaro system
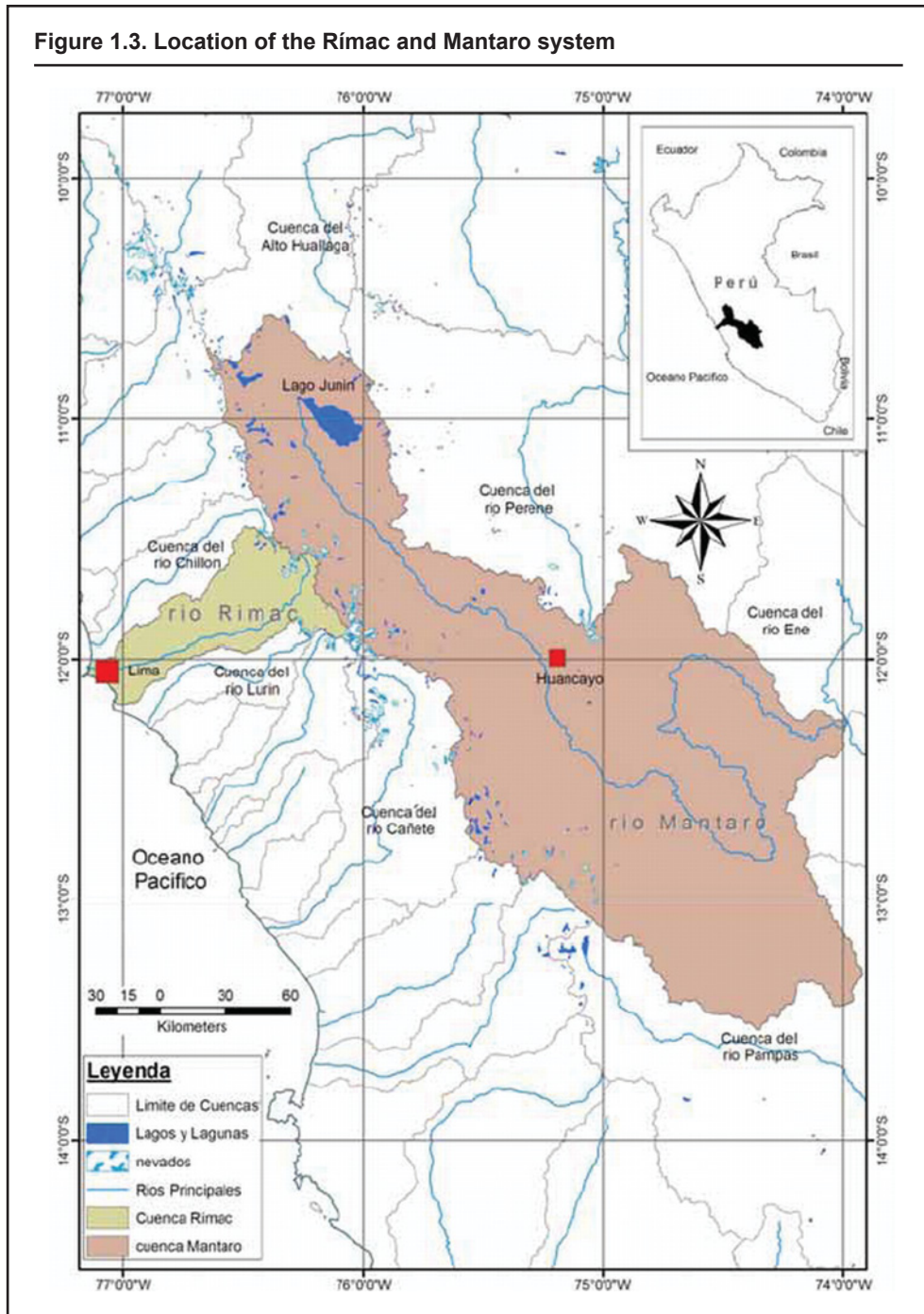
Source: Figure generated for this study by IRD 2009.

Context

There is an emerging consensus to support the view that climate change may have larger impacts at high altitudes, all around the world, and at a faster pace than previously predicted (Bradley et al. 2009; Duyrgerov 2003; IARU 2009; IPCC 2007a). Field measurements in the central range of the Andes already indicate a warming rate that exceeds the average registered for lowlands (Ruíz et al. 2010), and climate change is projected to result in even more significant temperature variation for the Andes in the future (Bradley et al 2006; see Figure 2.1). Reports based on future projections made using the Earth Simulator (Vergara et al. 2007) and ensemble results from various GCMs indeed estimate that surface temperature in the Andes mountains might increase as much as two times more than in the surrounding lowlands by the end of the century.

Besides the greater rate of overall warming anticipated for the American Cordillera, which includes mountainous terrains such as the Andes, the topography produces large climate variations along the mountain range. In particular, the Andean Cordillera

Figure 2.1. Anticipated temperature anomalies in the American Cordillera between 1990–1999 and 2090–2099
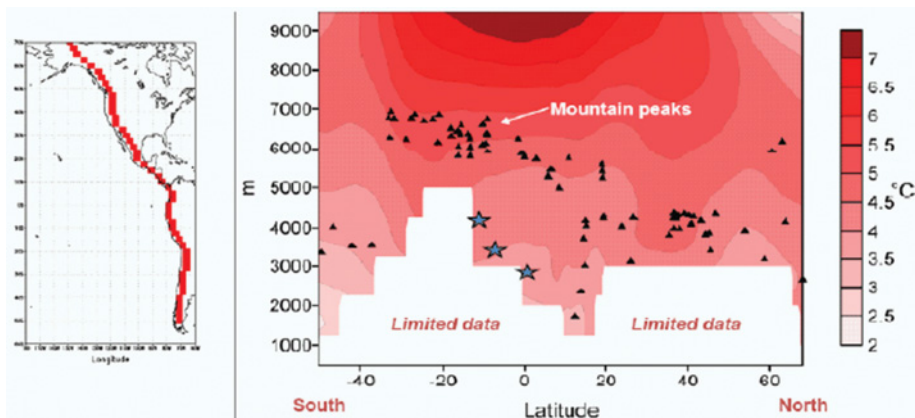
Source: Bradley et al. 2006.
Note: Projected changes in mean annual free-air temperatures between 1990–1999 and 2090–2099 along a transect from Alaska (68°N) to southern Chile (50°S), following the axis of the American Cordillera mountain chain. Results are the mean of eight different general circulation models used in the IPCC AR4, using CO2 levels from Scenario A2 (IPCC 2000; see also Appendix 1). Black triangles denote the highest mountains at each latitude; areas blocked in white have no data (surface or below in the models). In the figure: Blue stars = Quito, Cusco and La Paz, cities that derive water from higher-elevation sources.

acts as a barrier that drives variations in precipitation along and surrounding the range, which adds complexity to the analysis. These variations have significant implications for mountain climate and hydrology.

There is already clear evidence that the climate is changing in the Andes, particularly with respect to changes in temperature and rainfall. Recent studies from Peru's national meteorological and hydrological institute (SENAMHI 2007, 2009a and 2009b) have identified new climate patterns in mountainous areas in Peru, including changes in minimum daily temperatures, increases in maximum daily temperatures, reductions in relative humidity, changes in precipitation patterns, and changes in expected total precipitation. For example, with respect to temperatures, as summarized in Table 2.1, there are a decreasing number of cold nights and an increasing trend for warmer nights. These trends are not equally distributed throughout the year.

Table 2.1. Number of stations in the Peruvian Andes with significant (at 5% level) trends for seasonal temperature indexes during the 1960–2000 period

Indicator name	Negative	Nonsignificant	Positive	Indicator name	Season	Negative	Nonsignificant	Positive
Summer days	1	35	4	Warm days	Summer	5	47	3
Warmest day	1	40	2		Fall	3	46	6
Warm days	1	38	4		Winter	1	49	4
Cold days	5	37	1		Spring	1	48	5
Frost days	5	27	1	Cold days	Summer	6	48	1
Coldest night	2	35	9		Fall	4	51	0
Cold nights	19	26	1		Winter	5	50	2
Warm nights	0	25	21		Spring	4	48	1
Tropical nights	0	22	14	Warm nights	Summer	0	35	20
Diurnal temperature range	13	28	2		Fall	1	29	25
Extreme temperature range	6	36	0		Winter	0	43	10
					Spring	1	43	10
				Cold nights	Summer	22	33	0
					Fall	20	33	2
					Winter	8	43	2
					Spring	14	38	2

Source: Vincent et al. 2005 (c). American Meteorological Society. Reprinted with permission.
Note: The numbers in bold indicate that more than 25 percent of the stations have significant trends.

Summer days refer to number of days with daily maximum over 25°C. *Warmest day* means highest daily maximum temperature. *Warm days* refer to percentage of days with the maximum temperature above the 90th percentile. *Cold days* are the percentage of days with the maximum temperature below the 10th percentile. *Frost days* are the number of days with the daily minimum temperature below 0°C. *Coldest night* is the lowest daily minimum temperature. *Cold nights* are the percentage of days with the daily minimum temperature below the 10th percentile. *Warm nights* are the percentage of days with the daily minimum temperature above the 90th percentile. *Tropical nights* are the number of days with the daily minimum temperature above 20°C. *Diurnal temperature range* is the mean of the difference between the daily maximum and minimum temperatures, while *extreme temperature range* is the difference between the highest daily maximum and lowest daily minimum temperatures during the year.

Visible impacts of the changes caused by these new climate patterns are already evident. Warming temperatures have caused rapid retreat of glaciated areas, and variability and extremes in weather conditions have started to affect Andean ecosystems. Warmer temperatures are affecting evaporation rates, water storage in natural and man-made reservoirs, soil moisture and rates of evapotranspiration of mountain vegetation.

These changes are expected to have repercussions on water regulation and water and power supply, because rainfall is the source of runoff that feeds various power reservoirs, run-of-river plants, urban water supply systems and agriculture. The dynamic

behavior of tropical glaciers, Andean lakes and mountain wetlands also contribute to runoff seasonality by serving as storage or buffers during periods of rain and releasing the water stored over longer periods of time. From 2006 to 2009, over 50 percent of electric power in Peru was produced by hydropower, which is dependent on mountain water basins.

Some of the anticipated climate change impacts on water regulation, glaciers and mountain wetland ecosystems that might affect the runoff patterns of mountain water basins are summarized below.

Climate Impacts on Water Regulation

A growing set of data indicates that climate is affecting the land components of the water cycle. In reference to water and the water regime, the IPCC concludes (IPCC 2007a):

- There is high confidence[1] that **hydrological systems** are being affected: increased runoff and earlier spring peak discharge in many glacier- and snow-fed rivers, and warming of lakes and rivers in many regions, with effects on thermal structure and water quality. Increasing seasonal variability will also affect hydrological systems.
- Some **extreme** weather events have changed in frequency and/or intensity over the last 50 years: It is likely[2] that the frequency of heavy precipitation events (or the proportion of total rainfall from heavy falls) has increased over most areas.

Similarly, a wide array of satellite and field measurements documents that climate is affecting water stocks and flows in mountain systems. In practice, this would most likely mean higher fluctuations and loss of streamflows, which would have a direct impact on the available water resources, power supply and ecosystem integrity.

Climate Impacts on Glaciers

In Peru, glaciers had an area of 2,041 km^2 in 1970 but this number had declined nearly 22 percent to 1,595 km^2 by 1997 (see Figure 2.2; Bradley et al. 2006; CONAM 2001; Vuille and Bradley 2000).[3] Major additional reductions in surface area have been measured since. The largest of the studied glaciers in Peru's Cordillera Blanca lost 15 percent of its glacier surface area in 30 years. Figure 2.3 illustrates the rapid decrease in surface area being measured for the Santa Isabel Glacier in the central range of the Colombian Andes. The glacier is losing volume at a rate that would result in its disappearance in a few decades.[4] Similarly, many of the low-lying (below 5,500 m to 5,000 meters above sea level) and smaller glaciers in Peru have been heavily affected and some are likely to disappear within a generation (Francou et al. 2003).

Anticipated and already observed climate change-related impacts caused by glacier retreat include deterioration of river basins, depletion of water recharge capacities, and biotic changes in ecosystem thresholds and composition, which affect the ecosystem's ability to store water. Since glaciers have typically provided continuous meltwater to sustain river discharge through droughts and the dry season, glacier-fed rivers and streams will have lower dry-season flows and increased variability with a diminishing mass of glacier upstream (Francou and Coudrain 2005; Juen et al. 2007). The effects and consequences may be different at the initial and final stages of glacier retreat and depend on location.

Figure 2.2. Cumulative loss in length for selected glaciers in the Andes since 1870

Source: Vuille et al. 2008.

Figure 2.3. Reduction in surface area of the Santa Isabel Glacier in Colombia
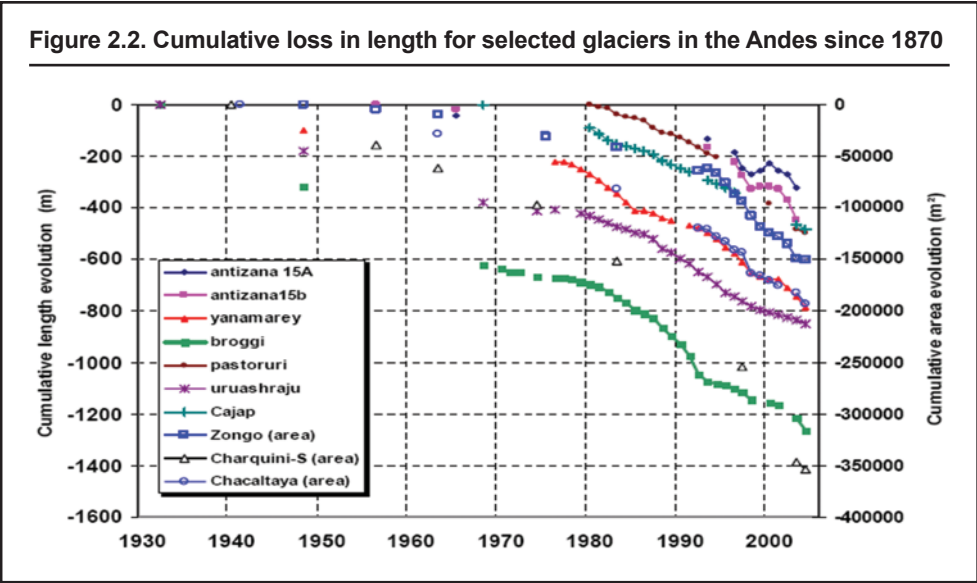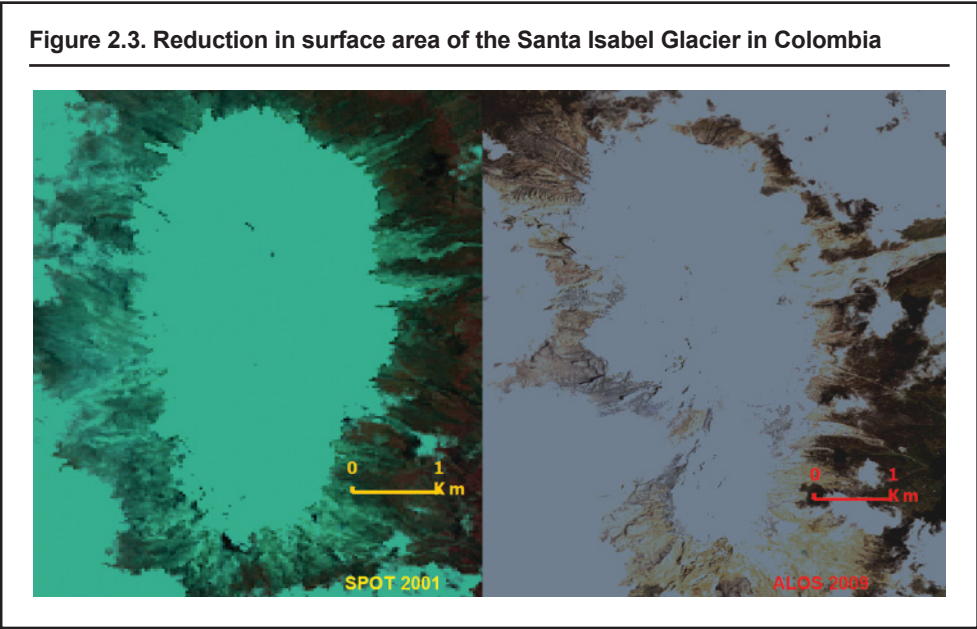
Source: SPOT and ALOS images collected by the INAP Project in Colombia and stored in IDEAM's archive.
Note: Documented through satellite images (2001–2009).

Climate Impacts on Mountain Wetlands

High-mountain ecosystems, including páramos, are among the environments most sensitive to climate change. These ecosystems have unique endemic flora and provide numerous and valuable environmental goods and services. Recently published data from a World Bank-funded study suggest that temperatures have indeed increased at a significant rate at páramo altitudes (Ruiz et al. 2010). See Figure 2.4 below.

In the abovementioned study, it is shown that minimum temperatures during the warmest days (MTmin) exhibit statistically significant trends at altitudes below 2,500 m, ranging from +0.1 to +0.5 C/decade. MTmin records gathered at higher altitudes do not show significant trends. Average minimum temperatures (ATmin) gathered at weather stations located below 2,500 m exhibit increasing trends that range from +0.1 to +0.6 C/decade. ATmin records observed at higher altitudes do not show significant trends. Minimum temperatures during the coldest days exhibit statistically significant increasing trends at all altitudes, ranging from +0.10 to +0.90 C/decade. Increases in these extreme temperatures at higher levels *are more than twice* what is observed on average at lower altitudes (Ruiz et al 2010).

Maximum temperatures during the warmest days exhibit statistically significant trends at all altitudes that range from +0.20 to +1.50 C/decade. Increases at higher levels are *more than three times* what is observed on average at lower altitudes. Average maximum temperatures exhibit increasing trends that range from +0.10 to +0.60 C/decade at all altitudes. Maximum temperatures during the coldest days exhibit statistically significant increasing trends in only three weather stations; their increasing trends in the mean reach +0.20, +0.30, and +0.90 C/decade, respectively.

Figure 2.4. Observed pattern of temperature changes at páramo and other altitudes during the 1950–2007 period in the Río Claro Valley in the Northern Andes
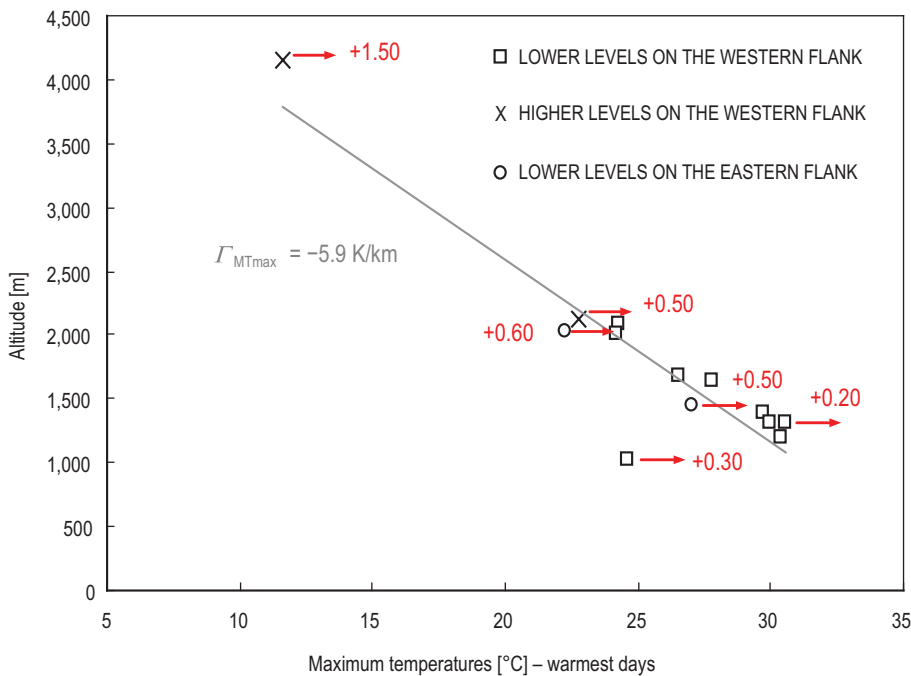
Source: Ruiz et al. 2010.
Note: Páramo starts at around 3,000 m at this location. Annual values (boxes, crosses and circles) and long-term trends (arrows) observed in the spatial domain 04° 25′N-05° 15′N and 75° 00′W-76° 00′W. Gray trends in temperature are expressed in °C/decade.

In addition, according to the study, climate impacts have already altered the atmospheric circulation patterns of producing and moving water vapor within these ecosystems. It is possible that these changes have contributed to the disappearance of high-altitude water bodies, as well as to the increased occurrence of natural and man-induced mountain fires (Ruíz et al. 2010).

Notes

1. High confidence means about an 8 out of 10 chance (IPCC 2007c). See also Appendix 1.
2. Likely means more than a 66 percent chance (IPCC 2007c). See also Appendix 1.
3. Glacier retreat is being monitored using a variety of techniques in the Andes. Some of these measurements are being facilitated through the Colombia: Integrated National Project and the Regional Andes: Adaptation to Glacier Retreat Project.
4. The second photograph is part of an archive being constructed through images taken every 48 days by the Advanced Land Observation Satellite (ALOS) of Japan.

Climate Analysis

As the consequences of global warming become more pressing, decisions related to the control, use and regulation of water resources need to take these into account. This chapter presents a process for the selection of "planning climate scenarios." First, a brief introduction of different approaches to building climate change scenarios is presented. It is followed by a summary presentation of projections made using GCMs in three different ways. To provide a comparison with current climate, a trend analysis of key climate variables is carried out with data selected from reliable weather stations (as defined by SENAMHI). The chapter then looks at the definition of criteria to rank alternative approaches. Once the criteria are defined, a semi-random sample of 10 "sites" is selected and the results are analyzed.

Available approaches for projection of climate scenarios can be grouped as follows:

- Use of a single GCM. If only one GCM is used, it has to be one that is well suited to the objective and the region under study.
- Use of an ensemble of GCMs to provide a wide range of possible future scenarios. Here the underlying assumption is that the ensemble does not provide one scenario but a range of results that help to deal with the uncertainty that is always associated with the modeled results.
- Use of a weighted ensemble of GCMs. In this method the GCMs are weighted by their ability to reproduce such climate conditions that are of interest considering the scope of the study. Normally, only a few (four or five at most) are used based on their contribution to explain past climate behavior.
- Use of dynamic downscaling models (also named Regional Circulation Models, or RCMs) to improve the resolution of the climate scenarios. Since GCMs set the boundary conditions for RCMs, the results of the RCM are associated with the use of one or several GCMs. Given the large computing time that this method requires, normally only one GCM is used with several "runs" of the downscaling routines.
- Use of statistical trend analysis on past climate observations to produce climate projections. This method can be used only in areas where some minimum adequate climate records are available.

The following four options were used:[1]

- **High-resolution projection.** The MRI-AGCM3.1 was used as a single GCM. Data were generated by running the MRI-AGCM3.1 model in a supercomputer called the Earth Simulator-2. For this application, only a few climate variables were downloaded and analyzed, including temperature, rainfall, soil moisture

and evaporation at a very high-resolution (20-km), capturing the intensity and frequency of extreme weather events.[2] Achieving such a high resolution in GCM is unique in global climate change studies; that is why the MRI-AGCM3.1 was chosen as a single GCM in this study. The challenge of this tool is that the available computing power is insufficient to enable multiple emissions scenario runs. Therefore, the application of the high-resolution GCM was limited to a single run. To address this limitation and strengthen the robustness of the projections made at a 20-km resolution, the same GCM was run at lower resolutions (60 km and lower). These results were compared with the 20-km version.

- **Ensemble of GCMs.** Since GCMs used for projecting the changing climate are imprecise representations of the earth's climate system, all of them are deemed to have "model errors". Therefore, an often recommended practice is to use the results of multiple GCMs in future climate projections. This study used combined output from 16 GCMs[3] presented in the Fourth Assessment Report of the IPCC. They were used in this study to project the potential range of precipitation and temperature changes that might be anticipated at a basin level.

- **Dynamic downscaling**. The use of the Subgrid Orography Dynamic Model has shown that downscaling could greatly improve the simulation of snowfall, temperature and precipitation in mountainous regions. In this study, the subgrid scheme was used to downscale outputs from the Community Climate System Model (CCSM). CCSM is a GCM developed by the US National Center for Atmospheric Research.

- **Rainfall trend analysis.** In order to further strengthen the robustness of the projections, the analysis used statistical analysis of observed meteorological data for over 20 years to verify the modeled GCM projections with local linear future projections.

High-Resolution Climate Projection for Peru for the 21st Century

The results from simulation runs from a high-resolution GCM were used to generate a climate projection for Peru, primarily for temperature, rainfall, and extreme events. This projection used the atmospheric GCM of the MRI of the Japan Meteorological Agency (JMA). It is a high-resolution atmospheric climate model.[4] The horizontal grid size is about 20 km (Mizuta et al. 2006), which offers unequaled high-resolution projection. The use of the Earth Simulator-2,[5] which has a top speed of 130 teraflops (TFLOPS), made the high-resolution simulation possible. A detailed description of the model and its performance can be found in Mizuta et al. (2006).

The MRI-AGCM3.1 was used to project Peru's hydrological response to climate change in the middle (2035–2049) and end of the 21st century (2075–2099). In previous Assessment Reports, the IPCC defined standard reference scenarios (SRES) that were used in its reports' GCM projections. These emissions scenarios are also widely used in modeling studies elsewhere (see Appendix 1 on the different IPCC-SRES emissions scenarios). The IPCC's emissions scenario used in this exercise was A1B,[6] which is considered a "middle-of-the-road" projection of greenhouse gas emissions. It results in an average temperature increase of between 1.3 and 3.5 degrees Celsius by the end of the century.

Only climate variables that are of direct relevance to the subsequent hydrology analysis are summarized here. These are annual mean rainfall, extreme rainfall patterns

(maximum 5-day precipitation and consecutive dry days), and top soil layer moisture. All of them are compared with historical data (1979–2003) to estimate changes over time. Since this model includes a river component option, its use enabled a direct assessment of countrywide river flow changes. Results of this model are used in Chapter 6 to make an overall estimate of the changes in runoff and river flow in Peru.

Results for Average Precipitation

To assess how well the model replicates present climate, historical data were compared to simulation results for a reference period (1979–2003). Figure 3.1 shows the distribution of annual mean rainfall averaged for this reference period. The top row presents the observed mean annual precipitation data, while the bottom row summarizes the results from a simulation analysis. Results are shown at different resolutions (20 km, 60 km, 120 km, and 180 km). In comparing these images, it is clear that the simulations reproduce general observed patterns reasonably well. However, these images also reveal the challenges of securing a good representation over the Andes, especially at lower resolutions (120 km and lower).

The annual mean rainfalls in the near future (2015–2039) and by the end of the 21st century (2075–2099) were simulated to visualize future changes. These data were then compared to the currently available data on mean rainfall. The projected changes are presented in Figure 3.2. The overall pattern of precipitation change simulated by the 20-km and 60-km models is similar. The largest anomalies (difference with the reference period) are seen over the Andes Cordillera while the smallest changes are seen in the eastern lowlands and the southern coastal areas.

Figure 3.1. Observed and simulated annual mean rainfall (mm d⁻¹) over Peru for 1979–2003
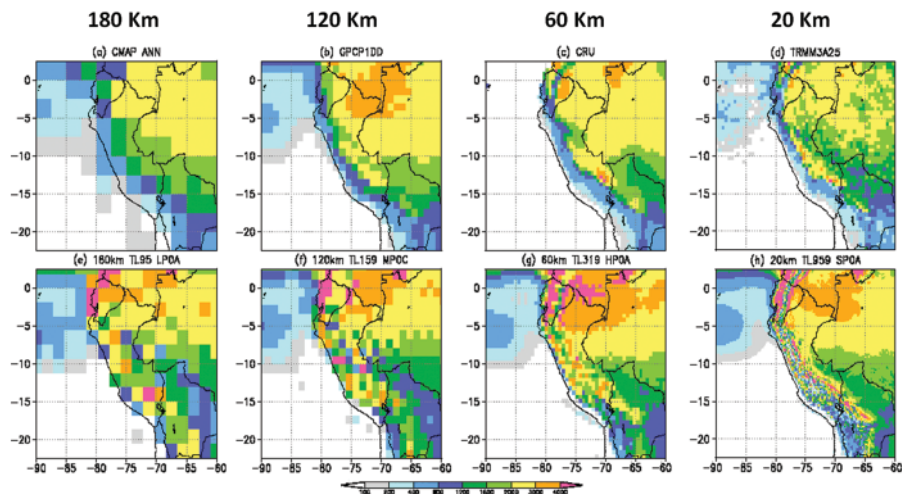
Source: Figure generated under the Memorandum of Understanding (MOU) between the MRI and the World Bank.
Note: Plots correspond to datasets of actual observations and different resolutions for projections.

Figure 3.2. Annual simulated mean precipitation changes (mm) for the a, b) near future (2015–2039) and c, d) end of the 21st century (2075–2099) for 60-km and 20-km resolutions
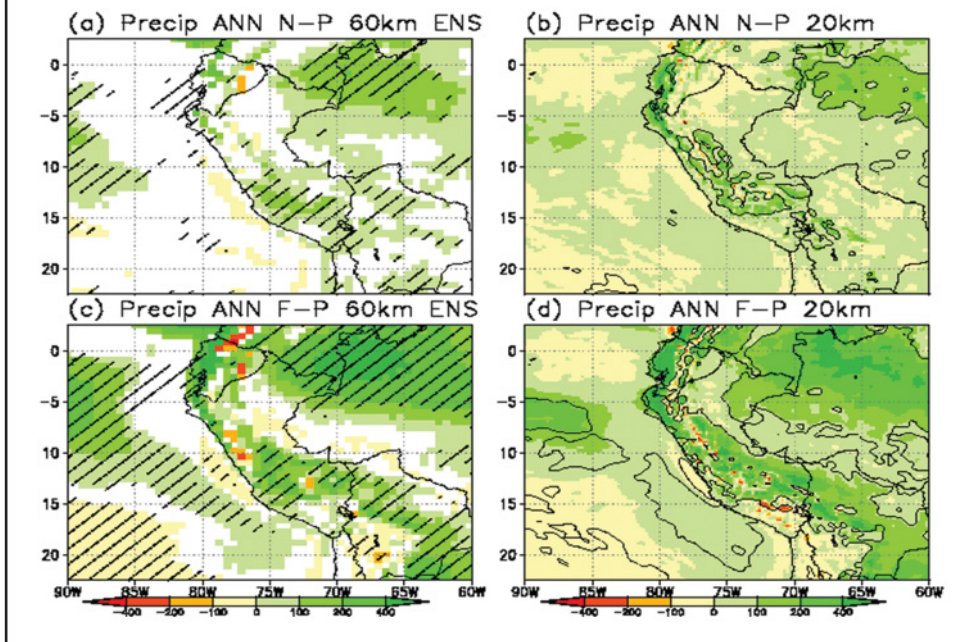
Source: Figure generated under the Memorandum of Understanding (MOU) between the MRI and the World Bank.
Note: Areas statistically significant at 95 percent level are hatched. Hatched areas only appear in the 60-km resolution, since only that one could be compared with the ensemble of GCMs. There was only a single run in the 20-km resolution. Therefore, the results obtained from it could not be compared with other results.

Extreme Precipitation Events

Global warming is not only expected to change the mean conditions of climate variables but also to increase the amplitude and frequency of extreme events. Understanding where these changes in extremes will take place is important for recognizing where adaptation measures are needed. Two distinct impacts can be identified: (i) changes in heavy precipitation (measured through the maximum total in five days, denoted as RX5D, in millimeters), and (ii) days without rain (measured through the number of consecutive dry days). These two extreme indexes for precipitation were calculated to illustrate changes in precipitation extremes over Peru. Figure 3.3 shows the projected changes in the heavy precipitation in comparison with today, at both 60-km and 20-km resolutions for the near future and end of the century. The model suggests that there will be an increase of heavier downpours throughout Peru, leading to an increased likelihood of floods and reduced stability of streamflows. As seen in the figure, the model projects even greater increases in heavy precipitation by the end of the century at a higher resolution (20 km). Overall, the largest rainfall intensification is found over the northwestern coast and the Andean Cordillera.

Figure 3.3. Changes in maximum annual five-day precipitation (total in mm) for the a, b) near future (2015–2039) and c, d) end of the century (2075–2099), for 60-km and 20-km resolutions
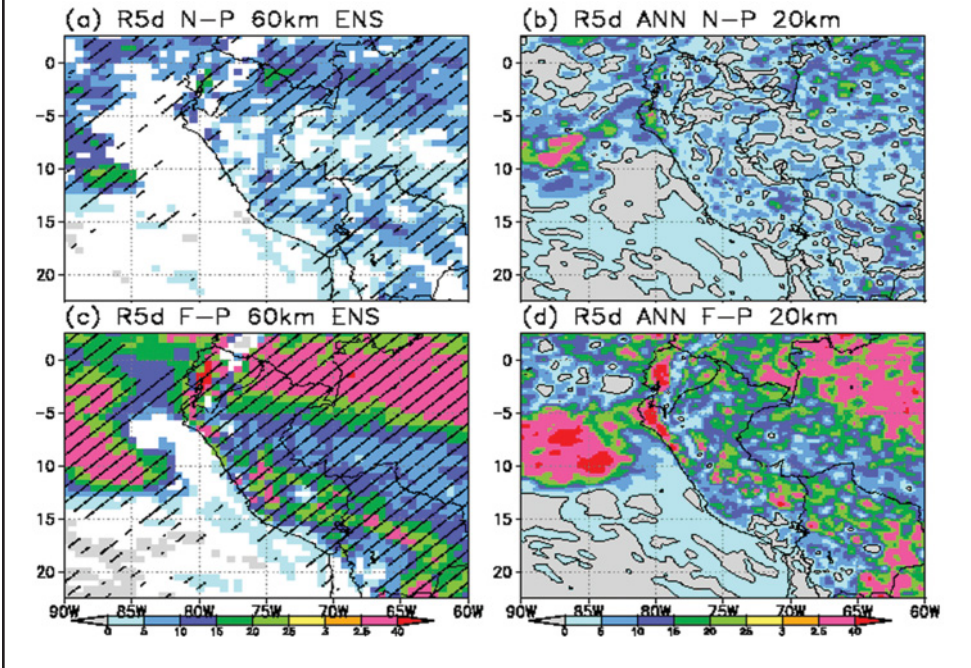
Source: Figure generated under the Memorandum of Understanding (MOU) between the MRI and the World Bank.
Note: Hatched areas show consistency in ensemble results at 60-km resolution.

According to the MRI-AGCM3.1 model, it seems likely that climate change would not only cause intensification of rain, but would also lead to an increased number of days without rain. To illustrate the changes in the extent of the dry season, the consecutive dry days (CDD) were estimated for the same period as heavy rainfalls. A "dry day" is defined as a day with precipitation of less than 1 mm d^{-1}. Figure 3.4 shows the changes in maximum number of CDDs over Peru for the near future and end of the century at 20 km and 60 km. The number of dry days is projected to increase over the entire country. This may lead to an increase in droughts over time.

Soil Wetness

Surface hydrology will be affected as a result of changes in precipitation. A key parameter for surface hydrology is the soil water content (wetness) of the upper layer of soil (WETSL1),[7] which may be estimated on the basis of a water budget calculation based on the GCM's modeling results. The calculations included an estimate of the change in top soil moisture made on the basis of evaporation and changes in rainfall and dry spells. The results of the calculations are presented in Figure 3.5. They indicate that soil would become considerably drier in most parts of the country and that the dryness would increase over time. According to the figure, drying of the soil would be the strongest in the
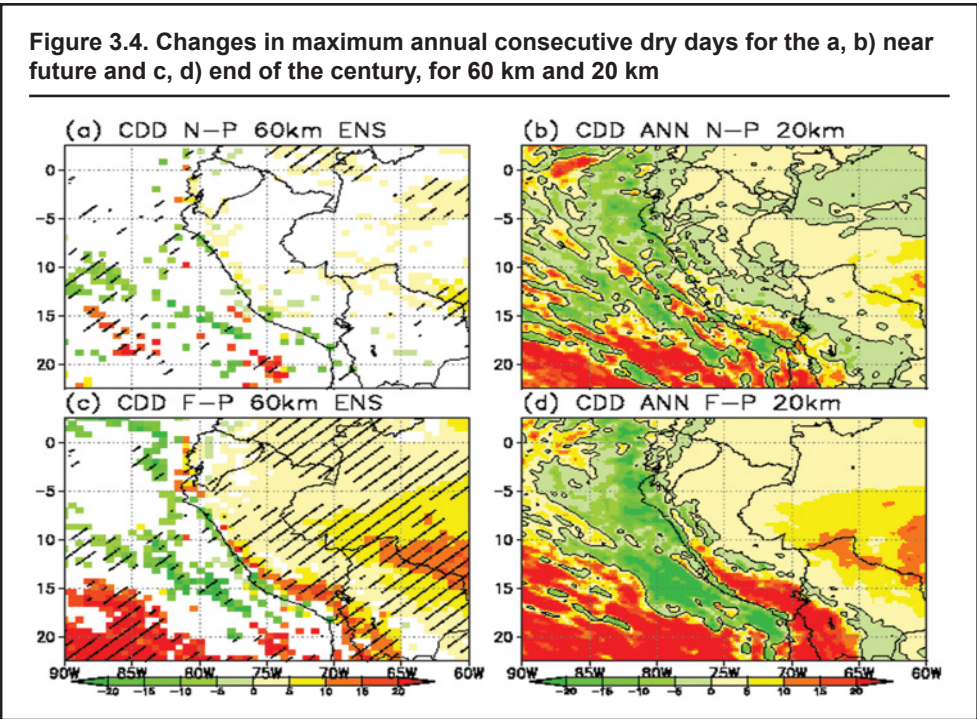
Figure 3.4. Changes in maximum annual consecutive dry days for the a, b) near future and c, d) end of the century, for 60 km and 20 km

Source: Figure generated under the Memorandum of Understanding (MOU) between the MRI and the World Bank.
Note: The scale is in days.
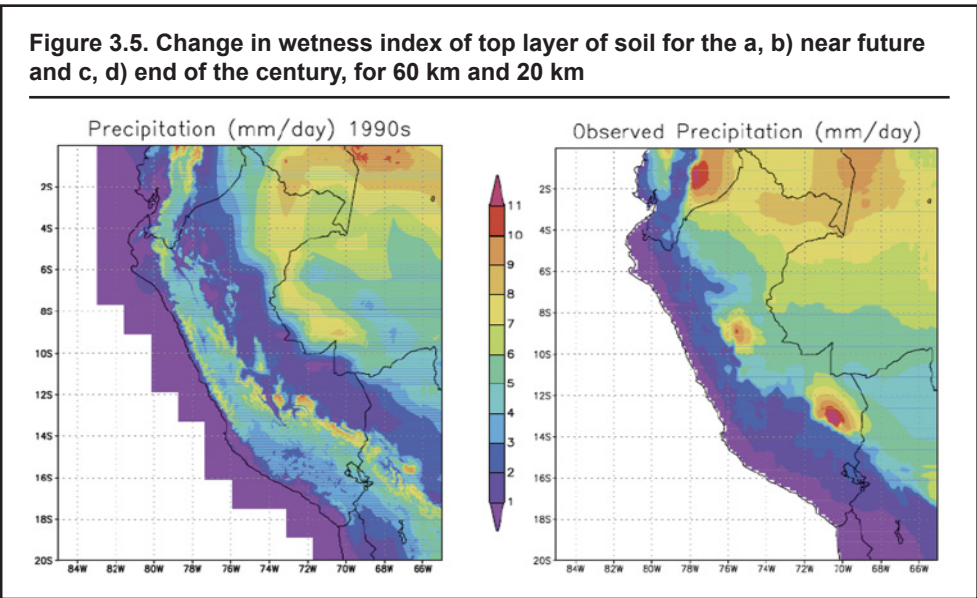
Figure 3.5. Change in wetness index of top layer of soil for the a, b) near future and c, d) end of the century, for 60 km and 20 km

Source: Figure generated under the Memorandum of Understanding (MOU) between the MRI and the World Bank.
Note: The wetness index WSLN is defined as average change in moisture content of the top 10 cm of surface soil.

Amazon region and southern coastal areas. The Andean Cordillera region is projected to experience mixed changes in soil moisture content.

The high resolution of the MRI-AGCM3.1 is ideal to help visualize climate extremes; in conjunction with GRiverT it can resolve hydrological impacts at large basin scale (+100,000 km²). However, large computing requirements limit the use to one or two emissions scenarios. The MRI-AGCM3.1 outputs are used in the study to project future climate nationwide and visualize weather extremes.

Ensembles to Simulate Future Climate

To complement the results obtained through the use of high-resolution projections of the MRI-AGCM3.1, an ensemble output from 16 other GCMs with lower resolutions (grid sizes of 200 km or more) was used to address uncertainty in the estimate of potential future temperature and precipitation changes. As with all GCMs, these 16 models were not run specifically for this study; instead, existing data were gathered from the IPCC's Fourth Assessment Report.[8] Data were used from two scenarios: (i) the A1B scenario, used in the previous subchapter in the application of the high-resolution GCM, and (ii) the B1 scenario, which is considered an optimistic scenario.

The range of precipitation and temperature changes obtained from the IPCC data was used to project changes at selected meteorological stations (the Collota, Huaraz, Parón and Caraz stations) in the Santa River Basin over the 21st century. The IPCC data were obtained on a monthly basis. The mean precipitation and temperature changes, along with the mean plus/minus one standard deviation, were calculated for each basin using all data points (16 models times two emission path scenarios). This exercise was done for each month in the simulation period from 2000 to 2100. The results estimate the upper and lower envelopes of precipitation and temperature change around 2040, as shown in Figure 3.6. The output from the 16 GCMs was generally consistent with the outputs from the Earth Simulator.

The two IPCC scenarios (A1B and B1) were used to create two temperature and precipitation conditions for the Santa River Basin for the 2040 decade, using the extremes: **Marginally warmer conditions** with a 0.5°C increase in temperature and a 15 percent increase in precipitation (roughly corresponding to the outputs from the MRI-AGCM3.1); and **Much warmer conditions** with a 2°C increase in temperature and a 10 percent decrease in precipitation.

These sets of conditions were used to project climate data for a 30-year period (2010–2040), building **two climate paths for the immediate future**, as shown in Figure 3.7.[9] For the baseline conditions (the average between 1979 and 2003), annual precipitation is around 870 mm/year. Under much warmer conditions, precipitation is reduced to 780 mm/year by 2040 while under the marginally warmer conditions, precipitation is projected at 1,000 mm/year. Precipitation is on the left side while temperature in on the right side. This approach produces the possible range of results to be expected from climate change. The results highlight the uncertainty associated with the use of the 16 independent GCMs deployed in the IPCC process. These results illustrate the approach often followed in building climate scenarios. Based on the results summarized in Figure 3.6, scenarios are selected, indicating the extreme (upper and lower bounds) climate conditions that might be expected. The underlying assumption is that projects (decisions) should prove resilient to the extreme climate projections.

Figure 3.6. Potential changes in temperature and precipitation in the Santa River Basin (Collota, Huaraz, Parón, and Caraz meteorological stations)
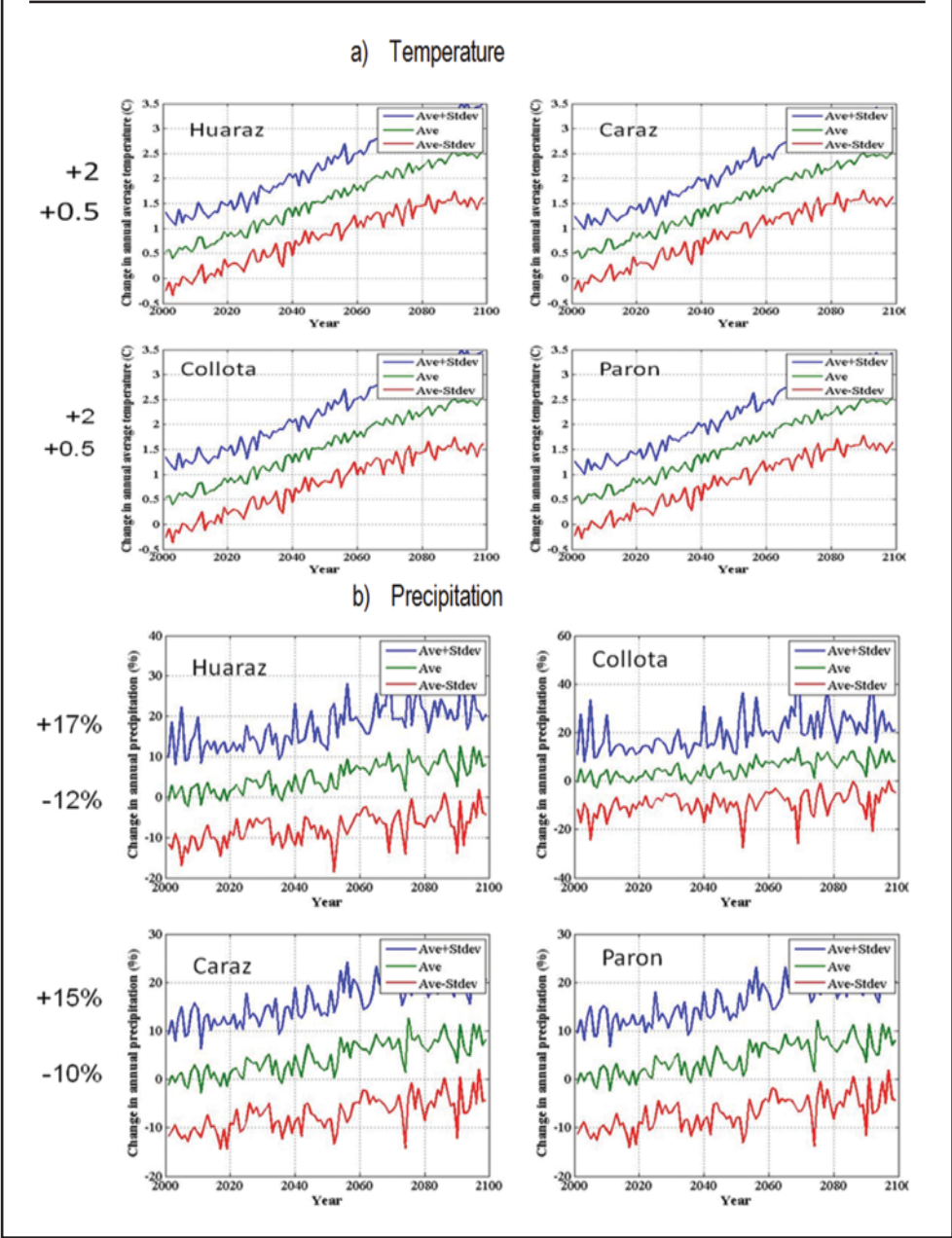
Source: Figure generated for this study by SEI, 2009.
Note: Outputs are from a set of 16 GCMs. The numbers on the Y axis indicate the values of the variables that would fall within one standard deviation in each direction.

Figure 3.7. Precipitation and temperature time series associated with two sets of conditions in the Santa River Basin
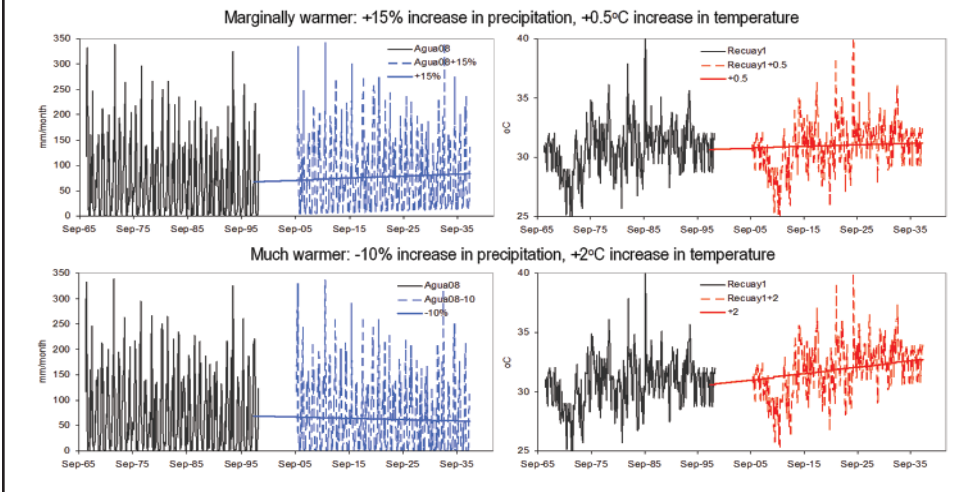
Source: Figure generated for this study by SEI, 2009.

To assess the uncertainty associated with the use of the ensemble of GCM, the variability in simulations of precipitation projections in the Santa Basin was estimated for the historical, mid-century and end-of-century periods. Figure 3.8 provides information on the variability and initial bias of GCMs. The horizontal axis indicates the individual GCM in the ensemble. For each GCM, Figure 3.8 presents the mean value of the precipitation and its quintiles. The ensemble analysis gives equal weight to each model and the combined information is used to calculate the expected variability.

The first panel shows the results for the simulation of the historical record. The next indicates the results for the mid-century and late-century simulations. Clearly, the GCMs do not yield consistent results. Some are able to simulate the current period with more accuracy than others but no attempt was made to weight these results.

The combination of outputs from 16 different models has the potential to reduce the range of uncertainty and identify areas where the models indicate common signs and magnitudes of anomalies; the combination of results can provide upper and lower levels for future climate variables at a basin level. However, as seen in Figure 3.8 below, the results show large variance between models. Unless weighted, these ensembles combine the projections of poor and good fits, masking the outputs from better individual models.

Subgrid Orography Dynamic Model (Downscaling Tool)

Assessments of the impacts of climate change at the project level typically require information at scales of 10 km or less. In regions with complex terrain, much of the spatial variability in climate (temperature, precipitation and snow water) occurs on scales below 10 km (IPCC 2007a) in contrast with the grid size of global climate model simulations, presently 200–300 km. Naturally, one can expect the grid size at which GCMs run to continue to decrease with time as computer speed and memory increase. However, the large increase in computer power required to reduce grid size (an eightfold increase in speed

Figure 3.8. Variability in precipitation (in mm) for the historical (1960–1999), middle (2000–2050) and end (2050–2099) of 21st century periods
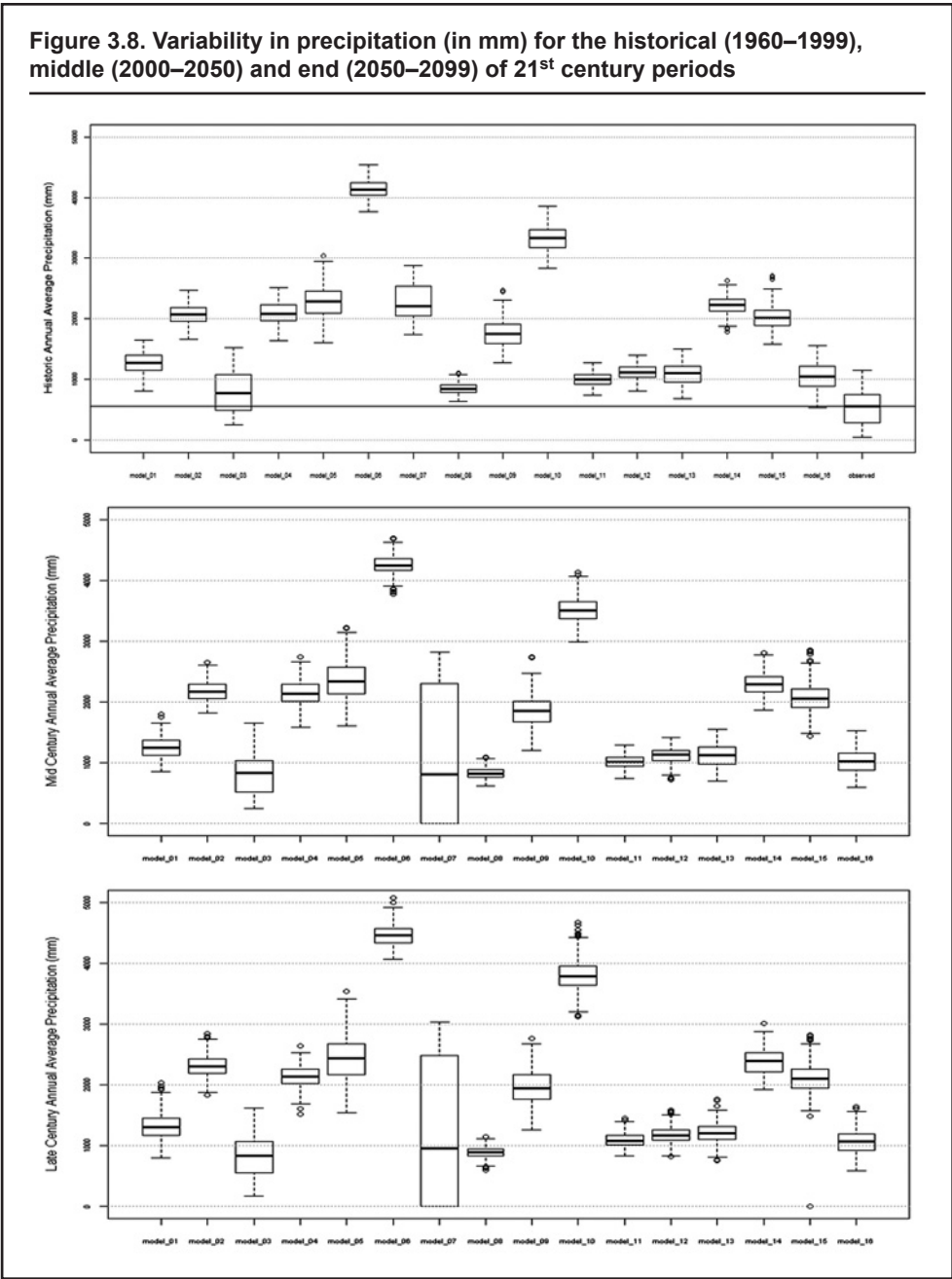
Source: Figure generated for this study by SEI, 2009.
Note: Annual average precipitation for the historical time period (1960–1999), mid-century (2000–2050) and late century (2050–2099) for 16 models from the WCRP CMIP3 multi-model database project (www. earthsystemgrid.org) for scenarios A1b and B1. Boxplots include data for stations Collota, Huaraz, Parón, and Caraz. The 16 GCMs used in this figure are Model 01: bcm2, Model 02: cccma_cgcm3, Model 03: cnrm_ cm3, Model 04: csiro_mk3_0, Model 05: gfdl_cm2_1, Model 06: giss_aom, Model 07: lap_fgoals1_0_g, Model 08: inmcm3_0, Model 09: ipsl_cm4, Model 10: miroc3_2_hires, Model 11: miub_echo_g, Model 12: mpi_echam5, Model 13: mri_cgcm2_3_2a, Model 14: ncar_ccsm3_0, Model 15: ncar_pcm1 and Model 16: ukmo_hadcm3. For the historical time period (1960–1999), the distribution of the observations and a horizontal line are added at 556.65 mm, which is the median annual precipitation of the observations for all four stations.

for a halving of the grid size) limits the rate of grid size reduction to discrete leaps as new supercomputers become available, roughly every six years. Despite concerted efforts, one therefore cannot expect the explicit resolution of global climate model simulations to reach the required resolution for impact assessment for present-day applications.

This gap between the resolution required for impact assessment and the resolution available from global climate models (Ghan 1992; von Storch 1995) has led to the development of a variety of downscaling techniques. These include high-resolution global atmospheric models run for selected time slices (Cubasch et al. 1995; May and Roeckner 2001), regional climate modeling (Giorgi 1990; Giorgi and Mearns 1999), and a variety of statistical downscaling methods (von Storch 1995; Wilby and Wigley 1997; Gyalistras et al. 1998; Murphy 1999, 2000). Each of these methods offers advantages but also has serious limitations.

Of particular interest for purposes of the assessment is the treatment of the atmospheric process in steep mountain ranges, such as the Andean Cordillera. Leung and Ghan's (1995, 1998) downscaling technique provides a phenomenological approach to the treatment of the subgrid influence of orography on temperature, clouds, precipitation and land surface processes. The use of the *Subgrid Orography Dynamic model* has shown that in a regional climate model, the treatment significantly improves the simulation of snow-water temperature and precipitation in mountainous terrain. The subgrid scheme was used to downscale the results of the CCSM3 GCM from the US National Center for Atmospheric Research.

In the subgrid orography scheme, each model grid cell is divided into a nominal number of subgrid elevation/vegetation bands based on high-resolution topographic and vegetation data, illustrated in Figure 3.9. The subgrid method estimates the vertical displacement of air parcels in each subgrid band based on the elevation difference be-

Figure 3.9. Subgrid orography scheme
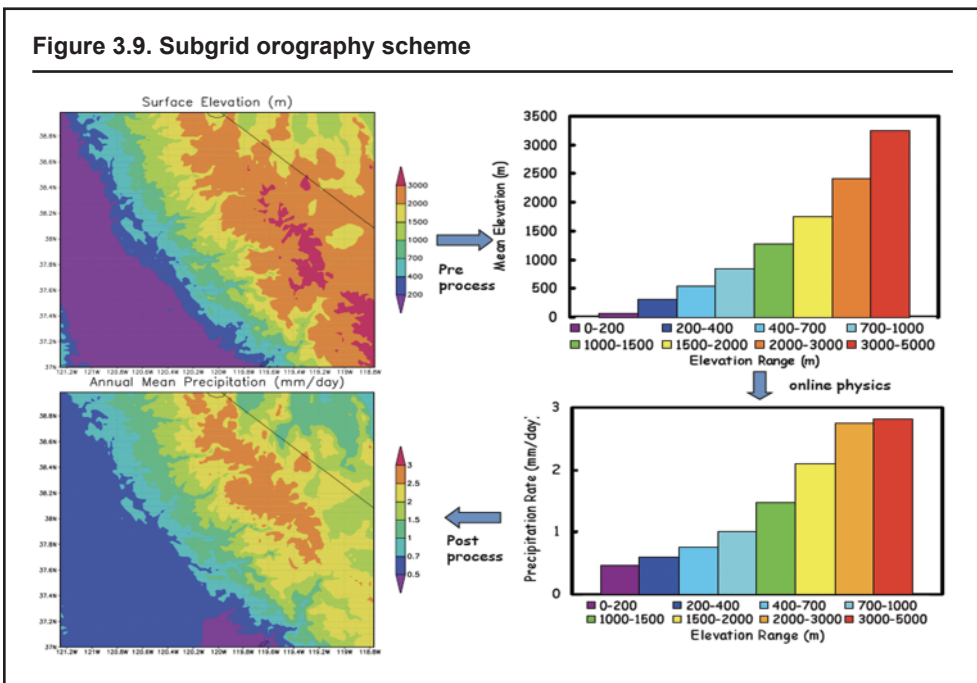
Source: Ghan and Shippert 2009.

tween the subgrid band and the grid cell mean, and the Froude number, which is used to distinguish whether the air parcel is blocked or lifted by the subgrid topography.

The estimated vertical displacement of the air parcel is then used to determine the subgrid vertical profiles of temperature and humidity based on conservation of energy and moisture. After that an orographic forcing term is applied to the prognostic equation of temperature and moisture for each subgrid class. This is done by nudging the temperature and moisture profiles to the diagnosed profiles over a relaxation time constant. The full suite of atmospheric physics and the land surface physics are applied to each elevation band within each grid cell, but atmospheric dynamics are only calculated based on the grid-cell mean variables. This method has been implemented and evaluated in a regional climate model (Leung and Ghan 1998, 1999) and a global climate model (Ghan et al. 2004).

The downscaled data using this technique were analyzed by comparing simulated results for the reference period with key statistics of observed climate variables for a semi-random[10] small sample of stations covering Peru (see Figure 3.11 for the location of the sample points). A statistical analysis was conducted for three periods of interest: the reference period as well as mid-century and end of century.

Figure 3.10 compares the simulated and observed distribution of precipitation for Peru. The simulation produces too much precipitation on the leeward (western) side of the Andes, and too little on the windward side. This is a consequence of the subgrid orography scheme's inability to distinguish between the windward and leeward sides of mountains. The mountain rain shadow must be explicitly resolved. The observed data (right figure) show the presence of three localized areas with very high precipitation on the eastern side of the Andean Cordillera where it meets the Amazon plateau: two in Peru and the third in Ecuador. The simulated precipitation fails to reproduce these features.

Figure 3.10. Simulated (left) and observed (right) precipitation for Peru
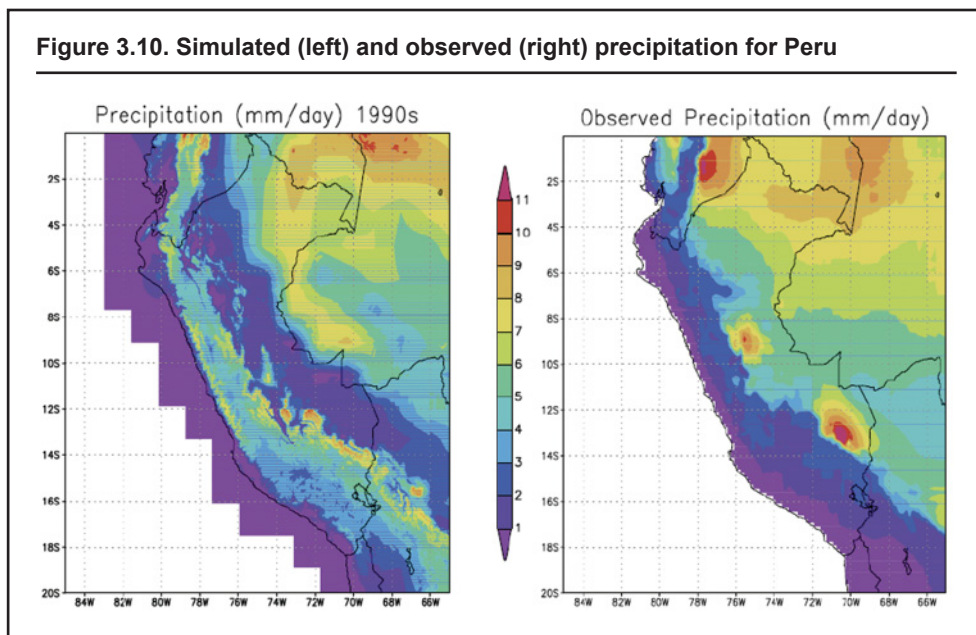
Source: Ghan and Shippert 2009.

The simulation shows some ability of the global model to reproduce the spatial distribution of annual precipitation where the Andes are broad, such as in southern Peru, but not where the Andes are narrow, such as in the middle and northern parts of Peru.

The detailed simulations are presented in Appendix 3. In summary, these simulations produce remarkably consistent but spatially complex distributions of changes in surface air temperature, total precipitation and snowfall that amplify with time. Total precipitation increases in most locations, but snowfall decreases. These changes are likely to produce strong effects on estimates of the impacts of global warming on surface water resources in Peru.

However, large biases are evident in the distribution of precipitation. The immediate solution would be to apply empirical corrections for these biases. Longer-term solutions would be to improve the subgrid orography scheme to account for subgrid rain shadows, or to employ explicit regional modeling for Peru and Bolivia. A treatment of rain shadows might be applied to this problem. Saved daily history from other global simulations could also be used to drive simulations with the regional climate model.

In conclusion, while the technique is able to model elevations in complex terrains and features high resolution that can potentially resolve basins in mountain areas, it still has limitations, that prevent its effective use at this time. These limitations include the inability to treat rain shadows, and the influence of slopes in runoffs, important in mountainous terrain. Once these are addressed, subgrid orography could play an important role in projections at a basin level.

Rainfall Trend Analysis

A trend analysis can provide a basis to ascertain the sign and magnitude (including confidence intervals) of a trend. Trend analyses were conducted at national and basin levels. For presentation purposes, ten sites were selected at the national level.

Regional trend analyses were conducted in the selected river basins. As an example of the results produced, Figure 3.11 shows the Mantaro River Basin as well as the location of meteorological stations upon which the analysis is based. A statistical analysis was conducted for each weather station in the basin (38 climate stations in the case of the Mantaro River Basin).[11] Precipitation trends for each station were plotted (Figure 3.11) to analyze their geographical consistency. The analysis resulted in the identification of six zones (Table 3.1 and Figure 3.11) where the data from the climate stations exhibit similar trends in precipitation.

Table 3.1 shows the observed annual precipitation trends in the Mantaro River Basin for the reference period (1979–2000). A positive precipitation trend was identified in the southern valley region (Zone III). In contrast, for the northern valley region (Zone I) and the eastern region (Zone VI), the trends indicate no, or hardly any, changes in annual precipitation. The remaining identified regions exhibit a decreasing trend, particularly significant in the high mountains surrounding the northern valley where substantial reductions in precipitation are anticipated. These results highlight the limitations of GCMs. Only high-resolution models have the possibility of reproducing the variability found in nature.

Figure 3.11. Trend analysis: Regionalization of observed trends in the Mantaro Basin
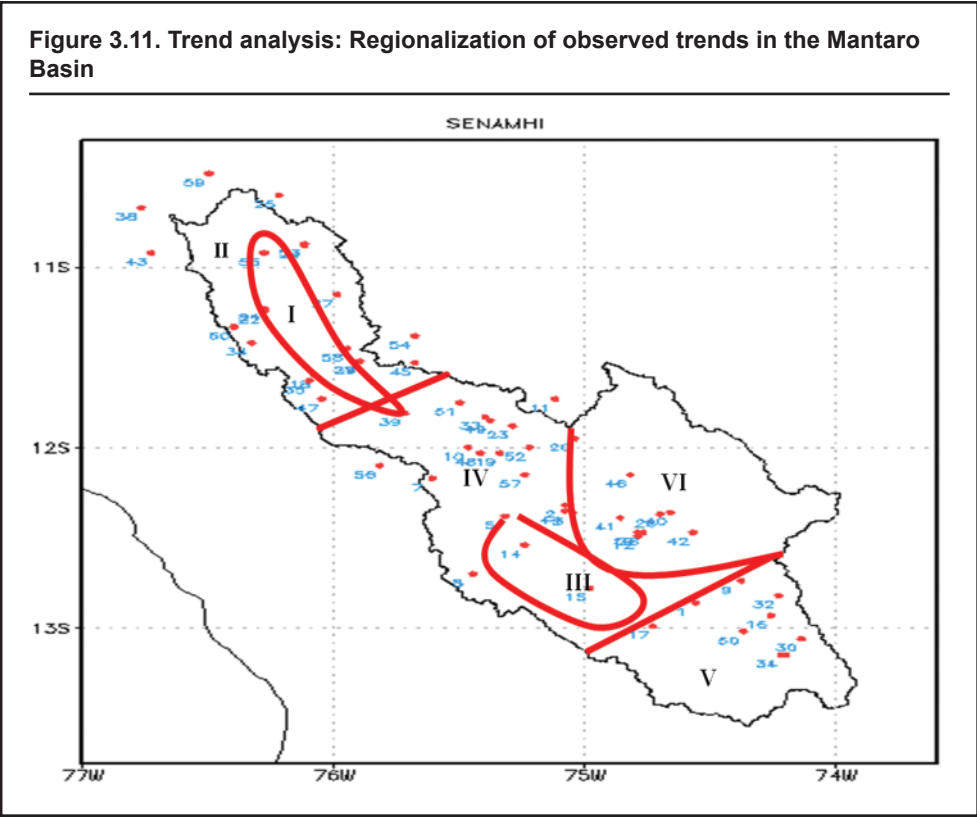
Source: Authors.
Note: This figure shows the distribution of the stations in the Mantaro Basin.

Table 3.1. Observed annual precipitation trends in the Mantaro River Basin (mm/period)

Zone	Location	Annual	DJF	MAM	JJA	SON
I	Northern Valley	0	0	0	0	0
II	North	-11	-6	-2	-1	-2
III	Southern Valley	7	3	1	1	2
IV	Central	-4	-2	-2	1	-1
V	South	-3	-1.5	-1.5	0	0
VI	East	-1	-1	0	0	0

Source: Authors.

These identified trends were used to make linear projections of future precipitation. The projections are summarized in Figure 3.12. The figure facilitates the identification of areas with similar behavior. Trend analysis only makes reference to the key trends, that is, to changes in the mean value with time.[12]

While trend analysis does not represent a modeling technique, it uses current climate as a basis for projections. The analysis requires adequate weather records for a period of 20 years or more and only addresses potential changes in mean values. It also

Figure 3.12. Average precipitation (mm/year) in the Mantaro River Basin for a) observed (1990–1999) and b) projected (2030–2039) time periods
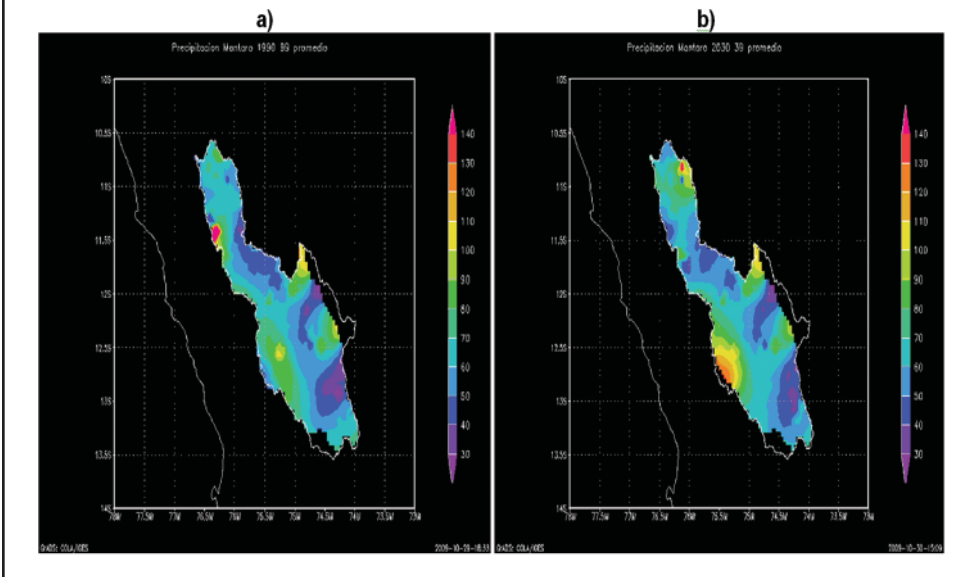
Source: Figure generated for this study by SENAMHI.

assumes that past linear trends will not change in the near future. On the other hand, the use of current trends may be misleading if emerging and substantially different trends are in play in the immediate future.

Limitations in Climate Projections

Although GCM models are powerful for representing global processes, they do not have the detailed resolution required for water resources planning at the basin level. The output of GCMs should be understood as the average climate condition found in the cell, which might encompass large areas that are thought to be homogeneous. This hypothesis is not valid in mountainous terrain. Interpretation of the models' results is therefore difficult. When using results from GCMs, the following general limitations should be considered:

■ **Model uncertainty**. Global oceanographic and atmospheric dynamic circulation models are representations, based on our scientific understanding, of very complex phenomena that span many levels of resolution. By definition, models are simplifications based on our present understanding. As more research becomes available and observations provide new insights into the many physical and chemical processes in the ocean and the atmosphere, models are expected to improve. The models used have considerable uncertainty, as indicated by the dissimilar estimates they offer of future climates.

■ **Emissions paths**. Future greenhouse gas emissions depend on economic activity and political decisions, both subject to great fluctuations and uncertainty. Nonetheless, for the next two to three decades such decisions are not expected to produce major deviations in climate response.

■ **Model resolution**. For hydrological application in complex terrain, as is the case in Peru, data input to hydrological models is needed at very detailed resolution. Such resolution is only available in one model among the 16 used in the Fourth Assessment Report, with the additional drawback that it has a limited number of independent simulations of future climate scenarios for sensitivity analysis. Most GCMs are run at resolutions of several hundreds of kilometers (parcel units are several hundreds of kilometers by side), which imply considerable theoretical and methodological difficulties.

■ **Model independence**. The use of model ensembles has become a common practice to assess future climate results. The underlying hypothesis is that the average of independent outcomes provides better mean estimates than single model experiments. Recent research suggests that this hypothesis is difficult to prove because models are not independent. They share similar routines; frequently one is the basis of improved versions—although they remain on the list of available models—and sharing of information and research among model developers prevents the use of the independent hypothesis. Some authors have proposed weighing the likelihood of model results based on a model's agreement with observation.

■ **Inability to accommodate the complex atmospheric process in mountain terrains**. A well-known limitation of GCMs is their inability to capture the many local atmospheric processes present in mountain landscapes. Several procedures have been developed to cope with these limitations, but they lack scientific and observational footing.

Hydrological trend analysis is a complementary approach that is based on observational data. However, data availability is a limitation. It would be desirable to analyze good-quality weather observation spanning 20 to 30 years. However, this record length is often not available. Even if such information is available, the basic hypothesis is that the identified trends are linear and will continue independent of the emission path. As a result, trend analysis can provide results by which to judge the accuracy of GCMs in simulating local conditions, as is done in this study. Thus, the selective use of those GCMs that reproduce (simulate) the observed trends should have more weight in the construction of future climate scenarios, as suggested in another recent World Bank analytical study (Vergara and Scholz 2011).

Criteria for Building Climate Scenarios

Choosing the Criteria

Two aspects should be considered in the selection of an approach for the generation of future climate scenarios:

1. Criteria need to be developed based on the purpose and potential use of the climate scenario.[13] This means that the scenario has to include those key variables relevant to the project. Often it is not enough that the projection shows only changes in mean values. Estimating changes in variability is equally important. Furthermore, demonstrating changes in short-duration events is sometimes more relevant than annual values. This is the case in small river basin applications, for example. At the same time, precipitation events of a few hours are especially important at the local level and should receive attention. In these cases,

evaporation and transpiration are climate variables with little influence on the final outcome. On the other hand, the impact of climate change on evaporation, transpiration, temperature and wind speeds are key factors for agricultural planning.

2. In addition, the modeling should use the observed climate data as a reference point, against which the capacity of the selected tool should be tested. The closer the model is able to simulate observed real climate conditions, the better its ability to simulate the future is expected to be.[14]

Since the emphasis of this study is on water resources planning, the following climate parameters are considered: the distribution of precipitation throughout a year (on a decadal, monthly or seasonal resolution), and the trends for precipitation in the next few decades (increasing, decreasing or neutral).[15] Other climate variables of interest, such as temperature, evaporation and transpiration, net radiation, relative humidity, wind speed, etc., are thought to be of secondary importance.

The criteria to assess the applicability of different methods for building climate scenarios used in this study are summarized below:

■ Rainfall regime, i.e., distribution of wet and dry seasons throughout the year. This criterion seeks to capture the ability to closely simulate (reproduce) the yearly distribution of precipitation (monthly basis) in selected areas of interest.

■ Annual direction and magnitude of the expected change in precipitation. This criterion assesses the skill[16] of the simulations to reproduce the precipitation (and temperature) trends exhibited by the observed data, on a yearly basis.

■ Model's capacity to reproduce seasonal trends for the climate variables of interest.

The indicators to assess the skill of different methods to build climate scenarios are presented in Table 3.2.

Testing the Criteria

The criteria were applied on a semi-random sample of 10 areas.[17] The sample was taken from the existing reference climate station in the country. Each of the 10 areas had an existing observed climate database of the past that included: (i) the monthly (mean) distribution of precipitation; (ii) the expected mean annual precipitation trend; and (ii) the monthly and seasonal trend exhibited in the rainfall data.

Table 3.2. Indicators used to assess the skill of different methods for building future climate scenarios

Criteria	Indicators
a) Annual distribution of precipitation, based on hietograms (diagram of mean monthly precipitation)	a.1) Location of "driest" and "wettest" months; a.2) Number of months with precipitation above average monthly precipitations (annual precipitation divided by 12); a.3) Distance (in months) between "driest" and "wettest" months.
b) Annual trend for key climate variables (precipitation in this case study) as estimated for a reference period. Only statistically significant values are used.	b.1) Agreement in sign (positive, negative or no trend); b.2) Agreement in sign and magnitude (low, medium and high).
c) Trends for hydrological seasons of interest (DJF and JJA) for climate variables of interest, estimated for a reference period. Only statistically significant values are used.	b.1) Agreement in trend (positive, negative or no trend); b.2) Agreement with sign and magnitude of observed trends (low, medium and high).

Source: Authors.

Some of the stations had collected climate data from a long period of time. Long records, spanning 50 years and more, were analyzed. Data from years 1979–2000 were chosen as the reference period. The underlying assumptions were that this period captures well the forcing of global climate change in precipitation, and that this trend is likely to continue in the foreseeable future or planning horizon.

Figure 3.13 shows the monthly distribution of observed precipitation in the selected sample sites. This figure highlights the large range of climates in Peru: from very rainy ecosystems, with average precipitation above 3,000 millimeters per year in San Roque,

Figure 3.13. Historical (1979–2000) monthly distribution of observed precipitation (mm/year) in reference stations used to describe precipitation regime in Peru
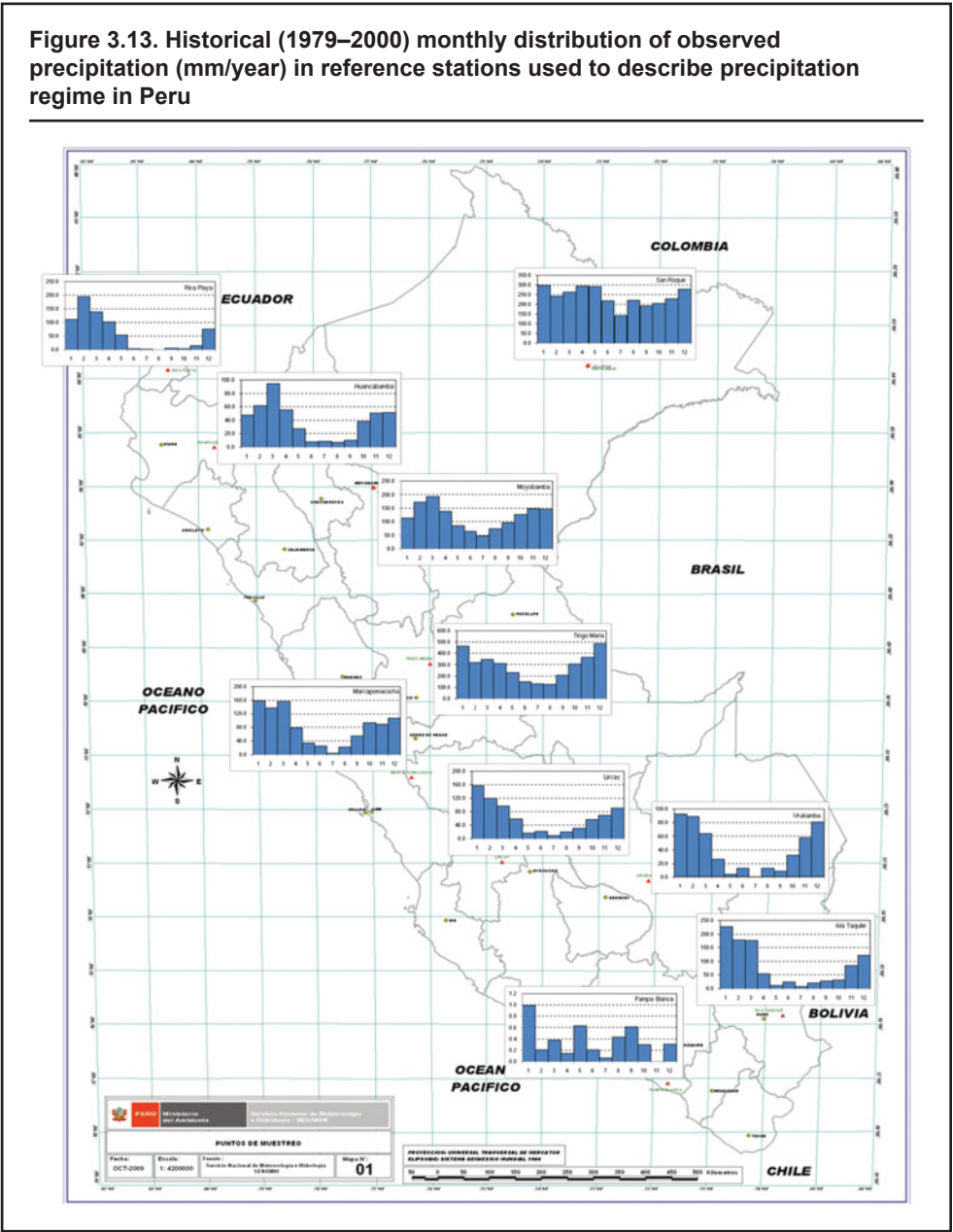
Source: Authors, based on SENAMHI's data.

to less than 100 millimeters per year in Pampa Blanca. Figure 3.14 shows the expected change in total annual precipitation (percentage) by 2030 to the reference period. It is a summary presentation of the observed trends combined with the use and analysis of a small ensemble of downscaled GCMs.

Figure 3.14. Projected percentage change in annual precipitation by 2030 using an ensemble of GCMs
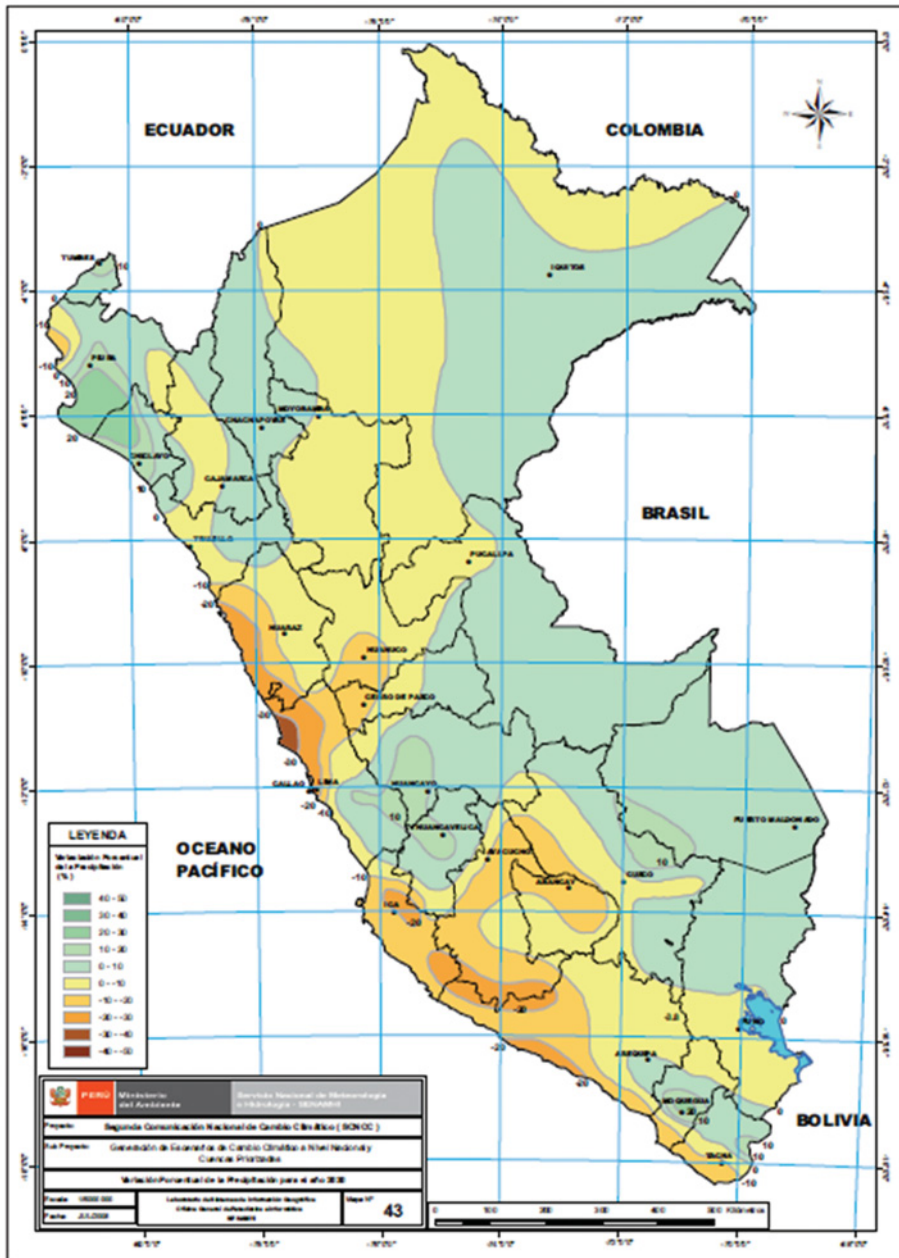
Source: SENAMHI 2009b.

Table 3.3 summarizes the trends[18] found in the observed record and compares them with model runs from the Earth Simulator and CCSM. The criteria used here show that such skill measurements are feasible, simple, and relevant to the application sought. Other possible uses of the climate scenarios might require a different set of criteria and indicators.[19] The table shows the results of the trend calculations for three sets of data. The first three columns present the statistics calculated from actual measurements at the selected weather stations. The wet season (see Figure 3.13) lasts from December to February and the dry season from June to August.

The trend in rainfall for the wet and the dry season are presented, as well as the value of the annual trend. Six sites show a positive annual trend (increasing precipitation with time) and the remaining four a negative trend. Table 3.3 also presents the trend statistics from the data generated by the MRI-AGCM3.1 and for the downscaled CCSM. Calculated trends from GCM simulations display great disparity when compared with observed trends. The lower three rows of Table 3.3 summarize the trends in direction magnitude.

Table 3.4 compares the three methods based on the criteria previously described. The "skill" measures how close the projections are to the observations. Note that the selected indicators do not apply to the ensemble of GCMs. This approach seeks to identify the possible range of future climate scenarios while the suggested methodology aims at selecting the approach that better simulates past climate.

Table 3.3. Statistically significant observed and estimated precipitation trends for 1979–2008

Station	Observed Change in precipitation (mm/year)			Earth Simulator (mm/year)			CCSM downscaled (mm/year)		
	DJF	JJA	Annual	DJF	JJA	Annual	DJF	JJA	Annual
RICA PLAYA	9.3	0	12.8	-5.7	-3.1	-22.5	16.2	0	23.8
SAN ROQUE	-4.5	-5.3	-12.2	-0.9	-2.4	-7.9	5.7	-0.8	15.1
HUANCABAMBA	1.3	0.7	3.8	8.5	-3.1	4.4	9.1	0.9	20.1
MOYOBAMBA	5.5	1.4	16.5	-2.0	0.3	-1.9	9.7	0.6	19.6
TINGO MARIA	-5.0	0.0	-18.1	-4.1	1.0	-3.2	-6.0	0.0	-4.1
MARCAPOMACOCHA	-13.6	0.3	-23.9	-2.0	-1.9	-8.9	-0.5	-0.6	-0.9
LIRCAY	2.4	-0.7	-2.0	0.2	-1.1	2.0	-1.2	-0.5	-3.7
URUBAMBA	8.0	1.0	14.0				-3.5	-2.9	-23.1
ISLA TAQUILE	-14.3	-1.9	-35.3	-2.0	0.1	-1.6	3.9	0.0	11.4
PAMPA BLANCA	-0.1	-0.1	-22.0	-0.1	0.0	-0.2	4.3	0.0	12.1
Number of positive or negative trends (trend indicators)*									
Positive trend — Large	3		3	1			4		6
Positive trend — Medium	2	2	1		1	1	2		
Positive trend — Small		4		1	3	1		6	
Negative trend — Small	1	2	1	2		3	1	3	1
Negative trend — Medium	1	1		4	5	3	2	1	2
Negative trend — Large	3	1	5	1		1	1		1
Total Positive	5	4	4	2	4	2	6	6	6
Total Negative	5	4	6	7	5	7	4	4	4

Source: Authors.
Note: * Definition of Small, Medium and Large for annual values correspond to the following ranges (1–3, 3–10, >10). For monthly/seasonal estimates the ranges are: 0–1, 1–5, >5, respectively.

Table 3.4. Assessment of skills: Application of criteria to alternatives for building future climate scenarios

Method	Annual precipitation distribution	Precipitation annual trend		Seasonal precipitation trends			
		Sign	Magnitude & sign	Sign		Magnitude & sign	
				DJF	JJA	DJF	JJA
Observations Descriptive statistics obtained from reliable weather stations operated by SENAMHI	Wet months fall between Dec. and April; dry months in April through August.; distances ranging 3 to 8 months. Numbers of months with above average precipitation range of 4 to 7.	4 positive 6 negative	+ L 3 + M 1 + S 0 - S 1 - M 0 - L 5 Concentration of trends in large trends	5 pos 5 neg	4 pos 4 neg	+ L 3 + M 2 + S 0 - S 1 - M 1 - L 3	+ L 0 + M 2 + S 4 - S 2 - M 1 - L 1
Single GCM MRI-AGCM3.1 with 20-km resolution	Similar ranges for the selected indicators: Skill below 30%	2 positive 7 negative *Indicates bias toward reduced precipitation.* Skill 67%	Skill below 35% Magnitude concentrated between S and M	Bias toward negative values. Skill 56%		For DJF concentration on negative M and S. For JJA negative M predominates. Combined skill 35%	
Downscaled input CCSM output downscaled with *Subgrid Orography Dynamic* routine	Reduced range for the selected indicators; wet months concentrated in Dec, dry months in July. Skill 35%	6 positive 4 negative Skill 60%	70% of trends grouped as L(Large) Skill 50%	Skill 75% No bias identified		Results for seasonal precipitation trends very good. Skill 80% for DJF and 70% for JJA	
GCM ensemble analysis	Not applicable: the basic premise of this approach is the identification of a wide range of possible future scenarios independent of their skill to simulate present climate						
Trend analysis Use of existing observations to assess future mean climate conditions	Not applicable: Uses precipitation observations (and their distribution) to project future average climate conditions.	Not applicable: Observed trends are used to project future mean climate conditions. The key assumption is that recent past trends are likely to continue with the same magnitude and sign. The trend analysis needs to be seen as an alternative tool that uses current climate as a basis for projections in the absence or as a complement of alternative tools.					

Source: Authors.

The analysis of Table 3.4 provides interesting insights. For this specific application it is possible to calculate an overall measure of skill to reproduce the key climate variables of interest. Under the assumption of equal weights for each criterion (and equal weight among indicators), the use of the single GCM provides a measure of skill of 42 percent and the downscaled approach 55 percent. Next, it is important to ask if such skill level is acceptable or if other approaches should be considered, such as the use of trend analysis directly or further exploration of alternative downscaling routines.

Figures 3.15, 3.16 and 3.17 provide a graphic representation of the results from the use of dynamic downscaling techniques, high-resolution GCM simulated by the Earth Simulator, and the historical record. A simplified comparison of the results for one site is provided in Figure 3.17.

Figure 3.15. Monthly precipitation (mm) and anomaly (%) as modeled by subgrid orography for 2050s
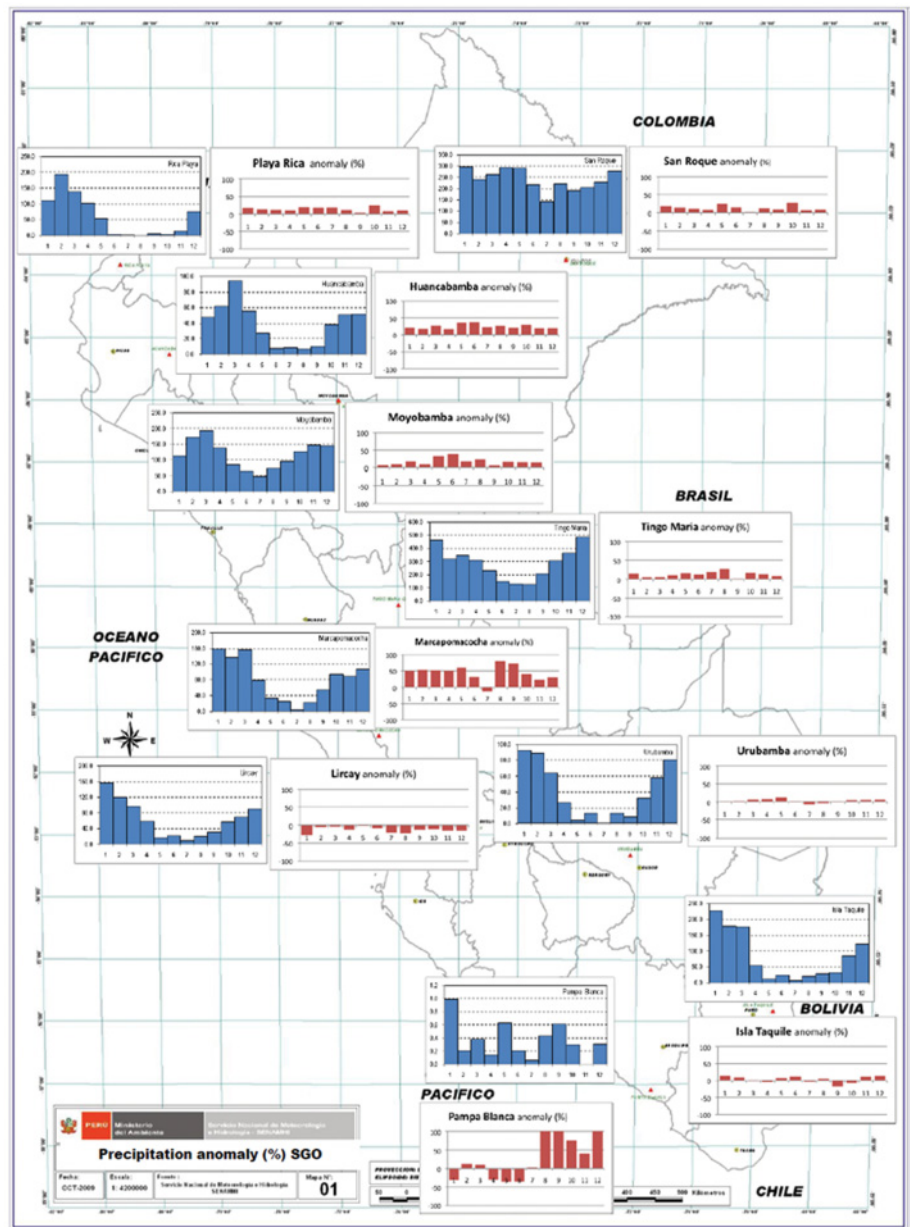
Source: Authors, based on SENAMHI data.

Figure 3.16. Monthly precipitation (mm) and anomaly (%) as modeled by MRI-AGCM3.1 (with Earth Simulator) for 2030s
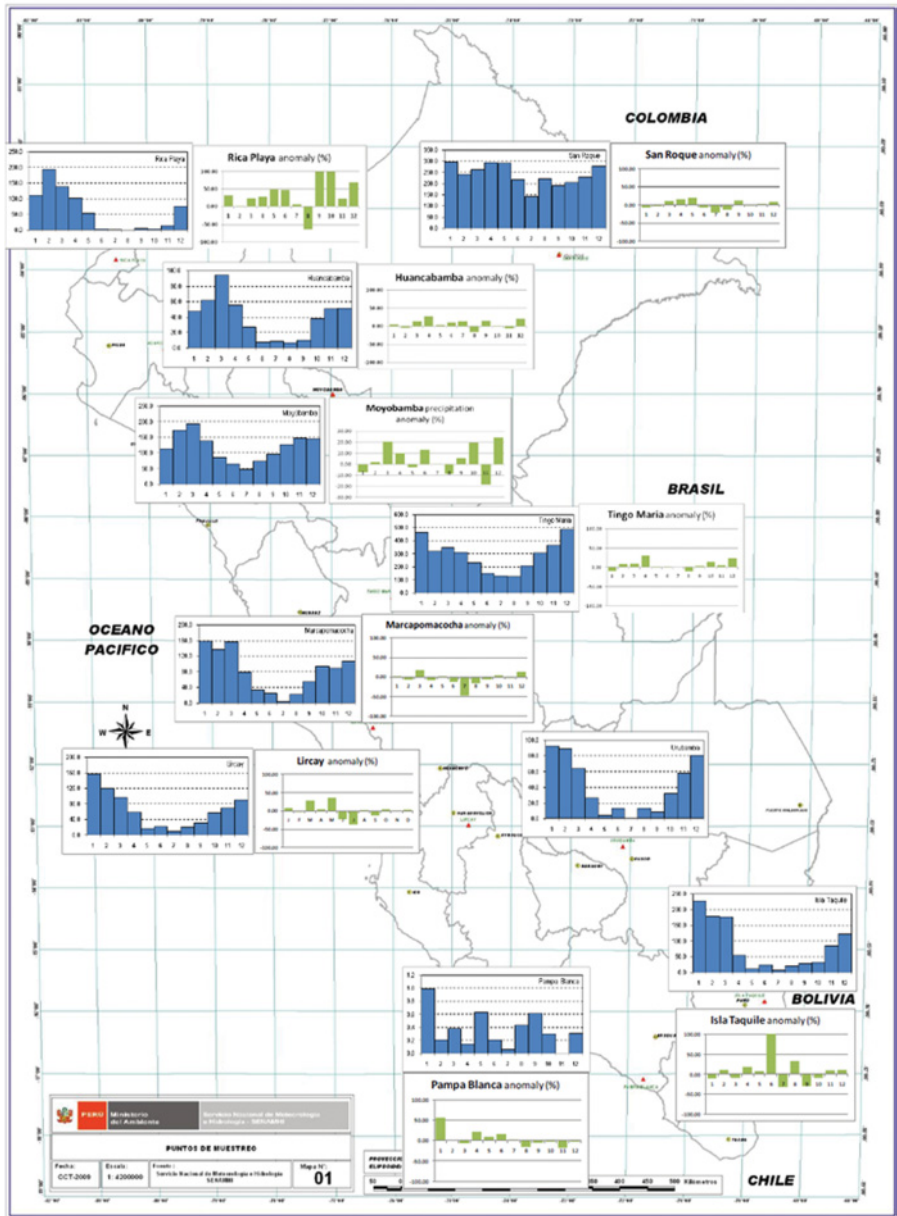
Source: Authors, based on SENAMHI data.

Figure 3.17. Monthly precipitation (mm) and anomaly (%) as modeled by trend analysis for 2050s
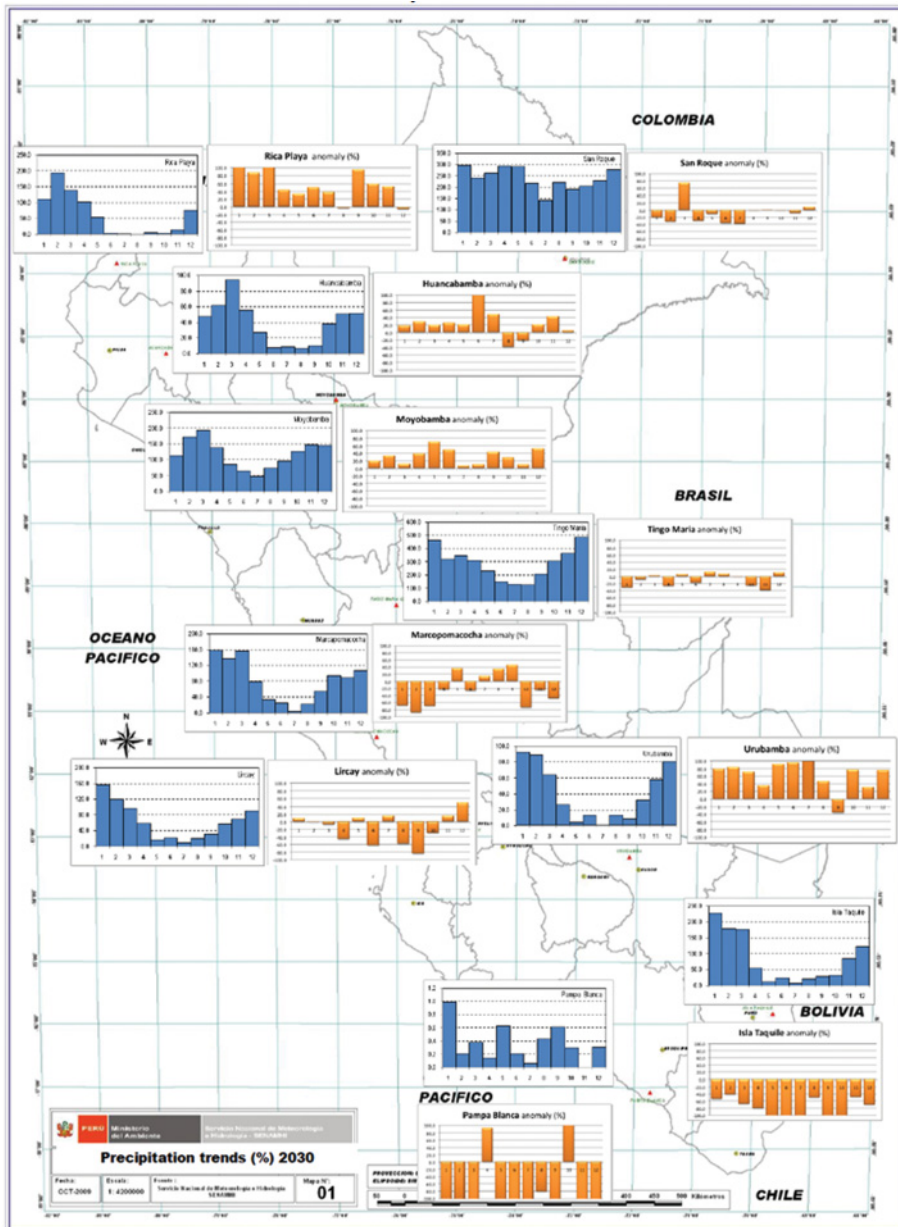
Source: Authors, based on SENAMHI data.

Figure 3.18. Comparative results analysis: Graphs indicate precipitation (observed) and anomaly estimated through different methods
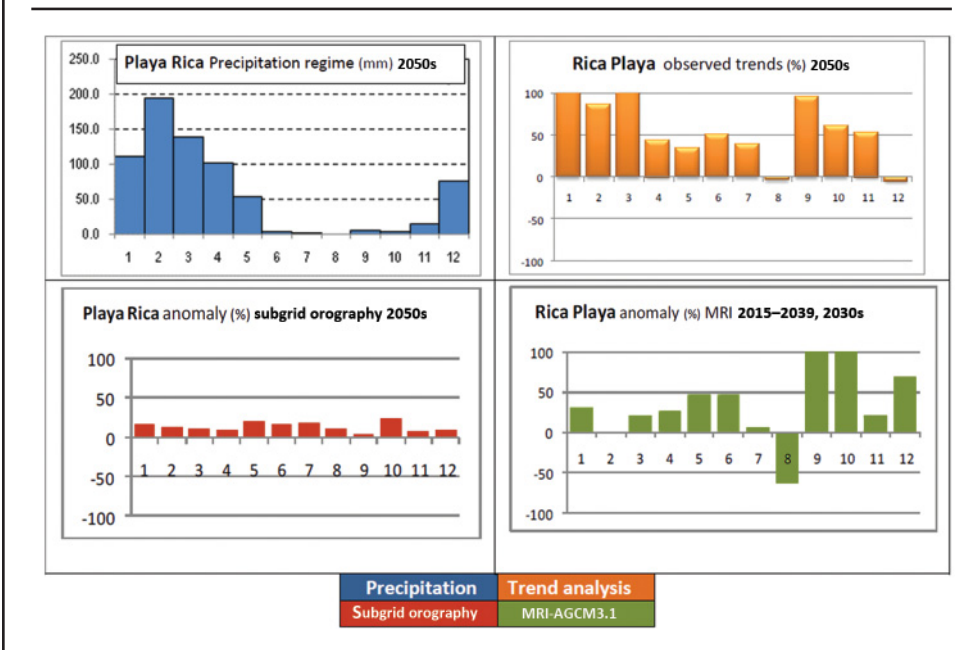
Source: Authors.
Note: More results are presented in the appendixes.

Figure 3.18 provides the results for the weather station at Rica Playa. The same representation is provided for all 10 sample sites in the appendixes.

In conclusion:

■ Four alternatives for climate scenario building are analyzed and compared through the use of criteria and indicators.

■ The analysis confirmed that the output from GCMs and dynamic downscaling require bias correction routines. Since many simple and effective bias correction methods are available, this does not represent a serious limitation to the use of GCM and/or RCM results.

■ Trends are not uniform in the area under study. Capturing this non-uniformity should be part of the criteria of selecting alternatives to define climate scenarios in mountainous regions.

■ The GCM (or RCM) ensemble method is an approach based on the objective of minimizing the maximum loss expected. The methodology proposed here does not provide elements to judge the effectiveness of this popular approach.

■ Trend analysis is a mathematical (statistical) procedure that gives great weight to existing information and assumes that observed trends are likely to continue in the future. However, future climate depends on numerous issues, such as economic and demographic growth as well as international climate policy. Still, for the relatively close future (next 20 to 30 years), trend analysis provides an estimate of potential climate change.

The following guidance can also be concluded on the basis of the results of the analysis of the ten stations:

- Avoid using approaches that do not use the past as a departure point for future climate (avoid the use of ensemble methods).
- Verify which GCM model or RCM approach is the best for local conditions (at basin or sub-basin resolution) by reviewing the skills of the most relevant indicators. If the application has a time horizon of a few decades (30 to 40 years), and reliable climate information is available, it is recommended that trend analysis be used to define a lower bound scenario.

Variability

The approach indicated by Tables 3.3 and 3.4 does not incorporate possible changes in the climate variables.[20] However, there is mounting evidence that extreme events are becoming more frequent: hurricanes are intensifying and severe storms are becoming common. The results of climate modeling through GCMs and the downscaled data show that variability (measured by the standard deviation) is expected to increase in the future (see appendixes for more information). Observed data from climate stations do not provide enough information to ascertain with confidence the direction and magnitude of the change in the variability of climate variables. For water resources planning, such future variability should be subject to sensibility analysis in order to study the possible responses to higher flow fluctuations.

Notes

1. Fusing of weighted ensembles was not applied because it became available only when the study was nearly completed (see Vergara and Scholz 2011).
2. AR4 of the IPCC uses a dataset of 24 global coupled atmosphere-ocean general circulation models (AOGCM, or GCM for short) to project future climate under various scenarios. The use of numerous models is intended to reduce errors and uncertainty. However, most of these models have a very coarse resolution (100 to 400 km); this has an undesirable impact on results, particularly as it relates to extreme weather events. This is because global warming would result not only in changes in mean climate conditions but also in increases in the amplitude and frequency of extreme events that would not be captured in a meaningful way with coarse resolutions. Changes in extremes are more important for assessing strategies for adaptation to climate changes.
3. The 16 models were chosen from a set of 25 models available through the World Climate Research Program (WCRP) Coupled Model Intercomparison Project (CMIP) Multi-Model Data Project. The criteria to select the models were: 1) availability of monthly mean atmosphere data available for both climate scenarios A1B and B1, and 2) the most updated version of a particular model (we chose GFDL-CM2.1 instead of GFDL-CM2.0), available at: http://www-pcmdi.llnl.gov/ipcc/data_status_tables.htm.
4. The atmospheric GCM is a global hydrostatic atmospheric general circulation model developed by MRI/JMA. This model is based on an operational short-term numerical weather prediction model of JMA and is part of the next-generation climate models for long-term climate simulation at MRI.
5. The data generated by the Earth Simulator were made available under the five-year Memorandum of Understanding between the MRI and the World Bank.
6. When initially developed, the A1B scenario was thought to be a description of the middle range of greenhouse gas emissions scenarios. Today's emissions trajectory is already well above the A1B scenario. Therefore, this scenario may no longer represent a plausible future.
7. Soil Wetness Index (SWI) represents the hydric stress of the vegetation. SWI ≤ 0 means evapotranspiration is zero (dry soils); at SWI ≥ 1, the vegetation evapotranspirates at the potential (maximal) rate (wet soils). The definition of SWI is:

$$SWI = \frac{(W_p - W_{wilt})}{(W_{fc} - W_{wilt})}$$

where: W_p is the total soil water content—liquid (water) and frozen (ice); W_{wilt} is the soil water content at wilting point; and, W_{fc} is the soil water content at field capacity.

8. Under the World Climate Research Programme (WCRP), the Working Group on Coupled Modelling (WGCM) established the Coupled Model Intercomparison Project (CMIP) as a standard experimental protocol for studying the output of coupled atmosphere-ocean general circulation models (AOGCMs). The CMIP provides diagnosis, validation, intercomparison, documentation, and data access. Virtually the entire international climate modeling community has participated in this project since its inception in 1995. The Program for Climate Model Diagnosis and Intercomparison (PCMDI) archives much of the CMIP data and provides other support for the CMIP. The 16 models are bcm2, cccma cgcm3, cnrm cm3, csiro mk3 0, gfdl cm2 1, giss aom, Iap fgoals1 0 g, inmcm3 0, ipsl cm4, miroc3 2 hires, miub echo g, mpi echam5, mri cgcm2 3 2a, ncar ccsm3 0, ncar pcm1, ukmo hadcm3. http://cmip-pcmdi.llnl.gov/

9. This approach has limitations, as described by Stone and Knutti (2010):

   (a) **All climate projections are necessarily uncertain** (Knutti et al. 2002). The largest contribution to this uncertainty is the limited understanding of many of the interactions and feedbacks in climate change. The ensemble hypothesis comes from the observation that combined information from many models performs better than a single model (for example: Yun et al. 2002; Thomson et al. 2006).

   (b) **The GCMs are interdependent**: many models are based on the same theoretical and sometimes empirical assumptions; all models have similar resolutions (too coarse to solve small-scale processes); model development is not independent: models are frequently compared and successful concepts are copied.

10. The sample was taken from a set of 141 geographical locations where SENAMHI operates weather stations classified as having reliable data. Ten points covering the entire country were selected.

11. The analysis, on a monthly basis, only used data for the reference period. Data collected prior to 1979 were not used under the hypothesis that global warming drivers have been noticeable only during the last two decades of the twentieth century.

12. This is a serious limitation, because variability (measured by the standard deviation) has not been projected. Thus, the analysis presented needs to be complemented in order to include hypotheses on the expected trends in the other relevant statistics. The results of the downscaling exercise described in Appendix 3 were used to assess the changes in variability. The analysis indicates that climate variables exhibit increased variability with time. The increase in variability also remained very similar among ten random sampling points when measured as percent increase over the variability of the 1990–1999 period. The project adopted these increases as a reasonable basis to assess the expected trends in variability as global warming continues for near-term projections (the next 20 to 30 years). From a statistical standpoint, the key statistics have been analyzed and projection-type methodologies have been used. Many uncertainties remain, among others those associated with the many, albeit reasonable, hypotheses made. A linear trend for the mean is assumed; variability is thought to follow the variability increases exhibited in GCM results; and temporal and spatial covariance is assumed to be time invariant. Although it is not possible to assess the uncertainty associated with the climate scenarios developed, it is clear that they represent good approximations for likely future climates. It is therefore suggested that the climate scenarios built through the approach developed here be called "climate planning scenarios," indicating that they closely resemble climate projections but retain enough uncertainty as to be called "scenarios." The use of these planning scenarios should be accompanied by thorough sensibility analyses to reduce the inherent uncertainties, and the need to search for water resources solutions that are resilient over a range of plausible "climate planning scenarios" to be used as inputs to the hydrological model.

13. The criteria need to be developed unless a third party has defined future climate scenarios applicable to the area of interest that already incorporates the best available information, validation of results and good practices. In some countries the governments have adopted official climate scenarios, based on the scientific work to produce the National Communications to the UNFCCC.

14. Note that the use of GCM results simultaneously provides estimates of expected changes in the mean and in the variability of climate variables. On the other hand, the use of data from meteorological stations to conduct trend analysis does not provide reliable estimates of expected changes in the variability of climate variables.

15. Trends normally refer to mean values, such as the expected increase or reduction in the climate variable of interest per year.

16. Skill is evaluated by testing how well the model can generate results that match the observations of each of the selected criterion.

17. Peru has 141 weather stations with long and reliable records, as reported by SENAMHI. The selected points were to provide a reasonable coverage of the entire country and coincide with a reliable weather station. In this way the results from each possible approach could be compared with existing information from reliable observations.

18. Only statistically significant trends (95 percent confidence level) are reported.

19. Note that the used criteria and results relate only to mean values (central tendency).

20. In statistical terms the analysis refers only to key trends; measures of dispersion and higher moments are excluded.

Hydrology Analysis

Before the outputs from the climate analysis could be fed into the hydrological model, this model had to be adapted to handle the specific conditions of the region. This chapter discusses the development of glacier and páramo modules to complement an existing and flexible water resources management tool aimed at integrating climate impacts in the hydrological response in mountainous regions. The glacier module allows the model to reflect the dynamic behavior of glaciers and estimate their net contribution to runoff. The páramo module does the same with high mountain wetlands. The Water Evaluation and Planning (WEAP) model was selected for its flexibility to integrate the addition of glacier and páramo modules.

After the initial development of these modules, a calibration and verification analysis was needed to assess the applicability of the complemented WEAP model. The calibration was done using historical climate data and observed runoffs at key points.

WEAP Model

The WEAP modeling software, developed by the Stockholm Environment Institute, was used as a basis for building the hydrology component. It is a generic, object-oriented water resources modeling system that includes options to simulate both the natural rainfall runoff processes and the management of installed water infrastructure. It was selected for this analysis based on a comparison exercise among hydrological tools for water resources management that was conducted for a Bank-financed project called the Regional Adaptation to Glacier Retreat Project (PRAA). The comparison concluded that the WEAP's water management component was an important characteristic, as was the model's adaptability to different basin configurations and to the flexibility in data requirements. The WEAP model was deemed suitable for use in the Andean countries where data availability represents a major barrier. To enhance the modeling system's appropriateness to the Andean region, glacier and páramo modules were developed and added to this model.

Development of a Glacier Module

A comparative analysis of different modeling approaches to glacier behavior was conducted as a starting point in the development of the glacier module. Multiple approaches are available to represent tropical glaciers and high-elevation wetlands, including statistical models, conceptual models, quasi-physical models and process-based models. A number of factors were considered in selecting the glacier dynamic representation; these included simplicity, correspondence with published information, the demand for data, and data availability in the basins under study. Appendix 4 (Technical Report on

glacier and high-elevation wetland model selection and parameterization) presents in detail several options for glacier modeling, as summarized in Table 4.1 below.

As indicated in the table, data availability was ultimately a limiting factor for models because only one of them could model all three basins. As a result, the simple degree-day model was selected and its application was adjusted to each of several elevation bands describing the glaciers.[1]

Table 4.1. Principal selection criteria for glacier modeling

Characteristics	Energy balance	Degree-day, index	Hybrid (balance+degree day)
Short description	Model based on the study of the exchange of energy between the surface glacier and the atmosphere	Energy balance which considers that all the physical processes are summarized in the temperature (the T° is a consequence and not a cause)	Similar to the degree-day, but to improve its efficiency it uses the albedo, radiation, etc. These variables are added one by one.
Complexity	High	Simple	Intermediate
Represents physical processes	Yes	No	Partially
Efficiency of the model	High	Intermediate – high	Intermediate – high
Number of parameters	6 to 9	2 or 3	2 to 5
Input variables for the entire model	More than 6: • Incident radiation • Diffuse radiation • Liquid and solid precipitation • Humidity • Long-wave radiation (incident and reflected) • Short-wave radiation (incident and reflected), etc.	• Precipitation • Evaporation • Temperature	Depending on the complexity: • Precipitation • Evaporation • Temperature • Albedo • Radiation
Level of specialization	Complex (generally grid)	Global or semi-distributed	Semi-distributed, global or grid
Advantages	Its efficiency: physical process representation	Few parameters Few input variables	Few parameters Few input variables
Disadvantages	Needs too much information (sometimes nonexistent)	Does not explain physical processes	Partially explains the physical processes
Possible application	Probably Santa	Santa, Rímac, Mantaro	Santa
Recommended bibliography	Hock 2005 Favier 2004 Juen 2006	Hock 2005 Schaefli et al. 2005 Martinec and Rango 1986	Hock 2005 Klok et al. 2001 Lang 1990 Zhang et al. 2007

Source: Table generated for the report by IRD, 2009.

The modeling of glacier dynamics follows the standard approach in WEAP, which involves simulating rainfall-runoff processes after first dividing a basin into sub-basins. These basins are each upstream from a "pour point," which is a point where streamflow is measured or where the river is actively managed. Next, the sub-basin area above a "pour point" is divided into *i* elevation bands. Each sub-basin/elevation band is defined as a unique WEAP catchment object, which represents an area with similar hydrological

behavior. Within each catchment object, temporally variable land cover and climate conditions can be added on a time-step by time-step basis. Each elevation band, i, is divided into either a glaciated (j=1) or nonglaciated (j=2) portion. In Figure 4.1 below, the blue portion represents the glacier, while the green area represents the subwatershed. Catchment object elevation bands are divided by the red lines.

Once the areas are split, runoff from the evolving glaciers and rainfall was assessed and added. The calculations were made on two timescales: a monthly time step, t, and an annual time step, T. The procedure to assess runoff is summarized as follows:

- *Step 0 – Initial Conditions:* The initial step is to define the base hydrological conditions within each sub-basin. Satellite data were used to determine the initial allocation of glaciated versus nonglaciated land. This area within each catchment is represented by A_i and is defined in units of km^2. Based on a published empirical relationship, the glacier ice volume (V) is estimated in km^3 (Bahr et al. 1997).
- *Step 1 – Estimated Runoff from Melting Snow and Ice:* The contribution to surface runoff from the glaciated portion of the catchment area is extrapolated from estimates of melting glacial snow and ice. This is done for each month, t, within a hydrological year, T.
- *Step 2 – Surface Runoff at the Sub-basin Level:* The volume of surface runoff within a sub-basin is calculated for each monthly time step as the sum of the contribution of a) melting snow and ice for the glaciated portion of the sub-basin, and b) the runoff coming from the simulation of rainfall-runoff processes in nonglaciated portions of the sub-basin.

Figure 4.1. Illustration of sub-basins and elevation bands
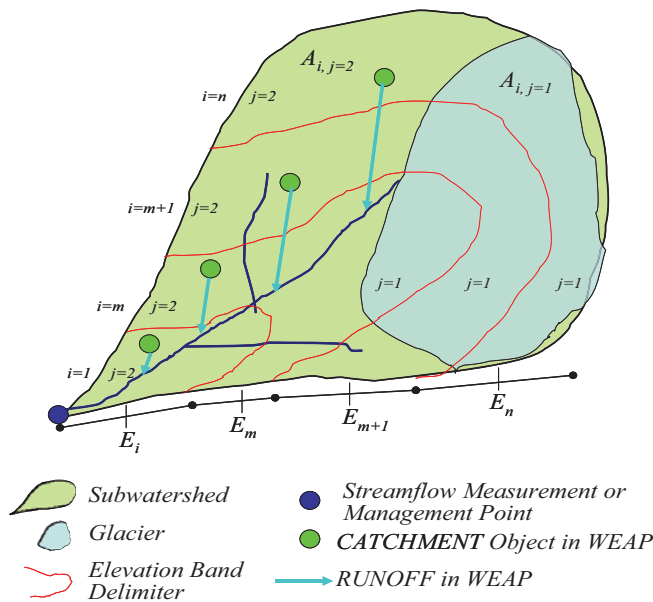
Source: Figure generated for the report by IRD, 2009.

- ■ *Step 3 – Annual Mass Balance:* A mass balance is used to assess changes in the area covered by glaciers within a sub-basin at the end of the 12 monthly time steps of a hydrological year.
- ■ *Step 4 – Annual Glacier Geometry Evolution:* The overall volume and extent of the glacial ice within a sub-basin are calculated prior to moving on to the subsequent hydrological year.
- ■ *Step 5 – Calibration:* The key criterion for calibration is the adjustment of parameters. This is needed to obtain a good fit with the surface area of the glaciers and the measured streamflow at selected pour points where gauging stations are available.

The glacier module was tested using available data on the evolution of glaciated areas over time (as estimated from satellite images) and the observed streamflows at key gauging stations below glaciers. The algorithm, which describes snow and ice accumulation and melt along with glacier area and volume evolution, was implemented using the WEAP software's user-defined variable functionality. This process is described in the calibration-verification section of the next chapter. Details about the glacier module are presented in Appendix 6.

Initial calibration and verification of the glacier module were conducted for the Arteson glacier in the Santa River Basin. The Arteson Sub-basin in the Santa River Basin is a 6.2 km^2 area with 80 percent glacier coverage. This site was selected because the *Institut de Recherche pour le Développement* (IRD) had, over number of years (2000–2007), collected extensive data on glacier evolution and glacier melt outflow for this sub-basin. The calibration statistics summarized in Table 4.2 indicate a good fit and low discrepancy between calculated and observed glacier extension (bias).[2]

Table 4.2. Statistics of glacier model results for the Arteson Sub-basin in the Santa River Basin

	Calibration				
	Period	n	RMSE	BIAS	NASH
Artesón	2000-2007	79	45%	5%	10%
Artesón	2001-2007	69	33%	-4%	51%

Source: Table generated for the report by SEI, 2009.

Module parameterization for the Arteson system was used in the estimation of parameter values in the wider Santa River Basin. In a similar manner, work with the glacier module in the Santa River system guided implementation of algorithms in the Mantaro/Rímac River system (see Appendix 6). The main outputs of the glacier routine include changes in glacier area, volume and contribution to runoff.

The Páramo Module

Two alternatives were used in the development of a páramo module:

- ■ The first linked the behavior of páramos to that of a reservoir (the páramo as storage of water, akin to a dam).

■   The second parameterized the already existing rainfall-runoff routine in WEAP to capture the unique nature of hydrological processes in river basins dominated by páramos.

The conclusion was that the first approach would require further refinement before it could be used to represent páramo hydrology. However, the second approach, the use of the existing WEAP rainfall-runoff routines, is likely sufficient to represent and model páramo hydrology.

Because there are no extensive páramo landscapes in the selected three river basins in Peru, the module was not applied to this study. Therefore, it is not explained in greater detail in this chapter. The results of the development of this module are presented in Appendix 5, which provides a technical presentation as well as the process to calibrate the existing rainfall-runoff routine in another basin dominated by páramos. Data from a small river basin near Quito, Ecuador, with 90 percent of páramo landscape, were used for this purpose. Both hydrological approximations were implemented. The results showed that the páramo module sufficiently modeled the dynamic behavior of the páramo and its impacts on runoff.

Notes

1. Represents an area with similar hydrological behavior.
2. Root Mean Square Error (RMSE) is a frequently used measure of the differences between values predicted by a model and the values actually observed. It is a good measure of precision or repeatability, which is the degree to which repeated measurements under unchanged conditions show the same results. Bias: perceptual bias; Ef: Nash-Sutcliffe efficiency coefficient is used to assess the predictive power of hydrological models. It is a criterion that measures the fraction of the variance of observed values explained by the model. It ranges from minus infinity to 1.0. An efficiency of 1 corresponds to a perfect match of modeled discharge to the observed data. Therefore, large positive values close to 1.0 are sought.

Testing the Hydrology Tool at Basin Level

Before the WEAP hydrological model was applied to the three selected basins, the glacier module was calibrated and validated to ensure that it satisfactorily represents glacier dynamics. The model was first calibrated in sub-basins that lack glacier coverage in order to check the existing rainfall-runoff routines. Based on the initial findings of the calibration in nonglaciated river basins, a preliminary set of parameters was applied when the adjusted model was calibrated in glaciated basins. The modeling period for calibration was 1970–1984, and the 1985–1998 period was used for validation.

Calibration in Nonglaciated Sub-basins

The modified WEAP model was initially calibrated in the nonglaciated Corongo and Tablachaca Sub-basins. Corongo has an area of 561 km^2. Discharge is recorded at the Manta gauging station. Tablachaca has an area of 3,179 km^2 and streamflow is measured at the Condorcerro gauging station. The time series of observed and simulated streamflows for Tablachaca and Corongo are presented graphically in Figure 5.1.

Rainfall-runoff parameters related to subsurface conductivity, soil water capacity, runoff resistance and flow direction were adjusted to obtain the peak flows in the winter and the baseflows in the summer that approximated the observed conditions. The calibration was rated as satisfactory.

The calibration parameters obtained for the nonglaciated sub-basin were applied uniformly in all three basins studied. However, a modified set of parameters was employed in the La Balsa Sub-basin in the Santa River Basin, as explained below, to implicitly account for agricultural water use in the region. See Appendix 7 for further details.

Calibration and Validation: The Santa River Basin

Once the modified WEAP model had been tested in nonglaciated sub-basins, it was calibrated and verified in the glaciated sub-basins of the Santa River, with particular focus on a comparison of observed versus simulated streamflow and observed versus simulated glacier area. During the calibration of the model in the Santa River, particular attention was paid to assessing the performance of the glacier module in a subset of the Llanganuco, Parón and La Balsa sub-basins.

Figure 5.2 presents the comparison of observed and simulated average annual streamflows for the entire calibration and validation period (1970–1998) for the selected sub-basins in the Santa Basin. The discontinuous line represents the observed data while the simulated data are shown on the solid line.

Figure 5.1. Calibration and validation of model in the Corongo Basin for two historical periods: 1967–1983 and 1984–1999

Periodo Calibracion 1967–1983

Caudal observado vs Caudal simulado Tablachaca

Caudal observado vs Caudal simulado en Corongo
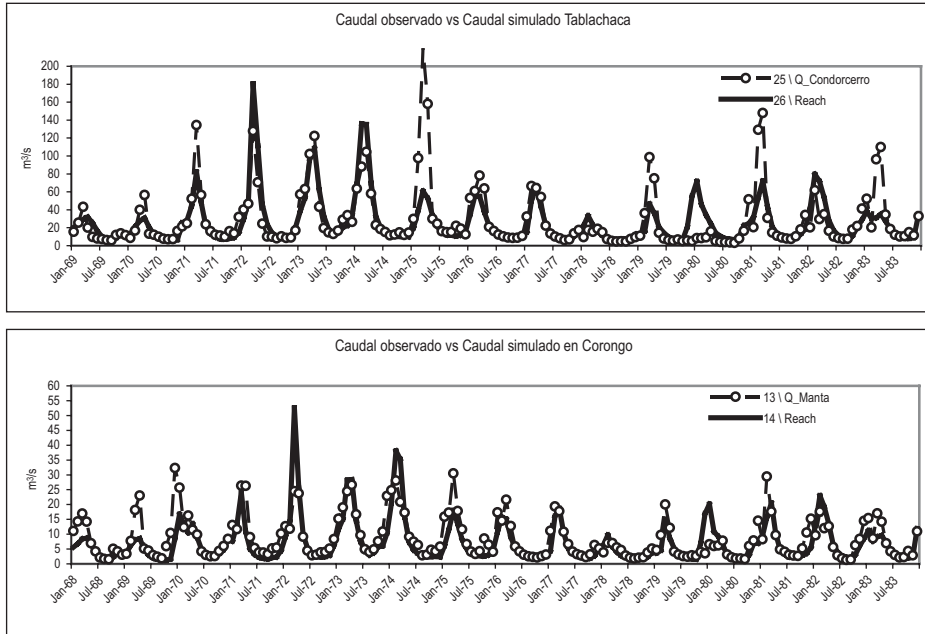
Periodo Validacion 1984–1999
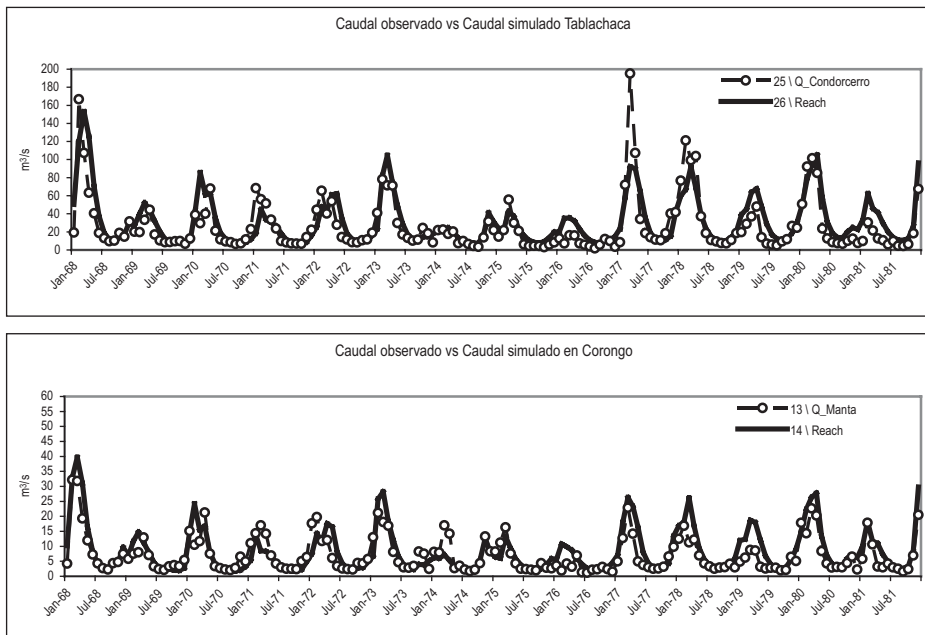
Caudal observado vs Caudal simulado Tablachaca

Caudal observado vs Caudal simulado en Corongo

Source: Figure generated for the report by SEI, 2009.

Figure 5.2. Observed and simulated streamflow in Llanganuco, Parón, and La Balsa in the Santa River Basin
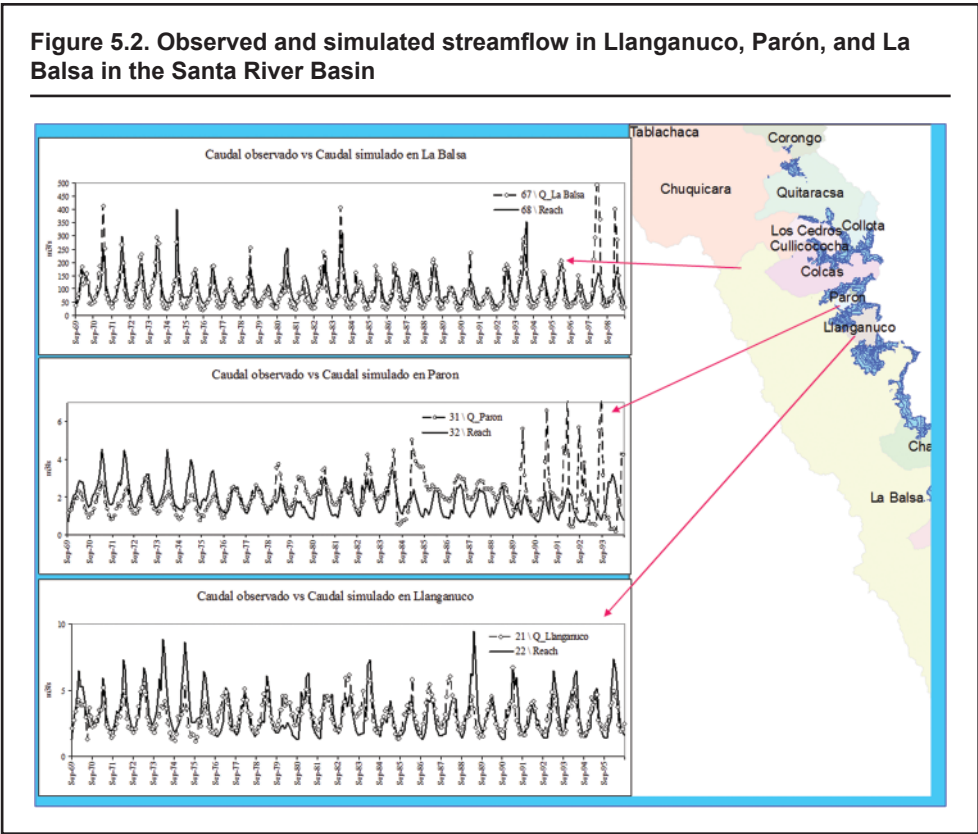
The simulation results show a basic agreement in the pattern of low and high discharge. However, there are significant differences between simulated and observed values. Most notably, some of the peak flows are missed, which is not surprising given the use of a monthly rainfall-runoff model applied at a fairly coarse spatial resolution. This indicates that more fine-tuning is desirable. However, the model captures well the conditions during the low-flow period, which is of critical importance to hydropower system operators, particularly at the tail end of the modeling period. To simplify these results, Figure 5.3 depicts the aggregated observed and simulated streamflow for the 1970–1999 period with the glacier module.

Table 5.1 shows the full calibration and validation statistics for the Santa River Basin. The calibration of larger glaciers is better than that of smaller glaciers, most likely because
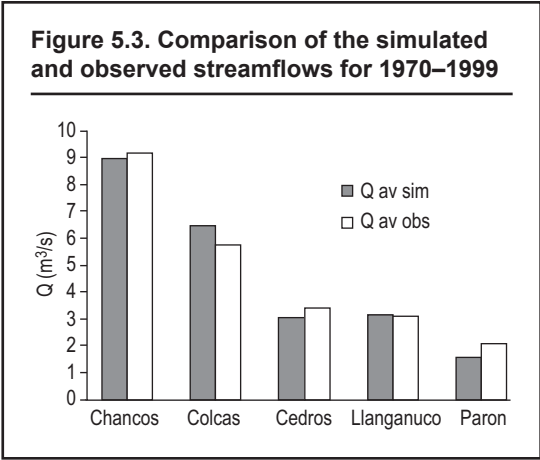
Figure 5.3. Comparison of the simulated and observed streamflows for 1970–1999

Table 5.1. Calibration and validation statistics for the Santa River

Sub-watershed	Calibration					Validation				
	Period	n	RMSE	BIAS	Ef	Period	n	RMSE	BIAS	Ef
1 - La Recreta	1969-1979	120	0.43	39%	0.63	1979-1989	120	0.43	44%	0.50
2 - Pachacoto	1969-1979	120	0.51	9%	0.64	1979-1989	120	0.53	13%	0.55
3 - Querococha	1969-1979	120	1.37	1%	0.72	1979-1989	120	1.50	20%	0.73
4 - Olleros	1969-1979	120	0.54	7%	0.73	1979-1989	120	0.55	-4%	0.63
5 - Quillcay	1969-1979	120	0.43	9%	0.65	1979-1989	120	0.45	-2%	0.63
6 - Chancos	1969-1979	120	0.26	20%	0.30	1979-1989	120	0.36	-4%	0.63
7 - Llanganuco	1969-1979	120	0.73	35%	-0.60	1979-1989	120	0.92	-15%	0.13
8 - Paron	1969-1979	120	1.70	6%	0.25	1979-1989	120	0.74	-44%	-1.60
9 - Artesoncocha	*	*	*	*	*	*	*	*	*	*
10 - Colcas	1969-1979	120	0.34	24%	0.34	1979-1989	120	0.38	4%	0.24
11 - Los Cedros	1969-1979	120	0.98	3%	0.34	1979-1989	120	0.79	-17%	0.20
12 - Quitaracsa	1969-1979	120	0.29	-7%	0.64	1979-1989	120	0.23	-23%	0.20
13 - La Balsa	1969-1979	120	0.03	3%	0.70	1979-1989	120	0.03	1%	0.72
14 - Corongo (Manta)	1969-1979	120	0.19	-12%	0.54	1979-1989	120	0.20	-9%	0.40
15 Chuquicara	1969-1979	120	0.01	4%	0.69	1979-1989	120	0.02	1%	0.77
16 - Tablachaca (Condorcerro)	1969-1979	120	0.05	17%	0.67	1979-1989	120	0.05	16%	0.61
17 - Puente Carretera	1969-1979	120	0.01	290%	-165.00	1979-1989	120	0.01	360%	-190.00

Source: Figure generated for the report by SEI, 2009.
Note: Root Mean Square Error (RMSE) is a good measure of precision or repeatability, which is the degree to which repeated measurements under unchanged conditions show the same results. Bias: perceptual bias; and Ef: Nash-Sutcliffe efficiency coefficient is used to assess the predictive power of hydrological models. It is a criterion that measures the fraction of the variance of observed values explained by the model. It ranges from minus infinity to 1.0. An efficiency of 1 corresponds to a perfect match of modeled discharge to the observed data. Therefore, large positive values close to 1.0 are sought.

small glaciers are more likely to be dominated by unique conditions that are not well captured by either the glacier module itself or the regional parameterization that was developed for the Santa River Basin. The final results of the Santa River's monthly discharges at La Balsa, which is the point of diversion to the Cañón del Pato hydropower project, and other points directly below glaciers provide reasonable calibration and validation statistics.

Table 5.1 summarizes the results of the calibration and validation statistics for the Santa River Basin. The 1969–1979 period was used for calibration; the observed data are used to estimate the model parameters. The 1979–1989 period is used for validation. The period is different from the calibration period because it seeks to confirm that the model is applicable to differing conditions. Three measures of goodness of fit are used; these include the Root Mean Square Error (RMSE), Bias and the Efficiency Coefficient, which are standard indicators used in this type of analysis.
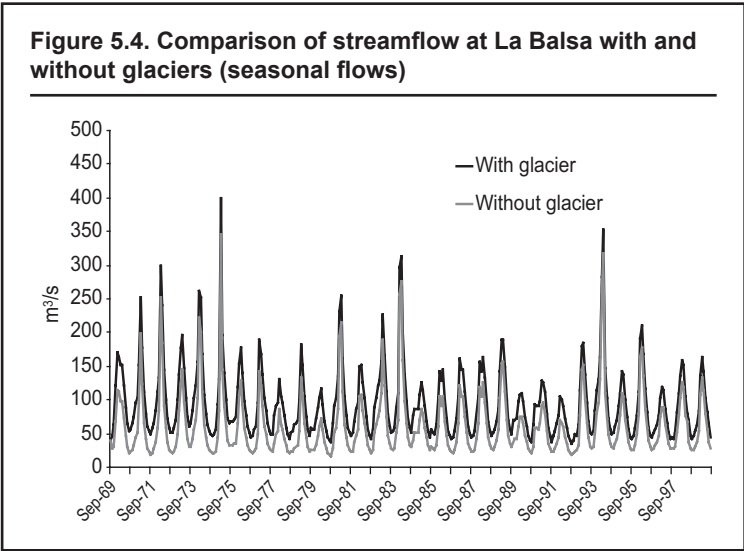
Figure 5.4. Comparison of streamflow at La Balsa with and without glaciers (seasonal flows)

Source: Figure generated for the report by SEI, 2009.

The final results of the Santa River's monthly discharges at La Balsa, which is the point of diversion to the Cañón del Pato hydropower project, and other points directly below glaciers, indicate a good model fit, as exemplified by the calibration and validation statistics, small biases and high-efficiency coefficient.

Figure 5.5. Comparison of streamflow at La Balsa with and without glaciers (average flows)

Source: Figure generated for the report by SEI, 2009.

Figure 5.4 illustrates the results at La Balsa with and without glacier retreat. Figure 5.5 represents the aggregated values shown in Figure 5.3 (above). These results show that the average simulated discharge of about 95 m^3/sec with glaciers are roughly 58 percent higher than the average discharge of 60 m^3/sec simulated in the absence of glaciers. These results thus confirm that glaciers are important in the production of water in the Santa River Basin (Vergara et al. 2007), and that the glacier module is important in accurately modeling the runoff in the glaciated basins.

In conclusion, the calibrated hydrological model results, at the selected discharge points of interest, provide a reasonable representation of the hydrological behavior of the basin under current climate conditions. These results represent the baseline for analyzing possible changes in hydrological behavior. Results from the final calibration-validation of the Santa River model are presented in detail in Appendix 7.

Calibration and Validation: Rímac-Mantaro River Basins

A similar calibration-validation effort was undertaken for the combined Rímac-Mantaro River Basins. These basins are more complex than the Santa River Basin, with many more sub-basins and a higher level of man-made infrastructure to regulate water flows such as reservoir storage and release. Consequently, the final calibration-validation of the application of the hydrological model in the Mantaro/Rímac River is less precise. It presents higher uncertainty and statistics denote medium fit.

The Rímac-Mantaro River Basin (Figure 4.3) includes 38 reservoir objects, 22 demand sites representing the urban and rural water demands in individual provinces, along with 276 subcatchment objects(102 for Rímac and 174 for Mantaro). Five diversion points and nine run-of-river hydropower objects are used to represent the hydropower production system. Twenty-eight streamflow gauges were available for calibration-validation of the hydrological routines.

The calibration-validation focused on the analysis of several gauge stations (19 stations for Mantaro, 6 stations for Rímac) with the 1970–1981 calibration period; the validation period was 1981–1996. For presentation purposes, the analysis is focused on sites with large mean water discharges. For the Mantaro River, stations include Pongor and Mejorada; for the Rímac River, the two main stations upstream from Lima: Chosica and Surco. While modeling in the Mantaro River Basin extends to the location of the projected hydropower facility at La Guitarra, information for calibration only reaches the Pongor hydrometric station. For practical purposes, input to the La Guitarra hydropower development is defined at the Pongor site. Similarly, while the Rímac River modeling extends to the point of water diversion to the city of Lima, the closest gauge in the system is Chosica, located upstream.

Parameter Setting

The calibration first focused on obtaining a set of parameters applicable to the entire river basin to reasonably represent the hydrology of the main course of the Mantaro and Rímac Rivers. The glacier parameters estimated for the Rio Santa were used, eliminating the need for separate calibration processes for glaciated and nonglaciated subcatchments. Because both rivers are located in different types of basins (the Mantaro is in the Amazon Basin, the Rímac drains to the Pacific), parameter values were adjusted separately for each basin. Each basin arrived at an internally uniform set of parameters, as indicated in Table 5.2. The table shows that the runoff resistance factor and the root zone conductivity parameters were defined in terms of land cover (crops, underbrush [*matorral*], coastal plain, tundra).

Temperature and humidity data were also needed. The only good-quality set of long and continuous time-series data that exists is collected from the Cercapuquio station in the Mantaro Basin (12.422°S, 75.417°W). Continuous temperature data for each catchment were obtained by adding a temperature gradient of -0.6°C/100m to the tempera-

Table 5.2. Land use parameter values for the glacier module

Land use parameters (part without glacier)				
Parameter		unit	Rimac	Mantaro
Crop coefficient			0.9	1.2
Root zone capacity		mm	425	425
Root zone conductivity	Cultivos	mm/month	840	420
	others	mm/month	600	300
Deep water capacity		mm	7500	300
Deep water conductivity		mm/month	800	300
Runoff resistance factor	Cultivos		1.2	1.2
	Matorral		0.9	0.9
	Planicie costera		0.6	0.6
	Tundra		0.6	0.6
Flow direction		% horizontal	0.2	0.2
Initial storage fractions	z1	%	30	30
	z2	%	10	30

Glacier parameters			
Parameter	unit	Rimac	Mantaro
T_0	°C	1.7	1.7
a_{snow}	$mm.month^{-1}.°C^{-1}$	300	300
a_{ice}	$mm.month^{-1}.°C^{-1}$	600	600

Source: Table generated for the report by IRD, 2009.

Note: Crop coefficient: Crop coefficients are crop-specific evapotranspiration values that are estimated by field experiments under no water limitation. Crop coefficients are multiplied by reference evapotranspiration data to estimate the potential crop's evapotranspiration requirement.

Root zone capacity: The effective water-holding capacity of the top layer of soil, represented in mm.

Root zone conductivity: Root zone (top "bucket") conductivity rate at full saturation (when relative storage z1 = 1.0), which will be partitioned, according to Preferred Flow Direction, between interflow and flow to the lower soil layer. This rate can vary among the land class types.

Deep water capacity: Effective water holding capacity of lower, deep soil layer (bottom "bucket"), represented in mm. This is given as a single value for the catchment and does not vary by land class type. This is ignored if the demand site has a return flow link to a groundwater node.

Deep water conductivity: Conductivity rate (length/time) of the deep layer (bottom "bucket") at full saturation (when relative storage z2 = 1.0), which controls transmission of baseflow. This is given as a single value for the catchment and does not vary by land class type. Baseflow will increase as this parameter increases.

Runoff Resistance Factor: Runoff Resistance Factor incorporates factors such as Leaf Area Index (represents vegetation canopy) and land slope to determine surface runoff. Higher values of Runoff Resistance Factor lead to lower values of runoff.

Flow direction: Parameter used to partition the flow out of the root zone layer (top "bucket") between interflow and flow to the lower soil layer (bottom "bucket") or groundwater, and can vary between 1.0 = 100% for horizontal, and 0 = 100% for vertical flow.

Initial storage fractions z1 and z2: Initial value of Z1 at the beginning of a simulation is the relative storage given as a percentage of the total effective storage of the root zone water capacity. Initial value of Z2 at the beginning of a simulation is the relative storage given as a percentage of the total effective storage of the lower soil "bucket" (deep water capacity). This rate cannot vary among the land class types.

T0: Threshold value for conversion of liquid precipitation into snow, or freezing threshold, which is defined by the user and may constitute a calibration parameter. T_0 is also used to estimate the temperature gradient that determines the potential snowmelt and icemelt when multiplied by the corresponding degree-day factors.

a snow and a ice: Degree-day factor for snowmelt and icemelt, respectively. In this particular application, this factor is applied at a monthly time step and has units of mm/month/ºC. This factor indicates the decreases of water content in the snow and ice cover caused by 1 degree above freezing in a time step. The degree-day factor for snow is lower than that for ice, because of the higher albedo of snow. More information on these parameters can be found at www.weap21.org.

Figure 5.6. Map of rainfall areas and location of data stations in the Mantaro River Basin
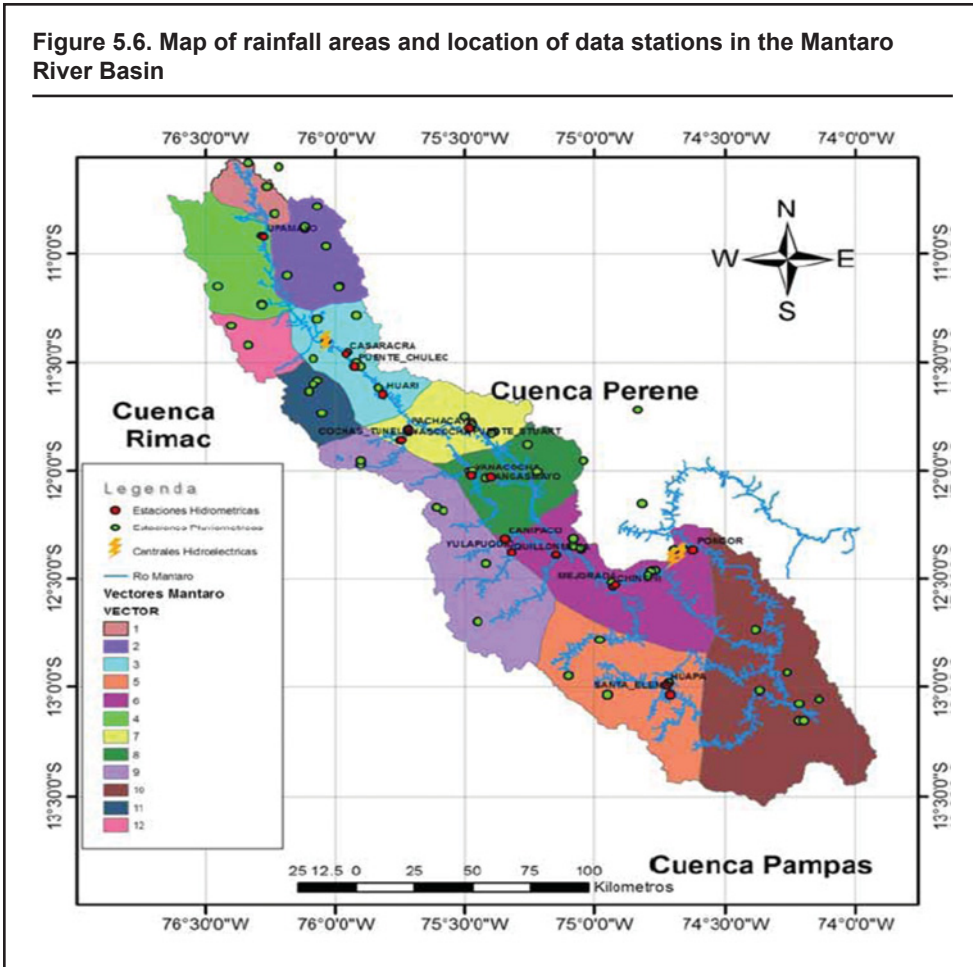
ture observed at Cercapuquio. For humidity and wind speed, the long-term monthly time series at Cercapuquio was assumed to apply to all catchments.

The Mantaro River Basin

Figure 5.6 shows the location of the data stations in the Mantaro River Basin.

The Mantaro River Basin was calibrated by using monthly average streamflow. Figure 5.7 presents the seasonal fluctuations of observed and simulated streamflows for the downstream stations of the Mantaro Basin, showing the relationship between the observed and simulated discharge values. The calibration indicates a good fit in reproducing the monthly distribution of discharges. An exception is the site at Pongor, where the simulated runoff fails to capture the pronounced high-flow characteristics of the February and March periods.

For validation in the Mantaro Basin, the simulated monthly flows for both the calibration and validation period (1966–1996) were plotted against the observed values, as shown in Figure 5.8. Good correlations appear to exist for these stations during this period, with the exception of the Sheque station.[1]

Figure 5.7. Observed (Qo) and simulated (Qs) monthly average streamflows for the Mantaro River Basin during the 1970–1981 calibration period
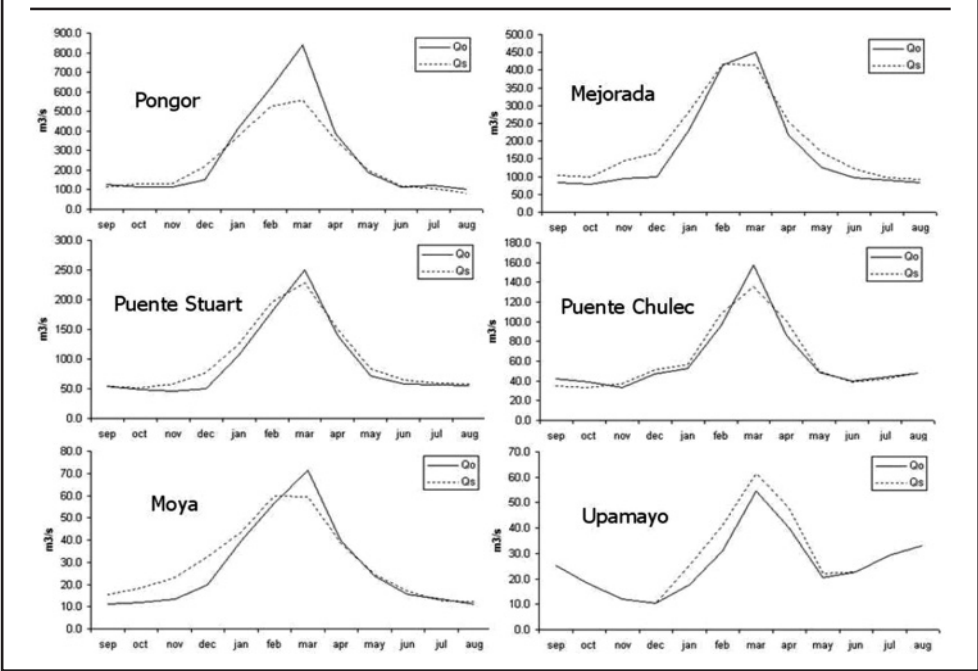
Source: Figure generated for the report by IRD, 2009.

Figure 5.8. Observed (blue line) and simulated (red line) flow rates for the 1966–1996 reference period at four gauge stations in the basin
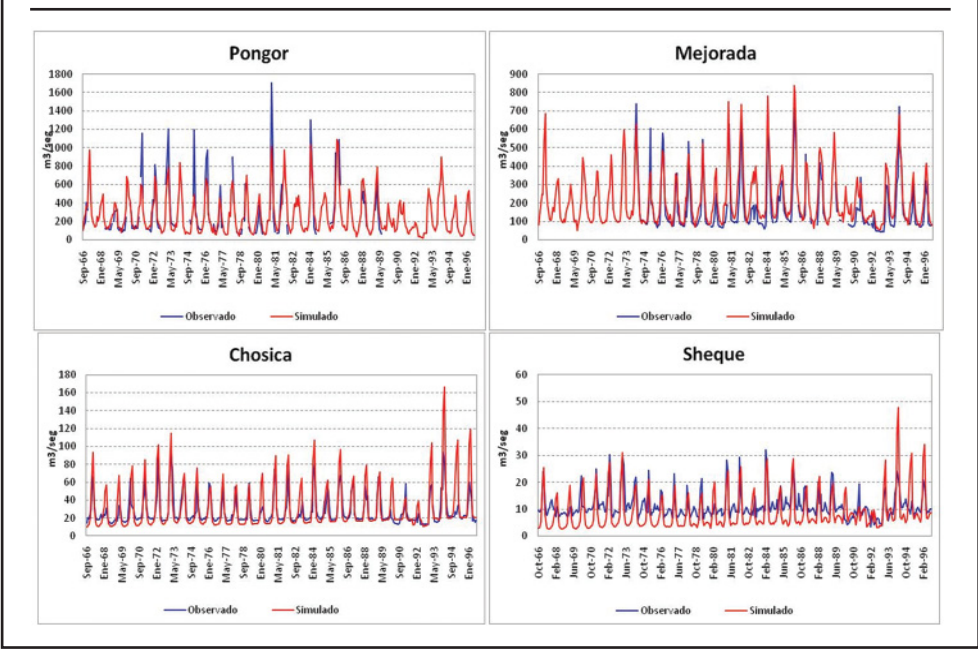
Source: Figure generated for the report by IRD, 2009.

Figure 5.9. Correlation between observed and simulated flow rates for the reference period
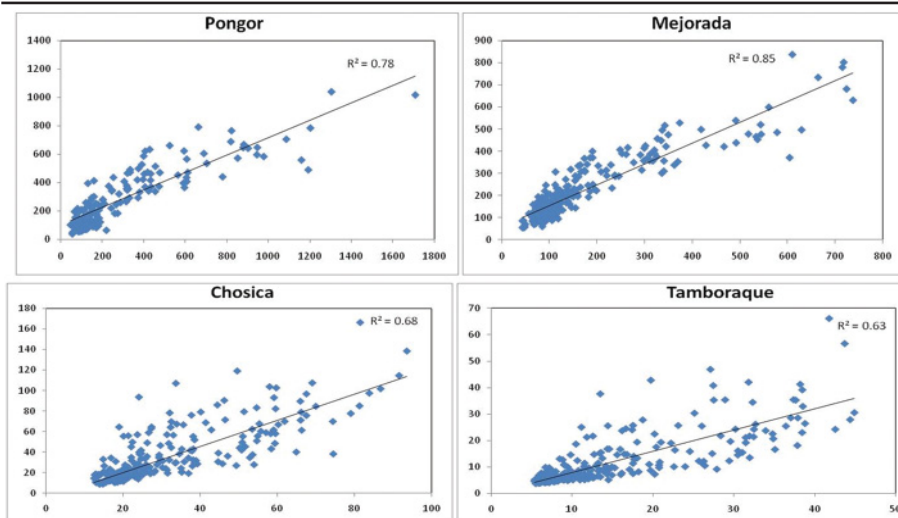
Source: Figure generated for the report by IRD, 2009.

To represent the results graphically, Figure 5.9 plots the simulated versus observed data during the reference period. In the case of these stations, the correlation coefficients are appropriate. Based on the results, the selected stations can be used in an analysis of the evolution of flow in the future.

In summary, validation results for the selected stations in the Mantaro Basin indicate a reasonable (good) fit, although bias and efficiency indicators are not as good. For detailed applications, it is recommended that calibration be improved by incorporating the spatial distribution of soil characteristics.

Table 5.3. Criteria for the calibration and validation periods in the Mantaro Sub-basins

station	Calibration period 1970-1981				Validation period 1981-1996				
	n	Qo m^3/s	RMSE	BIAS	Ef	n	Qo m^3/s	RMSE	BIAS	Ef
Pongor	90	310.2	53.76	-14%	0.74	39	375.2	44.57	5%	0.68
Mejorada	90	176.0	37.91	16%	0.81	158	170.6	48.14	36%	0.65
Puente Stuart	107	91.8	37.16	10%	0.81	142	81.9	72.33	50%	-0.25
Puente Chulec	91	57.5	37.40	5%	0.73	113	50.4	51.67	30%	-0.03
Moya	119	24.5	57.52	14%	0.62	115	23.7	65.82	40%	0.31
Upamayo	124	25.9	45.72	14%	0.65	161	23.5	84.65	41%	0.06
Chinchi	130	15.7	61.03	-5%	0.68	151	17.7	86.15	-8%	0.55
Angasmayo	132	17.5	52.95	10%	0.77	159	12.2	84.62	67%	0.46
Quillon	122	11.3	76.59	53%	0.36	99	8.2	128.62	98%	-0.55
Yanacocha	128	6.9	149.65	130%	-0.53	173	6.1	216.42	189%	-1.16
Pachacayo	131	10.7	61.60	-3%	0.60	174	9.4	107.50	82%	-0.26
Huapa	131	10.7	59.35	8%	0.68	164	11.0	54.47	3%	0.72
Santa Elena	126	8.4	78.52	-17%	0.59	174	10.7	115.89	-39%	0.33
Huari	131	6.8	54.37	-11%	0.70	174	6.1	131.36	97%	-0.69
Cochas Tunel	132	6.1	73.52	11%	0.36	156	2.3	79.91	33%	0.52
Yulapuquio	127	5.8	83.14	-13%	0.48	172	4.9	82.41	24%	0.47
Canipaco	119	3.8	88.02	-13%	0.55	159	4.2	163.14	-10%	0.31
Piñascocha	132	1.8	95.94	62%	0.17	177	1.5	225.38	181%	-2.94
Casaracra	122	1.8	82.99	49%	0.07	156	2.3	79.91	33%	0.52

Source: Figure generated for the report by IRD, 2009.

Figure 5.10. Observed and simulated monthly average streamflows for the Rímac River Basin during the 1970–1981 calibration period
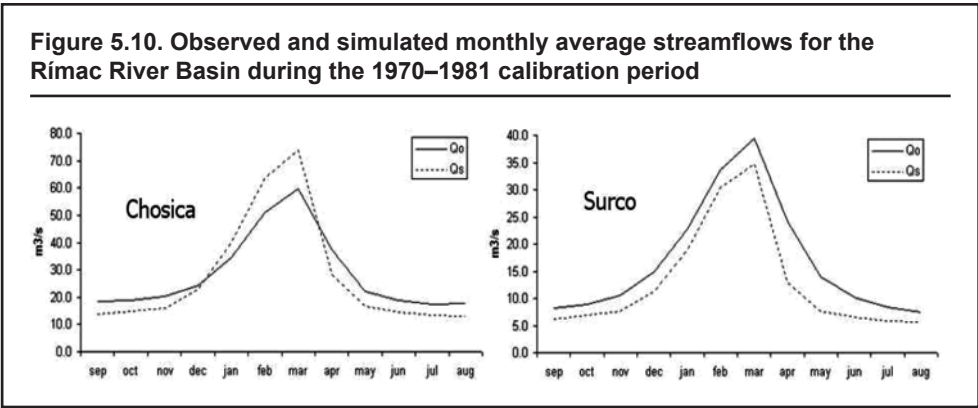
Source: Figure generated for the report by IRD, 2009.

The Rímac River Basin

Next, the calibration-verification focused on the Rímac River. Figure 5.10 presents seasonal fluctuations during the calibration period of observed and simulated streamflows at the Chosica and Surco stations. In Chosica the simulation seems to correlate the observed trend rather well, only showing clearly higher values during the high peak period (February–March).

Similar to the data for Mantaro, presented earlier, the monthly observed and simulated streamflows for the validation period are plotted for the Chosica and Surco stations in Figures 5.11 and 5.12. Good correlations appear to exist for these stations.

Conclusions of the Calibration-Validation in the Rímac-Mantaro River System

A double validation of the model was conducted by comparing observed and simulated streamflows at 25 control points in the Rímac-Mantaro system; and by comparing the glacier area observed with Landsat images nine years apart (1988 and 1996) with
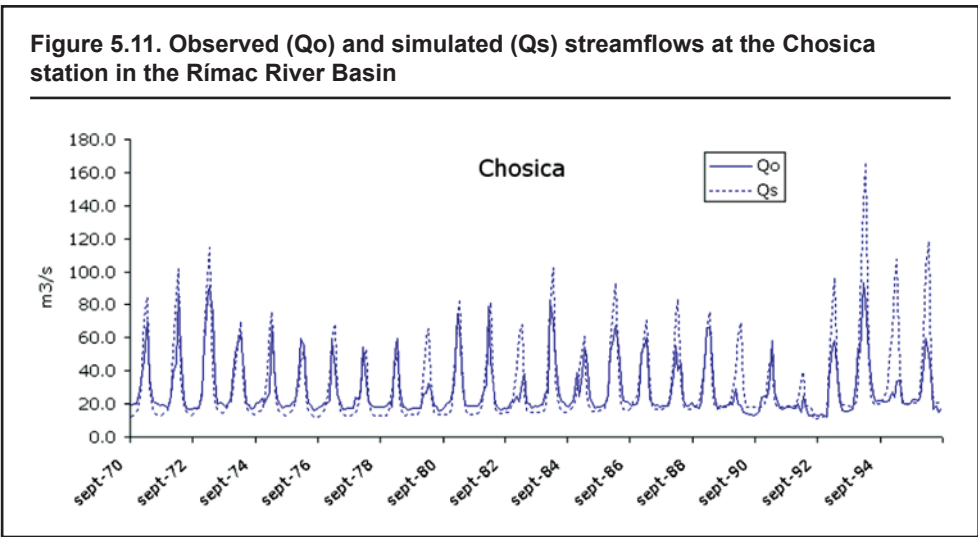
Figure 5.11. Observed (Qo) and simulated (Qs) streamflows at the Chosica station in the Rímac River Basin

Source: Figure generated for the report by IRD, 2009.

Figure 5.12. Observed (Qo) and simulated (Qs) streamflows at the Surco station in the Rímac River Basin
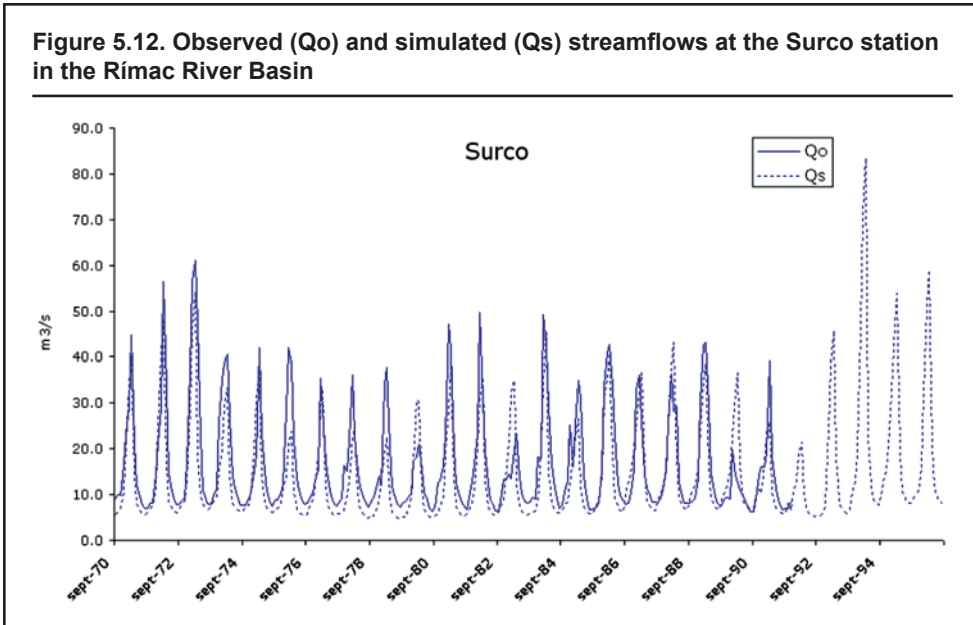
Source: Figure generated for the report by IRD, 2009.

that calculated by the model. This validation yielded reasonable results. However, for the Rímac-Mantaro system, future simulations would need to reproduce the reservoirs' operation and management: 16 reservoirs were operational from 1995 to 2000, and 28 reservoirs are planned for the future.

The flows in the Mantaro/Rímac River system are more hydraulically altered by the operation of reservoirs and diversions than are those in the Santa River. As a result, the model does not perform as well in some stations. However, it does perform better during the critical low-flow period. It is likely that the model's overall performance could be improved if the parameterization of the WEAP reservoir and diversion infrastructure is improved.

The results of the glacier area evolution simulation in the Mantaro/Rímac River system were satisfactory. The observed initial glacier area in these basins in 1970 was 113 km^2, which decreased to roughly 40 km^2 in 1997. This trend was well captured by the model when simulated and observed glaciated areas were compared at discrete times during the calibration-validation period (see Appendix 9 for more information). Compared to the Santa River, the glaciers in the Mantaro and Rímac River Basins are much smaller, and thus their runoff contribution is not significant.

Notes

1. However, this error can be explained by the fact that the station has problems in correctly estimating flows during low-water periods, and the simulation shows 50 percent of the amount observed.

Results from the Hydrology Analysis

In summary, up to this point, a procedure has been employed by which methodologies used to build planning climate scenarios are grouped and analyzed. Guidance has been developed to assess the skill of the methods in simulating (reproducing) key parameters of recent past climate. In parallel, a water resources management tool has been modified to incorporate the dynamic behavior of glaciers and high mountain wetlands when responding to global warming. The hydrological tool has been calibrated and validated for three basins in Peru. The next step is the use of the information provided by the climate component to ascertain the hydrological response to projected climate conditions. The main purpose of this chapter is to show how the planning climate scenario is incorporated in the hydrological model runs. At a practical level, the data generated provide a look at the anticipated changes in hydrology.

The chapter has been structured as follows: First, an overall picture of expected changes in river runoffs in Peru, generated by the MRI-AGCM3.1, is presented. Next, the chapter outlines the results of applying the calibrated WEAP hydrological model in the three river basins. **The analysis includes an estimate of increases in temperature, changes in precipitation, and rate of glacier retreat.** Although the purpose of this study is to develop a useful methodology, and not necessarily to produce an assessment of the impacts of climate change in the selected basins, this chapter nonetheless also discusses how hydrology may be impacted by the projected consequences of climate change in Peru.

Visualization of Climate Change Impacts on Rivers in Peru

The MRI-AGCM3.1 model, used as a tool to assess climate change impacts in Chapter 3, includes a river component that enables a direct assessment of changes in river runoffs at a country level. This tool was used to obtain an overall picture of the changes in runoffs. The runoff data were derived from the rainfall projections of the model (see Chapter 3, "High-Resolution Climate Project for Peru for the 21st Century"). Based on these, the net flow of rivers at a macro-basin level was calculated. The analysis used a "GRiverT" river model.[1] The results are presented in Figure 6.1: panel a) shows the current situation and panel b) shows the expected change in the river flows. The end-of-century projection seems to indicate a significant reduction in net discharges on the southern coast and in the northeastern part of the country. The results also indicate that in the Andean region some areas will experience increased runoff, while other areas will experience a reduction in the total volume of water in the hydrographic system. No simple generalization is

Figure 6.1. Changes in river flows: a) current annual flows (mm) and b) change between the present and the end of the century (%)
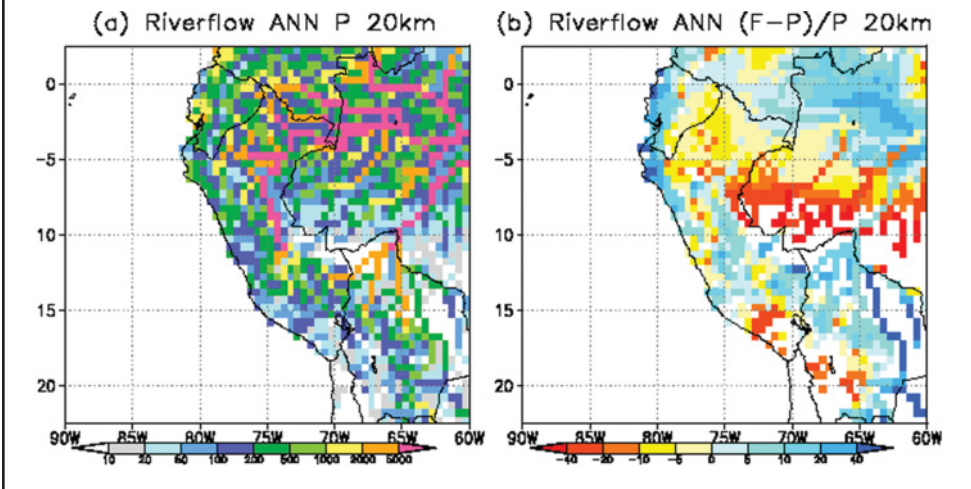
Source: Figure generated under the Memorandum of Understanding (MOU) between the MRI and the World Bank.
Note: Picture a) presents the absolute annual flow, and therefore the scale is in mm. Picture b) presents the change, and the scale is in percentage.

possible, nor is one desirable. Each area of interest needs studies and analysis at resolutions adjusted to the size of the basin and the details of the information needed.

Visualization of Climate Change in the Santa Basin

The two future climate conditions developed from the 16 GCM ensemble,[2] along with results from the trend analysis, were used as the basis for the hydrological analysis of the Santa River Basin. The ensemble results were used to simulate the future glacier dynamics, while the trend analysis provided the climate data to estimate the hydrological response to future climate change.

Simulation of Future Glacier Dynamics

According to the simulation, the glaciers of the Santa River Basin are likely to experience significant size reduction under warming climate scenarios. Using 2006 glacier coverage as a baseline, the simulated reduction in glaciated area in the Santa River Basin over the next 30 years would be 25 percent for the marginally warmer scenario and 47 percent for the much warmer scenario,[3] as shown in Table 6.1. A comparison of these scenarios with data from the past 40 years shows that the decline of glacier coverage is expected to accelerate in a nonlinear fashion in the future with faster-increasing temperatures. During the 1970–early 2000 period, the glaciers in the Cordillera Blanca declined more than 25 percent with an average temperature increase of 0.35–0.39°C per decade (Bradley et al. 2009; Racoviteanu et al. 2008; Urrutia and Vuille 2009; Vuille et al. 2008). Naturally, it is not only warmer temperatures that cause glacier melting. Other variables, such as humidity and precipitation, also play critical roles in the process (Bury et al. 2010)

Table 6.1. Simulated reductions in glaciated area between 2006 and 2036 under two climate projections

Total Area (km²)	2006	2021	2036	% Change		
				06-21	21-36	06-36
Dry	347	257	182	26%	29%	47%
Wet	347	300	260	14%	13%	25%

Source: Table generated for the report by IRD, 2009.

When the spatial distribution of the glacier retreat under much warmer conditions in the Santa River Basin by 2036 is assessed, it can be seen that the impacts will be distributed unevenly (Figure 6.2). Under these conditions, it is likely that the some small, low-altitude glaciers in the Santa River Basin would dramatically shrink in the future. Although the impact of these reductions may not be felt acutely everywhere in the basin, locally the effects of the loss of glacier ice could have a profound impact on streamflow conditions.

Based on these glacier cover reduction projections, a preliminary assessment was conducted on how changes in the seasonal patterns of streamflow may constrain the operations of the Cañón del Pato project. This assessment was made under both climate conditions: marginally warmer and much warmer. Over the entire period (2006–2036), the contribution of glacier melt to the total runoff at the Cañón del Pato diversion was

Figure 6.2. Simulated glacier coverage in 2036 under the much warmer climate projection
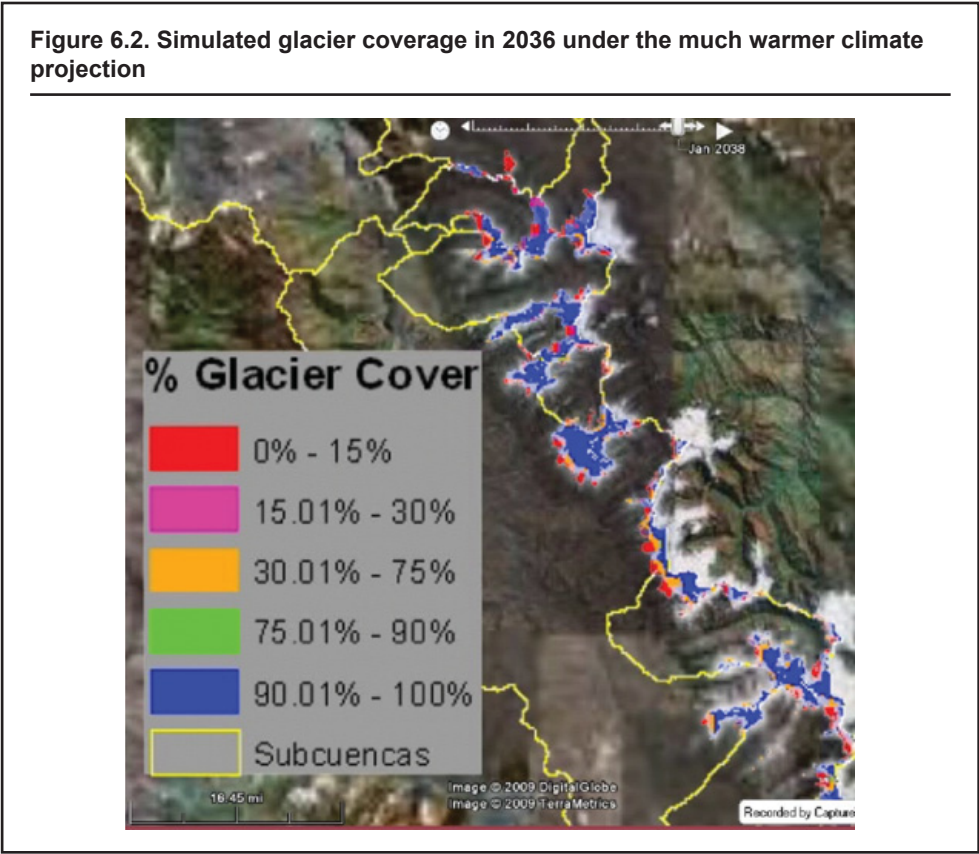
Source: Figure generated for the report by SEI, 2009.

estimated at 9 percent under marginally warmer conditions and 16 percent for the much warmer conditions. Based on these estimates under slower warming (and wetter) conditions, rainfall-runoff would create relatively more streamflow in nonglaciated regions of the Santa River Basin, reducing the relative contribution of glacier melt. At the same time, glacier retreat would be accelerated and more of the streamflow would come from glacier melt. This result is in line with some studies done on the impacts of glacier melt. They indicate that the streamflow is initially increasing with the glacier melt, but once a threshold is reached, the role of glacier melt in streamflows would diminish (Mark et al. 2010).

The assessment made for this report indicates that both scenarios would provide more water during the summer and autumn high-flow period (rainy season) when compared to historical conditions. At the same time, the flow would be reduced during the low-flow period in both scenarios (Figure 6.3).[4] Although these results are by no means

Figure 6.3. Flow through Cañón del Pato for historical conditions, marginally warmer and much warmer scenarios

Source: Figure generated for the report by SEI, 2009.

definitive, the repercussions of the increased variability and reduced minimum flows might require additional water regulation infrastructure to cope with increased variability and reduced minimum flows.[5]

Expected Overall Hydrological Response to Observed Trends

Data from the rainfall trend analysis (described in Chapter 3) were also used as an input to the WEAP hydrological model in the Santa River Basin in order to strengthen the analysis. The results are summarized by analyzing the expected hydrological changes at two sites: La Balsa and Condorcerro. To understand the future changes, it is important to have a historical record for comparison purposes. Figure 6.4 presents the flows for the baseline period, based on data provided by SENAMHI and the results from the WEAP simulations.

Figure 6.4. Observed (blue line) and simulated (red line) discharges using trend analysis at selected sites on the Santa River, 1966–1996
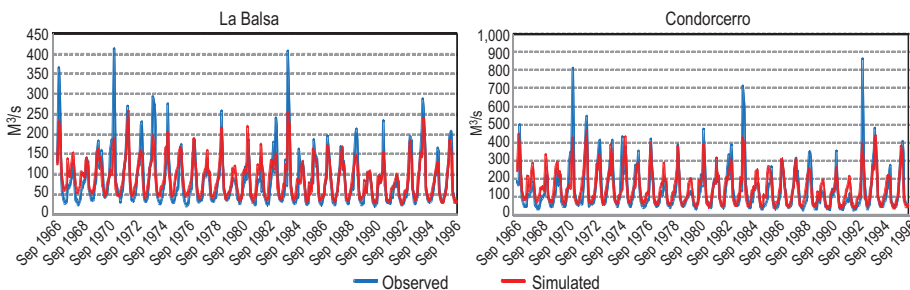
Source: Figure generated for the report by IRD and SEI.

Figure 6.5. Results of the trend analysis for mid-century in the Santa River
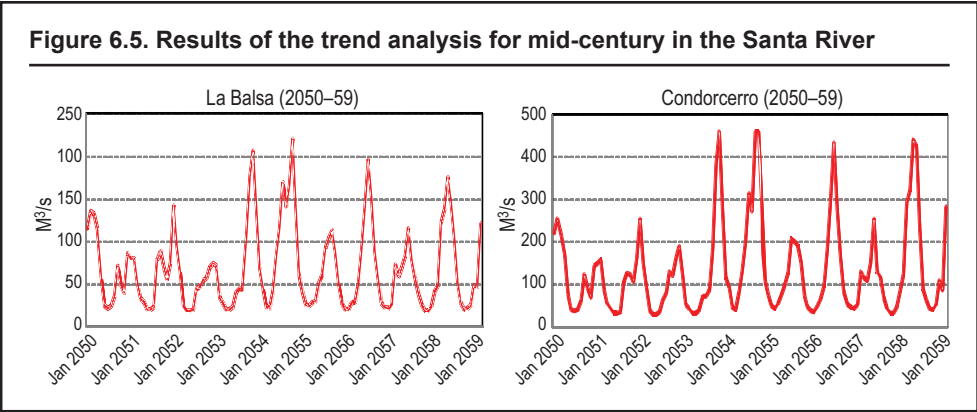
Source: Figure generated for the report by IRD and SEI.

In terms of projected impact, the expected discharges by mid-century are lower than the historical record (Figure 6.5 displays the results of the hydrological response in the 2050s), which summarizes the expected changes in the average monthly discharges at the selected sites.

Monthly discharges by 2050 at La Balsa (Figure 6.6) are expected to be lower year-round in comparison to historical values. The mean annual discharge in the observed period is 85.8 m³/sec and would be reduced by 21 percent by mid-century. Minimum values in August are also reduced by 28 percent. Similarly, average flow at Condorcerro is expected to decrease by more than 6 percent and its minimum flow by 18 percent.

As previously mentioned, the analysis assumes that the climate linear trends identified from the analysis of records from weather stations will continue into the future. This hypothesis may be considered a lower limit with respect to future climates, since it assumes that the warming will not intensify and that the trend is linear throughout the projection period. Moreover, no sensitivity analysis was conducted, since the main

Figure 6.6. Comparison of average monthly discharges in the Santa River between observed historical (blue line) and projected mid-century (red line) values (m³/s), based on trend analysis
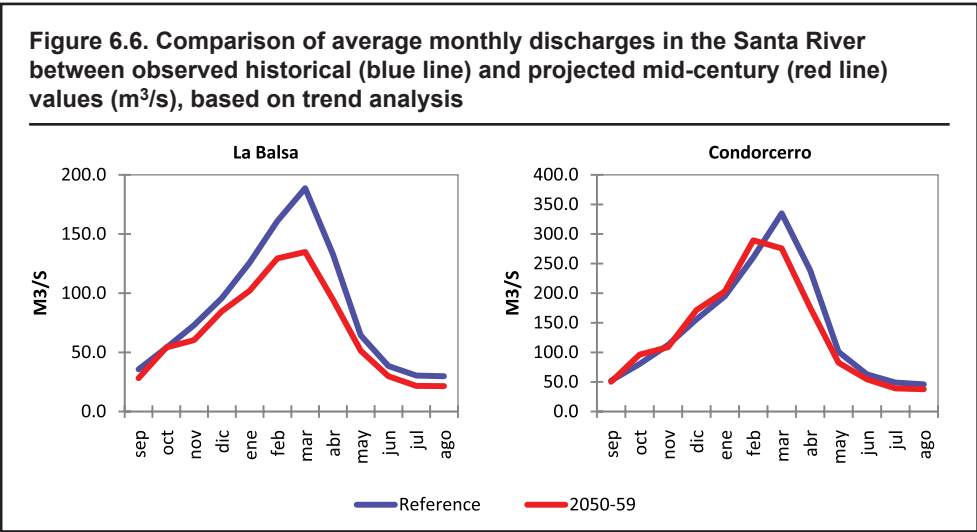
Source: Figure generated for the report by IRD and SEI.

objective of this study was to develop methodologies rather than to provide results for a particular application. However, a proper sensitivity analysis is required for any formal application on the possible range of climate impacts expected in Peru.

Visualization of Climate Change in the Rímac and Mantaro Basins

The glaciers in Mantaro and Rímac River Basins are rather small and their runoff contribution is less significant than in the case of the Santa River. Therefore, in addition to simulating future glacier dynamics, the study focuses on analyzing the consequences of expected changes in precipitation associated with future climates in these two basins. The trend analysis is used for this application. The results from the analysis are presented for four sites: Chosica and Surco in the Rímac River Basin, and Pongor and Mejorada in the Mantaro Basin. These control points have been selected to provide a summary view of the impacts of climate change in the basins, from upstream (small catchment areas) to the furthest point downstream with hydrometric information.

Again, the first step was to establish a baseline for comparison purposes. Figure 6.7 shows the comparison between the simulated and observed discharges in the selected control sites from 1966 through 1996. For the four gauge stations used in the analysis, the data show a good fit. In the Rímac Basin and especially at the Chosica station, simulated runoff gives higher values than the observed data during the peak periods.

The historical trends were compared with the projected hydrological response in the Rímac-Mantaro Basin in the 2050s (Figure 6.8). The decade of analysis includes a dry period similar to that observed during 1992–1993. The climate scenario is able to capture this extreme event, and the hydrological model describes the expected flows caused by such an extreme event. For the stations located upstream, Chosica and Surco, the first half of the decade is projected to be dry and the second half wetter. But this behavior has only limited influence on the flows downstream. The Pongor and Mejorada stations

Figure 6.7. Observed (blue line) and projected (red line) discharges using trend analysis at selected sites on the Rímac and Mantaro Rivers, 1966–1996
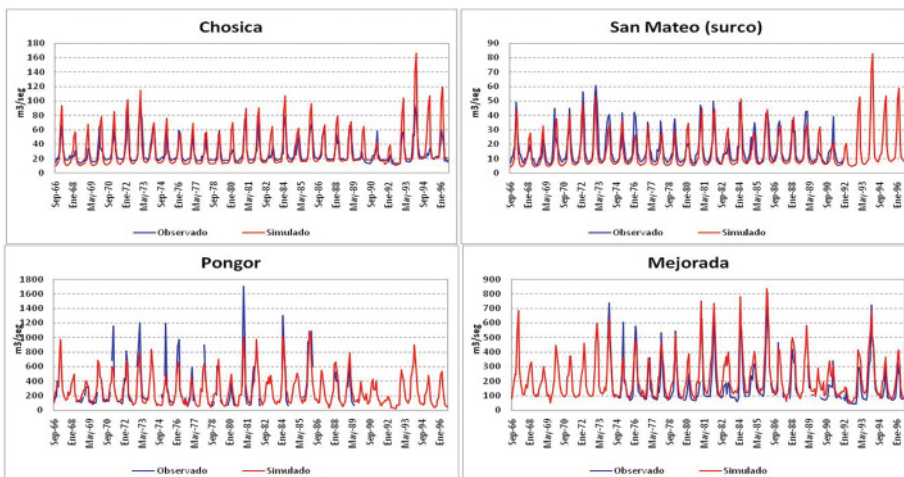
Source: Figure generated for the report by IRD and SEI.

Figure 6.8. Results of the trend analysis for mid-century in the Rímac and Mantaro Rivers
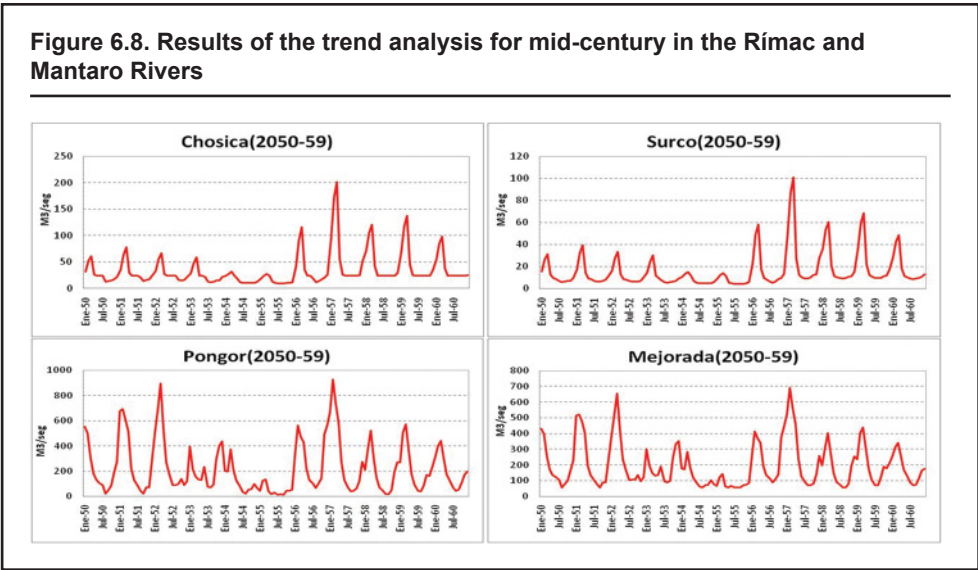
Source: Figure generated for the report by IRD and SEI.

show a dry spell only in the middle of the decade. Only a sustained dry period upstream produces drought conditions in the lower Mantaro Basin.

Summarizing the results for the Mantaro River Basin, Figure 6.9 provides the average monthly results for the historical data, for 2050–2059, and for 2090–2099, when the trend-line scenario is used as an input in the hydrological model. For the Mantaro River Basin, as indicated in the figure for the Pongor and Mejorada sites, overall water availability decreases. However, a shift in the distribution of runoff is projected, with reduc-

Figure 6.9. Comparison of average monthly discharges in the Mantaro River for observed historical, mid-century and end-of-century values (m³/s), based on trend analysis
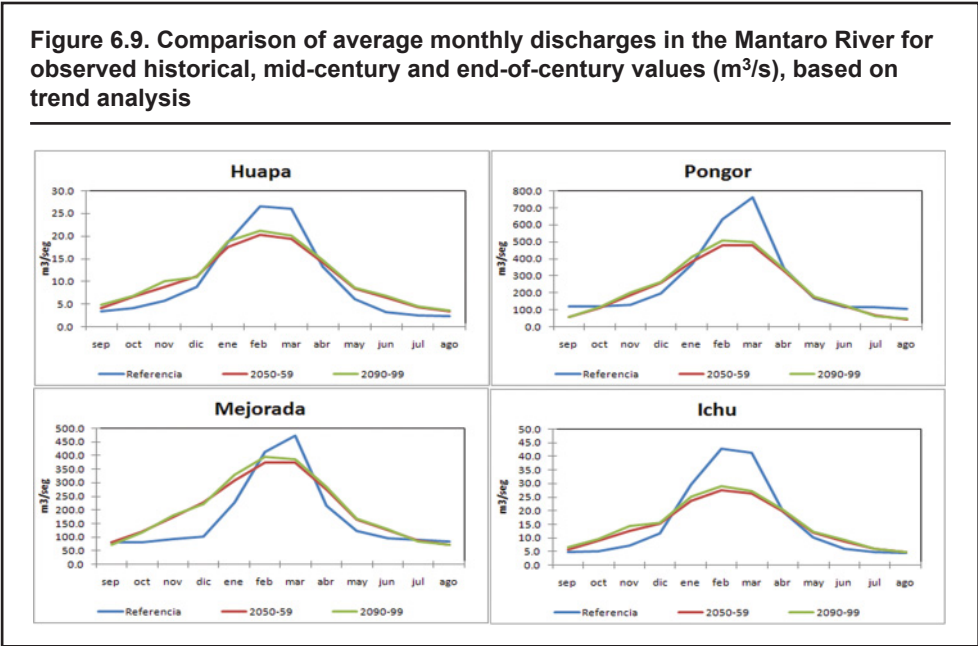
Source: Figure generated for the report by IRD and SEI.

Figure 6.10. Hydrological response by mid-century: Mantaro River Basin monthly discharges (cms)
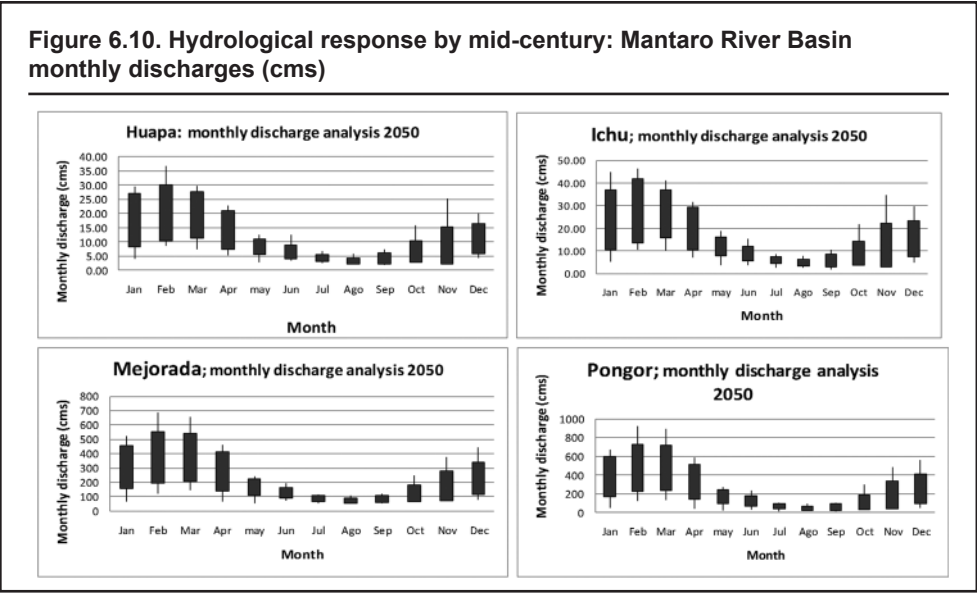
Source: Authors.

tion during the wet months. In Mejorada, the low-flow period is considerably reduced, with runoff increasing in November, December, and January and decreasing in the high-peak periods of February and March (Figure 6.10).

For the same climate scenario, the modeled hydrological changes along the Rímac River have different trends. As illustrated in Figure 6.11 for the Chosica and Surco stations, water availability is expected to increase, particularly with higher discharges in

Figure 6.11. Comparison of average monthly discharges in the Rímac River for observed historical (blue) and projected mid- (red) and end-of-century (green) values (m³/s), based on trend analysis

Source: Figure generated for the report by IRD and SEI.

Figure 6.12. Hydrological response by mid-century: Rímac River Basin monthly discharges (mcs)
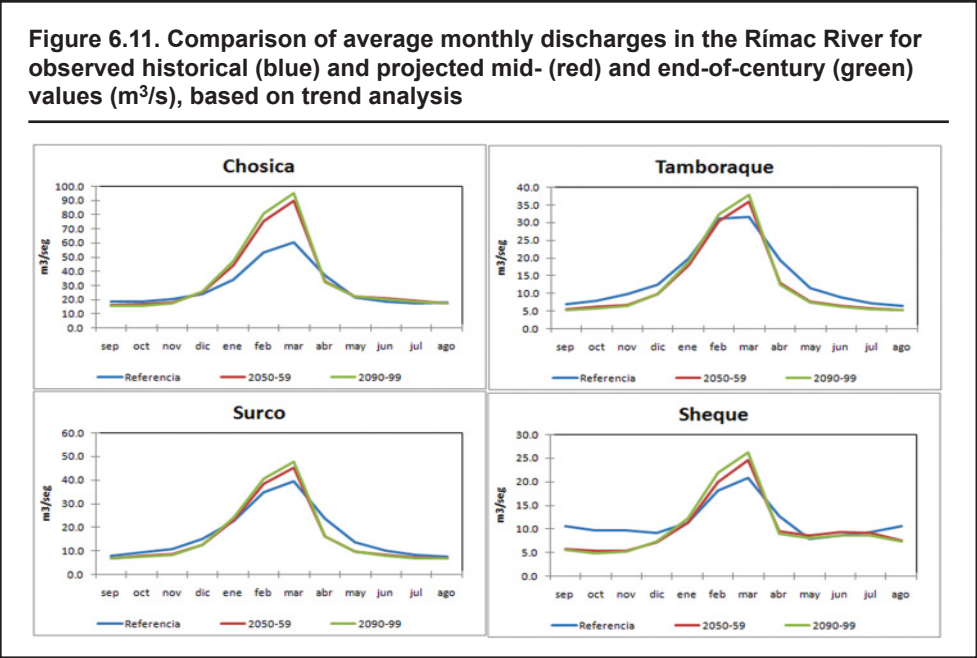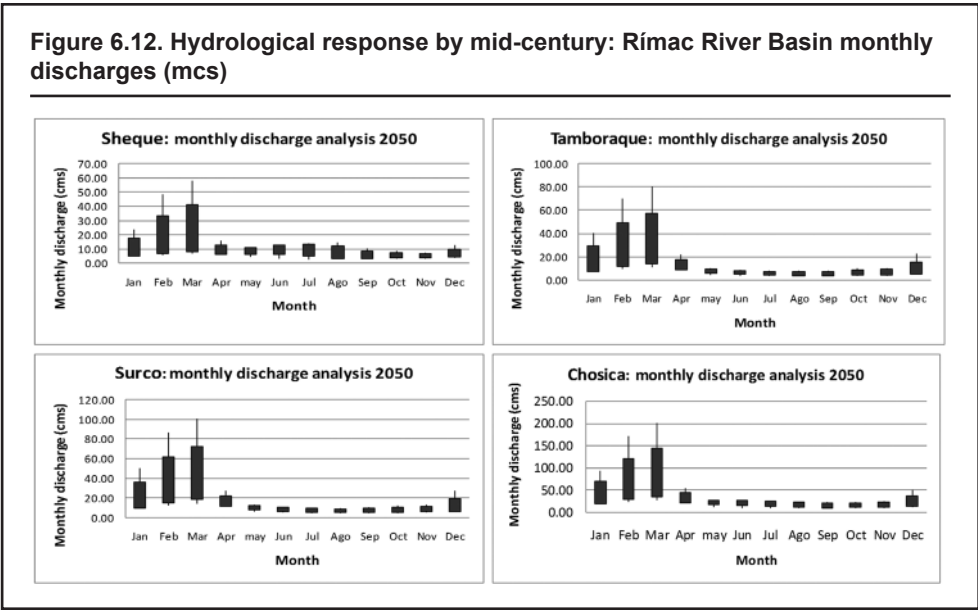
Source: Authors.

February and March, while there will be little or no reduction in the dry months from June to November. More water is welcome, especially for hydropower production, agriculture, and water supply to Lima. On the other hand, excessive runoff might lead to flooding, which could affect the most vulnerable inhabitants of Lima. Higher discharges imply increased sediment transport capacity in the stream. Such changes in sediment balances could enhance climate risks (Figure 6.12).

Results

The application of the methodology in the Santa, Rímac and Mantaro River Basins suggests that the hydrology model is appropriate. The combined expertise of glaciologists, hydrologists, researchers, and practitioners was needed to produce a module that provides good results in the sites studied.

   Although the purpose of this study is not to produce an assessment of climate change in the selected basins, the analysis of the data provides useful results. First, the assessment exemplifies the complexity of assessing the hydrological response to climate change in mountainous terrains such as those found in Peru. Each basin needs to be studied in detail. It is recommended that detailed sensitivity analyses on the hydrological and climate components be conducted to gain reliability in the results and possible recommendations.

   To illustrate the approach developed and the usefulness of the data generated under the selected climate scenarios, the following results are presented:

   ■   When looking at the changes in river runoffs in the country as whole, the MRI-AGCM3.1 model estimates a significant reduction in net discharges on the southern coast and in the northeastern part of the country. Some areas in the Andean region might experience increased runoff, while others might face a

reduction. No generalization for local levels can be made based on the use of this model. This observation highlights that: first, it is not possible to generalize what the impacts of climate change would be in areas with complex terrain; and second, rainfall runoff tools incorporating the dynamic response of glaciers and high mountain wetlands are needed to assess the impacts of global warming at the river basin resolution level.

■ The simulated flows for the 2050–2059 period show a reduction in their peaks for all the monitoring stations on the Mantaro River. Net increments in water availability are projected in the Rímac River. Monthly discharges at the La Balsa station on the Santa River are expected to decrease year-round in comparison to observed historical values. The mean annual discharge could be reduced by 21 percent by mid-century.

■ Glacier loss is expected to be significant during the period of analysis.

■ Simulated low water flows are expected to increase in the Mantaro River. There are no significant changes expected in low water flows in the Rímac River, with the exception of Sheque during September, October, and November when the flows at this station are expected to be lower. In the Santa River, low flows are estimated to decrease by around 28 percent, which raises immediate concerns due to their impact on energy and agricultural production.

■ No tipping point was observed for the loss of glacier runoffs.

Notes

1. GRiverT: Global Discharge model using Total Runoff Integrating Pathways (TRIP), the 0.5 x 0.5 version with global data for discharge channels (Nohara et al. 2006). The river runoff assessed in the land surface model is horizontally interpolated as external input data into the TRIP grid so that the flow volume is saved. A similar analysis made for the Magdalena River in Colombia has recently been published (Nakaegawa and Vergara 2010).

2. Marginally warmer conditions: a 0.5°C increase in temperature and a 15 percent increase in precipitation; and much warmer conditions: a 2°C increase in temperature and a 10 percent decrease in precipitation.

3. These conditions are developed in Chapter 3, section titled "Ensembles to Simulate Future Climate."

4. As the climate warms, less of the precipitation falls as snow and more falls as rain on snow- and ice-covered peaks. This produces reductions in the accumulation of snow during the wet season and in the melting of snow and ice during the dry season. Since snowmelt is an important water contribution during the dry season, there is concern that global warming will reduce the supply of water during the dry season in mountainous regions in many parts of the world (Vergara et al. 2009; Leung and Ghan 1999; Ghan and Shippert 2006).

5. Although the ensemble approach and the use of extreme climate scenarios reduce uncertainty, they do not provide guidance on the relative probabilities of such scenarios or their consistency with observed trends. Such scenarios represent extreme conditions at the high and low ends. The concurrence of this finding for the two extreme scenarios strengthens the conceptual argument that the loss of glaciers reduces the natural regulation of the water cycle, increasing flows in the wet season and reducing discharges in dry months.

Conclusions

This report describes a climate and hydrological analysis used to simulate current and projected future climate conditions in mountain regions and estimate the hydrological response at regional and basin levels. The tools used were applied to Peru but could be similarly deployed for other mountain basins to simulate current and predict future impacts of climate on hydrology.

General Conclusions

General context. This study is intended to provide guidance and options to explore the hydrological response to global climate change in mountainous landscapes. The guidance can be summarized as follows:

a. Define planning climate scenarios on the basis of existing climate data, using available modeling techniques. "Planning climate scenarios" are defined as future climate conditions at a scale and resolution appropriate for water resources planning.

b. Define criteria to judge the projections provided by the available techniques in order to define future climate scenarios.

c. Identify results (measurable, independent, simple) that characterize the most relevant properties of the criteria. Run several methods and calculate the adopted indicators.

d. Select likely climate scenarios for the next 30 to 40 years, the planning horizon for large-scale water resources infrastructure.[1]

e. Select hydrological planning tools suitable to the problem at hand. If required, complement the tools with new elements to incorporate the dynamic climate nature of the planning context. Use the best available information to calibrate and validate the hydrological model.[2]

f. Run the hydrological planning tools with the selected future planning climate scenarios and with the description of current climate for comparison purposes.

g. Conduct a sensitivity analysis.

h. Use the generated information as the basis for planning and decision making.

In this study, no planning or operational decision was incorporated in the analysis.

The use of outputs from large global climate change models. The use of GCM provides useful data, but at this time tits direct application in planning exercises is limited by various factors including coarse resolution, level of uncertainty, and the challenges posed by complex mountainous terrains. The main limitations are:

- Model uncertainty.
- Emission paths.
- Model resolution.
- Model independence.
- Calibration and verification problems.
- Inability to accommodate the complex atmospheric process in mountain terrains.

Appropriateness of GCM. The suggested criteria by which to judge the usefulness of outputs and associated downscaling techniques are:

- Ability to reproduce average annual distribution of precipitation, and its spatial distribution in the country.
- Ability to reproduce the annual trend for key climate variables (precipitation in the study cases) as estimated for a reference period.
- Ability to simulate the trends for hydrological seasons of interest (monthly or seasonal precipitation) for climate variables of interest, estimated for the reference period.

GCM outputs that best comply with these criteria are the best options for building planning climate scenarios as inputs for assessing future expected water availability at a basin level.

Trend analysis. The study identified trend analysis as a powerful method to produce "climate planning scenarios." As a general rule, long-term observations are preferable to short ones, but analysis beyond 30 years might not be very useful when trying to accommodate the dynamics of current changes driven by accelerating climate change. As illustrated in the analysis conducted for the Mantaro River Basin, a cluster of weather stations with similar trends does increase the reliability of the results. If such consistency is identified, the resulting trend should be incorporated into the analysis of future climate scenarios. Trend analysis builds on the hypothesis that the observed linear trend is likely to continue (without change) in the immediate future. The linear extrapolation of the observed trends was used in this study to define future planning climate scenarios. It is recommended that this be followed by a thorough sensitivity analysis. There is not enough information to estimate other than linear trends.

Hydrological modeling. Many existing tools and hydrological models continue to be useful in short-term water resources planning and operations but many require adjustments to reflect the dynamics of climate change over longer periods. The model selected is by no means unique. The WEAP system is a flexible, user-friendly software with good ability to minimize the demand for data, a characteristic very much appreciated in Peru and other developing nations.

Complementing the hydrological tools. A glacier dynamics module and a páramo routine were developed to complement the flexibility available in the WEAP system. The field of glacier dynamics is new to hydrology and is a consequence of the new paradigm shift. The hypothesis of a steady-state equilibrium for the glacier component is no longer valid. The module developed offers significant flexibility and could be replicated for other case studies.

Calibration and validation challenges. Once a hydrological model is selected, its use in a particular application goes through several stages from data collection, verification, and analysis, to calibration, validation and its use in the decision-making process. Calibration is the art of selecting model parameters congruent with field observations and recorded data that provide a good fit between the simulated and observed data. Such analysis ought to merit special consideration because the expected results depend on the selection of these parameters. Once the model is properly calibrated, the validation runs (with data not used in the calibration) should support the hypothesis made. If the validated results show poor fit, additional calibration work is called for, or a different hydrological tools should be used.

Multidisciplinarity. The assessment of the impacts of climate change on mountain hydrology involved a large group of researchers and practitioners, a condition that is common to this type of analysis and that accentuates the complexity of this endeavor. Atmospheric physicists, ocean modelers, mathematicians and statisticians, hydrologists and water resources experts joined forces with glaciologists, high mountain practitioners, geographers, foresters, and civil engineers in completing this task. This multidisciplinary characteristic is highlighted to emphasize to countries and development organizations the need to build teams to deal with emerging, challenging development issues. It also serves to indicate that the field of climate change is open to and requires the participation of many experts.

Some results. The followed approach produced useful insights into the hydrological response to climate change in three watersheds in Peru. In the Santa River Basin, it is estimated that climate change will bring a considerable reduction in water availability; in the Rímac Basin, that was not the case. In the lower reaches of the Mantaro River Basin, a change in the hydrography is projected. It includes very high discharges in the wet months and increasing water availability in otherwise dry months.

Limitations. There are limitations to keep in mind in the analysis of results. These limitations are:

- Deficiencies in data collection. Data related to hydrological soil characteristics were not collected, thus reducing the model's ability to account for variations in soil storage capabilities while constraining better model performance statistics.
- Calibration. More work is recommended before the results are used in the decision-making process. Greater flexibility should be allowed in the spatial variation of the hydrological parameters used.
- Planning climate scenarios. More research is needed: (i) to assess the variability of key climate variables and their trends; (ii) to assess the validity of the linear extrapolation of observed trends; and (iii) to develop improved statistical tools to assess the reliability of individual trends as well as in clusters.
- Need for sensitivity analysis. A thorough sensitivity analysis is strongly recommended in order to analyze the expected variability of the results. This sensitivity should span the climate planning scenarios to the land use changes driven by changes in precipitation and temperature. For purposes of supporting decision-making processes, the sensitivity analysis should include socioeconomic considerations as well.

Moving Forward

The study met the objective of developing a methodology to assess the hydrological response to global climate change in tropical mountain basins, but data availability remains a challenge. Gathering the required data may require a large share of the resources demanded by this type of analysis. Calibration of the models should provide good to very good model performance indicators. Also, a thorough sensitivity analysis is strongly recommended.

The study looked at the hydrological cycle from the supply side; only water availability and variability are considered. The work should be expanded to analyze the social and economic consequences associated with hydrological changes. In order to assess the economic consequence of climate change through water availability, the work should be complemented by an analysis of the economic consequences for the energy, agricultural and water supply sectors. Other socioeconomic impacts could also be explored.

Lessons Learned

Need for criteria to assess the suitability of results from GCM. How to select among the many models available? Should an ensemble of GCMs be used? Which models should be incorporated in the ensemble? How to assess the ability of the models to reproduce climate observations? How to weigh the different models? For practical purposes, criteria by which to judge model suitability should be clearly defined. The criteria should respond to the problem at hand (a function of the results sought) and the socioeconomic sensitivity to changes in the selected criteria.

A bag of tools instead of a single silver bullet. It may be better to use complementary tools, and in some instances to mix methods that appear to be competing, in order to produce similar results. As indicated in the climate component, the various methods used complement and enrich the results, reduce uncertainty, allow risk analysis and provide the basis to conduct sensitivity analyses.

Limitations when interpreting the results and the need for sensibility analysis. Good practice dictates that model limitations should be well understood by model users and should be an integral part of the analysis of results. It is recommended that a list of the limitations of the methodology/approach used and of each tool utilized be prepared. To cope with the uncertainties associated with these planning exercises, it is recommended that a thorough sensitivity analysis be conducted.

Conclusion

On the basis of the results obtained, **it seems that the combination of the climate and hydrology analysis can simulate current conditions at a regional and basin level and project future hydrological conditions**. The methods employed could be of use to predict future impacts of climate change on hydrology for other mountain basins in the Andes.

Notes

1. The reference to hydraulic infrastructure highlights the fact the climate change is having and will have great impact on the design and operation of water related works.
2. It is recommended that high standards be maintained in the calibration and verification tasks for the results to capture the basic hydrological response to existing climate conditions.

References

Aceituno, P. 1988. On the functioning of the southern oscillation in the South American sector, Part I: Surface climate. *Monthly Weather Review*. 116: 505-524.

Ames, A., S. Dolores, A. Valvedere, P. Evangelista, D. Corcino, W. Ganvini, J. Zúñiga, and V. Gomez. 1989. Inventario de glaciares del Perú. Fuente: Fotografias aeras de 1962, 1963, 1970, Part 1. Huaraz, Peru, Hidrandina S.A.

Bahr, D. B., M. F. Meier, and S. D. Peckham. 1997. The physical basis of glacier volume-area scaling. *J. Geophys. Res.* 102 (B9): 20355–20362.

Benestad R. E. 2004. Empirical-statistical downscaling in climate modeling. *Eos. Trans. Amer. Geophys. Union* 85: 417–422.

Beven, K. J., and M. J. Kirby. 1979. A physically based variable contributing area model of basin hydrology. *Hydrologic Sciences Bulletin* 24.

Bradley, R. S., M. Vuille, H. F. Diaz, and W. Vergara. 2006. Climate change: threats to water supplies in the tropical Andes. *Science* 312: 1755–1756.

Bradley, R. S., F. T. Keimig, H. F. Diaz, and D. R. Hardy. 2009. Recent changes in freezing level heights in the tropics with implications for the deglacierization of high mountain regions. *Geophys Res Lett* 36: L17701.

Brunet-Moret, Y. 1979. Homogénéisation des precipitations. Cahier ORSTOM, Série *Hydrologie* 16: 3-4.

Bury, J., B. G. Mark, J. M. McKenzie, A. French, M. Baraer, K. I. Huh, M. A. Z. Luyo, and R. J. G. López. 2010. Glacier recession and human vulnerability in the Yanamarey watershed of the Cordillera Blanca, Peru. *Climatic Change*. DOI 10.1007/s10584-010-9870-1.

Buytaert, W., B. De Bievre, G. Wysuere, and J. Deckers. 2004. The use of the linear reservoir concept to quantify the impact of changes in land use on the hydrology of catchments in the Andes. *Hydrology and Earth System Sciences* 8: 108–114.

Buytaert, W., R. Celleri, and L. Timbe. 2009. Predicting climate change impacts on water resources in the tropical Andes: Effects of GCM uncertainty. *Geophys. Res. Lett*. 36.

COES. 2009. Estadística Diaria de Operaciones. Comité de Operación Económica del Sistema Interconectado Nacional. Available at www.coes.org.pe/coes/Estadistica/Diario.asp.

CONAM. 2001. National communication of Peru to the United Nations Framework Convention on Climate Change (UNFCCC). National Council on the Environment, Lima.

Condom, T., A. Coudrain, S. J. E., and T. Sylvain. 2007. Computation of the space and time evolution of equilibrium-line altitudes on Andean glaciers (10oN-55oS). *Global and Planetary Change* 59: 189–202.

Croke, B. F. W., and A. J. Jakeman. 2004. A catchment moisture deficit module for the IHACRES rainfall-runoff model. *Environmental Modeling & Software* 19: 1–5.

Cubasch, U., J. Waszkewitz, G. Hegerl and J. Perlwitz. 1995. Regional climate changes as simulated in time-slice experiments. *Climatic Change* 31: 273–304.

Díaz-Granados, M. A., J. D. Navarrete González, and T. Suárez Lopez. 2005. Páramos: Hidrosistemas Sensibles. Revista de Ingeniería—Universidad de los Andes 22.

Dyurgerov, M. 2003. Mountain and subpolar glaciers show an increase in sensitivity to climate warming and intensification of the water cycle. *J Hydrol* 282: 164–176.

Escobar, M., T. Condom, W. Suarez, D. Purkey, J. C. Pouget, and C. Ramos. 2008. Construcción del Modelo WEAP del Río Santa. Report produced for the World Bank as a background for this report.

Favier, V., P. Wagnon and P. Ribstein. 2004. Glaciers of the outer and inner tropics: A different behaviour but a common response to climatic forcing. *Geophysical Research Letters* 31.

Francou, B., M. Vuille, P. Wagnon, J. Mendoza, and J.-E. Sicart. 2003. Tropical climate change recorded by a glacier in the central Andes during the last decades of the twentieth century. Chacaltaya, Bolivia, 16_S. *J. Geophys. Res*. 108(D5): 4154

Francou, B., and A. Coudrain. 2005. Glacier shrinkage and water resources in the Andes. *EOS Trans Am Geophys Union* 86: 415.

Frei C., R. Schöll, S. Fukutome, J. Schmidli, and P. L. Vidale. 2006. Future change of precipitation extremes in Europe: Intercomparison of scenarios from regional climate models. *J. Geophys. Res.* 111, D06105, doi:10.1029/2005JD005965.

Garreaud, R., M. Vuille, and A. Clement. 2003. The climate of the Altiplano: Observed current conditions and mechanisms of past changes. *Palaeogeogr., Palaeoclimatol., Palaeoecol.* 194: 5–22.

Ghan, S. J. 1992. The GCM credibility gap. Editorial, *Clim Change* 21: 345–346.

Ghan, S. J., and T. Shippert. 2006. Physically-based global downscaling climate change projections for a full century. *J. Clim*. 19: 1589–1604.

Ghan, S. J., and T. Shippert. 2009. Final report as a contribution to the Assessing the impacts of climate change on mountain hydrology: Development of a methodology through a case study in Peru. Report produced by Battelle, Pacific Northwest Division for the World Bank as a background for this report. May 10, 2009.

Ghan, S. J., X. Bian, A. G. Hunt, and A. Coleman. 2002. The thermodynamic influence of subgrid orography in a global climate model. *Climate Dynamics* 20: 31–440. DOI: 10.1007/s00382-002-0257-5.

Ghan, S. J., T. Shippert, and J. Fox. 2006. Physically-based global downscaling: Regional evaluation. *J. Climate* 19: 429–445.

Giorgi, F. 1990. Simulation of regional climate using a limited area model nested in a general circulation model. *J Clim* 3: 941–963.

Giorgi, F., and L. O. Mearns. 1999. Introduction to special section: regional climate modeling revisited. *J Geophys Res 104*: 6335–6352.

Gyalistras, D., C. Schär, H. C. Davies, and H. Wanner. 1998. Future Alpine climate. In: *Views from the Alps. Regional perspectives on climate change*. P. Cebon, U. Dahinden, H. C. Davies, D. Imboden, and C. C. Jaeger, eds. Massachusetts: MIT Press, Cambridge, pp 171–223.

Hiez, G. 1977. L'homogénéité des données pluviométriques. Cahier ORTSTOM, *série Hydrologie*, 14:129–172.

Hock, R. 2003. Temperature index melt modelling in mountain areas. *Journal of Hydrology* 282: 104–115.

Hock, R. 2005. Glacier melt: A review of processes and their modelling. *Progress in Physical Geography* 29: 362–391.

IARU. 2009. Rising sea levels set to have major impacts around the world. In *Conference on Climate Change: global risks, challenges and decisions*. March 10–12, International Alliance of Research Universities, University of Copenhagen, Copenhagen.

IGP. 2005a. Diagnóstico de la cuenca del río Mantaro bajo la visión de cambio climático. Fondo Editorial CONAM, Lima, Perú.

IGP. 2005b. Vulnerabilitdad y adaptación al cambio climático en la cuenca del río Mantaro. Fondo Editorial CONAM, Lima, Perú.

IPCC. 2000. IPCC Special Report on Emissions Scenarios. Nebojsa Nakicenovic and Rob Swart, eds. Cambridge, UK: Cambridge University Press, pp 570. http://www.ipcc.ch/ipccreports/sres/emission/index.php?idp=0.

IPCC. 2005. Guidance notes for lead authors of the IPCC Fourth Assessment Report on Addressing Uncertainties.

IPCC. 2007a. Climate change 2007: The physical science basis. Contribution of Working Group I to the Fourth Assessment Report of the Intergovernmental Panel on Climate Change. S. Solomon, D. Qin, M. Manning, Z. Chen, M. Marquis, K. B. Averyt, M. Tignor, and H. L. Miller, eds. Cambridge, UK, and New York, NY, USA: Cambridge University Press.

IPCC. 2007b. Climate Change 2007: Synthesis Report. Contribution of Working Groups I, II and III to the Fourth Assessment Report of the Intergovernmental Panel on Climate Change [Core Writing Team, R. K. Pachauri and A. Reisinger, eds.]. Geneva, Switzerland: IPCC, 104 pp.

IPCC. 2007c. Climate change 2007: Impacts, adaptation and vulnerability. Contribution of Working Group II to the Fourth Assessment Report of the Intergovernmental Panel on Climate Change. M. L. Parry, O. F. Canziani, J. P. Palutikof, P. J. van der Linden, and C. E. Hanson, eds. Cambridge, UK: Cambridge University Press, 976 pp.

IRD. 2009. Final report as a contribution to: Assessing the impacts of climate change on mountain hydrology: Development of a methodology through a case study in Peru. Report produced by Institut de Recherche pour le Développement (IRD) for the World Bank as background for this report.

Johannesson, T., O. Sigurdsson, T. Laumann, and M. Kennett. 1995. Degree-day glacier mass-balance modeling with applications to glaciers in Iceland, Norway and Greenland. *J. Glaciol.* 41(138): 345–358.

Johnson, A. M. 1976. Climate of Peru, Bolivia, and Ecuador. In *World Survey of Climatology*, vol. 12, W. Schwerdtfeger, ed. New York: Elsevier, 147–218.

Juen, I. 2006. Glacier mass balance and runoff in the tropical Cordillera Blanca, Perú. Institute of Geography. Innsbruck, University of Innsbruck: 194.

Juen, I, G. Kaser, and C. Georges. 2007. Modelling observed and future runoff from a glacierized tropical catchment (Cordillera Blanca, Peru). *Glob Planet Change* 59: 37–48.

Kaser, G., and H. Osmaston. 2002. *Tropical Glaciers*. New York: Cambridge University Press.

Kayastha, R. B., Y. Ageta, and M. Nakawo. 2000a. Positive degree-day factors for ablation on glaciers in the Nepalese Himalayas: case study on glacier AX010 in Shoron Himal, Nepal. *Bull. Glaciol. Res.* 17: 1–10.

Kayastha, R. B., 2001. Study of glacier ablation in the Nepalese Himalayas by the energy balance model and positive degree-day method. PhD Thesis. Graduate School of Science, Nagoya University, 95 pp.

Klein, A., and B. Isacks. 1998. Alpine glacial geomorphological studies in the Central Andes using Landsat thematic mapper images. *Glacial Geology and Geomorphology.* rp01/1998 http://ggg.qub.ac.uk/papers/full/1998/rp011998/rp011901.htm.

Klok, E. J., K. Jasper, K. P. Roelofsma, J. Gurtz, and A. Badoux. 2001. Distributed hydrological modelling of a heavily glaciated Alpine river basin. *Hydrological Sciences Journal* 46: 553–570.

Knutti, R., T. F. Stocker, F. Joos, and G. K. Plattner. 2002. Constraints on radiative forcing and future climate change from observations and climate model ensembles. *Nature* 416: 719–723.

Kuzmin, P. P. 1961. Melting of snow cover. Israel Program for Scientific Translation. 290 pp.

Lang, H., and L. Braun. 1990. On the information content of air temperature in the context of snow melt estimation. *International association of hydrological sciences* 190: 347–354.

Leung, L. R., and S. J. Ghan. 1995. A subgrid parametrization of orographic precipitation. *Theor Appl Climatol* 52: 95–118.

Leung, L., and S. Ghan. 1998. Parameterizing subgrid orographic precipitation and surface cover in climate models. *Mon. Wea. Rev.* 126: 3271–3291.

Leung, L., and S. Ghan. 1999. Pacific Northwest climate sensitivity by a regional climate model driven by a GCM. Part II: 2 x CO_2 Simulations. *J. Climate* 12: 2031–2053.

Leung, L. R., and Y. Qian. 2003. The sensitivity of precipitation and snowpack simulations to model resolution via nesting in regions of complex terrain. *J. Hydrometeorol.* 6: 1025-1043.

Mark, B. G., and G. O. Selzer. 2003. Evaluation of recent glacier recession in the Cordillera Blanca, Peru (AD 1962-1999): spatial distribution of mass loss and climatic forcing. *Quat Sci Rev* 24: 2265–2280.

Mark, B. G., J. Bury, J. M. McKenzie, A. French, and M. Baraer. 2010. Climate change and tropical Andean glacier recession: Evaluating hydrologic changes and livelihood vulnerability in the Cordillera Blanca, Peru. *Annals of Association of American Geographers* 100(4): 794–805. Published by Taylor & Francis, LLC.

Martinec, J., and A. Rango. 1986. Parameter values for snowmelt runoff modelling. *Journal of Hydrology* 84: 197–219.

Martínez, A. G., E. Núñez, Y. Silva, K. Takahashi, G. Transmonte, K. Moquera, and P. Lagos. 2006. Vulnerability and adaptation to climate change in the Peruvian central Andes: Results of a pilot study. In *International Conference on Southern Hemisphere Meteorology and Oceanography (ICSHMO), 8, 2006.* Foz do Iguaçu. Proceedings, São José dos Campos, INPE, CD-ROM ISBN 85-17-00023-4, 297-305.

Maurer, E. P., and H. G. Hidalgo. 2008. Utility of daily vs. monthly large-scale climate data: an intercomparison of two statistical downscaling methods. *Hydrology and Earth System Sciences* 12: 551–563.

May, W., and E. Roeckner. 2001. A time-slice experiment with the ECHAM4 AGCM at high resolution. The impact of horizontal resolution on annual mean climate change. *Clim. Dyn*. 17: 407–420.

Meehl, G. A., W. M. Washington, B. D. Santer, W. D. Collins, J. M. Arblaster, A. Hu, D. M. Lawrence, H. Teng, L. E. Buja, and W. G. Strand. 2006. Climate change projections for the twenty-first century and climate change commitment in the CCSM3. *J. Climate* 19: 2597–2616.

Miura, H., H. Tomita, T. Nasuno, S. Iga, M. Satoh, and T. Matsuno. 2005. A climate sensitivity test using a global cloud resolving model under an aqua planet condition. *Geophys. Res. Lett.* 32: L19717, doi:10.1029/2005GL023672.

Mizuta R, K. Oouchi, H. Yoshimura, A. Noda, K. Katayama, S. Yukimoto, M. Hosaka, S. Kusunoki, H. Kawai, and M. Nakagawa. 2006. 20-km-mesh global climate simulations using JMA-GSM model—mean climate states. *Journal of the Meteorological Society of Japan* 84: 165–185.

Murphy, J. M. 1999. An evaluation of statistical and dynamical techniques for downscaling local climate. *J Clim* 12: 2256–2284.

Murphy, J. M. 2000. Predictions of climate change over Europe using statistical and dynamical downscaling techniques. *Int J Climatol* 20: 489–501.

Nakaegawa, T., and W. Vergara, 2006. First projection of climatological mean river discharges in the Magdalena River Basin, Colombia, in a changing climate during the 21st century. *Hydrological Research Letters* 4: 50–54 (2010). Published online in J-STAGE (www.jstage.jst.go.jp/browse/HRL). DOI: 10.3178/HRL.4.50.

New, M., D. Lister, M. Hulme, and I. Makin. 2002. A high resolution data set of surface climate over global land areas. *Climate Res.* 21: 1–25.

Nohara, D., M. Hosaka, A. Kitoh, and T. Oki. 2006. Impact of climate change on river runoff using multi-model ensemble. *J. Hydrometerol.* 7: 1076–1089.

Pouyaud, B., M. Zapata, J. Yerren, J. Gómez, G. Rosas, W. Suárez, and P. Ribstein. 2005. Devenir des ressources en eau glaciaire de la Cordillère Blanche. *Hydrological Sciences Journal* 50: 999–1022.

Qian, Y., S. J. Ghan, and L. R. Leung. 2009. Downscaling hydroclimatic changes over the Western U.S. based on CAM subgrid scheme and WRF regional climate simulations. *Int. J. Climatology*, DOI: 10.1002/joc.1928.

Racoviteanu, A., Y. Arnaud, and M. Williams, 2008. Decadal changes in glacier parameters in Cordillera Blanca, Peru derived from remote sensing. *J Glaciol* 54: 499–510.

Ruiz, D., W. Vergara, A. Deeb, and D. G. Martinson. 2010. Trends, stability and stress in the Colombian central Andes. Not published.

Salathé, E. P. Jr., P. W. Mote, and M. W. Wiley. 2007. Considerations for selecting downscaling methods for integrated assessments of climate change impacts. *Int. J. of Climatology* 27: 1611–1621.

Schaefli, B., B. Hingray, i. M. Niggl, and A. Musy. 2005. A conceptual glaciohydrological model for high mountainous catchments. *Hydrology and Earth System Sciences* 9: 95–109.

SEI. 2009. Final report as a contribution to Assessing the impacts of climate change on mountain hydrology: Development of a methodology through a case study in Peru. Report produced by Stockholm Environment Institute (SEI) for the World Bank as a background for this report.

SENAMHI (Servicio Nacional de Meteorología e Hidrología). 2007. Escenarios de cambio climático en la cuenca del Río Mantaro para el año 2100. Centro de Predicción Numérica—CPN.

SENAMHI. 2009a. Climate scenarios for the Santa River Basin to 2030. In *Second National Communication on Climate* Change.

SENAMHI. 2009b. Climate scenarios for Peru to 2030. In *Second National Communication on Climate* Change. Prepared with the collaboration of the Ministry of Environment and UNDP.

Silva, Y., K. Takahashi, N. Cruz, G. Transmonte, K. Mosquera, E. Nickl, R. Chavez, B. Segura, and P. Lagos, 2006. Variability and climate change in the Mantaro River basin, Central Peruvian Andes. In *International Conference on Southern Hemisphere Meteorology and Oceanography (ICSHMO), 8, 2006.* Foz do Iguaçu. Proceedings, São José dos Campos, INPE, CD-ROM ISBN 85-17-00023-4, 407-419.

Silva, Y., K. Takahashi, and R. Chavez, 2007. Dry and wet rainy seasons in the Mantaro river basin (Central Peruvian Andes). *Adv. Geosci* 14: 1–4. Published by Copernicus Publications on behalf of the European Geosciences Union.

Singh, P., N. Kumar, and M. Arora. 2000. Degree-day factors for snow and ice for Dokriani Glacier, Garhwal Himalayas. *Journal of Hydrology* 235: 1–11.

Smith, C. A., and P. Sardeshmukh. 2000. The effect of ENSO on the intraseasonal variance of surface temperature in winter. *International J. of Climatology* 20: 1543–1557.

Stone, D. A., and R. Knutti. 2010. Weather and climate. In: *Climate Change and Water Resources Modelling*, C. F. Fung and A. Lopez, eds. In press.

von Storch, H. 1995. Inconsistencies at the interface of climate impact studies and global climate research. *Meteorol* Z 4 NF: 72–80.

Suarez, W. 2007. Le bassin versant du fleuve Santa (Andes du Pérou) : dynamique des écoulements en contexte glacio-pluvio-nival. Doctoral Thesis, Université Montpellier 2, Montpellier.

Suárez, W., P. Chevallier, B. Pouyaud, and P. López. 2008. Modeling the water balance in the glacierized Parón lake (White Cordillera, Peru). *Hydrological Sciences* 53.

Thomson, M. C, F. J. Doblas-Reyes, S. J. Mason, R. Hagedorn, S. J. Connor, T. Phindela, A. P. Morse, and T. N. Palmer. 2006. Malaria early warnings based on seasonal climate forecasts from multi-model ensembles. *Nature* 439: 576–579.

Urrutia, R., and M. Vuille. 2009. Climate change projections for the tropical Andes using a regional climate model: temperature and precipitation simulations for the end of the 21st century. *J. Geophys. Res*. 114: 1823–1825, 1828, 1832, 1837. D02108, doi:10.1029/2008JD011021.

Vauchel, P. 2005. HYDRACESS: Software for management and processing of hydro-meteorological data. Available at www.mpl.ird.fr/hybam/outils/logiciels.htm.

Vergara, W., A. Deeb, A. Valencia, R. S. Bradley, B. Francou, S. Hauessling, A. Grunwaldt, and A. Zarzar. 2007. Economic consequences of rapid glacier retreat in the Andes. *Journal of the American Geophysical Union*, *EOS* 88(25), June.

Vergara, W., N. Toba, D. Mira-Salama, and A. Deeb. 2009. The consequences of climate-induced coral loss in the Caribbean by 2050–80. In *Environment Matters at the World Bank. Valuing Coastal and Marine Ecosystem Services.* The World Bank, Washington, DC.

Vergara, W., and S. Scholz, eds. 2011. Assessment of the risk of Amazon Dieback. World Bank, Washington, DC.

Vicuña, S., R. Garreaud, and J. McPhee. 2010. Climate change impacts on the hydrology of a snowmelt driven basin in semiarid Chile. *Climatic Change*. DOI 10.1007/s10584-010-9888-4.

Vincent, L. A., T. C. Peterson, V. R. Barros, M. B. Marino, M. Rusticucci, G. Carrasco, E. Ramirez, L. M. Alves, T. Ambrizzi, M. A. Berlato, A. M. Grimm, J. A. Marengo, L. Molion, D. F. Moncunill, E. Rebello, Y. M. Anunciacäo, J. Quintana, J. L. Santos, J. Baez, G. Coronel, J. Garcia, I. Trebejo, M. Bidegain, M. R. Haylock, and D. Karoly. 2005. Observed trends in indices of daily temperature extremes in South America 1960–2000. *J. Climate* 18: 5011–5023.

Vuille, M., and R. S. Bradley. 2000. Mean annual temperature trends and their vertical structure in the tropical Andes. *Geophys Res Lett* 27: 3885–3888.

Vuille, M., R. S. Bradley, B. Francou, G. Kaser, and B. G. Mark. 2007. Climate change in tropical Andes. Impacts and consequences for glaciations and water resources. Part I: The scientific basis. A report for CONAM and the World Bank. Amherst, Massachusetts, 24 January, 2007.

Vuille, M., B. Francou, P. Wagnon, I. Juen, G. Kaser, B. G. Mark, and R. S. Bradley. 2008. Climate change and tropical Andean glaciers: past, present and future. *Earth-Sci Rev* 89: 79–96.

Wilby, R. L., and T. M. L. Wigley. 1997. Downscaling general circulation model output: A review of methods and limitations. *Prog. Phys. Geogr.* 21: 530–548.

Wood A. W., L. R. Leung, V. Sridhar, and D. P. Lettenmaier. 2004. Hydrologic implications of dynamical and statistical approaches to downscaling climate model outputs. *Climate Change* 62: 189–216.

Yates, D., J. Sieber, D. Purkey, and A. Huber-Lee. 2005. WEAP21: A demand-, priority-, and preference-driven water planning model. Part 1: Model characteristics. *Water International* 30:487–500.

Yun, X., B. Y. Liu, and M. A. Nearing. 2002. A practical threshold for separating erosive and non-erosive storms. *Transactions of the American Society of Agricultural Engineers* 45(6): 1843–1847.

Zhang, Y., S. Liu, and Y. Ding. 2007. Glacier meltwater and runoff modelling, Keqicar Baqi glacier, southwestern Tien Shan, China. *Journal of Glaciology* 53: 91–99.

Appendixes

Appendix 1. IPCC—Emissions Scenarios

In 1992, for the first time the IPCC released emissions scenarios for use in driving global circulation models to develop climate change scenarios.

In 1996, the IPCC decided to develop a new set of emissions scenarios (the Special Report on Emissions Scenarios, or SRES), which provided input to the IPCC's Third Assessment Report (TAR) in 2001. The SRES scenarios were also used for the Fourth Assessment Report (AR4) in 2007. Since then, the SRES scenarios have been subject to discussion because emissions growth since 2000 may have made these scenarios obsolete. It is clear that the IPCC's Fifth Assessment Report will develop a new set of emissions scenarios.

This study used two of the IPCC's SRES emissions scenarios for its analyses (A1B and B1). The following paragraphs provide a brief background on the IPCC's SRES scenarios and show the expected range of temperature increase toward the end of the 21st century under each of these scenarios.

The SRES scenarios cover a wide range of the main driving forces of future emissions, from demographic to technological and economic developments. None of the scenarios includes any future policies that *explicitly* address climate change, although all scenarios necessarily encompass various policies of other types and for other sectors. The set of SRES emissions scenarios is based on an extensive literature assessment, six alternative modeling approaches, and an "open process" that solicited wide participation and feedback from many scientific groups and individuals. The SRES scenarios include a range of emissions of all relevant greenhouse gases and sulfur, as well as their underlying driving forces.

As an underlying feature of all emissions scenarios, the IPCC developed four different narrative storylines to describe the relationships between emission-driving forces and their evolution over time (Figure A1.1). Each storyline represents different demographic, social, economic, technological, and environmental developments. Each emissions scenario represents a specific quantitative interpretation of one of the four storylines. All the scenarios based on the same storyline constitute a scenario "family."[1]

■ The **A1 storyline** and scenario family describes a future world of rapid economic growth, global population peaks by mid-21st century and declines there-

Figure A1.1. Schematic illustration of SRES scenarios
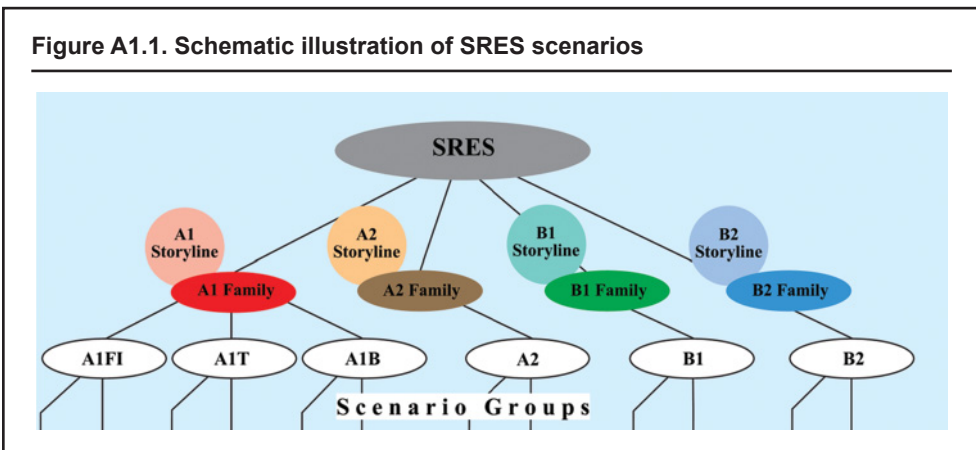
Source: IPCC 2000, modified.

after, and the rapid introduction of new and more efficient technologies. Major underlying themes of the A1 storyline are convergence among regions, capacity building, and increased cultural and social interactions, with a substantial reduction in regional differences in per capita income. The A1 scenario family develops into three groups that describe alternative directions of technological change in the energy system. The three A1 groups are distinguished by their technological emphasis: **fossil fuel intensive (A1FI)**, **non-fossil energy sources (A1T)**, or a balance across all sources (A1B).

■ The **A2 storyline** and scenario family describes a rather heterogeneous world. The underlying theme is self-reliance and preservation of local identities. Global population increases continuously. For the most part, economic development is regionally oriented, and per capita economic growth and technological change are more fragmented and slower than in other storylines.

■ The **B1 storyline** and scenario family describes a convergent world with the same global population that peaks in mid-century and declines thereafter, as in the A1 storyline, but with rapid changes in economic structures toward a service and information economy, with reductions in material intensity, and the introduction of clean and resource-efficient technologies. The emphasis is on global solutions to economic, social, and environmental sustainability, including improved equity, but without additional climate initiatives.

■ The **B2 storyline** and scenario family describes a world in which the emphasis is on local solutions to economic, social, and environmental sustainability. It is a world with global population continuously increasing at a rate lower than that of A2, intermediate levels of economic development, and less rapid and more diverse technological change than in the B1 and A1 storylines. While the scenario is also oriented toward environmental protection and social equity, it focuses on local and regional levels.

The overview in Table A1.1 summarizes the likely temperature changes under each of the scenarios described above. It shows that B2 would lead to a temperature change of

Table A1.1. Projected global average surface warming and sea level rise at the end of the 21st century according to different SRES scenarios

Case	Temperature change (°C at 2090-2099 relative to 1980-1999) [a, d]		Sea level rise (m at 2090-2099 relative to 1980-1999)
	Best estimate	*Likely* range	Model-based range excluding future rapid dynamical changes in ice flow
Constant year 2000 concentrations[b]	0.6	0.3 – 0.9	Not available
B1 scenario	1.8	1.1 – 2.9	0.18 – 0.38
A1T scenario	2.4	1.4 – 3.8	0.20 – 0.45
B2 scenario	2.4	1.4 – 3.8	0.20 – 0.43
A1B scenario	2.8	1.7 – 4.4	0.21 – 0.48
A2 scenario	3.4	2.0 – 5.4	0.23 – 0.51
A1FI scenario	4.0	2.4 – 6.4	0.26 – 0.59

Notes:
a) Temperatures are assessed best estimates and *likely* uncertainty ranges from a hierarchy of models of varying complexity as well as observational constraints.
b) Year 2000 constant composition is derived from Atmosphere-Ocean General Circulation Models (AOGCMs) only.
c) All scenarios above are six SRES marker scenarios. Approximate CO_2-eq concentrations corresponding to the computed radiative forcing due to anthropogenic GHGs and aerosols in 2100 (see p. 823 of the Working Group I TAR) for the SRES B1, AIT, B2, A1B, A2 and A1FI illustrative marker scenarios are about 600, 700, 800, 850, 1250 and 1550ppm, respectively.
d) Temperature changes are expressed as the difference from the period 1980-1999. To express the change relative to the period 1850-1899 add 0.5°C.

Source: IPCC 2007.

approximately 2.4°C toward the end of the century, under A1B the temperature change is estimated to be 2.8°C, while A2 is more extreme with a 3.4°C projected change.

It is important to note that the projected surface temperature changes toward the end of the 21st century exhibit a broad range of likely estimates, as shown by the bars next to the right panel of figure A1.2.

Figure A1.2. Scenarios for GHG emissions from 2000 to 2100 (in the absence of additional climate policies) and projections of surface temperatures
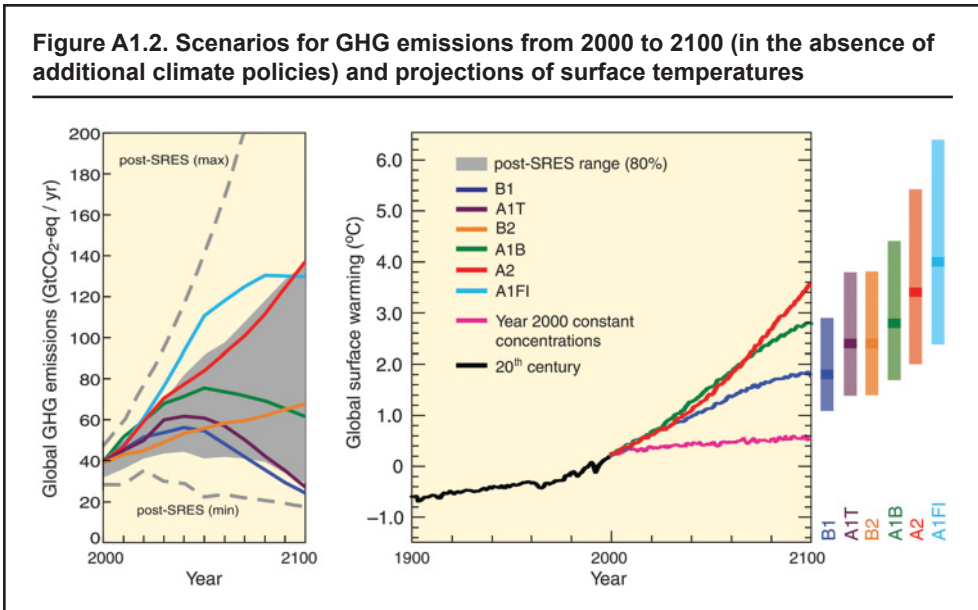
Source: IPCC 2007.
Notes: **Left Panel:** Global greenhouse gas emissions (in $GtCO_2$-eq) in the absence of climate policies: six illustrative SRES marker scenarios (colored lines) and the 80th percentile range of recent scenarios published since SRES (post-SRES) (gray-shaded area). Dashed lines show the full range of post-SRES scenarios. The emissions include CO_2, CH_4, N_2O and F gases.

Right Panel: Solid lines are multimodel global averages of surface warming for scenarios A2, A1B and B1, shown as continuations of the 20th-century simulations. These projections also take into account emissions of short-lived greenhouse gases and aerosols. The pink line is not a scenario, but is for Atmosphere-Ocean General Circulation Model (AOGCM) simulations where atmospheric concentrations are held constant at year 2000 values. The bars at the right of the figure indicate the best estimate (solid line within each bar) and the likely range assessed for the six SRES marker scenarios at 2090–2099. All temperatures are relative to the 1980–1999 period.

IPCC Statements of Confidence

Quoting the IPCC Fourth Assessment Report Guidance Note on Uncertainty (IPCC, 2005):

> **Likelihood**, *as defined* [below], *refers to a probabilistic assessment of some well defined outcome having occurred or occurring in the future.*

The categories defined in this table should be considered as having 'fuzzy' boundaries. The central range of this scale should not be used to express a lack of knowledge… There is evidence that readers may adjust their interpretation of this likelihood language according to the magnitude of perceived potential consequences.

Terminology	Likelihood of outcome
Virtually certain	>99% probability of occurrence
Very likely	>90% probability
Likely	>66% probability
About as likely as not	33 to 66% probability
Unlikely	<33% probability
Very unlikely	< 10% probability
Exceptionally unlikely	< 1% probability

Source: IPCC 2005.

A *level of confidence* was defined as well, and the terminology is reproduced below and can be used to characterize uncertainty that is based on expert judgment as to the correctness of a model, an analysis, or a statement. The last two terms in this scale are reserved for areas of major concern that need to be considered from a risk or opportunity perspective, and the reason for their use should be carefully explained.

Terminology	Degree of confidence in being correct
Very High confidence	At least 9 out of 10 chance of being correct
High confidence	About 8 out of 10 chance
Medium confidence	About 5 out of 10 chance
Low confidence	About 2 out of 10 chance
Very low confidence	Less than 1 out of 10 chance

Source: IPCC 2005.

Notes

1. For each storyline, several different scenarios were developed using different modeling approaches to examine the range of outcomes arising from a range of models that use similar assumptions about driving forces.

Appendix 2. Verification of the Ability of the Simulated Dataset to Reproduce Observed Precipitation Behavior (draft)

The simulations utilizing the CCSM3 from National Center for Atmospheric Research (NCAR) and the downscaling activities resulted in an ensemble of five simulations for the 1990–1999 decade, as well as for the decades comprising 2050–2059 and 2090–2099. The simulations of the 1990–1999 existing climate were made to be compared with observed data and verify the fit between simulations and observed meteorological data. Data for all three time periods (including mid- and end of century) were made available to SENAMHI for archiving and processing.

- **Ensemble outputs.** For each of the three decades of interest, Pacific Northwest National Laboratory (PNNL) with the cooperation of NCAR produced five simulations (experiments) of an ensemble based on ocean surface temperature and sea ice cover data (adjusted to correct for biases with respect to the 1979–1996 period) needed to drive a global atmosphere/land simulation using the NCAR-GCM (Community Atmosphere Model/Community Land Model) from 1977 to 2100. The A1B greenhouse gas emissions scenario was used. In addition, PNNL ran simulations with the subgrid orography version of the CAM/CLM model for the 1990–1999, 2050–2059, and 2090–2099 periods.
- **Downscaling of projections.** PNNL produced downscaled scenarios of key climate parameters. These include rainfall, snowfall, surface air temperature, surface air specific humidity, surface wind speed, and downward solar radiation. All downscaling was done for daily mean fields to 2.5-minute spatial resolution for the regions bounded by latitudes 20S and EQ and by longitudes 85W and 65W (Peru) and by 60W to 70W and by 10S to 30S (Bolivia).[1]

Validating Simulation Results

The value of climate scenarios depends on the ability of the simulations to mimic the climate system in Peru. Climate is a very complex scientific field. To characterize climate, several variables are used here, based on their relevance to the availability and variability of water resources. The special distribution of precipitation, humidity, wind velocity, etc. are core elements for assessing the ability of a simulation model to produce datasets that are statistically undistinguishable from the observed record. The following criteria were used for the case at hand:

- Ability to simulate the monthly distribution of precipitation in selected areas of the country;
- The ability of the simulations to reproduce the precipitation trends exhibited by the observed data, on a yearly basis; and
- The performance of the simulations in reproducing the trends observed on a monthly basis.

Data Processing for Validation: Annual Precipitation

Simulation results were sampled at ten locations, each comprising areas of 50 km x 50 km, for a total of 100 points (control elements). The analysis conducted treats each

sample location as a point for comparison with observed data. SENAMHI's analysis of future climate scenarios is summarized in Figure A2.1, which describes the expected percentage change in annual precipitation by 2030 based on the observed early trends in the past. The map covers the entire country.

Figure A2.1. Expected percentage change in annual precipitation by 2030
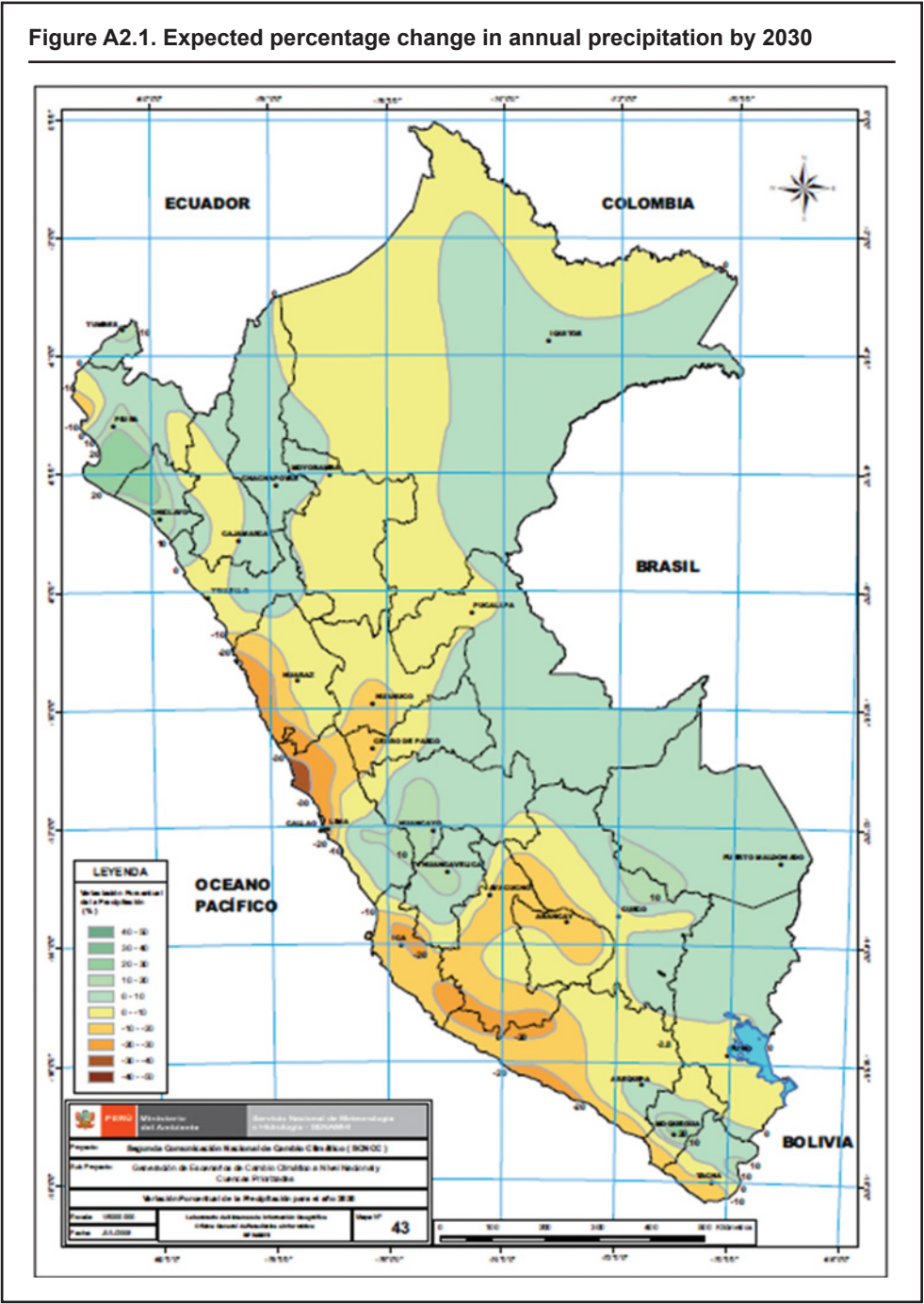
Source: SENAMHI 2009b.

The following observations can be made from the map:

■   Precipitation trends show large disparities in Peru, with some areas indicating increased precipitation and other zones exhibiting sharp reductions.

■   Most Pacific coastal areas show trends toward a drier climate, with a strong trend 100 km north of Lima. However, a trend toward increased precipitation is noted in northern Peru (Chiclayo and Piura).

■   Yearly precipitation is expected to increase in most of Amazonia as well in as some portions of the Mantaro River Basin.

The downscaled information from PNNL/NCAR was compared against this background. The analysis is summarized in Table A2.1, which indicates the expected precipitation change estimated from trends and from PNNL's simulation runs. In summary, the trends indicate that of the ten locations selected for analysis, four showed expected increases, four showed reductions and two showed no changes. In contrast, the data from PNNL/NCAR indicate expected increases in nine locations and decreased precipitation in one location. This contrast indicates a serious discrepancy between observed trends and simulated results.

Interannual Precipitation Analysis; Monthly Precipitation Distribution

Table A2.1 shows the distribution of median monthly precipitation for the ten selected locations from the simulated sets. In general, it can be observed that precipitation peaks in December (altogether in 8 locations) or in March (locations 6 and 7). It should be mentioned that location 6 is in southern Peru (south of Arequipa) while location 7 is close to Tumbes in the Pacific north. After a comparison of the observed precipitation regimes and the simulated results, it is concluded that these observed characteristics are not captured well by the simulation.

Interannual Precipitation Trends

Analyses conducted by SENAMHI for the Second National Communication to the UNFCCC indicate that precipitation trends at subannual scales show contrasting values. In general the information suggests that precipitation tends to increase for high precipitation months, while the trend is toward lower values during low precipitation months. This behavior is summarized in Table A2.1. As highlighted in the table, actual observation records exhibit contrasting trends. The data from the simulations, summarized on the right side of the Table A2.1, show some contrasting trends. But these contrasting trends are associated with location where the overall trend is weak (low slope and correlation values), in particular for locations 8 and 9. The trend observed in location 6 merits greater scrutiny. The simulation results indicate a substantial increase in precipitation by 2050 (48 percent) followed by a large decrease that brings precipitation almost back to the starting value. This behavior is unique and it is difficult to find a plausible technical explanation for it.

Table A2.1. Monthly precipitation from PNNL/NCAR simulations

Area	Monthly precipitation in milimeters													Precipitation as a percentage of 1990 mean value.													
	1	2	3	4	5	6	7	8	9	10	11	12			1	2	3	4	5	6	7	8	9	10	11	12	
1	331.1	326.5	273.9	117.2	60.0	32.1	15.8	46.0	128.7	221.7	244.1	502.0		2090	1.16	1.22	1.26	1.14	1.13	1.57	1.17	1.36	1.30	1.29	1.09	1.08	1.18
1	332.9	300.2	241.1	112.6	63.6	24.0	15.9	37.4	102.6	214.2	241.2	509.6		2050	1.17	1.13	1.11	1.10	1.20	1.18	1.18	1.11	1.03	1.25	1.07	1.10	1.12
1	285.3	266.8	217.3	102.5	53.0	20.4	13.4	33.8	99.2	171.3	224.7	464.8		1990	1.00	1.00	1.00	1.00	1.00	1.00	1.00	1.00	1.00	1.00	1.00	1.00	1
2	321.3	333.9	282.9	132.2	66.3	37.5	16.1	45.2	124.5	210.5	197.6	422.2		2090	1.12	1.18	1.18	1.04	1.04	1.54	1.03	1.33	1.29	1.31	1.02	1.02	1.13
2	340.8	325.6	267.3	137.9	79.6	28.2	15.8	38.4	106.2	203.2	208.0	453.7		2050	1.18	1.15	1.12	1.09	1.24	1.15	1.02	1.13	1.10	1.27	1.07	1.10	1.14
2	288.1	283.8	239.1	126.9	64.1	24.4	15.5	34.0	96.4	160.2	194.2	413.1		1990	1.00	1.00	1.00	1.00	1.00	1.00	1.00	1.00	1.00	1.00	1.00	1.00	1
3	229.7	276.3	293.7	189.3	79.3	41.5	29.4	60.2	125.7	223.2	218.0	391.5		2090	1.08	1.18	1.21	1.12	1.15	1.71	1.41	1.42	1.25	1.28	1.20	1.17	1.19
3	255.1	276.3	310.5	197.6	93.7	33.3	25.8	54.3	121.3	225.8	216.9	400.1		2050	1.20	1.18	1.28	1.17	1.35	1.37	1.23	1.27	1.20	1.30	1.19	1.19	1.22
3	212.0	235.0	243.0	169.1	69.3	24.3	20.9	42.6	101.0	173.7	182.1	335.6		1990	1.00	1.00	1.00	1.00	1.00	1.00	1.00	1.00	1.00	1.00	1.00	1.00	1
4	194.2	221.5	229.4	148.7	67.3	35.9	23.2	59.3	119.1	190.1	185.1	353.1		2090	1.06	1.22	1.23	1.16	1.23	1.68	1.17	1.38	1.18	1.19	1.20	1.18	1.19
4	198.1	202.0	220.4	142.0	73.2	29.8	23.4	53.3	108.6	188.0	179.1	344.7		2050	1.09	1.11	1.18	1.11	1.33	1.40	1.18	1.24	1.07	1.17	1.16	1.16	1.15
4	182.6	182.2	186.5	128.3	54.9	21.3	19.8	43.1	101.0	160.4	154.1	298.1		1990	1.00	1.00	1.00	1.00	1.00	1.00	1.00	1.00	1.00	1.00	1.00	1.00	1
5	176.5	162.6	151.6	72.3	42.6	26.9	18.7	17.8	30.0	52.7	101.4	251.2		2090	1.18	1.01	1.18	1.19	1.28	1.31	1.16	1.21	1.42	1.15	1.05	1.08	1.12
5	172.7	169.8	135.7	67.1	39.0	22.9	19.3	18.7	21.4	53.6	109.1	252.5		2050	1.15	1.05	1.06	1.10	1.17	1.12	1.19	1.27	1.01	1.17	1.13	1.08	1.10
5	149.7	161.2	128.4	60.9	33.4	20.5	16.2	14.7	21.1	45.6	96.5	233.5		1990	1.00	1.00	1.00	1.00	1.00	1.00	1.00	1.00	1.00	1.00	1.00	1.00	1
6	47.6	69.4	78.7	65.8	27.1	13.1	1.4	4.7	12.3	31.2	17.9	36.9		2090	0.95	1.11	0.88	0.96	0.98	1.71	0.68	1.79	1.36	1.73	1.12	1.03	1.04
6	75.0	95.5	134.9	102.6	44.2	10.1	1.8	4.7	15.6	25.2	19.6	46.7		2050	1.50	1.52	1.51	1.50	1.61	1.32	0.87	1.79	1.73	1.40	1.23	1.31	1.48
6	50.0	62.7	89.1	68.4	27.6	7.7	2.0	2.6	9.0	18.0	16.0	35.7		1990	1.00	1.00	1.00	1.00	1.00	1.00	1.00	1.00	1.00	1.00	1.00	1.00	1
7	28.7	51.5	53.2	35.4	24.5	10.9	7.5	6.8	8.7	13.2	11.9	26.8		2090	0.70	0.85	0.72	0.81	0.98	0.97	0.77	0.76	0.89	0.94	0.83	0.78	0.80
7	29.6	57.4	71.1	38.7	24.7	10.3	7.7	6.9	8.6	12.5	12.1	28.6		2050	0.72	0.95	0.96	0.88	0.99	0.92	0.78	0.77	0.88	0.89	0.84	0.84	0.89
7	40.9	60.7	74.3	44.0	24.9	11.2	9.8	8.9	9.7	14.0	14.4	34.1		1990	1.00	1.00	1.00	1.00	1.00	1.00	1.00	1.00	1.00	1.00	1.00	1.00	1
8	332.5	314.8	348.2	308.8	182.4	90.7	97.2	185.6	216.8	251.9	306.5	660.4		2090	1.13	1.14	1.08	1.07	1.19	1.22	0.89	0.95	1.04	1.10	1.08	1.15	1.09
8	294.4	284.3	342.1	310.0	172.2	75.7	100.5	185.4	208.0	241.1	299.7	609.8		2050	1.00	1.03	1.06	1.07	1.12	1.02	0.92	0.95	1.00	1.05	1.05	1.06	1.04
8	293.5	277.1	322.2	288.6	153.9	74.1	109.0	194.8	208.1	229.8	284.3	575.2		1990	1.00	1.00	1.00	1.00	1.00	1.00	1.00	1.00	1.00	1.00	1.00	1.00	1
9	283.6	225.3	198.0	67.0	31.4	17.9	11.4	20.8	44.8	71.3	151.6	401.0		2090	1.23	1.03	1.15	1.01	1.09	1.26	0.98	1.09	1.10	0.91	1.09	1.20	1.13
9	262.4	238.3	172.1	62.9	31.0	15.8	11.2	20.2	34.0	72.4	155.3	377.4		2050	1.14	1.09	1.00	0.95	1.08	1.12	0.96	1.05	0.83	0.92	1.11	1.13	1.07
9	230.8	218.2	171.4	66.2	28.8	14.2	11.7	19.2	40.9	78.3	139.4	333.4		1990	1.00	1.00	1.00	1.00	1.00	1.00	1.00	1.00	1.00	1.00	1.00	1.00	1
10	353.4	361.9	332.0	189.9	104.9	62.7	47.4	92.7	182.1	266.6	296.0	595.3		2090	0.70	1.21	1.13	0.68	0.66	0.80	1.18	2.59	2.69	1.84	1.44	2.37	1.22
10	344.0	337.3	324.5	190.7	102.4	50.2	41.0	78.1	162.3	256.9	288.4	578.9		2050	0.68	1.12	1.11	0.69	0.64	0.64	1.02	2.19	2.40	1.77	1.41	2.31	1.17
10	506.2	299.8	293.5	278.1	159.5	77.9	40.0	35.7	67.6	145.0	204.9	251.2		1990	1.00	1.00	1.00	1.00	1.00	1.00	1.00	1.00	1.00	1.00	1.00	1.00	1

Source: SENAMHI 2009b

Note: Highlighted values show maximum precipitation months in the left columns; trends are highlighted in the right columns.

Conclusions

This validation exercise indicates that the PNNL/NCAR dataset does not closely simulate the precipitation regime observed in Peru. As shown, the simulations do not capture the monthly precipitation distribution or the monthly and yearly trends that were observed and verified.

Notes

1. The projection using NCAR-GCM and the downscaling have included Bolivia for reasons of cost-effectiveness and bearing in mind the potential future application of results in that country.

Appendix 3. Subgrid Orography Scheme

Produced by Steven Ghan and Tim Shippert, Battelle, Pacific Northwest Division.

Global climate models lack the necessary spatial resolution to explicitly resolve the spatial variability of future temperature, precipitation, and snow water in regions with complex terrain. The spatial resolution required is roughly 5-km grid size, which is far finer than the typical 100-km grid size employed in most simulations of global warming.

Recognizing the disparity between the resolution of global climate models and the resolution required for impact assessment in regions with complex terrain, the climate impacts community has employed a variety of methods for downscaling the climate information from global climate models to the spatial scales required for impact assessment (Wilby et al. 1997; Wood et al. 2004; Salathé et al. 2007).

One solution uses data to identify relationships between local and large-scale conditions and then correct for the local biases in the global climate simulations (Benestad 2004; Maurer and Hidalgo 2008). This approach works well in regions with a high density of measurement stations, but is questionable when applied to conditions far beyond those observed in the past.

A second solution is called high-resolution time-slice, in which the atmosphere and land components of a climate model are run at much finer resolution for selected periods (typically a decade) of a global warming scenario, driven by ocean surface conditions from coarse-resolution coupled climate simulations (Cubasch et al. 1995; May and Roeckner 2001). In such a configuration, it should be possible to run a global atmosphere model at 5-km resolution for a decade, although published simulations are only for several years at 7-km resolution without topography (Miura et al. 2005).

A third solution is to apply a regional model to the region of interest and run it at high resolution, driven by daily boundary conditions interpolated from a global coupled simulation. This approach has been employed many times (Leung and Ghan 1999; Leung and Qian 2003; Frei et al. 2006; Qian et al. 2009) and has been shown to be an effective downscaling method if the region of interest is not too large.

A fourth solution applies a physically based downscaling method to a global model to produce global high-resolution results at a very modest computational cost (Ghan et al. 2002, 2006; Ghan and Shippert 2006). In this method, illustrated in Figure A3.1, each model grid cell is divided into a nominal number of subgrid elevation/vegetation bands based on high-resolution topographic and vegetation data. The subgrid method estimates the vertical displacement of air parcels in each subgrid band based on the elevation difference between the subgrid band and the grid cell mean, and the Froude number, which is used to distinguish whether the air parcel is blocked or lifted by the subgrid topography. The estimated vertical displacement of air parcels is then used to determine the subgrid vertical profiles of temperature and humidity based on conservation of energy and moisture, and an orographic forcing term is then applied to the prognostic equation of temperature and moisture for each subgrid class through nudging of the temperature and moisture profiles to the diagnosed profiles over a relaxation time constant. The full suite of atmospheric physics and the land surface physics are applied to each elevation band within each grid cell, but atmospheric dynamics is only calcu-

Figure A3.1. Subgrid orography scheme
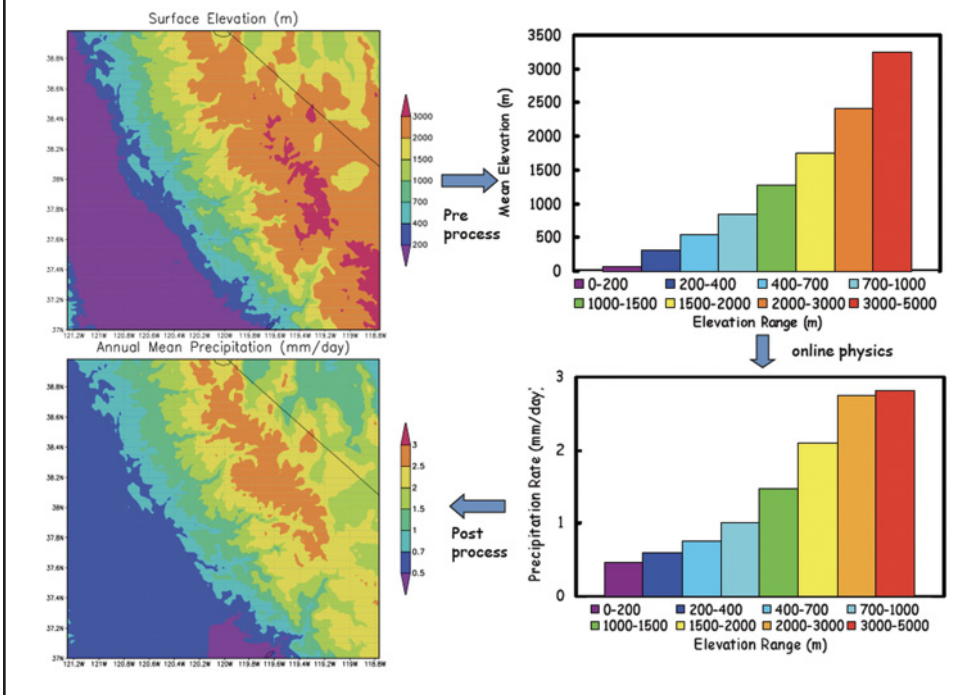
Source: Authors.

lated based on the grid cell mean variables. Model output is written for each elevation band during the simulation and then spatially distributed in postprocessing according to the elevation of the subgrid band and the high-resolution surface elevation data. This method has been implemented and evaluated in a regional climate model (Leung and Ghan 1998; 1999) and a global climate model (Ghan et al. 2004).

In this study, the physically based subgrid orography scheme described above is used in a global model to produce high-resolution information about future climate change in Peru and Bolivia. The global model is the community atmosphere model (CAM3) coupled to the community land model (CLM3) run at T85 (about 1.4° latitude and longitude) resolution. The same subgrid scheme and application methodology described by Ghan and Shippert (2006) is used. The ocean surface temperature and sea ice cover are interpolated to the grid from an ensemble of five climate simulations by the Community Climate System Model (CCSM3) for an Intergovernmental Panel on Climate Change A1B greenhouse gas emissions scenario (Meehl et al. 2006). For each member of the ensemble simulations of the four decades (1990–1999, 2030–2039, 2050–2059 and 2090–2099) are performed after initializing four months earlier to permit the atmosphere and land to adjust to the new boundary conditions.

For each of the five simulations of the periods 1990–1999, 2030–2039, 2050–2059 and 2090–2099, the following daily mean fields to 2.5 minute (about 5 km) spatial resolution are downscaled for the regions bounded by latitudes 20S and EQ and by longitudes 85W and 65W (Peru) and by 60W to 70W by 10S to 30S (Bolivia): rainfall, snowfall, surface air temperature, surface air specific humidity, surface wind speed and downward solar radiation.

Figure A3.2. Surface elevation used for downscaling for Peru (left) and Bolivia (right)
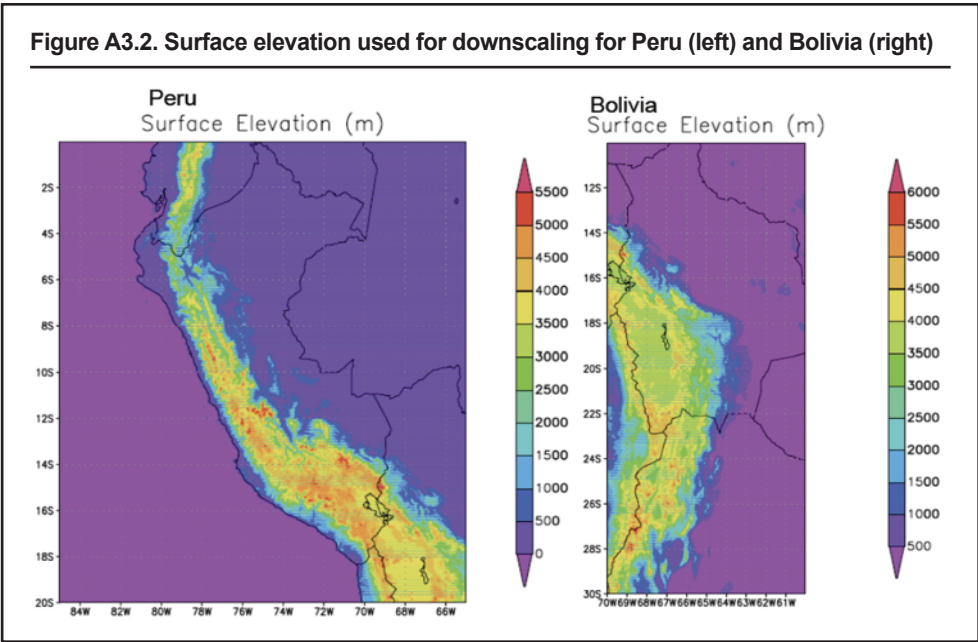
Source: Authors.

Figure A3.2 shows the spatial distributions of surface elevation used for the downscaling for Peru and Boliva. This distribution should be kept in mind because it has a strong influence on the distributions of the climate variables.

Although all members of the ensemble of simulations are completed, only the results from a single member of the ensemble are presented here.

Figure A3.3 compares the simulated and observed distribution of surface air temperature for Peru during the 1990s. The simulated surface air temperature has a significantly stronger orographic signature than is observed.

Figure A3.3. Simulated (left) and observed right distribution of surface air temperature for Peru during the 1990s
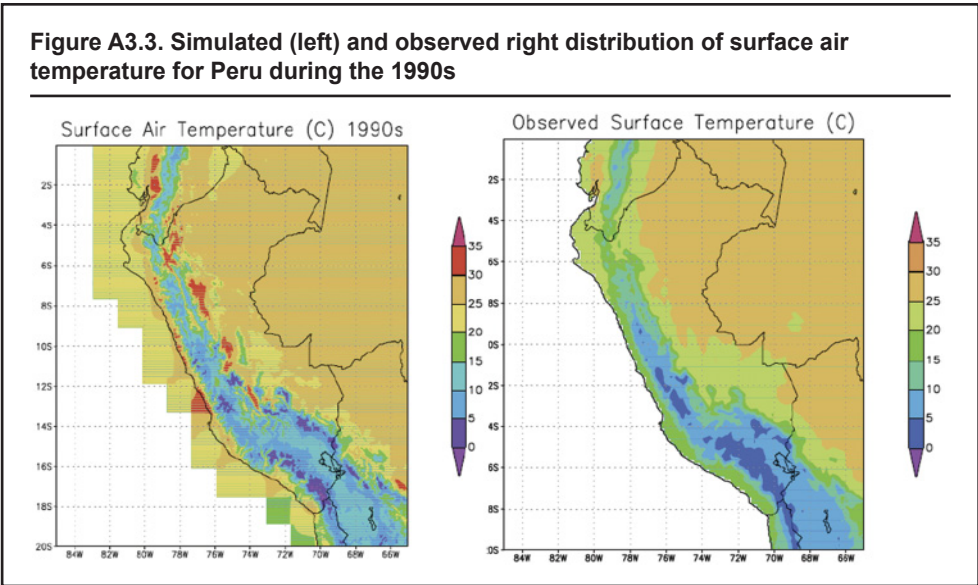
Source: Observations are from New et al. (2002)..

Figure A3.4. Simulated (left) and observed right distribution of surface air temperature for Bolivia during the 1990s
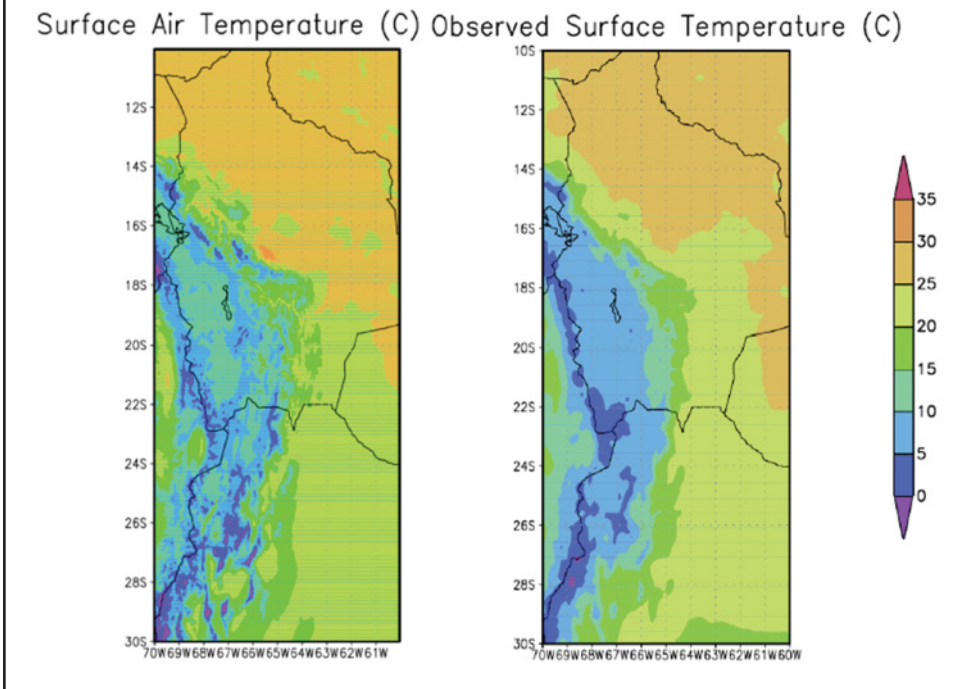
Source: Authors.

Figure A3.4 shows the simulated and observed surface air temperature for Bolivia. The exaggeration of the orographic signature of temperature is not as severe for Bolivia as it is for Peru.

Figure A3.5 compares the simulated and observed distribution of precipitation for Peru. The simulation produces too much precipitation on the leeward (western) side of the Andes, and too little on the windward side. This is a consequence of the inability of the subgrid orography scheme to distinguish between the windward and leeward sides of mountains. The mountain rain shadow must be explicitly resolved. The simulation shows some ability of the global model to do this where the Andes are broad, such as in southern Peru, but not where the Andes are narrow, such as in the middle and northern parts of Peru. This serious bias has obvious implications for water resources in this region, and must be corrected.

Figure A3.6 compares the simulated and observed precipitation for Bolivia. Large biases are also evident for this domain, with excessive precipitation on the western side of the Andes and too little precipitation on the eastern side.

Figure A3.7 shows the distribution of the surface warming for Peru for each decade. The spatial pattern of the warming is remarkably coherent, being amplified over time as the warming increases.

Figure A3.5. Simulated (left) and observed (right) precipitation for Peru
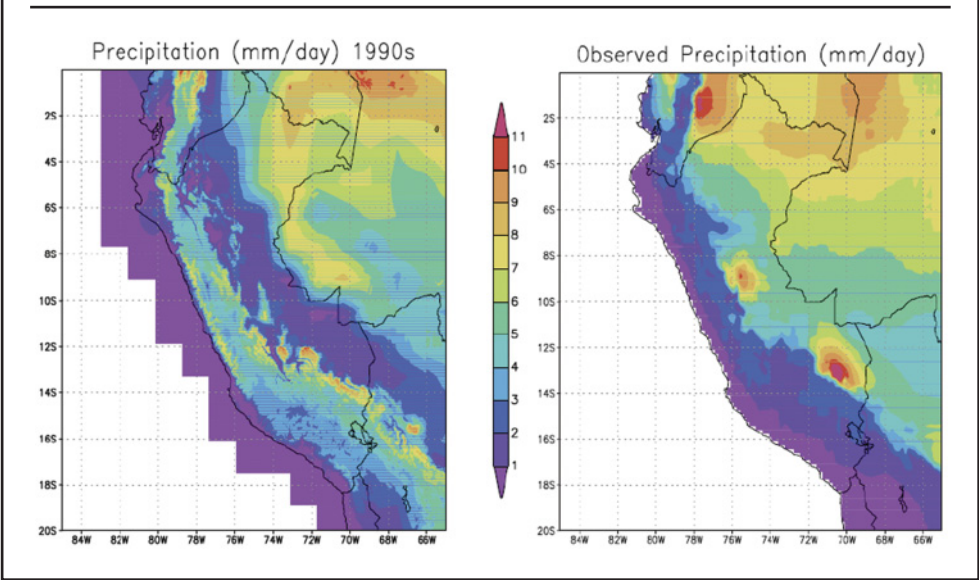
Source: Authors.

Figure A3.6. Simulated (left) and observed (right) precipitation for Bolivia
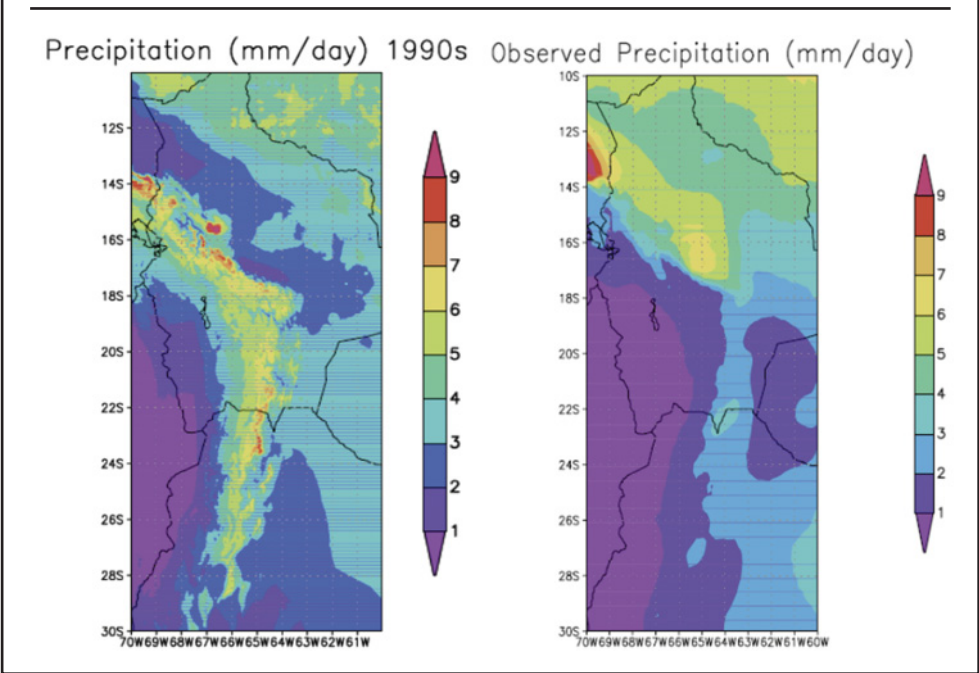
Source: Authors.

Figure A3.7. Simulated change in surface air temperature for Peru during the 2030s, 2050s, and 2090s
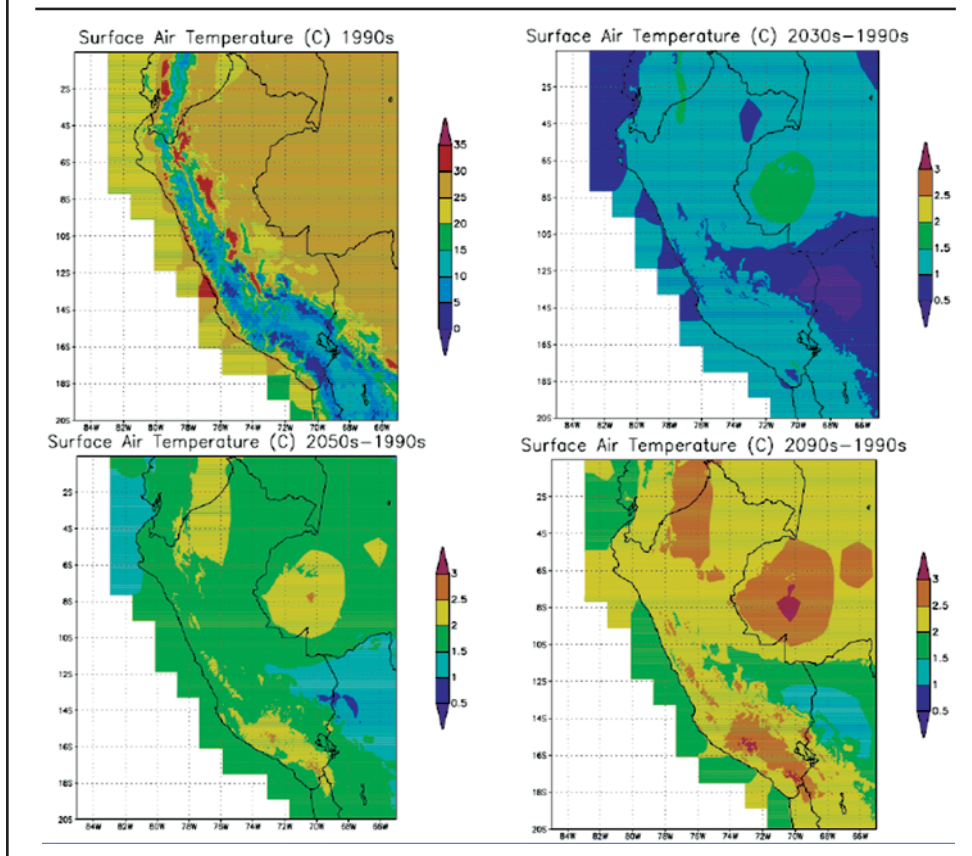
Source: Authors.

Figure A3.8 shows the simulated surface warming for Bolivia for each decade. Greater warming is evident at higher elevations, which is consistent with results from global models.

Figure A3.9 shows the distribution of the change in precipitation for Peru for each decade. The distributions of the change are remarkably complex and consistent from decade to decade, amplifying in time. Precipitation increases exceeding 2 mm/day are simulated along the eastern side of the Andes. Decreases are less than 0.5 mm/day except in one small region.

Figure A3.10 shows the distribution of precipitation changes for Bolivia for each decade. Precipitation increases are greatest over the Andes, with increases exceeding 2 mm/day at some elevations.

Figure A3.11 shows the distribution of snowfall for Peru, and the change in snowfall for each decade. Snowfall is limited to higher elevations, but is not greatest at the highest elevations. Figure A3.12 shows that the greatest snowfall occurs at elevations between 4 and 5 km rather than at higher elevations. This is to be expected because the air is drier at higher elevations. The distribution of the reduction in snowfall shown in Figure A3.11 is similar to the distribution of the 1900s' snowfall and amplifies with time. Figure A3.13 shows that the largest reduction in snowfall (up to 2.5 mm/day) during the 2090s occurs

Figure A3.8. Simulated change in surface air temperature for Bolivia during the 2030s, 2050s, and 2090s
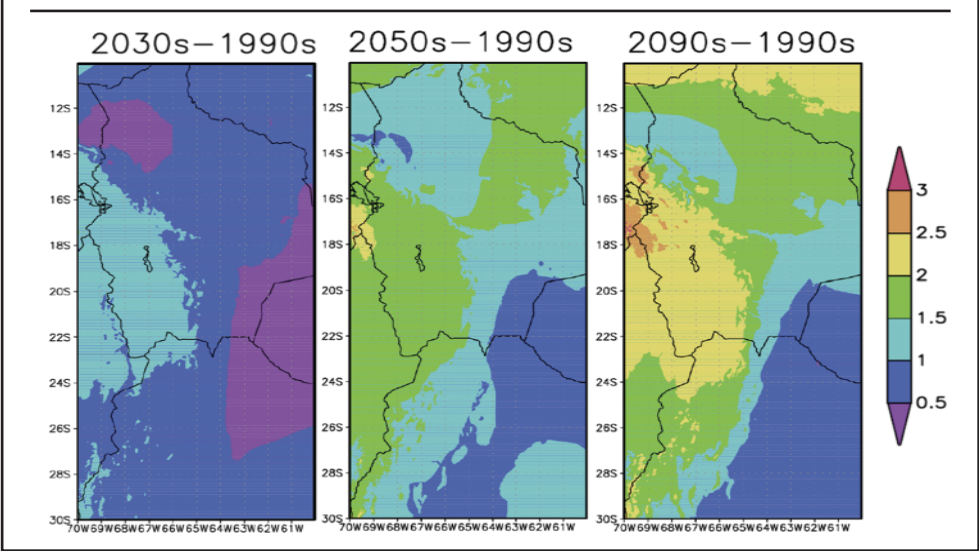
Source: Authors.

Figure A3.9. Precipitation for Peru for the 1990s decade (upper left) and the change in snowfall for the 2030s (upper right), 2050s (lower left), and 2090s (lower right)

Source: Authors.

Figure A3.10. Precipitation for Bolivia during the 1990s (left) and the change in snowfall for each decade (right)

Source: Authors.

Figure A3.11. Snowfall for Peru for the 1990s decade (upper left) and the change in snowfall for the 2030s (upper right), 2050s (lower left) and 2090s (lower right)
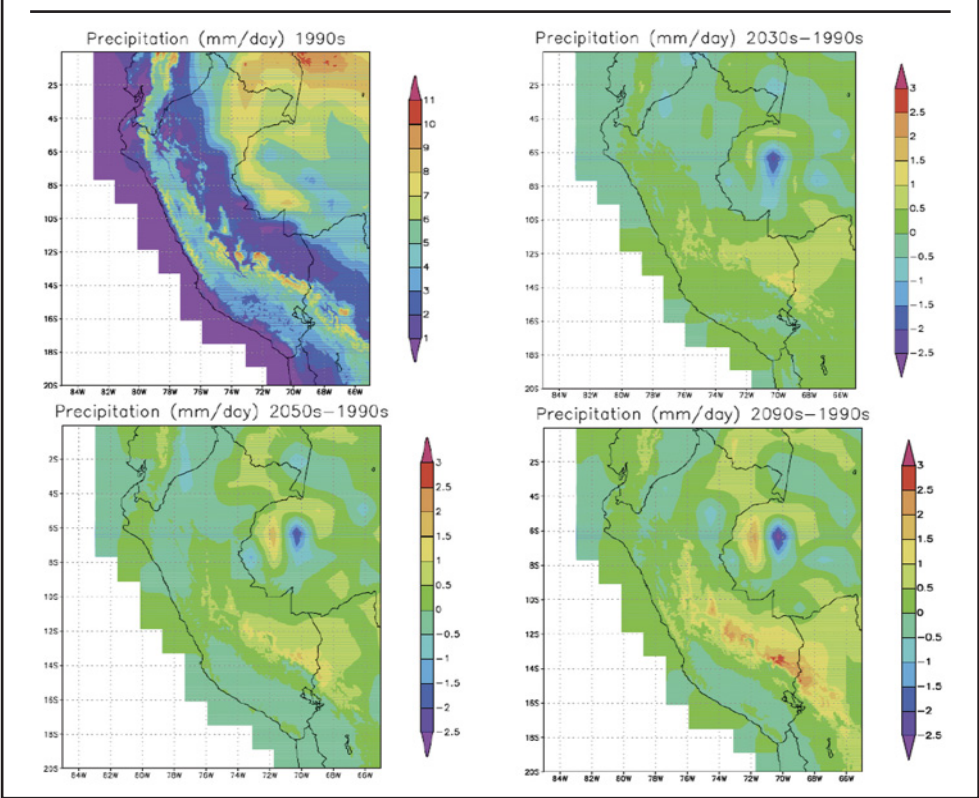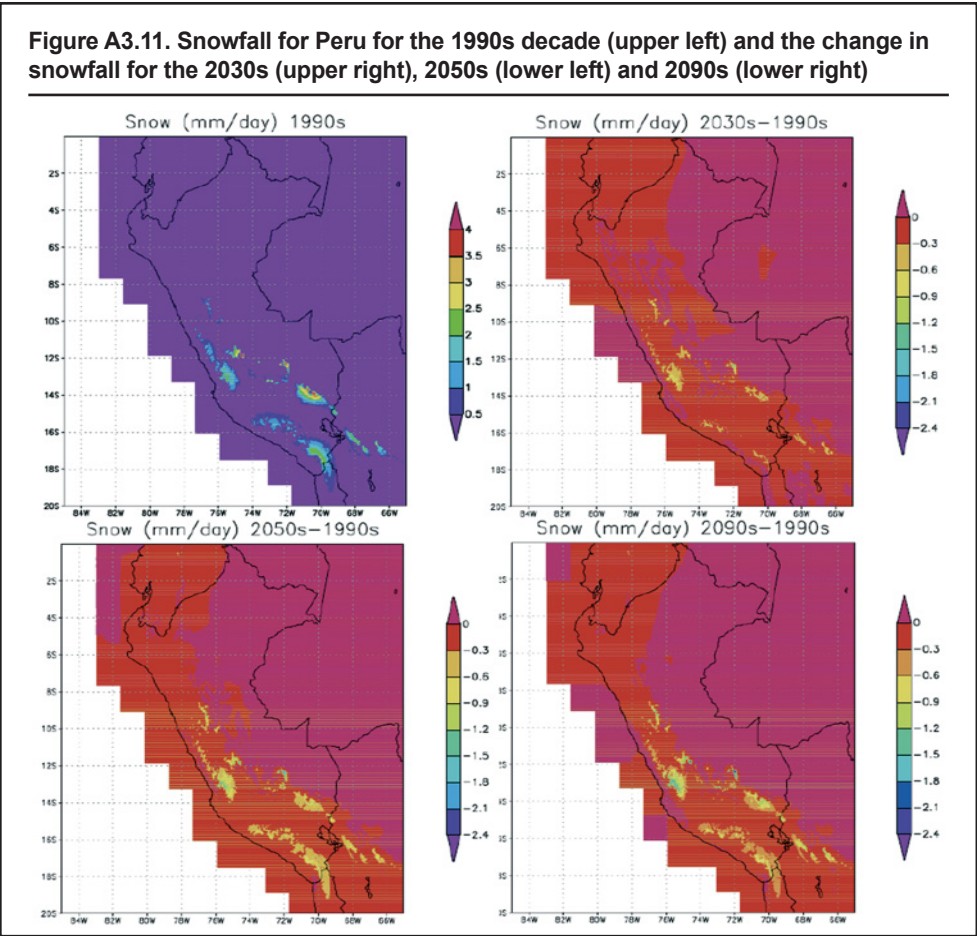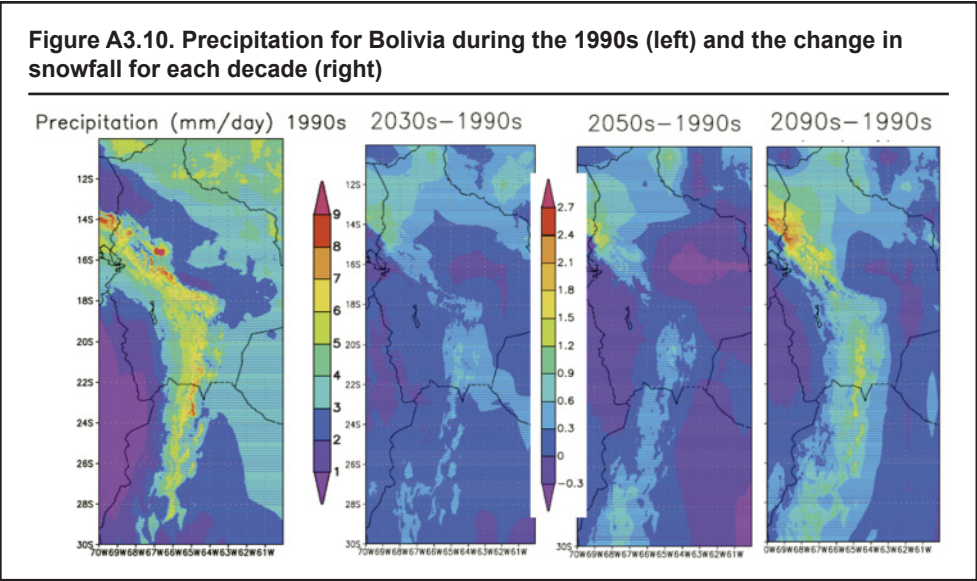
Source: Authors.

Figure A3.12. Relationship between snowfall during the 1990s and surface elevation for Peru
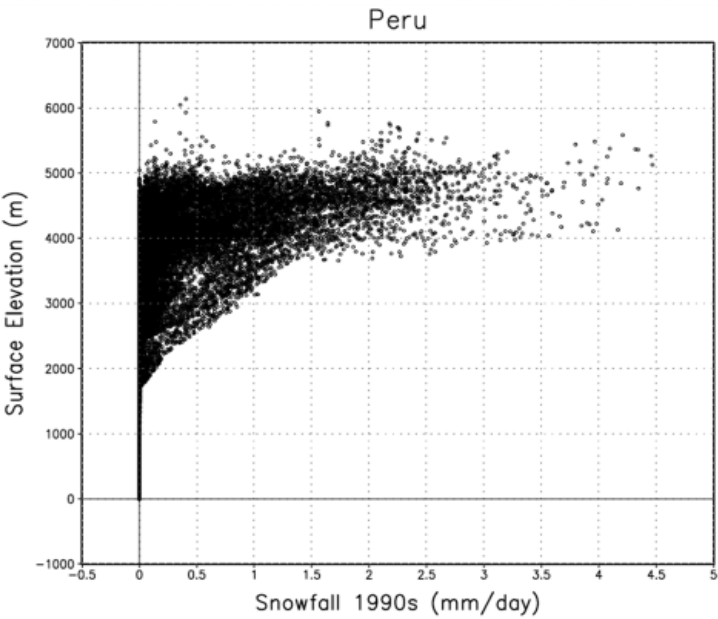
Source: Authors.

Figure A3.13. Change in snowfall (mm/day) (2090s–1990s) versus surface elevation for Peru
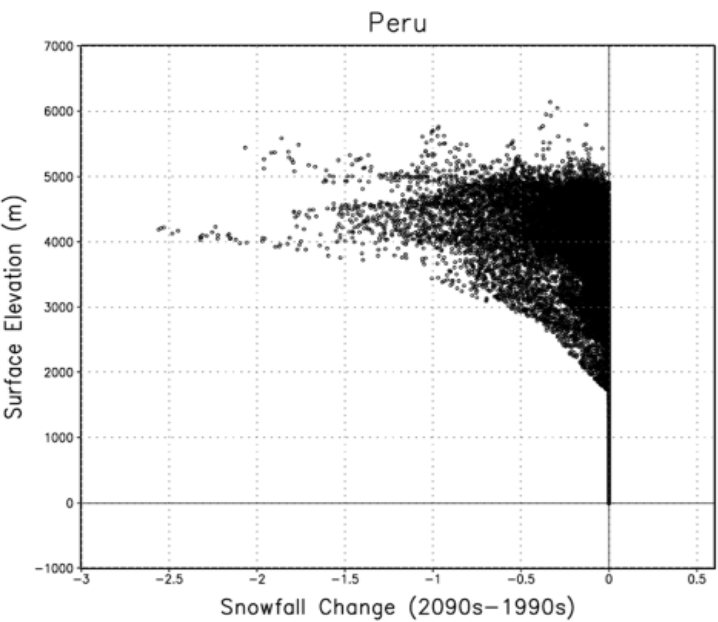
Source: Authors.

Figure A3.14. Snowfall for Bolivia during the 1990s (left) and the change in snowfall for each decade (right)
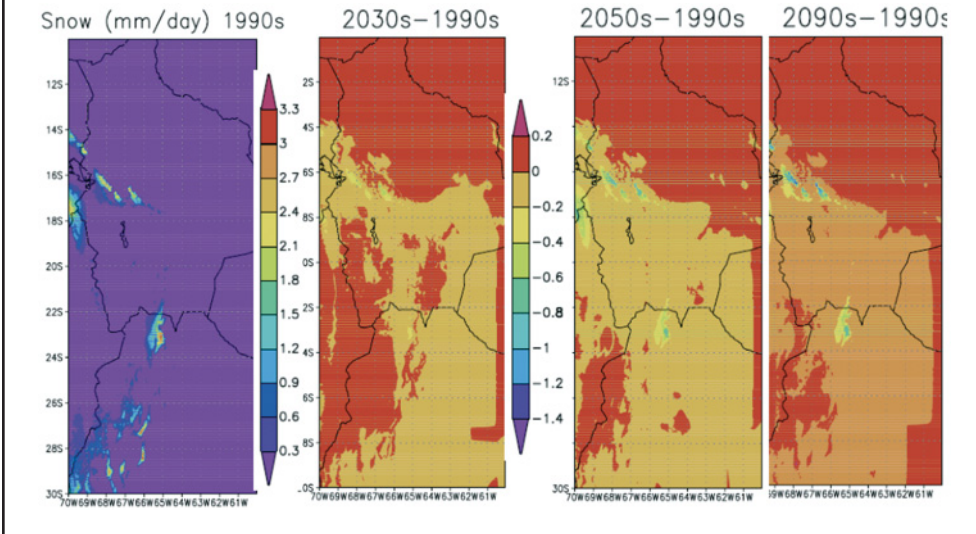
Source: Authors.

at an elevation of about 4.2 km; at lower elevations the snowfall reduction is limited by the amount of snowfall in the 1990s, because almost all precipitation is rain, while at higher elevations the warming is insufficient to convert the snowfall to rain. These distributions are likely to have a strong influence on the distributions of snow water and snowmelt.

Figure A3.14 shows the distribution of snowfall for Bolivia for the 1990s and the change in snowfall for the 2030s, 2050s, and 2090s. The results are comparable to the results for Peru.

In summary, these simulations produce remarkably consistent but spatially complex distributions of changes in surface air temperature, total precipitation, and snowfall that amplify with time. Total precipitation increases in most locations, but snowfall decreases. These changes are likely to produce strong effects on estimates of impacts of global warming on surface water resources in Peru and Bolivia.

However, large biases are evident in the distribution of precipitation. The immediate solution would be to apply empirical corrections for these biases. Longer-term solutions would be to improve the subgrid orography scheme to account for subgrid rain shadows, or to employ explicit regional modeling for Peru and Bolivia. A treatment of rain shadows might be applied to this problem. Saved daily history from other global simulations could also be used to drive simulations with the regional climate model.

Appendix 4. Technical Report on Glacier and High-elevation Wetland Model Selection and Parameterization

World Bank Project "*Assessing the Impacts of Climate Change on Mountain Hydrology: Development of a Methodology through a Case Study in Peru*"

Introduction

This report corresponds to product p. 5.1 of Contract 7148343 between the Institut de Recherche pour le Développement of France (IRD) and the World Bank, corresponding to the project "Assessing the Impacts of Climate Change on Mountain Hydrology: Development of a Methodology through a Case Study in Peru." The IRD contributors are Wilson Suárez, Thomas Condom, Jean-Christophe Pouget and Patrick Le Goulven.

Description of the Content

This appendix contains three parts:

- PART 1. SEVERAL KINDS OF GLACIER MODELING
  - 1.1. General analysis of the models
  - 1.2. Study of ice-snow melt models
  - 1.3. Studies in the Santa River basin

- PART 2. MODELING APPROACH ADOPTED
  - 2.1. General formulation
  - 2.2. Calculation steps

- PART 3. PROGRESS OF THE PARAMETERIZATION
  - 3.1. Progress in glacier parameterization module (2000–2007)
  - 3.2. Progress in parameterization module in the entire Santa River Basin (1969–1997)

PART 1. SEVERAL KINDS OF GLACIER MODELING

General Analysis of the Models

A model is a schematic representation of a physical phenomenon; the purpose of the model is to study or analyze the influence that the phenomenon exerts. The representation may be mathematical or physical. A mathematical model is the result of analytical expressions of observed complexity and is usually presented as a set of equations. Physical models are adapted representations (scale models) of different physical processes, most of them difficult to represent mathematically because of their complexity (example: dams, siphons, etc).

The physical model is not used in this study.

Mathematical models: These models can be presented in two groups: **deterministic** and **stochastic models**. The difference between these two models is that the former considers the physical process to be a consequence of a fact prior to the event or situation to be represented (for example, the unit hydrograph that considers floods to be a consequence of precipitation; if the rainfall patterns are presented again, they will have the same kind of flooding). In contrast, stochastic models are more complex in their analytical concept; they depend in part on random phenomena (randomness). In summary, they consider that the same input data in the model should not deliver two similar outputs. These models do not consider all the variables existing inside the physical environment to be represented.

First place is assigned to the analysis of the deterministic models. These models can be divided into four large groups, depending on the physical concept: **empirical, statistical, conceptual, and physics-based models.**

Empirical models are the simplest and need fewer input data; they are strongly based on the hydrologist's observations and judgment. An example is the rational model.

$$Q = i * A * C$$

Q is the flux; i is the intensity of rainfall; A is the area of the basin; and C is the runoff coefficient.

Statistical models tend to predict or evaluate a specific behavior observed (for example, observed peak flows), based on the laws of statistical distribution (for example, normal law or Gumbel distribution). These models are inductive since they use observations to determine the proper law to be used. A separate feature is that these models do not consider the number of parameters.

Conceptual models seek to reproduce the response of a physical space (such as a basin), replacing the reality for a strongly simplified idealization of the real situation, in the geometric matter as well in the physical (real) process. For the hydrological case, hydrometeorological data are used to estimate the parameters. These models are therefore **deductive;** their main basis is the perceptual aspect of water behavior within the basin.

These models include the classic reservoir models, the most representative of which is the Nash instantaneous unit hydrograph model, in which the reservoirs tend to represent the evolution of the surface runoff during water flow in the basin.

Physics-based (mechanistic) models almost completely resolve all the possibilities of the equations of continuity and movement quantity connected with the transportation of water and/or energy. This equation system aims to describe the various phenomena

encountered, such as Darcy-Richards concerning underground drainage. These models are complex and may require spatialized information (2D or 3D grid system), robust numerical schemes, and the assignment of physical parameters for each physical unit (each cell of the grid). A classical model in hydrology is the European MIKE SHE, which is an integrated modeling framework to simulate all components of the land phase of the hydrologic cycle (surface water and groundwater).

Another important classification of deterministic models in hydrology is that related to the degree of complexity concerning the physical measurements of the basin or the area to be studied. These can be divided into **global** or **distributed** models. Global models generally consider the studied area as a whole, a total; all the parameters and characteristics are similar, but they fail to explain all the processes that occur within the studied area. However, they properly represent the physical process in one particular point. The **distributed** and **semi-distributed** models can represent the processes that take place throughout the studied area, but their operation is difficult and requires a large amount of data as well as parameters (usually physics-based models).

Within the deterministic models, there are other series of classifications; those that analyze the evolution of the physical process: **linear models** (for example, flow as a direct consequence of precipitation) and **nonlinear models** (such as flow as a nondirect consequence of precipitation, use of fictitious reservoirs). These are analyzed by the variation of physical parameters in time (**seasona**l and **nonseasonal**) and will not be addressed in this analysis because their characteristics may be within the models already described above.

Stochastic models: As noted, stochastic models give several outputs for one input in the model. These models are used to simulate complex physical processes that appear to be directed by randomness. The simplest examples of stochastic models are time series in which the variables given at a particular moment are according to their previous values and random error. In this case, the function that unites the values of the variable at different times are deterministic and the error is stochastic. The classical examples are the Markov chains, ARMA (Auto Regressive and Moving Average), etc.

Figure A4.1 shows a descriptive picture of the different types of existing models for hydrological modeling.

Figure A4.1. Simplified structure of the models
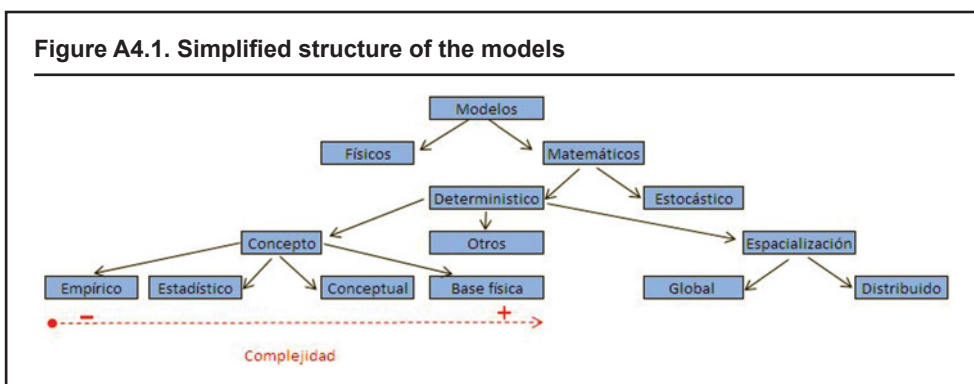
Source: Authors.

Study of Ice-Snowmelt Models

After the applicable existing general models and the general concepts used in hydrology are analyzed, it is necessary to evaluate the most-used and specialized models in the representation of the fusion of ice and snow.

It is important to analyze several basic concepts of the processes of melting that appear in the snow or ice.

The process of ice and snow melt is produced by different aspects such as the exchange of energy, albedo, temperature, slope, orientation, etc.

For tropical zones, the modeling of ice and snow melt can have the same behavior as that of medium-latitude regions, with the difference of conditions of seasonal climate variations. The seasons in the tropical zones are humid and dry, and precipitation occurs during four to five months; the dry period is the opposite. The fusion processes are constant due to the high variations of temperature during the day and the night. In other latitudes, the seasons are cold and warm so the fusion occurs at the end of the cold season (major inflows) and the daily variations of temperature are not as important as in the tropical zones.

Choosing a model among those presented previously is somewhat difficult since the runoff coming from the glacier zones is not only related to land parameters (slope, filtration, etc.), but is also related to climate parameters that determine the melting of the ice or snow (exchange of energy, albedo, temperature, slope and orientation of the glacier, etc.)

Currently, two types of models are most often used for the representation of glacier and snow melt: Energy balance models and the "degree-day" models.

Energy Balance

Mostly used for simulations of short time steps (daily or hourly), although it can be used for longer periods. It is a mathematical-deterministic model that works under physical bases (interconnection of complex equations) and operates in a distributed manner (spatialization grids). It analyzes the exchange of energy produced between the glacier and the snow through atmospheric radiation.

The models based on the "energy balance" consider a runoff factor (M):

$$M = \frac{Q_M}{\rho_w L_f}$$

where ρ_M is the water density and L_f the latent heat of fusion; parameter QM is the energy consumed during the runoff and is calculated through the following equation:

$$Q_N + Q_H + Q_L + Q_G + Q_R + Q_M = 0$$

where Q_N is net radiation; Q_H is the flux of sensitive heat; Q_L is the flux of latent heat; Q_G is the flux of the floor heat ;and Q_R is the flux of sensitive heat related to rainfall.

Value QN (net radiation) is the parameter that requires more understanding and is represented in the following equation:

$$Q_N = (I + D_S + D_t)(1 - \alpha) + L_S^{\downarrow} + L_t^{\downarrow} + L \uparrow$$

where I is direct sun radiation; D_s is diffuse radiation of the sky; D_t is radiation reflected by land; α is albedo; $L_s\downarrow$ is radiation in long-incident wave; $L_t\downarrow$ is radiation in long wave over land; $L\uparrow$ is radiation in emitted long wave.

Parameter I can then be calculated through the following equation:

$$I = I_o * (\frac{R_m}{R})^2 * \psi_a^{\frac{p}{\cos z}} * \cos \theta$$

where I_o is the solar constant; R is the distance between the sun and earth; Ψ is the sky-atmosphere transitivity under clear sky; P is the atmospheric pressure at sea level; Z is the local angle of the zenith; and θ is the incidence angle between the normal slope and solar radiation.

Some parameters such as the diffuse radiation of the sky (D_s) and reflected radiation (D_t) are very difficult to measure but they can be calculated through the following equation:

$$D_S = \int_0^{2\pi} \int_{h(\varphi)}^{\pi/2} D(h,\varphi) * \cos \theta * \cos \partial h \partial \varphi$$

where D(h,φ) is the radiation for a specific direction concerning the maximum angle "*h*" on the horizontal plane and the azimuth angle "φ".

The albedo (α) can be represented by the equation:

$$\alpha = \alpha_o + be^{-n_d * k}$$

where α_o is the minimum snow albedo; n_d is the number of days during a significant snow; *b* and *k* are constant.

The outgoing long-wave radiation (L↑) can be represented by the following equation:

$$L\uparrow = \varepsilon_c * \sigma * T_s^4 + (1 - \varepsilon_s)L\downarrow$$

where: ε_s is the emissivity of snow cover; σ is the Stefan-Boltzmann constant (5.67 X 10^{-8} W m^{-2} K^{-4}); T_s is the temperature of the air on the surface; and L↓ is the radiation in long-incident wave.

The turbulent heat-flow analysis (sensitive and latent QH QL) is conducted by temperature and moisture gradient between the air and surface:

where $\mathbf{Q_H}$ is represented by the equation:

$$Q_H = \rho_a * C_p * K_H * \frac{\partial \bar{\theta}}{\partial Z}$$

and $\mathbf{Q_L}$ is represented by the equation:

$$Q_L = \rho_a * L_V * K_E * \frac{\partial \bar{q}}{\partial Z}$$

where, for these two equations, ρ_a is the density of the air; C_p is the specific air heat; L_v is the latent heat of evaporation; Z is the height to the surface; K_H and K_L are the efficiency-in-transfer processes and depend on air speed, surface roughness and atmospheric stability; θ is the potential gradient of temperature; and "q" is the specific humidity on the edges of the surface.

The heat flux of ice is the energy needed for the ice/snow temperature to increase above 0° C and for runoff to take place.

$$C = \int_0^Z \rho(z) * C_P * T(z)\partial z$$

where: $\varrho(z)$ is the density of ice and snow; C_P is the specific heat of ice and snow; T is the temperature as a function of depth "z"(°C); and Z is the maximum depth of under-freezing temperature.

This parameter is strongly connected with the heating flux coming from the soil (QG) which can be represented by the equation:

$$Q_G = \int_0^Z \rho C_P * \frac{\partial T}{\partial t} dz$$

where: $\partial T/\partial t$ is the rate of ice temperature change.

The last element is the flux of heat generated by rainfall Q_R, as represented by the equation:

$$Q_R = \rho_W * C_W * R(T_r - T_s)$$

where: ϱ_W is water density; C_W is specific water heat (4.2 Kj* Kg^{-1}*°K^{-1}); R is rainfall; T_r is rain temperature; and T_s is ground temperature.

This last flux (Q_R) does not greatly affect the energy balance but rain indirectly influences the increase in liquid water contained in the ice and decreases the albedo.

This model requires special equipment on the glacier in order to measure the entire number of variables, and at the same time special training for the modeling worker to operate this type of model. Figure A4.2 shows a station fully equipped for this kind of work, as well as the outputs of the model displayed in a GIS format.

Figure A4.2. Information measured by a complete station located on the Swedish glacier Storglacien (Hock 2005) for an energy balance model and glacier station
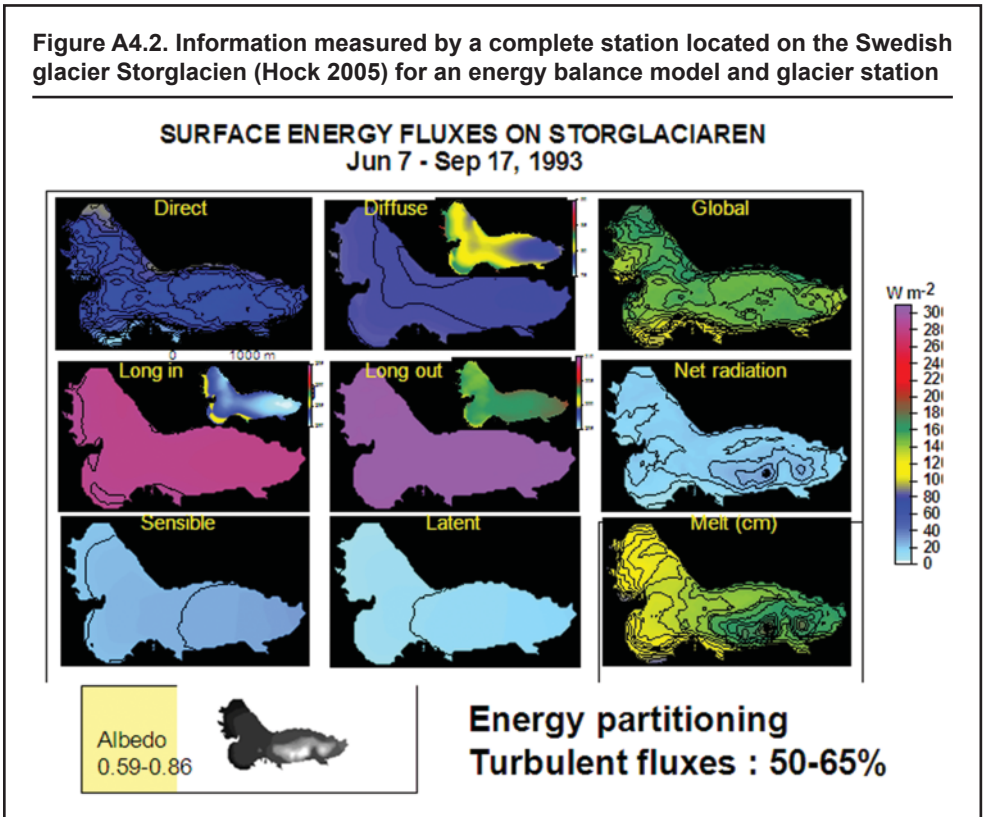
Figure A4.2 (continued)

An automatic weather station was placed on the ablations zone of Sørbreen in October 2007. The station measures air temperature (2m, 5m). relative humidity (2m, 5m). wind speed and direction (5m), long and short wave radiation (5m), snow depth, ice melt, snow temperatures (0m to 2,5m) and ice temperatures (0m to -15m).

Source: Hock 2005.

Degree-Day Models

These are conceptual models (reservoirs) that work at a global or semi-distributed level.

They are based on empirical relationships between the melting and the air temperature, and are also based on a strong and frequently observed correlation between these two variables, although the net radiation dominates the balance.

The study of the physical basis of this model emphasizes the role of long-wave radiation: Usually this is by far the largest source of heat for melting; along with the sensible heat flux, it provides nearly three-quarters of the energy for melting. Both heat fluxes are strongly affected by air temperature, which is the main reason for the close relationship between the melting and the air temperature. Moreover, the temperature is inside the affected parties because of global radiation, which is the second source for the melting.

These models can be used at different time steps: hourly, daily and monthly.

The temperature data are easily available in a direct (measured) or indirect (re-analysis) manner. Their broad application includes the prediction of melting for flow forecast operations and hydrologic models, modeling of glacier mass balance and evaluation of the snow and ice response applied to climate change predictions (see Schaefli et al. 2005).

The classical relative model for ice and snow melting: M(mm) over a period of "n" interval time Δt, to the positive sum of air temperatures for each time interval, T^+ during the same period:

$$\sum_{i=1}^{n} M = DDF * \sum_{i=1}^{n} T^+, \Delta t$$

where DDF is the degree-day factor (mm*day^{-1}*°K^{-1}), for Δt expressed in days and temperature in °C.

The DDF values can be calculated by direct comparison using snow lysimeters, ablation stakes or from the melting obtained by calculating the energy balance. This factor does not necessarily have a constant value throughout the world, as shown in Table A4.1.

Table A4.1. Different values of DDF for snow and ice in different parts of the world

Site	DDF snow	DDF ice	Latitude	Altitude (m.a.s.l)	Period	Reference
Qamanarssup	2.8	7.3	64°28' N	370–1410	1979–1987	Johannesson et al. 1995
Former European USSR	5.5	7.0		1800–3700		Kuzmin 1961
Satujökull (Iceland)	5.6	7.7	65°N	800–1800	1987–1992	Johannesson et al. 1995
Dokriani Glacier	5.9		31°45'N	4000	June 4–6, 1995	Singh and Kumar 1996
Glacier AX010	7.3	8.1	27°45'N	4956	Jun–Aug 1978	Kayastha et al. 2000
Khumbu Glacier		16.9	28°00'N	5350	May 21–Jun 1, 1999	Kayastha et al. 2000
Rakhiot Glacier		6.6	35°22'N	3350	Jul 18–Aug6, 1986	Kayastha et al. 2000
Yala Glacier		9.3	28°14'N	5120	Jun 1–Jul 31	Kayastha 2001

Source: Authors.

The difference between the term degree-days is attributable to the relative difference (significance) of the energy balance components that provide energy for the melting, considering that the energy balance may change in space and in time; the environmental conditions (altitude, climate) will not be the same in a glacier in Greenland as in another one situated in an intermediate or low latitude. Because of the important relative turbulence of flows, including condensation and marine environment, the areas with continental regimes probably have a lower "degree-days" factor.

Table A4.1 shows that the values of DDF$_{snow}$ are lower than those of DDF$_{ice}$. This is mainly because ice density is more important than snow density and therefore requires more energy to change its condition. DDF$_{ice}$ values usually have a ratio of 1.5 to 3 with respect to DDF$_{snow}$.

The advantages of this model can be summarized as follows: there is a good availability of air temperature data (direct or indirect measurements); there is also a relative easy interpolation and probable prediction of this variable. It is a generally good model with high efficiency and simplicity and with a simple calculation process (computer).

Hybrid Models

A last group could be called hybrid models, which consider a part of the energy balance model and a part of the degree-day model. These models usually add one or two variables to the temperature data used in the degree-day model. This variable is generally the albedo.

The choice of the most optimum model to simulate the hydrologic functioning of the three basins (Santa, Rímac and Mantaro) will depend on several characteristics of the studied area and on the models that will be analyzed.

Studies in the Santa River basin

To implement the glacier model, we must select a pilot area for calibration and validation. Because of its location in the Cordillera Blanca, the Santa River Basin is an important case studied by several Peruvian and international working teams. This chain of mountains is the subject of the largest number of studies concerning glaciers: Paleo-Climatology (University of Ohio and IRD), Glacier Dynamics (IRD, INRENA-Peru and University of Innsbruck), Remote Sensing (IRD, INRENA-Peru and University of Geneva); and Modeling of Glacier Melt (IRD and University of Innsbruck).

Prior to the presentation of our chosen approach, it is important to introduce the already existing work done on the glacier modeling. Three main works published to date are described below.

Studies by Bernard Pouyaud et al. (2005)

The first work, conducted by Bernard Pouyaud et al. in 2005, proposes the possible simulated glacier flow of four sub-basins of the Santa River under future temperature scenarios. This work used an empirical model based on simple equations that link runoff from the glacier with temperature.

This purely mathematical modeling used as its single indicator the air temperature at 500 hPa (taken from the National Oceanic and Atmospheric Administration [NOAA] re-analysis). This work does not take into account the physics or concept of ice melting (from a glaciological standpoint) and considers the glacier as whole (there is no ablation or accumulation zone). The entire glacier surface is constantly melting and the decrease is calculated based on topographic observations obtained on the Yanamarey glacier since the 1940s. These observations have revealed a coefficient of glacier retreat, which takes into account the size of the glacier for four different sub-basins (Llanganuco, Parón, Artesonraju and Yanamarey) in the Cordillera Blanca.

The results were presented for these four glacier sub-basins and glaciers and the probable flow was simulated until the complete disappearance of glaciers for each basin. The date of complete disappearance of glaciers is 2200, calculated with an annual time-step (Figure A4.3).

The most important point in this work is that it provides evidence of the good relationship between the air temperature and the depth of runoff (Llanganuco Sub-basin, Figure A4.4). For a better understanding, see Pouyaud et al. 2005.

Figure A4.3. Results simulation conducted by Bernard Pouyaud on different sub-basins of the Santa River

Source: Pouyaud et al. 2005.

Figure A4.4. Re-analysis of temperature (500 hPa) versus depth of runoff in the Llanganuco Sub-basin
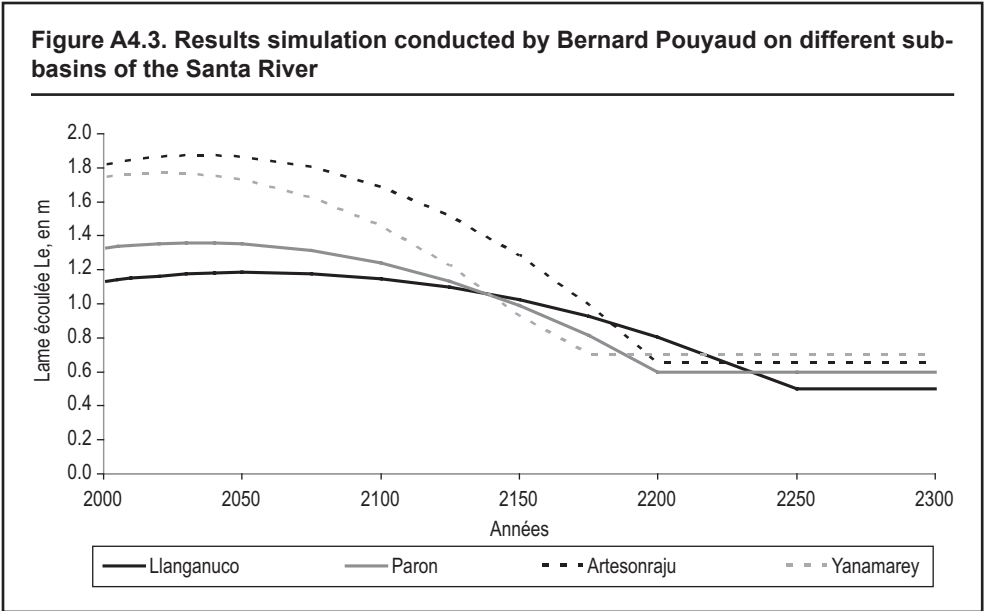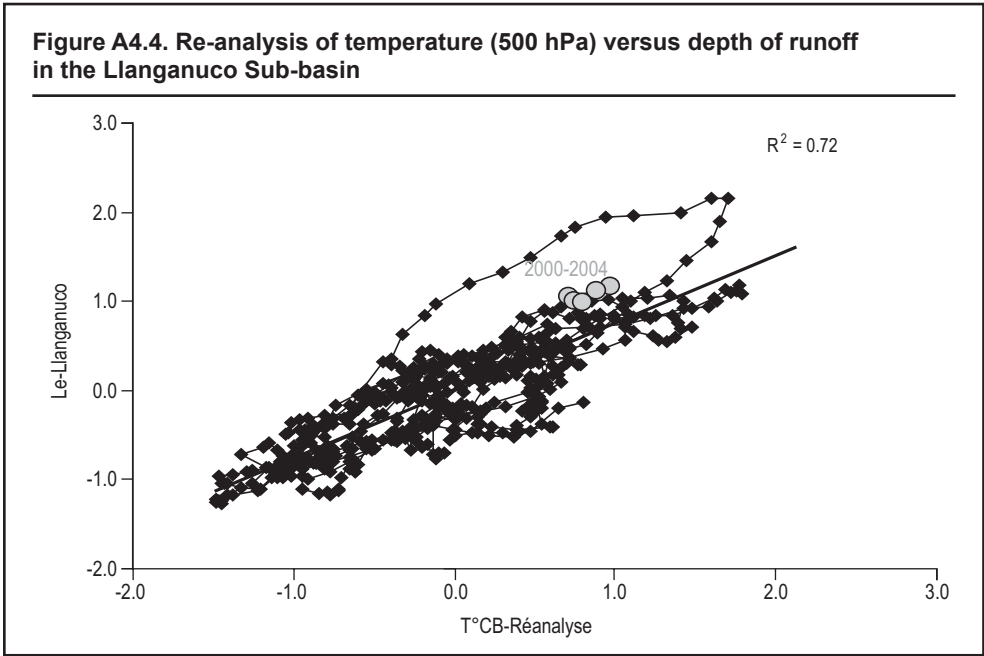
Source: Pouyaud et al. 2005.

Studies by Irmgard Juen (2006)

This important second work was conducted by Irmgard Juen (2006) as a part of his doctoral thesis at the University of Innsbruck (Austria). The aim of this study was to simulate the seasonal and interannual variations of glacier runoff for a period of 44 years and then to simulate the future runoff under different climate change scenarios. This mod-

eling was made based on the ITGG-2.0-R model. This model is in the group of hybrid models but has an important proximity to the energy balance model.

This work used many hypotheses based on observations on the Zongo glacier (Bolivia) due to the lack of data required by the model. It is important to describe this model in greater detail because it considers glaciological (glacier mass balance, analysis of albedo) and hydrological (soil water capacity, runoff coefficient) parameters.

The work is based on the use of the ITGG-2.0-R model, which uses the 2.0-ITGG model for modeling the glacier mass balance. This model not only considers the ablation depending on temperature but also some other atmospheric variables.

The ITGG-2.0-R at first takes a set of hypotheses to begin operating. The snow located outside the glacier disappears quickly and is not considered. All the precipitation that falls on the glacier is snow and there is no feedback for the albedo; this means that the snow covers the glacier tongue for only a few days and ultimately the influence of different aspects of the glacier surface is negligible. The model calculates all at monthly time steps and the runoff for the q_G glacier zone and the glacier-free zone q_N in order to obtain:

$$q_{Tn} = q_{Gn} + q_{Nn}$$

a) The calculation of the melting glacier is based on the ITGG-2.0 model, which was extended from the profile of the model of vertical mass balance VBP until reaching the model of total mass balance. The profile of vertical absolute balance is VBP_a; it is calculated by adding VBP to the specific net mass balance and a reference level bl_{zr}.

$$VBP_a = b\big|_{Zr} + VBP$$

Similar to VBP but with the atmospheric "emissivity" for wet and dry conditions, the following calculation is made:

$$b\big|_{Zr} = C\big|_{Zr} - \tau F(f)[SWin(1-\alpha)\big|_{Zr} + \varepsilon_a \sigma T_a^4\big|_{Zr} - \sigma T_s^4\big|_{Zr} + Cs(T_a\big|_{Zr} - T_s\big|_{Zr})]$$

where Cl_{Zr} is the accumulation with a reference level; ζ is the length of time of the ablation; SWin is the short-wave radiation; α is the albedo; ε_a is the emissivity of the atmosphere; σ is the Stefan-Boltzman constant; T_a is the air temperature, T_s is the surface temperature of the glacier; and Cs is the transfer coefficient.

The ITGG-2.0-R takes out the glacier runoff for each band (specialization) along the VBPa with the vertical gradient of the air temperature $\partial Ta/\partial Z$, accumulation $\partial C/\partial Z$, and the albedo $\partial\alpha/\partial Z$. The contribution of the melting ice from the glacier to the deep runoff of the total collecting zone Δ_T is:

$$q_G = \sum (q_{Gi} * AG_i)/\Delta T$$

where A_G is the glacial area.

Due to a considerable delay in the response of the "firn" glacier, 30 percent of the melted water is considered a contribution to the runoff for the next month.

$$q_{Gn} = q_{Gn} * 0.7 + q_{Gn-1} * 0.3$$

b) The runoff coming from the areas that are not situated over the glacier is calculated with precipitation P and has a vertical gradient $\partial P/\partial Z$. Precipitation P_i for each band (step) of elevation ΔZ is:

$$P_i = P + \partial P/\partial Z * \Delta Z$$

and the total space average P_A for the nonglaciated area is:

$$P_A = \sum (P_i * A_{Ni}) / \Delta T$$

A portion of (1-K) goes to the evaporation, transpiration, and baseflow.

Baseflow represents 20 percent of total runoff and it appears the next month after the flooding of the river. The value of K varies between 0.5 and 0.6 of rainfall.

The variable part of the baseflow was considered q_o and the total runoff for each month of the nonglaciated area is calculated as follows:

$$q_{Nn} = P_{An} * K_n + P_{An-1} * (1 - K_{n-1}) * 0.2 + q_O$$

In summary, the data used to operate this model were: f, SWin, α, $\in_a$ and T_a. From all these, the first three were taken from the Zongo glacier in Bolivia between 1996 and 1998 (provided by the IRD); the SWin was taken from two stations located in the Cordillera Blanca at 4,600 and 5,000 meters, respectively, in 1999. Air temperature was taken at Querocha Lake (3,980 meters) south of the Cordillera Blanca, data available from 1965 to 1994, and re-analysis data from NOAA at 500 hPa level.

In the case of melted water coming from the firn, the subsequent month was considered; this is a simple reservoir.

The results of this model were correct; simulations were made over six subglacial basins belonging to the Santa River (Parón, Llanganuco, Chancos, Quillcay, Pachacoto and Querococha).

Figure A4.5 shows the results of the modeling at the Llanganuco Basin. For a better understanding, see Juen et al. 2007.

Figure A4.5. Results of the modeling made at the Llanganuco Sub-basin, conducted by Juen
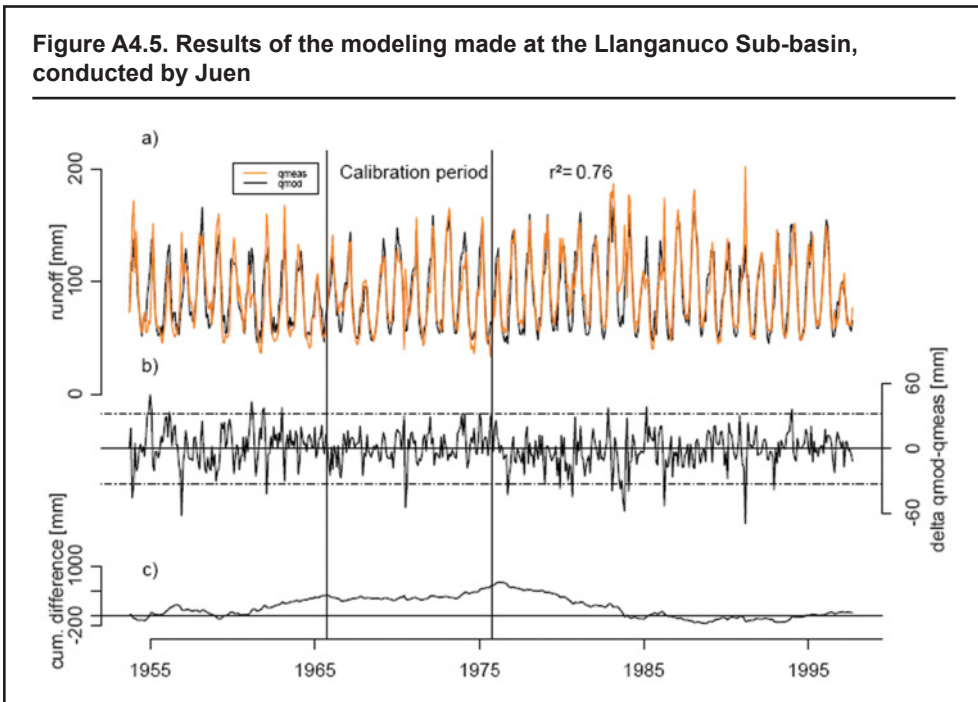
Studies by Wilson Suárez (2008)

The last work is the modeling of the glaciers of the Cordillera Blanca belonging to this basin. This modeling was conducted by **Wilson Suárez** as a part of his doctoral thesis at the University of Montpellier II (France) (2007) under the auspices of IRD. The work used a variation of the degree-day model at monthly time steps and is presented in Suárez et al. (2008). The model was calibrated on the Artesonraju glacier and the available temperature data were used as well as the outflow data situated at the front of the glacier.

This work modeled 11 subglacial basins of the Santa River with a starting point made on a pilot of the basin (Artesoncocha) that was used to extrapolate the model in a second time.

The model considers the glacial part and the nonglaciated part.

To study the glacial part, an adaptation of the degree-day model was used, still considering temperature as the only variable responsible for the ice.

This divides the glacier into two parts: a contributory part (Zc) and a noncontributory part (Znc). In theory, Zc is the only part of the glacier that will melt and where rainfall is considered liquid (the melting of snow is negligible throughout the process for the little time it remains on the soil). The separation between Zc and Znc is done by the temperature (calibration parameter), which is within a range of 0–2°C, coinciding with the proximity of the snow line and the Equilibrium Line Altitude (ELA).

This Zc is multiplied by a melt factor, equivalent to the DDF from the degree-day model, to find the contributions of glacier water to final runoff. The Baker equation (1982) was used to represent the response time from month to month in the model.

$$Q_{ice}(ti+1) = Q_{ice}(ti) \cdot e^{-\frac{ti+1-ti}{Kice}} + \left[P_{liq,ice}(ti+1) + M_{ice}(ti+1) \cdot T(ti+1) \right] \cdot \left(1 - e^{-\frac{ti+1-ti}{Kice}} \right)$$

where M is the equivalent of the degree-day factor (DDF) in mm/month; K_{ice} is a numerical constant; and $P_{liq,ice}$ (mm/month) is the liquid precipitation over the Zc.

For the nonglaciated area, an adaptation of the GR2M model was used. This is a simple reservoir model that uses only rainfall and evapotranspiration as input variables, and adjusts the input data with an X1 parameter and the maximum water retention capacity of the ground (Kapa) as regulating parameters of the model.

Figure A4.6 presents the results of the modeling operated in the Llanganuco Basin and Table A4.2 shows the general results in all sub-basins under the Nash coefficient, volume balance and r². For a better analysis of this methodology, see Suárez et al. 2008.

Figure A4.6. Modeling of the Llanganuco Basin and Sub-basin
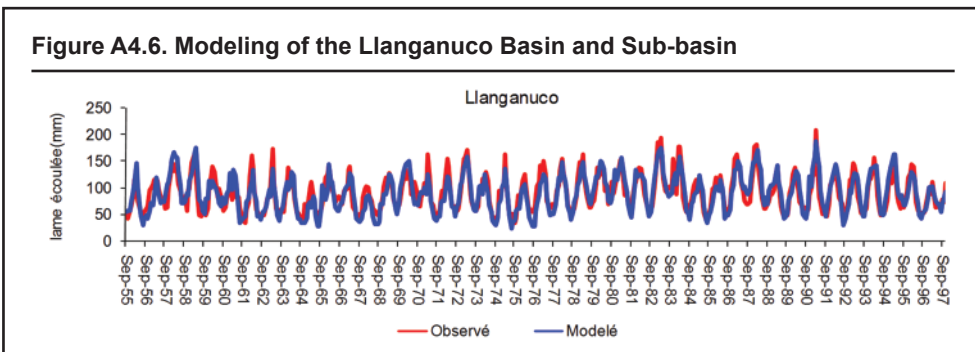
Source: Suárez 2007.

Table A4.2. Results for the modeling of 10 sub-basins g in the Santa River Basin

	Calibration				Validation			
	Nash	Balance	r²	Date	Nash	Balance	R²	Date
Los Cedros	0.43	0.97	0.42	Sep91–Aug94	0.34	1.19	0.48	Sep94–Aug97
Colcas	0.69	0.97	0.63	Sep91–Feb95	0.69	1.16	0.85	Mar95–Aug98
Artesón	0.78	0.99	0.69	Sep00–Feb03	0.72	0.99	0.74	Mar03–Aug05
Llanganuco	0.64	0.96	0.70	Sep55–Aug76	0.75	1.08	0.77	Sep76–Aug97
Chancos	0.76	1.04	0.69	Sep91–Aug95	0.63	0.73	0.76	Sep95–Aug98
Quillcay	0.74	1.01	0.75	Sep70–Aug84	0.71	0.99	0.67	Sep84–Aug97
Olleros	0.75	0.89	0.74	Sep70–Aug84	0.71	1.01	0.66	Sep84–Aug97
Yanamarey	0.76	0.95	0.73	Sep02–Mar05				
Pachacoto	0.76	0.90	0.71	Sep70–Aug84	0.72	0.97	0.70	Sep84–Aug97
Recreta	0.58	0.85	0.60	Mar91–Dec95				

Source: Suárez 2007.

Conclusion

From these three studies, the model proposed by Juen provides the best results, but with few differences from the model proposed by Suárez (based on the optimization criteria; for example, r²). But the quantity of information required in Juen's model is impossible to collect in the remaining part of the Santa Basin or in the other basins (Rímac and Mantaro). A common point of the three models is that they consider air temperature as a determining factor of glacier melting and the monthly time step is considered to be the correct one.

Taking into account the advantages and disadvantages of the existing models and considering the preceding works conducted on the Santa River, the model chosen as a starting point will be the degree-month model in order to implement the glacier functioning in the WEAP model (monthly time step).

PART 2. ADOPTED MODELING APPROACH

This section corresponds to an adaptation of a working paper entitled, "An Approach for Modeling the Hydrologic Role of Glaciers in WEAP," proposed by SEI-US and IRD.

General Formulation

The general formulation of glaciers in WEAP will use the standard approach to building a WEAP rainfall-runoff model of a mountainous region as a starting point. In WEAP, rainfall-runoff processes are simulated by first dividing a watershed into subwatersheds, which are the contributing areas above points of streamflow measurement or management control (Figure A4.7). Furthermore, a subwatershed area above a "pour point" is divided into i elevation bands. Each subwatershed/elevation band is then represented as a unique WEAP catchment object within which temporally variable land cover and temporally variable yet spatially homogeneous climate conditions can be imposed on a time-step by time-step basis. This section describes an approach for adding a representation of evolving glacial contributions to simulate hydrologic processes to be incorporated into the WEAP rainfall-runoff representation by dividing each elevation band, i, into either a glaciated (j=1) or nonglaciated (j=2) portion (Figure A4.8).

Figure A4.7. Example of WEAP model of Santa Basin

Source: Authors.

Figure A4.8. Subcatchment with glacier

Source: Authors.

Calculation Steps

The calculations made in implementing the procedure will occur on two timescales: a monthly time step, t, and an annual time step, y, as indicated in a particular equation. In this notation, a subscript $t=0$ suggests that the expression pertains to conditions at the beginning of a hydrologic year, y, before any of the monthly time-step calculations are carried out. Conversely, the subscript $t=12$ indicates that the expression pertains to conditions at the transition between hydrologic years following the completion of all monthly time-step calculations within a year. In this notation y, $t=12$ is equivalent to $y+1$, $t=0$. The notation for initial conditions is $y=0$, $t=0$.

Step 0. Initial Conditions

The first step in the process of representing glaciers within a WEAP application will be to define the initial conditions within each computational object used to simulate hydrologic processes. This section deals only with the role played by glaciers located within these computational objects in determining subwatershed-scale hydrologic response, because the hydrologic processes in nonglaciated areas will be captured using a separate rainfall-runoff routine that has already been integrated into the WEAP software (Yates et al. 2005).

From recent GIS databases of the spatial extent of glaciers, the surface area of glacier ice within each elevation band of each subwatershed (a unique WEAP catchment model object) can be calculated. The overall initial allocation of the actual area within each catchment, A_i, defined in units of km^2 will then be defined as:

Figure A4.9. Schematic of the two-layer soil moisture store, showing the different hydrologic inputs and outputs for a given land cover
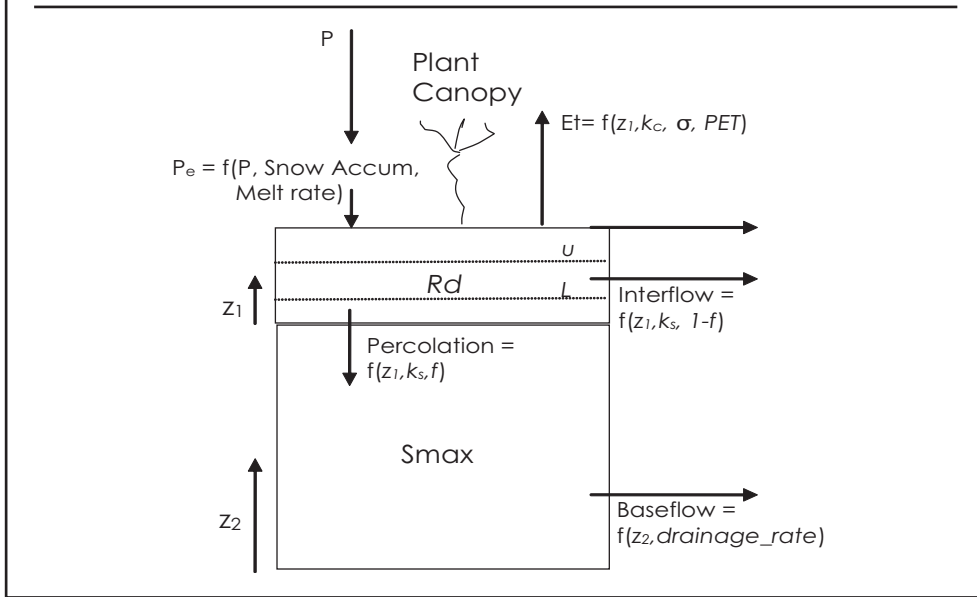
Source: Yates et al. 2005.

$$A_i = \sum_{j=1}^{2} A_{y=0,t=0,i,j} \tag{1}$$

and the total initial extent of glaciers in a subwatershed will be defined as:

$$A_{glacier,\,y=0,t=0} = \sum_{i=m}^{n} A_{y=0,t=0,i,j=1} \tag{2}$$

where n is the total number of elevation bands within a subwatershed and m is the lowest elevation band containing glacier ice. This glacial area value has already been calculated for each of the 20 subwatersheds in the Santa River WEAP application, suggesting that the GIS analysis pursued to estimate the initial glacier extent is feasible in the Peruvian context. Note that A_i is constant but the relative proportion between $A_{j=1}$ and $A_{j=2}$ will vary after the end of each hydrologic year.

Based on a published empirical relationship that relates glacier ice volume (V) expressed in km³ to glacial area for individual glaciers (Bahr et al. 1997), the initial glacier volume in each subwatershed will be estimated as:

$$V_{glacier,\,y=0,t=0} = c \cdot A_{glacier,\,y=0,t=0}^{b} \tag{3}$$

where c and b are scaling factors related to the width, slope, side drag and mass balance of a glacier. Analysis of 144 glaciers around the world suggests factor values of $b = 1.36$ and $c = 0.048$ (Bahr et al. 1997; Klein and Isacks 1998). The research team decided to use these volume-area correlation factors (Figure 1 in Bahr et al. 1997) despite the fact that no Andean glaciers were included in the correlation due to the lack of studies in the zone. It is expected that similar studies will be developed for Andean glaciers, in which case

the correlation factors will be verified (J. C. Pouget, personal communication). Note that this volume corresponds to the entire initial ice mass within a WEAP subwatershed and that in using (3) there is an implicit assumption that water equivalent depth over the total glacier surface is uniform. An allocation of this volume between glaciated elevation bands is not attempted. The reason why the volume is not allocated between elevation bands stems from the fact that the existing area-volume ratios are based on total glacier volume and area (Figure 1 in Bahr et al. 1997).

Step 1. Estimate Runoff from Melting Snow and Ice

For each monthly time step, t, within a hydrologic year, y, the contribution to surface runoff from the glaciated portion of a unique catchment area, i, will be estimated based on a modification to the method proposed by Schaefli et al. 2005. This method, which was developed for the estimation of daily contributions to streamflow from melting snow and ice from glaciers, was modified by Suárez et al. (2008) for use in modeling Peruvian glaciers on a monthly time step. The streamflow contribution due to snow melt from the surface of a glacier within a particular elevation band is:

$$Q_{snow,y,t,i,j=1} = \left\{ Q_{snow,y,t-1,i,j=1} \cdot e^{-\frac{t-(t-1)_i}{K_{snow}}} + \left[P_{liq,y,t,i,j=1} + M_{snow,y,t,i,j=1} \right] \cdot \left(1 - e^{-\frac{t-(t-1)}{K_{snow}}} \right) \right\}$$

(4)

where for monthly time step, t, during hydrologic year, y:

$Q_{snow,y,t,i,j=1}$ = ith catchment discharge from snow reservoir (mm/month)

K_{snow} = time constant (month)

$P_{liq,y,t,i,j=1}$ = liquid rainfall on snow surface in ith catchment (mm/month)

$$= \begin{cases} P_{y,t,i}, & T_{T,t,i} \geq T_0 \\ 0, & T_{T,t,i} < T_0 \end{cases}$$

(4a)

$P_{y,t,i}$ = ith catchment total monthly precipitation, also used in j=2 (mm/month)

$T_{y,t,i}$ = ith catchment monthly average temperature, also used in j=2 (ºC)

T_o = threshold temperature (°C)

$M_{snow,y,t,i,j=1}$ = snow melt from glacier surface in ith catchment (mm/month)

$$= \min \begin{cases} SInitial_{y,t,i,j=1} \\ M_{pot\,snow,y,t,i,j=1} \end{cases}$$

(4b)

$SInitial_{y,t,i,j=1}$ = snow-water equivalent on the glacier surface in ith catchment (mm)

$$= SFinal_{y,t-1,i,j=1} + P_{snow,y,t,i,j=1}$$

(4c)

$P_{snow,y,t,i,j=1}$ = snow accumulation on glacier surface in ith catchment (mm/month)

$$= \begin{cases} 0, & T_{y,t,i} \geq T_0 \\ P_{y,t,i}, & T_{y,t,i} < T_0 \end{cases} \tag{4d}$$

$M_{pot\ snow,\ y,\ t,\ i,\ j=1}$ = potential snow melt in the *ith* catchment (mm/month)

$$= \begin{cases} a_{snow}(T_{y,t,i} - T_0), & T_{y,t,i} \geq T_0 \\ 0, & T_{y,t,i} < T_0 \end{cases} \tag{4e}$$

a_{snow} = degree-day factor for snow melt (mm/month/°C)

T$_o$ constitutes a threshold value for conversion of liquid precipitation into snow that is defined by the user and may constitute a calibration parameter. According to (4c), for the first month of each hydrologic year the value of SInitial will be exclusively the value of P$_{snow,y,t,I,j=1}$, given that at the end of the previous year snow either melted or was converted to ice. After the first time step of the water year, each month P$_{snow,y,t,I,j=1}$ is defined as a function of the current temperature and the threshold temperature for converting water to snow according to (4d).

At the end of each monthly time step, the snow-water equivalent accumulated on the surface of the glacier must be updated to account for snow-melt runoff.

$$SFinal_{y,\ t,\ i,\ j=1} = SFinal_{y,\ t-1,\ i,\ j=1} + P_{snow,\ y,\ t,\ i,\ j=1} - Q_{snow,\ y,\ t,\ i,\ j=1} \tag{6}$$

In (4b) it is possible that the potential snow melt in a given month, *t*, will exceed the actual accumulated amount of snow-water equivalents on the surface of the glacier within elevation band *i*. In this case, all of the snow-water equivalents within the band will be melted and the surface of the glacier ice will become exposed. To calculate the portion of a monthly time step during which the glacier surface is snow free, the expression

$$SFree_{y,t,i,\ j=1} = \begin{cases} 0, & P_{snow\ y,t,i,\ j=1} \geq 0 \\ (1 - \dfrac{SFinal_{y,t,i,\ j=1} - Q_{snow\ y,t,i,\ j=1}}{SFinal_{y,t,i,\ j=1}}) & 0 < (1 - \dfrac{SFinal_{y,t,i,\ j=1} - Q_{snow\ y,t,i,\ j=1}}{SFinal_{y,t,i,\ j=1}}) < 1 \\ 1, & (1 - \dfrac{SFinal_{y,t,i,\ j=1} - Q_{snow\ y,t,i,\ j=1}}{SFinal_{y,t,i,\ j=1}}) > 1 \\ 1, & SFinal_{y,t,i,\ j=1} < 0 \end{cases}$$

$$\tag{7}$$

is evaluated once the final snowmelt contribution to runoff is calculated. The fraction inside the parenthesis indicates the portion of the time that the surface was covered with snow, so the complement indicates the portion of the time that the surface was free of snow.

The preceding set of equations will be executed during each time step, *t*, to approximate the contribution of melting snow on the surface of the glacier within a given band to surface flow in the catchment. During time steps, *t*, when $SFree_{y,\ t,\ i,\ h=1}$ is non-zero, an additional set of equations will be executed to estimate the contribution of melting glacier ice to surface flow in the *ith* catchment.

$$Q_{ice,\,y,t,\,i,\,j=1} = \left\{ Q_{ice,\,y,\,t-1,i,\,j=1} \cdot e^{-\frac{t-(t-1)_i}{K_{ice}}} + \left[P_{liq,\,y,t,i,\,j=1} + M_{ice,\,y,t,i,\,j=1} \right] \cdot \left(1 - e^{-\frac{t-(t-1)}{K_{ice}}} \right) \right\}$$ (8)

where the preceding definitions for snow apply for ice with the modifications that
$M_{pot\,ice,\,y,\,t,\,i,\,j=1}$ = potential ice melt from the *ith* catchment (mm/month)

$$= SFree_{y,t,i,\,j=1} \cdot \begin{cases} a_{ice}(T_{y,\,t,i} - T_0), & T_{y,t,i} \geq T_0 \\ 0, & T_{y,t,i} < T_0 \end{cases}$$ (7a)

a_{ice} = degree-day factor for ice melt (mm/month/ºC)

In (7) the term $P_{liq,y,t,I,j=1}$ corresponds to the portion of rain that falls in a snow-free area, so it was not accounted for in (4), where what is accounted for is the portion of rain that falls in a snow-covered area. (7) is only estimated when ice is exposed; in other words, when $SFree_{y,\,t,\,i,\,h=1}$ is non-zero.

The assumptions implicit in (7) are that icemelt from the snow-free exposed surface of a glacier within an elevation band is not volume limited and that icemelt is blocked when there is snow covering the glacier.

In the preceding equations, the parameters k_{snow}, k_{ice}, a_{snow} and a_{ice} were calibrated by Suárez based on observations of glaciers in Peru. These values will be used as the starting point for the WEAP modeling that will occur for the current project.

Note that the outputs from (4) and (7) are in units of mm, or equivalent depths of water. The actual volumes of water in m³ associated with precipitation on the surface of a glacier with an elevation band *i*, the contribution of snow and ice melt to surface flow from the *ith* catchment, and the accumulation of snow on the surface of the glacier are determined by accounting for the surface area of the glacier within the elevation band.

$$VQ_{snow,y,t,i,\,j=1} = \left(Q_{snow,y,t,i,\,j=1} / 1000 \right) \cdot A_{y,t=0,i,\,j=1} \cdot 1000^2 \,(\text{m}^3)$$ (8a)

$$VQ_{ice,y,t,i,\,j=1} = \left(Q_{ice,y,t,i,\,j=1} / 1000 \right) \cdot A_{y,t=0,i,\,j=1} \cdot 1000^2 \,(\text{m}^3)$$ (8b)

$$VP_{liq,\,y,i,\,j=1} = \left(P_{liq,\,y,i,\,j=1} / 1000 \right) \cdot A_{y,t=0,i,\,j=1} \cdot 1000^2 \,(\text{m}^3)$$ (8c)

$$VSFinal_{y,t,i,\,j=1} = \left(SFinal_{y,t,i,\,j=1} / 1000 \right) \cdot A_{y,t=0,i,\,j=1} \cdot 1000^2 \,(\text{m}^3)$$ (8d)

$VP_{liq,y,t,j=1}$ in (8c) is the synthesis of the volume of water that fell within the time step, which uses the same $P_{liq,y,i,j=1}$ variable and is intended for volume calculation, different from the use of $P_{liq,y,t,j=1}$ in (4) and (6) to estimate snow and ice melt. The annual balance of $\Delta VP_{liq,y,t,j=1}$ is estimated in (10) to identify how much liquid water did not make part of snow or ice contributions to streamflow. The sum of liquid and snow phase that do not run off from the subwatershed at the end of the year is converted to ice and added to the total glacier volume (Step 3, eq. 12).

According to the approach presented in the previous section, there is outflow from each band as snowmelt and icemelt. However, areas and volumes at each elevation band are not tracked. Instead, the volume of icemelt, snowmelt and liquid runoff are added at the end of the year to estimate total runoff, which is compared to actual measured runoff data at the downstream point of the subwatershed. This comparison constitutes the main criterion for calibration of the model.

Step 2. Surface Runoff at the Subwatershed Level

For each monthly time step, the volume of surface runoff within a subwatershed will be the sum of the contribution of melting snow and ice for the glaciated portion of the subwatershed and the runoff coming from the simulation of rainfall-runoff processes in nonglaciated portions of the subwatershed.

$$Q_{sub-watershed,y,t} = \sum_{i=m}^{n} \left(VQ_{snow,y,t,i,j=1} + VQ_{ice,y,t,i,j=1} \right) + \sum_{i=1}^{n} Q_{WEAP,y,t,i,j=2} \quad (\text{m}^3) \tag{9}$$

Note that in (9) the simulated contribution to surface runoff from nonglaciated portions of the subwatershed will be provided by the internal rainfall runoff routines already implemented in WEAP (Yates et al. 2005). Note also that the WEAP model assumes that all contributions to surface runoff flows from a subwatershed coming from the several elevation bands arrive at the subwatershed pour point within the time step, *t*, during which they are generated. Ice and snow flows, on the other hand, as calculated based on Schaefli et al. (2005) and Suárez et. al. (2008), contain an autocorrelation component that implies that the flow from a current time step is a function of the flow from the immediately preceding time step. For monthly time steps, this autocorrelation may tend to 0 in relation to the glacier area in the watershed.

Step 3. Annual Mass Balance

At the end of the 12 monthly time steps, *t*, in a hydrologic year, *y*, it is possible to carry out a mass balance that can be used to assess changes in the overall volume of glacier ice within a subwatershed. This will be done by implementing a mass balance, carried out in units of m³ on each of the *n-m+1* elevation bands within a subwatershed that contained glacier ice at the start of a hydrologic year. The goal is to account for all water that has entered a particular elevation band, *i*, and has not flowed from the band during the hydrologic year. The input of water to a band comes either through liquid precipitation or snowfall. Outputs of water include the estimated runoff from melting snow and the melting of glacier ice, (4) and (7), which take into consideration runoff associated with liquid precipitation falling on the surface of a glacier within elevation band *i*, $P_{liq,y,t,i,j=1}$. Considering first the liquid phase, the annual mass balance is:

$$\Delta V_{liq,y,t=12,i} = \sum_{t=1}^{12} VP_{liq,y,t,i,j=1} - \left(\sum_{t=1}^{12} VQ_{snow,y,t,i,j=1} + \sum_{t=1}^{12} VQ_{ice,y,t,i,j=1} \right) \quad (\text{m}^3) \tag{10}$$

If this balance is positive, the implication is that some portion of the liquid water that has fallen within the elevation band has not been offset by liquid water leaving the band, and as a result, on a net basis, there is a volume of liquid water free within the elevation band at the end of the hydrologic year.

The annual mass balance in snow is actually being calculated dynamically throughout the hydrologic year based on (4) and (5). The mass balance for the snow phase at the end of the hydrologic year *y* is:

$$\Delta V_{snow,y,t=12,i} = VSFinal_{y,t=12,i,j=1} \quad (\text{m}^3) \tag{11}$$

expressed as a water equivalent. The total net accumulation of water within the *ith* catchment during hydrologic year, *y* , expressed as a mass (*ΔM*) in units of g, is:

$$\Delta M_{water,y,t=12,i} = \left(\Delta V_{liq,y,t=12,i} + \Delta V_{snow,y,t=12,i} \right) \cdot \rho_{water} \cdot 100^3 \quad (\text{g}) \tag{12}$$

where ρ_{water} is the density of liquid water expressed in units of g/cm³.

Here an assumption is invoked that at the end of the hydrologic year, y, all water mass within a catchment, i, is frozen and converted to ice. In this case, the change in the volume of ice within the *ith* catchment during hydrologic year, y, is:

$$\Delta V_{ice,\ y,t=12,i} = \frac{\Delta M_{water,y,t=12,i}}{\rho_{ice} \cdot 100^3} \quad (\text{m}^3)$$

(13)

where ρ_{ice} is the density of frozen ice expressed in units of g/cm^3.

Based the change in ice volume within each elevation band, i, in (12), it is possible to estimate the position of the point where the change in mass is essentially zero for the hydrologic year. This will be done by sequentially comparing $\Delta V_{ice,y,t=12,i}$ to $\Delta V_{ice,y,t=12,i+1}$ to find a point where the mass balance transitions from a negative value to a positive value. Once this point is found, the approximate elevation of the point of equilibrium will be:

$$E_{equib} = -\Delta V_{ice,\ y,t=12,i} \cdot \frac{E_{i+1} - E_i}{\Delta V_{ice,\ y,t=12,i+1} - \Delta V_{ice,\ y,t=12,i}} - E_i$$

(14)

where E_i, E_{i+1}, and E_{equib} are the mid-elevations of bands i and $i+1$ and the elevation of the approximate point of annual water balance equilibrium.

From the annual mass balance conducted on each of the m elevation bands containing ice at the start of a hydrologic year, y, it will also be possible to estimate the overall change in the mass of glacier ice within a subwatershed.

$$\Delta V_{glacier,\ y,t=12} = \sum_{i=m}^{n} \Delta V_{ice,\ y,t=12,i} \quad (\text{m}^3)$$

(15)

Step 4. Annual Evolution of Glacier Geometry

Based on the value of (15), it will be possible to adjust the overall volume and extent of glacier ice within a subwatershed prior to moving on to the subsequent hydrologic year. Ideally this would be done by assessing the internal dynamics of ice movement within the glacier. This is likely beyond the scope of both the current project, which focuses on the water management implication of glacier change and the available data in most glaciated regions of the world. As such, a simplifying model of the redistribution of ice, which assumes that changes in the total volume of ice manifest themselves at the low part or tongue of the glacier, will be used. The first step in the process is to estimate the new estimated surface area of the glacier at the end of hydrologic year y.

$$A_{glacier,\ y,t=12} = \sqrt[b]{\frac{V_{glacier,\ y,t=0} + \dfrac{\Delta V_{glacier,\ y,t=12}}{1000^3}}{c}} \quad (\text{km}^2)$$

(16)

The next step is to assess the estimated change in the surface area of the glacier during the hydrologic year.

$$\Delta A_{glacier,\ y,t=12} = A_{glacier,\ y,t=12} - A_{glacier,\ y,t=0}$$

(17)

Two approaches will be explored for adjusting the glacial area at the lowest elevation bands.

APPROACH 1: DEFINING A MAXIMUM GLACIAL AREA, MAXA$_i$, AT THE LOWEST BAND

The assumption is that the change in surface area will be concentrated within the lowest elevation band containing ice, $i=m$, during the hydrologic year, within limits. The minimum limit is that all of the glacier surface area within the band is removed and the maximum limit is a user-defined maximum extent of glacier ice within the elevation band, $MaxA_i$. In this case, the updated area in elevation band $i=m$ will be:

$$A_{y,t=12,i=m} = \begin{cases} 0, & A_{y,t=0,i=m} + \Delta A_{glacier,y,t=12} < 0 \\ A_{y,t=0,i=m} + \Delta A_{glacier,y,t=12}, & MaxA_i \geq A_{y,t=0,i=m} + \Delta A_{glacier,y,t=12} > 0 \\ MaxA_i, & A_{y,t=0,i=1} + \Delta A_{glacier,y,t=12} > MaxA_i \end{cases} \qquad (18)$$

With this approach, $MaxA_i$ could be defined based on geomorphic parameters that would indicate the likelihood of an area within the elevation band glacier to be lost. For instance, the slope of sub-bands within a given elevation band could be used to decide what portion of area is likely to be lost, so that areas with higher slopes will be likely to melt and areas with lower slopes will be likely to remain. $MaxA_i$ will be an estimate of the glacial areas that are likely to remain. A drawback of this approach is that the model will be dependent on additional GIS processing, implying additional controlling variables inside the glacier model.

From (18), it is possible to calculate the residual of the overall change in the glaciated area that could not be accounted for within elevation band $i=m$.

$$RA_{y,t=12,i=m} = \begin{cases} A_{y,t=0,i=m} + \Delta A_{glacier,y,t=12}, & A_{y,t=0,i=m} + \Delta A_{glacier,y,t=12} < 0 \\ 0, & MaxA_i \geq A_{y,t=0,i=m} + \Delta A_{glacier,y,t=12} > 0 \\ A_{y,t=0,i=m} + \Delta A_{glacier,y,t=12} - MaxA_i, & A_{y,t=0,i=m} + \Delta A_{glacier,y,t=12} > MaxA_i \end{cases}$$

$$(19)$$

If $RA_{y,t=12,i=m}$ is negative, then (18) is repeated for next upslope elevation band, $i=m+1$, by replacing $\Delta A_{glacier,y,t=12}$ with $RA_{y,t=12,i=m}$ in the expression. In an extreme case of $\Delta A_{glacier,y,t=12}$, a residual for $RA_{y,t=12,i=m+1}$ could also be calculated according to a recalculation of (19), and (18) could be implemented for elevation band $i=m+3$, and so on.

If $RA_{y,t=12,i=m}$ is positive, then a new downslope elevation band that contains ice will be added for the subsequent hydrologic year. Here $A_{y+1,t=0,i=m-1}$ will be set equal to $RA_{y,t=12,i=m}$ with the possibility—in the extreme case that $RA_{y,t=12,i=m}$ exceeds $Amax_{m-1}$—that additional downslope elevation bands could be added.

The final step in the annual adjustment to the glacial extent in a subwatershed will be to compensate for change in the extent of glacier ice in the areas defining the nonglaciated portion of a particular elevation band i.

$$A_{y,t=12,i,j=2} = A_i - A_{y,t-12,i,j=1} \qquad (20)$$

APPROACH 2: DEFINING A DEPTH PARAMETER, $k_{i=M}$, AT THE TWO LOWEST BANDS

An alternative approach to the one proposed above involves the assumption of a differential depth at the two lowest elevation bands. Instead of defining $MaxA_i$, the adjustment of the areas within the two lowest elevation bands will be based on a depth parameter, $k_{i=m}$ and $k_{i=m+1}=c * k_{i=m}$, so that the area is reduced as a function of the depth of the glacier in the elevation band.

$$A_{y,t=12,i=m} = A_{y,t=0,i=m} \cdot k_{i=m} \tag{21}$$

$$A_{y,t=12,i=m+1} = A_{y,t=0,i=m+1} \cdot ck_{i=m} \tag{22}$$

An implication of this approach would be that the depth of the glacier would no longer be uniform. With an initial $c=1.2$, $k_{i=m}$ would constitute a parameter that will be adjusted during calibration and would allow the control of the depth evolution of the two lowest elevation bands, given that

$$h_{y,t=12,i=m} = h_{ave} \cdot k_{i=m} \tag{23}$$

$$h_{y,t=12,i=m+1} = h_{ave} \cdot ck_{i=m} \tag{24}$$

where

$$h_{ave} = \frac{A_{glacier,y,t=12}}{V_{glacier,y,t=12}} \tag{25}$$

The final implementation of Approach 2 will depend on whether there are depth data to corroborate parameters $k_{i=m}$ and c. It may be possible to obtain data on specific subwatersheds, but there may not be data for corroboration at the scale of the entire watershed.

Step 5. Calibration

The key criterion for calibration is the adjustment of parameters to obtain measured glacier flow. The volume of icemelt, snowmelt and liquid runoff are added at the end of the year and compared to actual measured runoff data at the downstream point of the subwatershed. The observed streamflow at the subwatershed pour points will be used as another calibration target through a comparison with the results of (9).

The threshold value for conversion of liquid precipitation into snow, T_o, will be defined by the user and, although the value needs to be between a physically based range, it can also be used as calibration parameter.

The approaches for adjusting the area of the glacier at the lower elevation bands will also make use of calibration parameters, either $MaxAi$ or $k_{i=m}$. Depending on data availability for comparing model data to glacial areas and depths, the parameters will be calibrated until modeled areas are comparable to actual areas.

An additional calibration metric will use the E_{equib} calculated in (14), comparing it to field data where available and to the value to the position of the Equilibrium Line Altitude (ELA), which is defined for the hydrologic year according the equation derived in Condom et al. (2007):

$$ELA_T = 3427 - 1148 \left(\log_{10} \sum_{i=1}^{n} \frac{A_{y,i,j=1}}{A_{glacier,y}} \sum_{t=1}^{12} P_{t,i} \right) + \frac{\sum_{i=1}^{n} \frac{A_{y,i,j=1}}{A_{glacier,y}} \frac{1}{12} \sum_{t=1}^{12} T_{t,i}}{0.007} + \frac{1}{n} \sum_{i=1}^{n} E_i \tag{26}$$

   The calculation of ELA will allow additional checking of the results for calibration runs, but will also allow the tracking of the evolution of the glacier for future climate change scenarios.

   The values of calibration parameters k_{snow}, k_{ice}, a_{snow}, a_{ice}, and T_o will be adjusted until a reasonable correspondence between the observed and simulated streamflows at the pour points is obtained, and until a correspondence between annual evolution of E_{equib}, ELA field data and ELA_T in (26) is achieved.

PART 3. PROGRESS IN PARAMETERIZATION

Progress in Glacier Parameterization Module (2000–2007)

The collected data from Arteson were used to build the modeling of the glacier.

Artesonraju Glacier Basin

The Arteson Basin is located within the Parón Lake watershed (integrated system). This basin has a total area of 8.8 km², of which 0.6 km² belong to Arteson Lake; 72.9 percent of this area is covered by glaciers (Image SPOT5 2003). The basin has a limnimeter (operated by IRD and the National Water Agency–ANA, formerly INRENA) at its outlet point (Arteson Lake) and a hydraulic structure (overflow channel in V) that makes it possible to calculate this basin's output flow. The team has operated from 1996 to the present, with a gap between 1997 and 2001.

There are four pluviometers on the Artesonraju glacier situated approximately between 4,900 and 5,100 meters above sea level, operating since 2001, under the responsibility of ANA. IRD and ANA installed a climate station (at 4,980 meters) that has provided humidity and temperature data since 2002.

The 1970 National Glacier Inventory, Landsat satellite imagery (1987 and 2006) owned by SENAMHI and a 2003 SPOT image make it possible to have mapping information that allows access to the variation in glacier coverage (area) information.

Figure A4.10a shows the positions of the basin and the Artesonraju glacier, and Figure A4.10b shows a view of the limnimetric station at the exit point of the basin.

Progress in Parameterization

The glacier module was developed jointly with SEI-US. The IRD team was responsible for verifying the equations and hypothesis used for the Arteson basin; SEI was responsible for software coding (algorithms) and for connecting the module to the WEAP.

The principles that have guided the implementation of the glacier in WEAP were:

■ The principle of parsimony which means taking the minimum of calibration parameters.
■ Once the calibration is done, save the calibrated parameters for the entire basin since there are no other well-known sites with long-term hydrometeorological records.
■ Parameters of fusion (ice and snow) degree-days were changed to monthly step fusion parameters or "degree-months."

Finally, to correspond with the principle of parsimony, equations (5) and (8) have been simplified as equations 5bis and 8bis. Thus, the melting of snow and glacier is controlled by only three parameters: the T0 temperature limit, the parameters of degree-month fusion of ice (a_{ice}) and snow (a_{snow}).
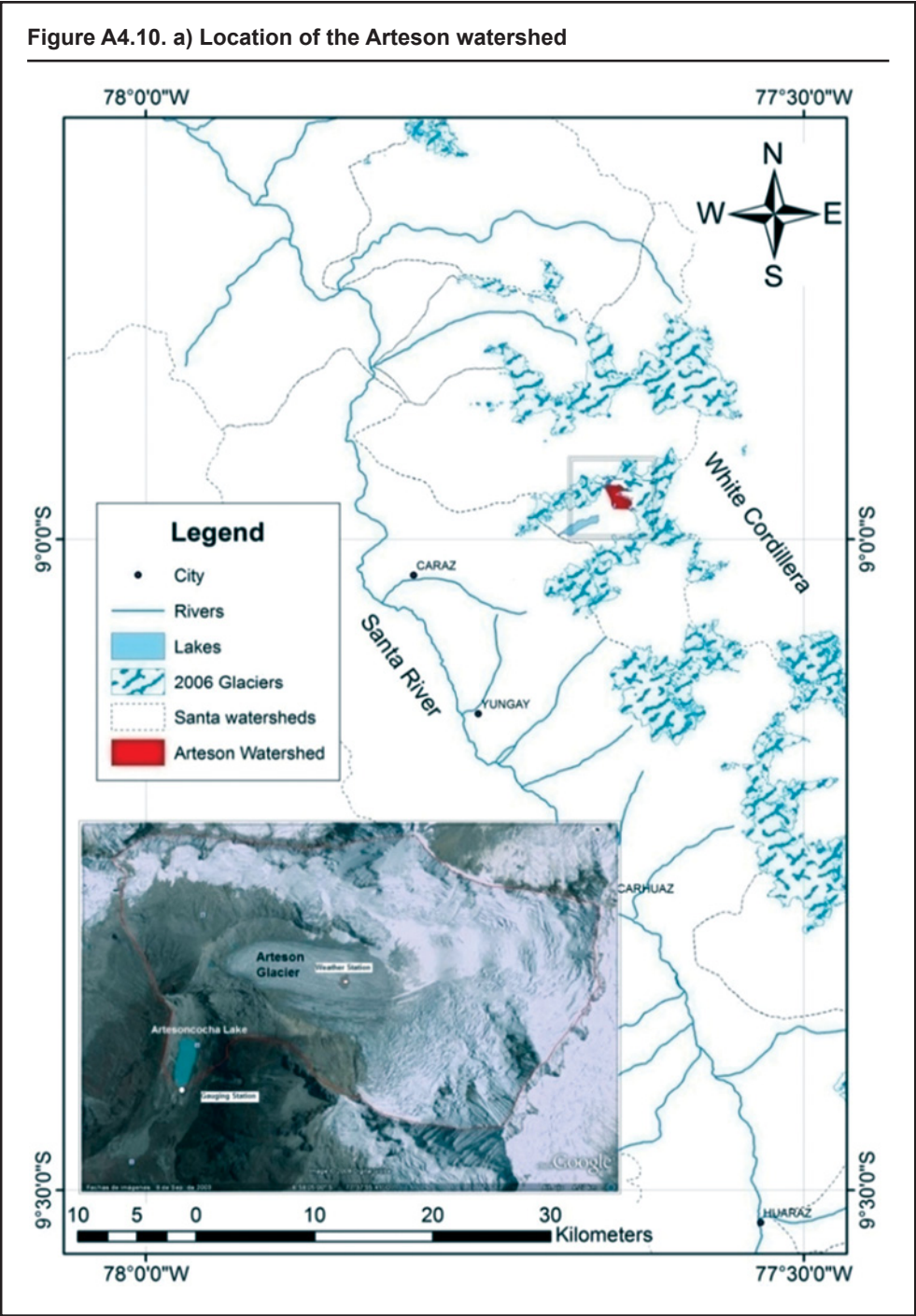
The equations used for calibration were:

$$Q_{snow,T,t,i,\ j=1} = P_{liq,T,t,i,j=1} + M_{snow,T,t,i,j=1} \qquad\qquad \text{eq. 4bis (modification of eq. 4)}$$

and

$$Q_{ice,T,t,i,\ j=1} = P_{liq,T,t,i,j=1} + M_{ice,T,t,i,j=1} \qquad\qquad \text{eq. 7bis (modification of eq. 7)}$$

Figure A4.10. a) Location of the Arteson watershed

Source: Authors.

Figure A4.10. b) Hydrometric station installed at the outlet of Arteson Basin in the upper glacier


Source: Photo: Bernard Pouyaud.

To carry out the range optimization used by T0, it was contained between -2 and +2°C; and for the degree-day parameter it was limited in the range of values used in the bibliography (see Table 1.1).

Figure A4.11 presents the results of calibration for the Arteson Sub-basin during the 2001–2005 period and shows a good correlation between simulated and observed data. The optimized parameters are:

T0 =1.45°C ; a_{ice} =600 mm/month/°C y a_{snow} =380 mm/month/°C.

Figure A4.11. Outflow at Artesoncocha gauge station: comparison between observed and simulated values between September 2001 and August 2005, R^2=0.67 p≤0.05
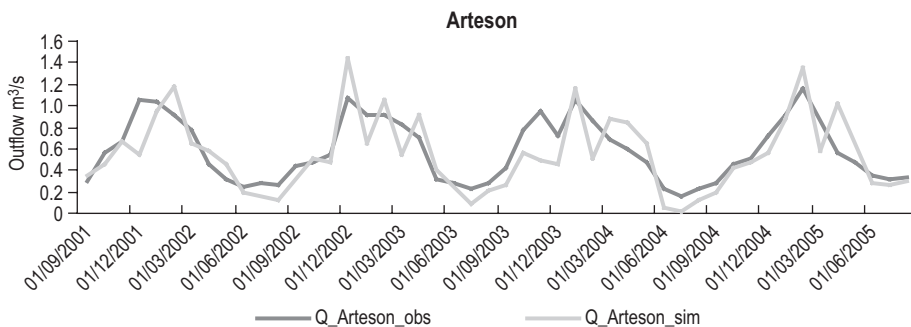
Source: Authors.

Progress in parameterization in the entire Santa River Basin Module (1969–1997)

The principles applied for the entire Santa River Basin were to:

- Control and interpolate the input data in the module;
- Use the calibrated parameters from Arteson for the glacier part (see above);
- Start the system from September 1969 with the extensions of the glaciers observed in 1970;
- Calibrate the parameters for the nonglaciated part and keep the same parameters for all subwatersheds;
- Conduct calibration by considering not only the flow in each control station, but also changes in glacier length.

With regard to rainfall, 43 stations with databases using monthly time steps were used. An interpolation with the 43 stations (inverse distance type) was made to generate data from 164 catchments for the period beginning in September 1969 and ending in August 1996.

With regard to temperatures, only the Recuay station has good-quality data without gaps. Thus, to make the interpolation across the entire Santa River Basin (164 catchments), the numerical model of terrain (DEM) and a temperature gradient equal to $0.6°/100$ m were used to generate the time series for the 164 catchments for 1969–1996.

Finally, to operate the calibration of soil (sub-surface and deep) parameters (Table A4.3), several samples were taken, considering the range already used in other models of WEAP in mountain areas (personal communication with scientists from SEI).

Table A4.3. Calibrated parameters in the Santa River Basin of the WEAP hydrological model, considering two-layer soil moisture storage

| Parameter	Unit	Value
Crop coefficient		1.1
Root zone capacity	mm	80
Root zone conductivity	mm/month	500
Deep water capacity	mm	500
Deep water conductivity	mm/month	50
Runoff Resistance Factor		
Crops		4.0
Matorral (shrub)		3.2
Tundra		0.8
Coastal Plain		0.8
Flow Direction	**% horizontal**	**0.68**
Z1	%	35
Z2	%	35

Source: Yates et al. 2005

Some of the results obtained by the WEAP-Glacier model are presented in Figures A4.12, A4.13, and A4.14 and in Table A4.4.

Figure A4.12. Correspondence between simulated (continuous thick line) and observed (broken thick line) streamflow at La Balsa gauge station between September 1969 and August 1997
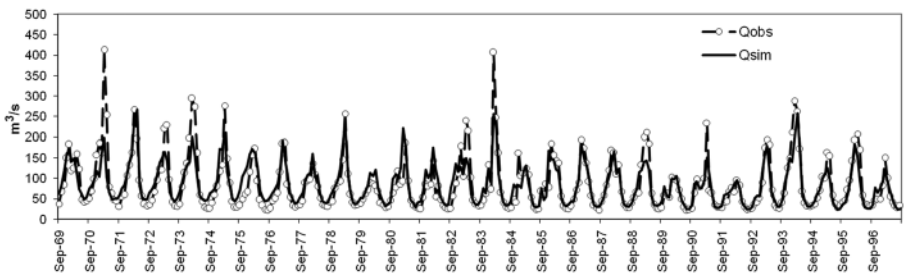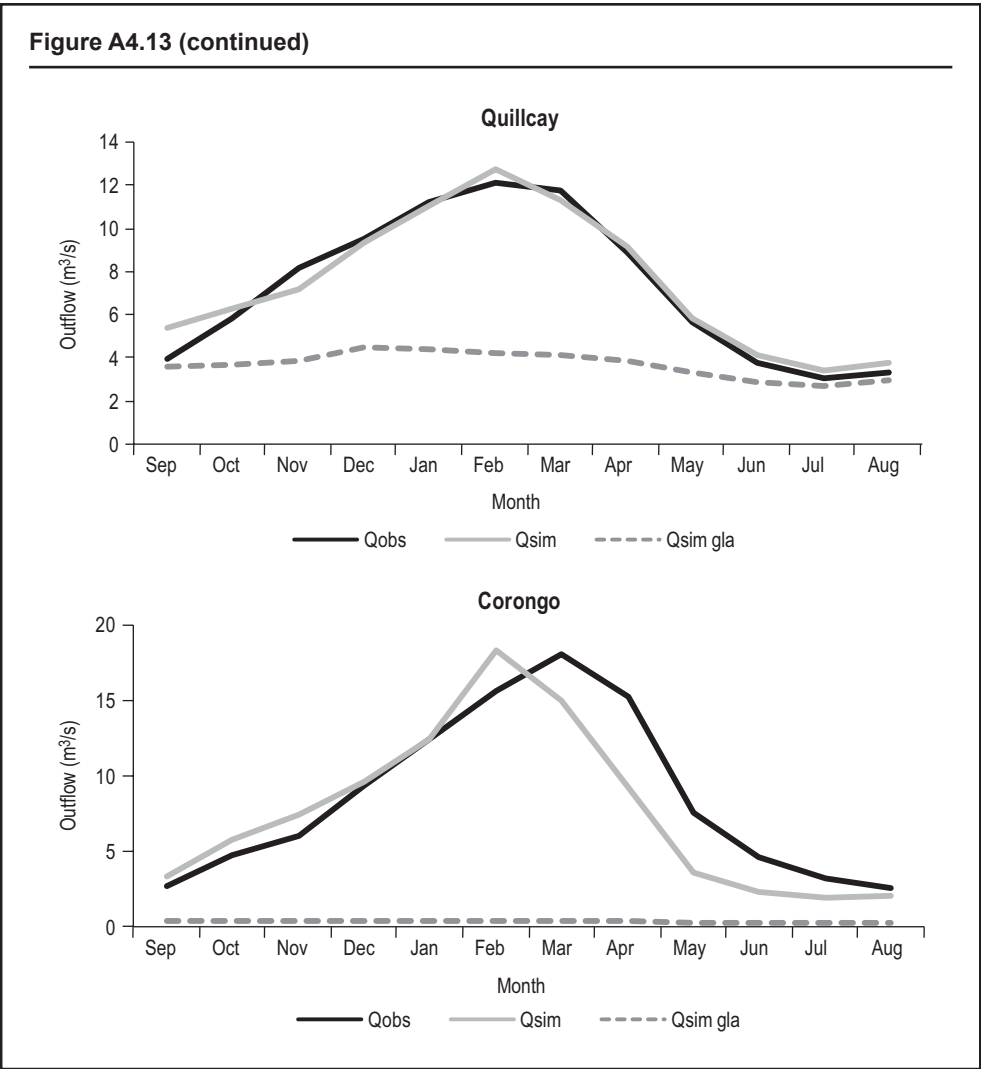

Source: Authors.
Note: This is at the lowest pour point before the Cañón del Pato hydroelectric facility, which includes the aggregated response of most glaciated subwatersheds in the Santa River Basin.

Figure A4.13. Mid-monthly calculated and simulated streamflows (m³/s) for three watersheds, 1969–1997
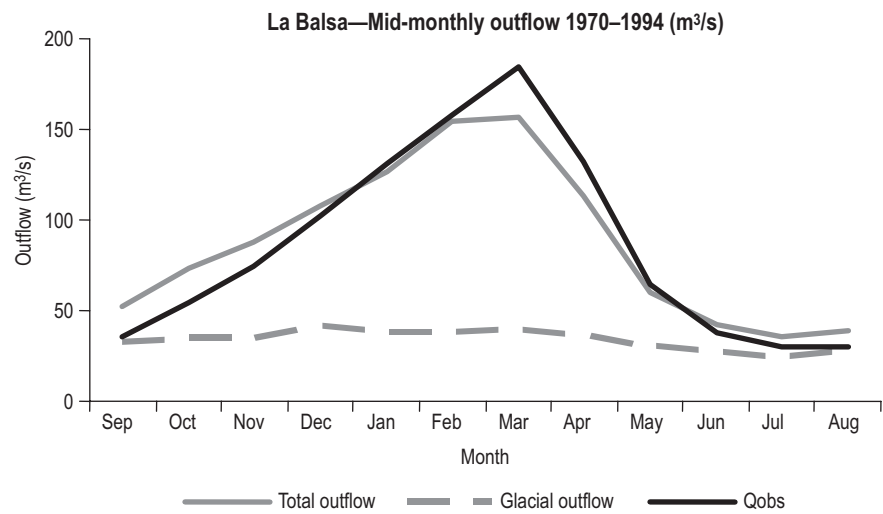
(Figure continues on next page)

Figure A4.13 (continued)

Source: Authors.
Note: For each calculated subwatershed, streamflows are indicated the total streamflow (continuous gray line) and the glacial part (dashed line); the subwatersheds presented are Quillcay (highly glaciated), La Balsa (mildly glaciated), and Corongo (lowly glaciated).

Table A4.4. Simulation results in calibration and validation periods using three statistics: (a) Root Mean Square Error (RMSE); (b) BIAS; and (c) Nash-Sutcliffe parameter efficiency (Ef)

	Calibration				Validation			
	Period	n	RMSE	BIAS	Ef	Period	n	RMSE	BIAS	Ef
Chancos	1970–1984	180	0.38	9%	0.42	1985–1998	180	0.87	-20%	0.05
Colcas	1970–1984	180	0.43	13%	0.22	1985–1997	156	0.50	14%	0.22
Cedros	1968–1982	180	0.31	4%	0.15	1982–1998	192	0.45	-25%	0.00
Llanganuco	1970–1984	180	0.40	17%	(0.27)	1985–1996	144	0.35	-21%	0.07
Parón	1968–1980	180	0.44	0%	(0.75)	1980–1994	144	0.80	-46%	(0.94)
Balsa	1968–1982	180	0.44	12%	0.65	1982–1998	192	0.58	-13%	0.58

Source: Authors.

Figure A4.12 presents the results of simulated and observed flows for the La Balsa station (located in the middle part of the Santa River). The seasonal dynamics and the flow ranges are simulated in good agreement with the observed data.

Figure A4.13 shows for three control stations the influence of glacier contributions related to surface and underground runoff. Note that, depending on the basin considered, glacier contributions are more or less important over the year. This justifies the choice of the half-distributed model.

Figure A4.114 presents the extensions of glaciers per catchment related to the observed extensions. The matching is quite good between the observed and simulated extensions. This makes it possible to confirm the way to calculate changes in glaciers dynamically related to climate (extension calculated for each year).

Figure A4.14. Scatter plot graph with observed versus simulated glacial areas for the two periods (1987 and 1998)
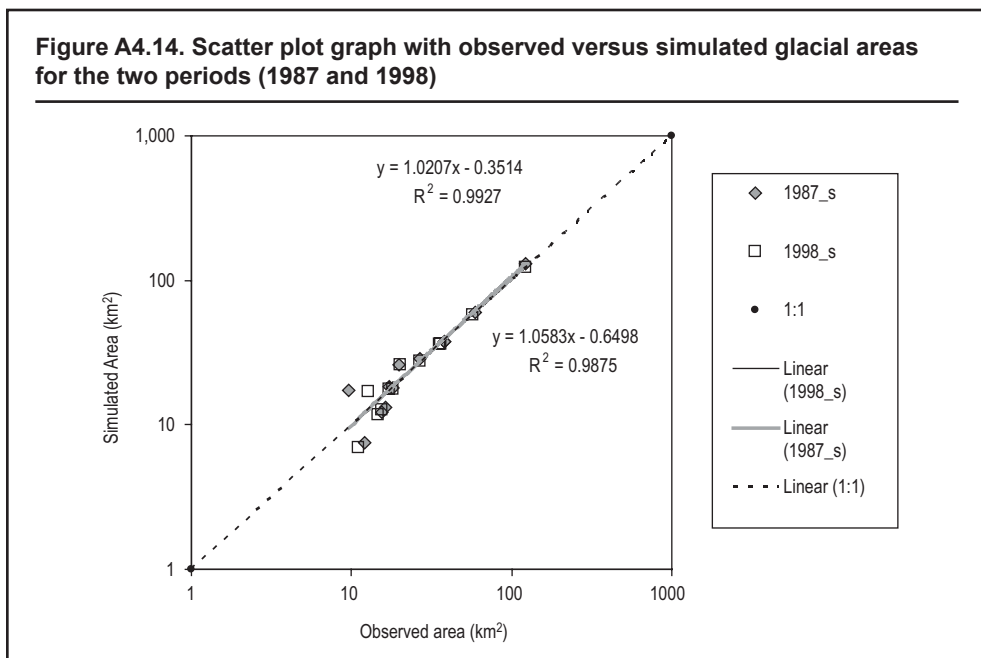
Source: Authors.

CONCLUSION

Part 1 of this report presents various approaches for glacier modeling. According to basin data availability, the selection of the degree-day (degree-month) model for the glacier representation was justified.

Part 2 presents the adopted modeling approach. Since September 2008, IRD worked closely with SEI-US to propose and evaluate a conceptual modeling of mountain basins partially covered with glaciers. They produced several versions of a working paper entitled, "An Approach for Modeling the Hydrologic Role of Glaciers in WEAP." An initial proposal was sent to the World Bank on October 30, 2008. Part 2 corresponds to the latest updated version.

Part 3 presents the latest progress in parameterization. Since January 2009, IRD has taken active part in the equations, in checking the glacier model within WEAP, and in the calibration. The proposed methodology was first to prepare and calibrate the glacier module using data for the high glaciated subwatershed (Arteson) for the recent period (2000–2007). According to several tests, we justified the simplification of equations (4) and (7) of the streamflow contribution due to snowmelt and icemelt from the glacier surface. The new formulation of equations (4bis) and (7bis) consider only three parameters (T0 limit, a_{ice}, a_{snow}). These three parameters were optimized in the Arteson Sub-basin. Next, the new WEAP model, which takes into account the hydrologic role of the glaciers, was used for the historic period (1969–1999) in the entire Santa basin. A double validation of the model has been done, on the one hand, with the comparison of the glacial area calculated by the model and observed with Landsat images for two periods (1987 and 1998), and on the other hand, with the comparison between observed and simulated outflow in 16 control points (or subwatersheds) distributed throughout the entire Santa watershed. An observation of the trends of the glacial area's evolution indicated good correspondence between simulated and observed data (see Figure A4.14, with R2 = 0.993). In summary, the model is able to reproduce glacier shrinkage and runoff in the different watersheds. The latest tests appear to demonstrate the robustness of the model so that it can be used with future climate scenarios. However, because the climate change scenario data required to complete the effort was not provided in a timely manner, the Santa River Basin model could not be run for future simulations. IRD has been working closely with SEI-US in 2009 to model and calibrate the Rímac and Mantaro River Basins.

Appendix 5. Páramo Module in WEAP

Produced by the Stockholm Environment Institution (SEI) for the project.

This appendix documents efforts undertaken by the Stockholm Environment Institute to evaluate possible strategies for integrating a representation of páramo hydrology into the WEAP water resource modeling software.

Modeling Approach for Páramos: Initial Definition

The preliminary modeling approach was based on the linear reservoir concept proposed by Buytaert (Buytaert et al. 2004). According to the linear reservoir concept, the discharge from the páramo can be represented as:

$$Q = k \cdot S \tag{1}$$

where

Q is discharge in units of L^3/T

S is storage (L^3)

K is a time constant that represents the rate of discharge (T^{-1})

With $k=1/T$, where T represents the buffering capacity of the reservoir, Eq. 1 can be transformed by restating as a change in storage over time as shown in Eq. 2:

$$LnQ = LnQ_o - t/T \tag{2}$$

This plots as a linear function on a semi-log plot. According to Eq. 1, discharge and storage in a hypothetical system would change over time, as shown in Figure A5.1, if no further water were added to storage.

The linear reservoir approach presents challenges to represent the discharge from páramos. For instance, storage is not a function of discharge alone, but also varies as a function of inflows (precipitation) and other potential outflows (evapotranspiration). Moreover, hydrographs do not typically have this smoothly decaying structure. Rather, the structure of the hydrograph changes over time (Figure A5.2). Linear portions of the hydrograph can be analyzed to estimate different values of 1/T, or k.


Figure A5.1. Change in discharge and storage over time according to the linear reservoir approach

Day	Q (m³/day)	S (m³)
1	10.0	90.0
2	9.0	81.0
3	8.1	72.9
4	7.3	65.6
5	6.6	59.0
6	5.9	53.1
7	5.3	47.8
8	4.8	43.0
9	4.3	38.7
10	3.9	34.9

$S_0 = 100$ m³
$k = 0.1$ day^{-1}

Source: Authors.

**Figure A5.2. Structure of a páramo hydrograph in Ecuador**
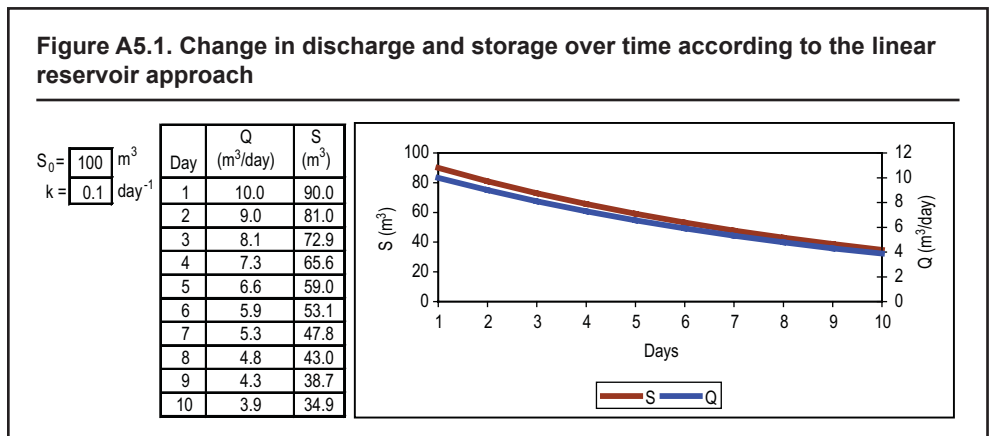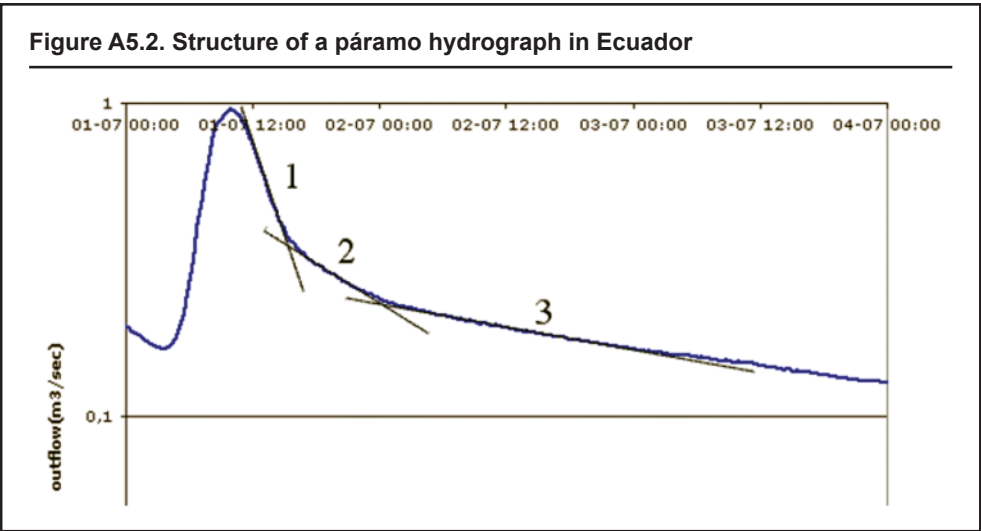
Source: Buytaert et al. 2004.

Buytaert hypothesized that the hydrograph structure of páramos (Figure A5.2) is formed by three potential reservoirs: 1) water stored on the soil surface, 2) water stored in the upper soil H-horizon, and 3) water stored in the lower soil A-horizon. Each of these reservoirs can be represented with the linear reservoir equation (Eq.1) where $k=1/T$ is different for each reservoir. The representation of these three reservoirs is shown in Figure A5.3.

Figure A5.3. Representation of three-reservoir páramo model

Source: Authors.

Figure A5.4. Implementation of three-reservoir model in Excel
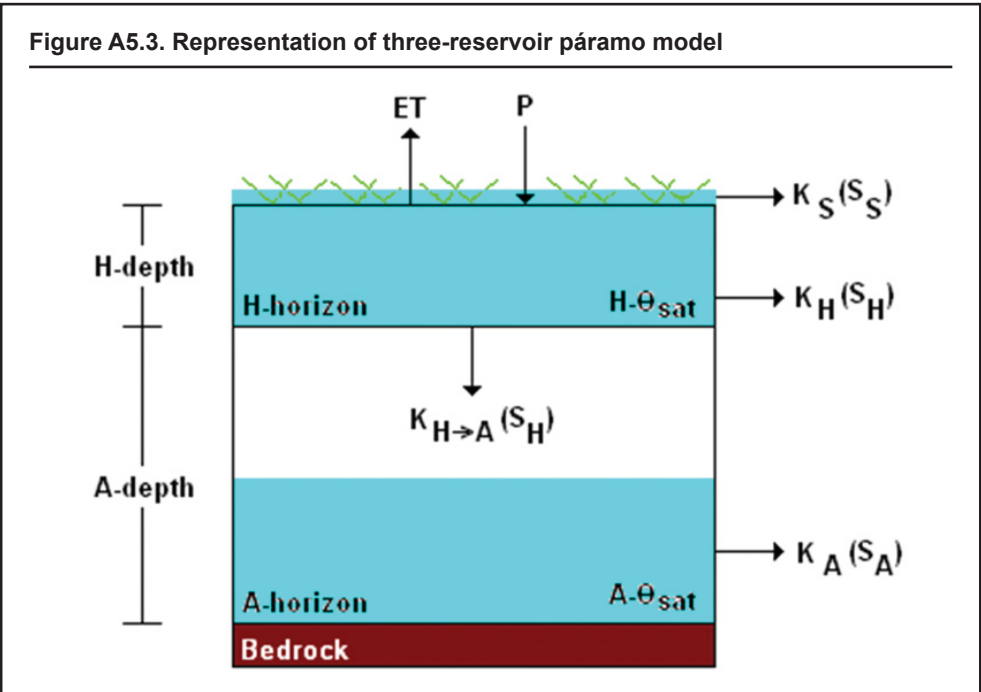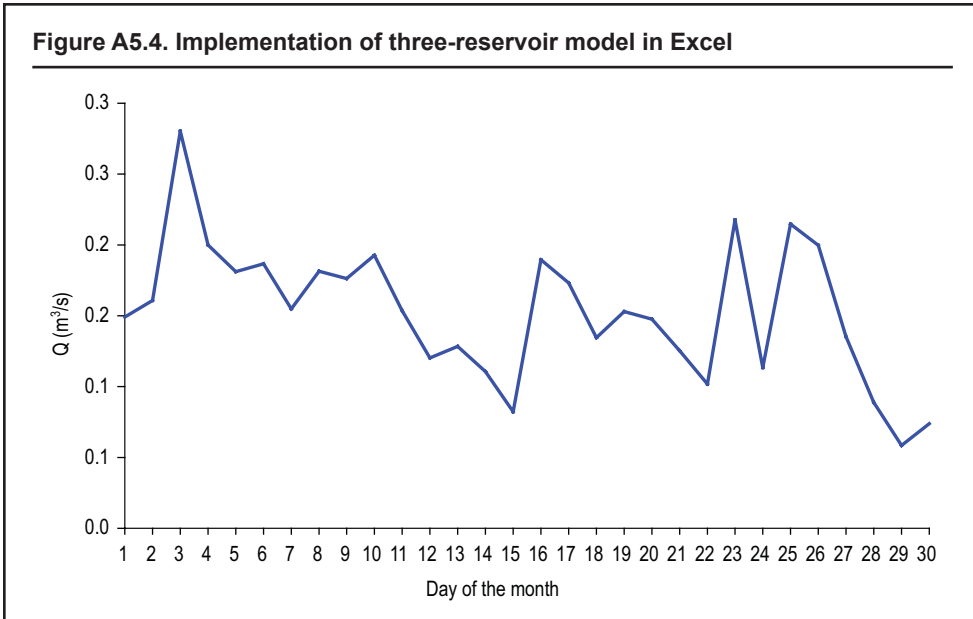
Source: Authors.

When implemented in Excel, these routines can be used to produce a hydrograph of the structure shown in Figure A5.4. This was the conceptual model that was presented by David Purkey at Paramundi in late June.

Modeling Approach for Páramos: Revised Definition

The modeling strategy proposed, in Croke and Jakeman (2004) and Buytaert et al. (2009), to have the advantage of providing a more parsimonious model because it relied on only one linear reservoir rather than three. With this approach, the simplicity in the definition of the model is counteracted by the complexity in the representation of the geographic setting, which is characterized by using high-resolution land cover and hydrologic input data. This model is structured to allow for continuous tracking of evapotranspiration, which is a critical-state variable in páramo hydrology owing to its correspondence to the critical point where páramo peat soils begin to desiccate. The model incorporates a catchment moisture deficit and a routing function. The catchment moisture deficit links soil water content to evapotranspiration losses (Croke and Jakeman 2004). The routing function is represented by one linear reservoir (Buytaert et al. 2009), which differs from the approach described in the Initial Definition section of this document in which three flow routes are used but where explicit tracking of soil moisture status is less well represented.

The modeling approach finally implemented in WEAP was based on this literature. Figure A5.5 provides a graphic representation of the model.

The moisture deficit is estimated as:

$$M_k = M_{k-1} - P_k + ET_k \qquad (3)$$

where

Figure A5.5. Moisture deficit approach to model páramo hydrology
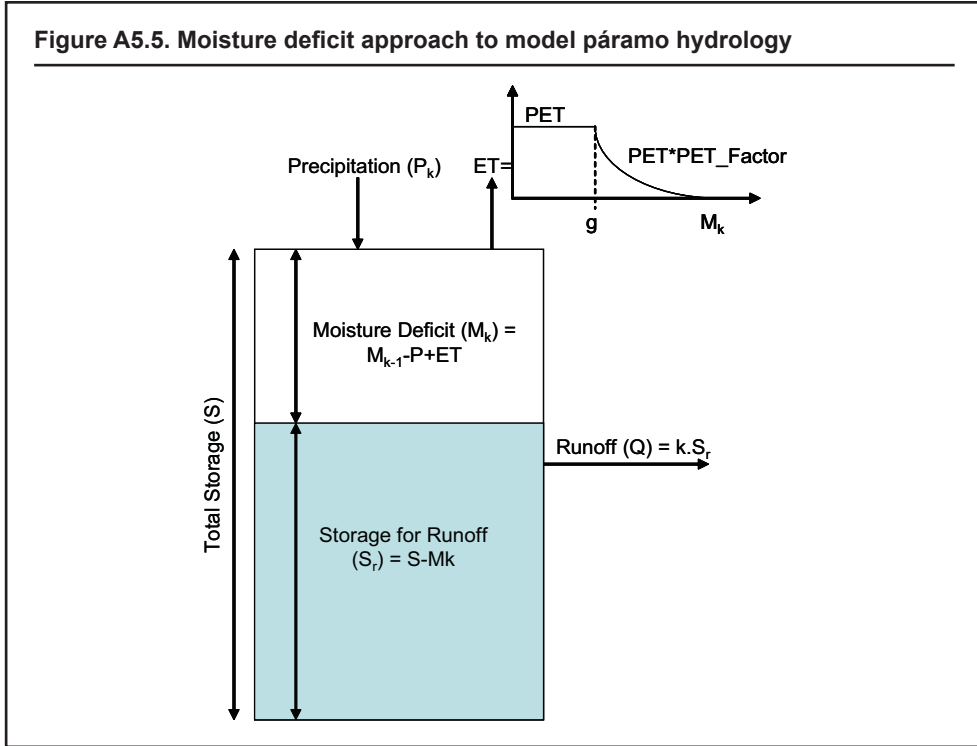
Source: Authors.

k is the current time step

M_k is the moisture deficit of the current time step

M_{k-1} is the moisture deficit of the previous time step

ET_k is the actual evapotranspiration of the current time step

The runoff from the reservoir is estimated with Eq. 1. The updated storage is:

$$S_k = S_{k-1} - Q_k \tag{4}$$

The updated moisture deficit is:

$$M_k = S_T - S_k \tag{5}$$

and the evapotranspiration, ET_k, is given by:

$$ET_k = \begin{cases} PET, & M_k < g \\ PET * PET\_factor, & M_k > g \end{cases} \tag{6}$$

where PET is the potential evapotranspiration estimated using the FAO-Penman Monteith method and g is a factor that represents a threshold above which ET is a function of the moisture deficit (M_k). The PET_factor is estimated as:

$$PET\_factor = Exp^{c*(M_k - g)} \tag{7}$$

where c is a constant that controls the monotonic decay when soil moisture falls below the assumed deficit threshold and it is estimated as:

$$c = Ln(\sqrt[A]{0.0001}) \tag{8}$$

where A is M_k-g for the conditions when M_k=S_T

The final calibration parameters of the algorithm include g (threshold parameter), S_T (total storage), M_k (initial moisture deficit) and T (reservoir buffering capacity). For simplification purposes, the model will be named the four-parameter model in this document.

Implementation and Calibration of a Páramo Hydrology Model in WEAP

The algorithm of the four-parameter module was implemented in WEAP in which a new data category called páramo and associated variables were added to the interface (Figure A5.6).

Given that the existing two-bucket model in WEAP estimates the *PET* using the Penman-Monteith approach, the estimated *PET* from the two-bucket model was used as input to estimate *ET* for the four-parameter model according to Eq. 6.

Using one year of daily climate variables (precipitation, temperature, wind speed, and relative humidity) and hydrologic variables (streamflow) measured in a small páramo test watershed in Ecuador, a test of the model was undertaken.

The test focused on 1) adjusting the parameters of the four-parameter in WEAP, and 2) adjusting the parameters of the existing two-bucket hydrologic model in WEAP to see if these routines approximated observed hydrology to any significant degree. For this exercise, two rivers were created in WEAP, one for each test (Figure A5.7).

**Figure A5.6. Implementation of páramo hydrology algorithm in WEAP**

Source: Authors.

gions of the watershed would be parameterized to capture flashy behavior while others would be tuned to provide more of a baseflow profile. On aggregate, a calibration exercise would involve adjusting parameters for these different zones in order to produce a reasonable hydrograph.

Parameterization of Two-Bucket Model

Using the native hydrology routine in WEAP, a model test run on a daily time step was attempted. The hydrology in this model is regulated by seven parameters (Figure A5.9): Kc (crop coefficient), Sw (soil water capacity), Dw (deep water capacity), RRF (runoff resistance factor), Ks (conductivity of root zone), Kd (conductivity of deep zone) and f (preferred flow direction).

Figure A5.9. Two-bucket model schematic and parameters
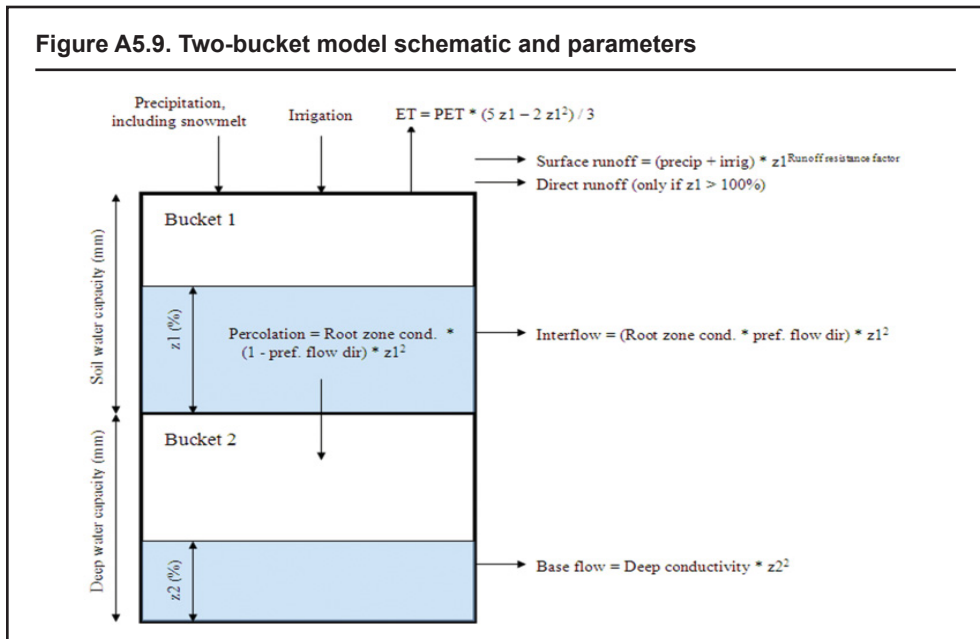
Source: Authors.

Figure A5.10 shows the final results after calibration. The six degrees of freedom provided by the two-bucket model provide a better representation of the hydrology of this particular páramo watershed. With this test, the model well represents the peak flows and provides a good approximation of baseflows.

Discussion

From the test exercises, it is evident that the four-parameter model implemented does not give enough degrees of freedom to adjust the hydrology of a modeled watershed to produce water that follows the daily fluctuations existing in the páramo setting unless it is combined with a detailed spatial analysis, disaggregation and calibration of the watershed. For this, Buytaert is currently using the TOPMODEL to support this analysis (Beven and Kirby 1979). In addition, there are a number of uncertainties associated with páramo hydrology that are not taken into account in the model, including the horizontal precipitation (Díaz-Granados et al. 2005).

Figure A5.10. Two-bucket parameter calibration
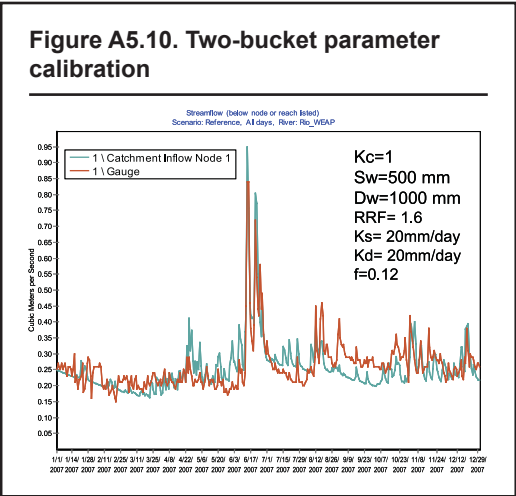
Source: Authors.

In contrast, the existing two-bucket model hydrology in WEAP provided a good aggregate representation of páramo daily runoff patterns within the year of the dataset. This short experiment with the existing two-bucket model in WEAP, implemented at a daily time step, provided promising results. Most WEAP models are implemented at a weekly and monthly time step, given the typical regional planning applications of this modeling platform. However, even without taking into account planning considerations, the results of the model at the daily time step provided a good representation of the páramo hydrology.

To further test the four-parameter model, a modified version of the TOPMODEL needs to be explored (Beven and Kirby 1979).

Possible collaborations will be explored in subwatersheds of the Paute River Basin. Moreover, a model of this watershed was already built within a project implemented by the Centro de Cambio Global of the Universidad Católica de Chile and PROMAS (Programa para el Manejo del Agua y del Suelo of the Universidad de Cuenca, Ecuador) for the PACC (Proyecto de Adaptación al Cambio Climático (Figure A5.11).

The existing WEAP model in the Río Paute watershed was implemented using a monthly time step. Consequently, it will be necessary to coordinate modeling páramo hydrology using the daily time step to track soil moisture, with the reality of modeling for planning purposes using the monthly time step to observe management and climate change scenarios.

Figure A5.11. Río Paute model schematic in WEAP
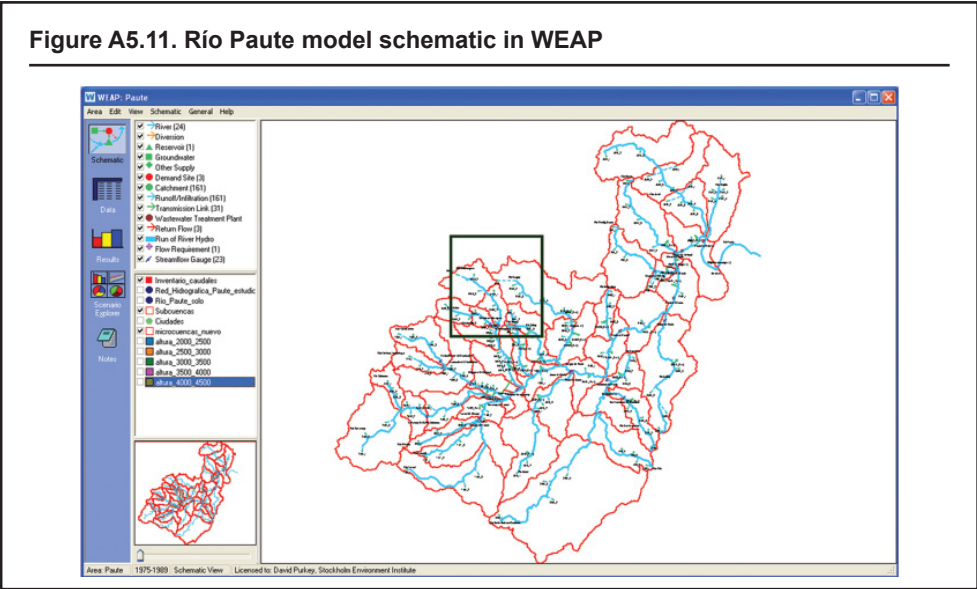
Source: Authors.

Appendix 6. Calibration of Nonglaciated Sub-basins

Relevant parts taken from "Construcción del Modelo WEAP del Río Santa," ("Construction of the WEAP Model for the Santa River") by Marisa Escobar (SEI), Thomas Condom (IRD), Wilson Suárez (IRD-SENAHMI), David Purkey (SEI), Jean-Christophe Pouget (IRD) and Cayo Ramos (U. La Molina).

Model Calibration

The calibration was conducted manually with the objective that the volumes produced by the model would follow the behavior of the volumes measured in the sub-basins with no glacier coverage. The selected sub-basins were Corongo, with an area of 561 km^2, whose volume is measured at the Manta station; and Tablachaca, with an area of 3,179 km^2, whose volume is measured at the Condorcerro station. The parameters obtained here will be applied to the entire basin once the glacier module is introduced. The calibration period was 1967–1983 and the validation period was 1984–1999. The parameters of conductivity, water storage capacity, runoff resistance factor, and direction of flow were adjusted to generally reproduce the behavior of peak flow in winter and baseflow in summer. Because precipitation in both sub-basins was estimated on the basis of data from the Collota pluviometric station, which is approximately 40 and 80 km, respectively, from the central points of the Corongo y Tablachaca sub-basins, rainfall data show an uncertainty that may be transferred to volumes obtained by the model.

The parameters obtained are within the normal ranges for monthly time-step models (Table A6.1). For comparison purposes, the values used in the modeling of the Limari River Basin in Chile (Vicuña et al. 2010) are presented. There is an exception in the conductivity of the deep zone, which is lower in the Santa River, indicating that this lower value was necessary so that the baseflows in summer could be released slowly from the subsoil toward the river.

The model's precision was measured using the following parameters: root mean square error (RMSE), BIAS and Nash-Sutcliffe efficiency (Ef):

Table A6.1. Calibration parameters

Parametro	unidad	Valor Cuenca Río Santa	Valor Cuenca Río Limari (Chile)
Coeficiente de cultivo		1.1	n.r.
Capacidad de agua en zona de raices	mm	712.5	108-4320
Conductividad en zona de raices	mm/mes	600	120-900
Capacidad de agua en zona profunda	mm	1,000	300-7500
Conductividad en zona profunda	mm/mes	20	140-600
Factor de resistencia a la escorrentia			0.9-5.85
Cultivos		3.2	
Matorral		2.4	
Tundra		1.6	
Planicie Costera		1.6	
Direccion del flujo	% horizontal	0.68	n.r.
Z1	%	35	n.r.
Z2	%	35	n.r.

Source: Authors.

$$RMSE = \frac{100}{\overline{Q}_o} \sqrt{\frac{\sum_{i=1}^{n}(Q_{s,i} - Q_{o,i})^2}{n}}$$,

$$BIAS = 100[(\overline{Q}_s - \overline{Q}_o)/\overline{Q}_o]$$, y

$$E_f = 1 - \frac{\sum_{i=1}^{n}(Q_{s,i} - Q_{o,i})^2}{\sum_{i=1}^{n}(Q_{o,i} - \overline{Q}_o)^2}$$

(1)

where $Q_{s,i}$ and $Q_{o,i}$ are simulated and observed volumes for each time step $_i$, and n = 193 for the calibration period, 168 for the validation period, and 12 for average monthly estimates for the entire validation and calibration period. The results are presented in Table A6.2. Generally, in the validation period the RMSE and BIAS are lower and the efficiency is greater, indicating better correspondence between observed and simulated volumes.

Table A6.2. Statistics of correspondence between observed volume and simulated volume in the Tablachaca and Corongo sub-basins

Calibracion 1967-1983	Todos los pasos de tiempo (n=193)			Promedio mensual		
	RMSE	BIAS	Ef	RMSE	BIAS	Ef
Tablachaca	113%	50%	29%	7%	-1%	89%
Corongo	58%	-17%	53%	10%	-17%	70%
Validacion 1984-1999	**Todos los pasos de tiempo (n=168)**			**Promedio mensual**		
	RMSE	BIAS	Ef	RMSE	BIAS	Ef
Tablachaca	69%	19%	54%	8%	19%	88%
Corongo	30%	18%	79%	12%	18%	74%

Source: Authors.

Looking at the monthly averages, one can see an overestimate of volumes in the validation period (Figure A6.1).

Figure A6.1. Calibration and validation
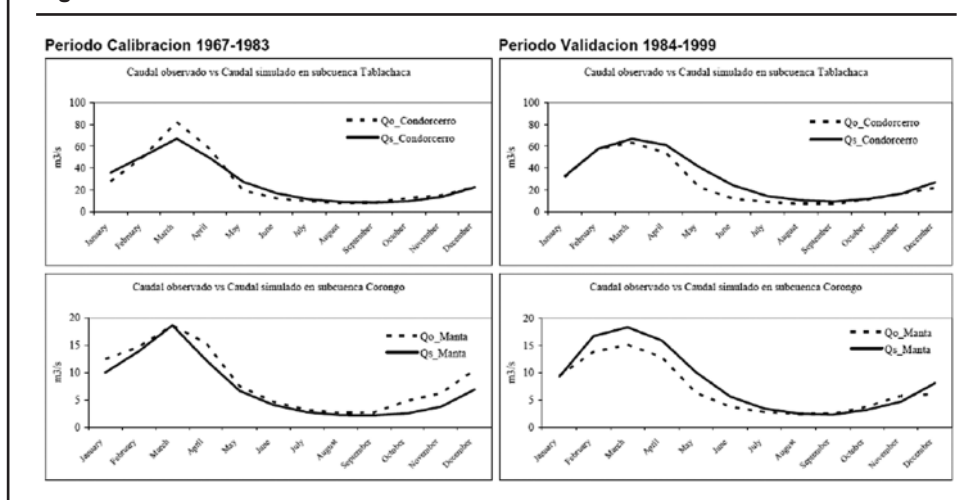
Source: Authors.

The model was calibrated using a set of standard parameters in the Tablachaca and Corongo sub-basins. The set of parameters made it possible to obtain acceptable results in both sub-basins, despite a significant difference in their sizes: the Corongo sub-basin is approximately 20 percent of Tablachaca's size. These land use parameters will be applied to all of the model's sub-basins so that, during the process of implementing the glacier model, it will be possible to achieve the calibration of glacier parameters exclusively. However, there remains a possibility to review the parameters in each sub-basin, in terms of soils if specific information on soils and geology is obtained, or in terms of the sub-basin's geometry if patterns are observed suggesting that other characteristics such as size and form may have an effect on the results.

Appendix 7. Final Calibration-Validation of the Santa River Model

R elevant parts taken from "*Modeling the Hydrologic Role of Glaciers within a Water Evaluation and Planning System (WEAP): A case study in the Santa River watershed (Peru)*", by T. Condom, M. Escobar, D. Purkey, J. C. Pouget, W. Suárez, C. Ramos, J. Apaestegui, M. Zapata, J. Gómez and W. Vergara.

CASE STUDY: THE SANTA RIVER AND THE CORDILLERA BLANCA

Climate Settings

The regional climate is strongly marked by the mountain barrier of the Andes. In the tropical Andes the main source of precipitation comes from the Atlantic Ocean and the Amazon Basin. The latter plays the role of recycling water through intense evapotranspiration; the principal transport mechanism of this humidity into the Andes is the seasonal easterly wind (Johnson 1976; Aceituno 1998). This seasonality allows the development of one wet season centered during the December-January-February (DJF) austral summer and a dry season during the July-August-September (JAS) austral winter. Along South American's entire western coastal strip, the proximity of the South Pacific anticyclone and its accompanying subsidence, reinforced by the cold Humboldt current, which flows parallel to the Pacific coast, generate a dry climate. Garreaud et al. (2003) give a detailed description of climate in the tropical Andes.

At the scale of the Cordillera Blanca, longitudinal and a latitudinal gradients of precipitation are present. For the dry Pacific coast and the humid summits, the mean annual values ranged between 93 and 1,542 mm.y^{-1} for the 1967–1998 period. The weighted average for the entire Santa River watershed was 868 mm.y^{-1}. With regard to temperature, the inner tropical location of the watershed (Kaser and Osmaston 2002) makes the annual variation less important than the diurnal variation. Nevertheless, seasonal variation is observed and the range of mean annual temperature values falls between -7°C.y^{-1} (higher parts of the watershed) and 30°C.y^{-1} (lower parts of the watershed) for the 1967–1998 period with a weighted mean value of 8°C.y^{-1}.

In summary, both the mean annual temperature and precipitation for the Santa River watershed show strong latitudinal, longitudinal, and altitudinal gradients. These gradients offer a great contrast between the hot arid zone to the west and the cold and wet high-elevation zone to the east with an average annual precipitation of more than 1,500 mm.y^{-1} at the Huascarán glacier.

Input Data

Terrain Data Pre-processing

The Digital Elevation Model (DEM) issued by the maps of the National Geographic Institute of Peru (IGM) (scale 1/100000) was used to define subwatersheds above all the points where gauging of streamflow volumes, reservoirs, managed natural lagoons for hydroelectric production, points of water extraction and points of water return exist. The DEM was also processed to define elevation bands within each subwatershed, with a range of 700 m in the lower parts of the basin and 300 m in the higher parts of the basin, in order to afford a greater level of detail in the zone occupied by glaciers (Table A7.1).

Table A7.1. Altitude bands for the different subcatchments and notification of the presence or absence of glacier for each band

Elevation Bands		Low level (masl)	High level (masl)	Mid point (m)	Spacing (m)
	1	0	500	250	500
	2	500	1200	850	700
	3	1200	1900	1550	700
Land use	4	1900	2600	2250	700
	5	2600	3100	2850	500
	6	3100	3600	3350	500
	7	3600	4000	3800	400
	8	4000	4400	4200	400
Land use	9	4400	4700	4550	300
and Glacier	10	4700	5000	4850	300
	11	5000	5300	5150	300
	12	5300	5600	5450	300
	13	5600	5900	5750	300
Glacier	14	5900	6200	6050	300
	15	6200	6500	6350	300
	16	6500	6800	6650	300

Source: Authors.
Note: The spacing of altitude is accurate for the higher zone (300m) in order to correctly report the glacier behavior.

The intersection between subwatersheds and elevation bands constituted a WEAP catchment. The area of each catchment was calculated as well as the percentage of various land cover types within the catchment. The land cover dataset was obtained from the Chavimochic project (ATA-INADE 2002) and was reclassified from its original classification scheme into tundra, coastal plain, shrub and agriculture categories (Table A7.2).

Two datasets on the spatial evolution of glaciated area were used: one for the Artesoncocha subwatershed alone (2001–2007) derived from Landsat images, and another for the entire Santa River watershed (1969–1999) from an inventory published by Ames et al. (1989) based on analysis of 168 aerial photos. This latter set was used to define initial glaciated area conditions. The different glaciated areas in the Santa River watershed are shown in Figure A7.1.

Table A7.2. Land cover classification from ATA-INADE (2002) and simplification in the WEAP model

Initial Land Cover Classification	Reclasification of Land Cover for WEAP
Andean highlands without vegetation	Glaciers
Bofedal	Tundra
Tundra	
Pajonal	
Pajonal/puna	
Agriculture	Agriculture
Shrubs	Shrub
Coastal plain	Coastal plain

Source: Authors.

Figure A7.1. Evolution of the glacier extension between the three periods (1970, 1987 and 2006), with a zoom on the Huascarán Massif
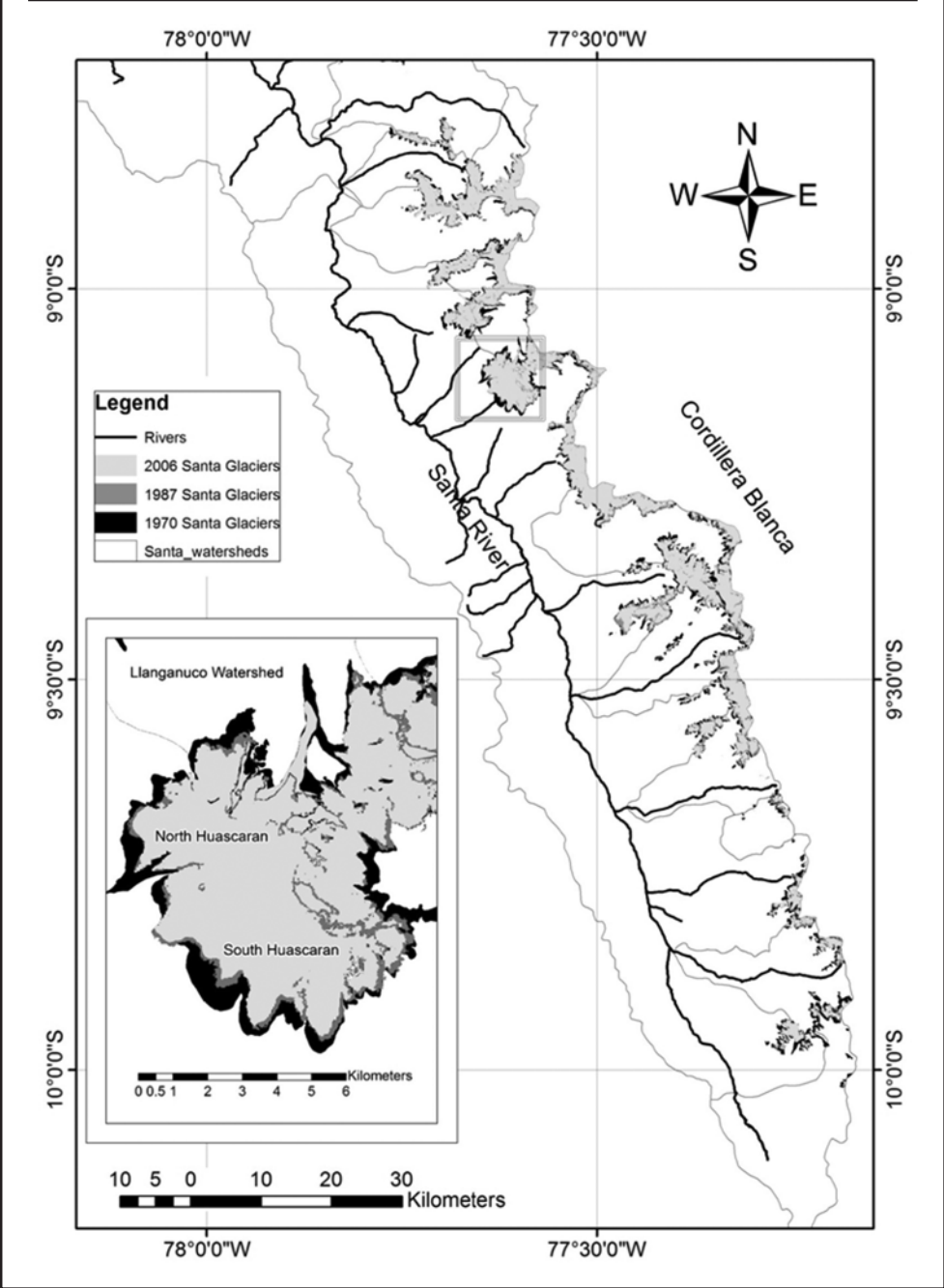
Source: Authors.

In order to characterize human and agricultural water consumption in the Santa River watershed, we added water demand nodes to represent each province, including information on the number of inhabitants (rural and urban). Total water demands in each province were estimated by multiplying the number of inhabitants by a per capita water use of 300 l/day, which is a rough estimate of the combined urban and agricultural water use in each region.

Meteorological Data Pre-processing

PRECIPITATION

Because the objective of this study was to obtain a continuous simulation of the evolution of glaciers in the Santa River watershed, continuous climate time series were required for each of the catchments in the model. A total of 39 pluviometric stations are located within the Santa River watershed. The time series of available data from the stations extended from 1968 to 1999 on a monthly basis. The stations were submitted to the Regional Vector Method–RVM (Hiez 1977; Brunet-Moret 1979) to assess their data quality and to isolate climatological regions (see Espinoza et al. 2008 for more details about this method). Data from other stations within a group were used to fill gaps in the record of individual stations. From these stations, an inverse distance squared interpolation scheme was used to generate a precipitation time series for each catchment. This analysis was done using Hydracess software (Vauchel 2005) for the RVM and with ArcGIS for the spatial interpolation. Although precipitation in this watershed might be controlled by spatial variability due to barrier effects and altitudinal gradient, the interpolation technique used is well suited to maximize utility of the available data. The 39 stations are evenly distributed in the watershed and thus provide a reliable starting point to obtain a dataset that can approximate the actual spatial variability of precipitation in the watershed.

TEMPERATURE, HUMIDITY, AND WIND SPEED

With regard to temperature and humidity data, only one good-quality, long, continuous time series exists for the Santa River watershed: the Recuay station (9°50′S, 76°20′W). Continuous temperature data for each catchment were obtained using a temperature gradient of 0.6°C/100 applied to the temperature observed at Recuay. For humidity and wind speed, we assumed that the long-term monthly average time series at Recuay applied to all catchments. The simplicity of the interpolation of the temperature, humidity, and wind speed for each subwatershed was driven by the scarcity of the weather station data. Although the temperature gradient can vary, the classical range is given between 0.5 and 1°C/100m as a function of the atmospheric humidity. In order to simplify the modeling, we assumed that the gradient would be stable and equal to 0.6°C/100m as is classically done for zones where the number of air temperature stations is scarce. While we recognize that the quality of the modeling would be improved by more spatially continuous information on actual climatic conditions, it is our opinion that model calibration can accommodate uncertainty in the climate inputs. Furthermore, the type of analysis we propose cannot wait until a perfect input dataset is available.
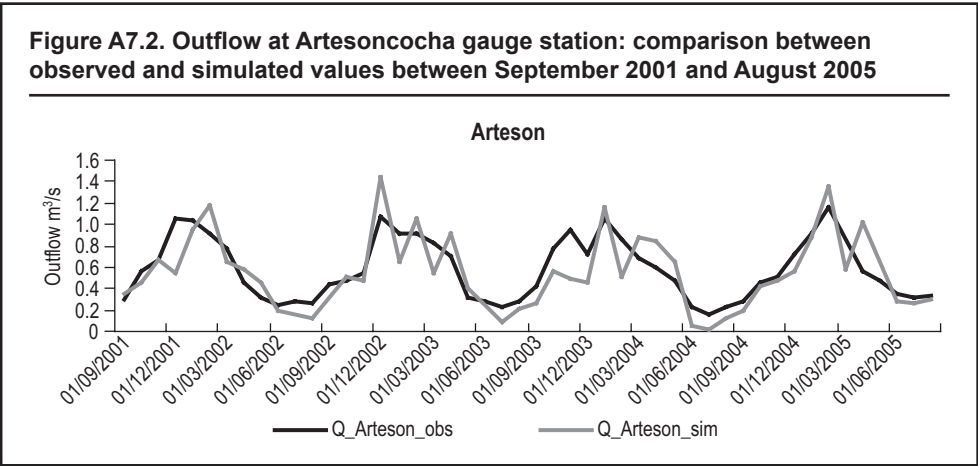
Results

Calibration of the Glacier Module for the Recent Period (2000–2007)

The first effort to calibrate the proposed glacier module focused on the well-documented Artesoncocha subwatershed (n°9 in Figure A7.1). This watershed extends over 8.8 km² with an initial percentage of glacier coverage equal to 73 percent. Researchers from IRD in collaboration with the Instituto Nacional de Recursos Naturales (INRENA), a Peruvian public entity dealing with environmental studies, have studied the evolution of the glacier in the Artesoncocha since 2000 (Pouyaud et al. 2005). At the Artesoncocha streamflow gauging station, pluviometers and temperature sensors have been installed and maintained by researchers to continuously monitor the climate conditions in the watershed. The calibration procedure was structured to understand the role of each glacier module parameter in the simulation of glacier evolution; this constitutes a critical precursor to the effort to calibrate the glacier module for all of the glaciers in the Santa River watershed.

The Artesoncocha subwatershed is characterized by a vertical gradient of temperature and precipitation. For the 2000–2007 period, conditions at the bottom of the subwatershed between 4,000 and 4,400 meters above sea level (masl) were on average 900 mm.y^{-1} (total precipitation) and 5.9°C (average temperature). At the top of the watershed between 5,900 to 6,200 masl, the annual averages are 1780 mm.y^{-1} and -3.7°C. To calibrate the degree-day factors a_{ice} and a_{snow} without access to specific reference values for the Cordillera Blanca, the research began with the compilations provided by Singh et al. (2000) and Hock (2003). These suggest that the degree-day factor for ice is generally higher than the degree-day factor for snow and that the ranges are 1.3 to 11.6 mm.d^{-1}.°C^{-1} for snow and 5.5 to 20 mm.d^{-1}.°C^{-1} for ice (we scaled these daily values for use in our monthly time-step model). To calibrate T_0, we assumed that the value fell somewhere between -2°C and 2°C.

Monthly comparisons between simulated and observed outflow from the Artesoncocha subwatershed are presented in Figure A7.2. Given that the available time series was relatively short, all the data were used to calibrate the three glacier parameters T_0,

Figure A7.2. Outflow at Artesoncocha gauge station: comparison between observed and simulated values between September 2001 and August 2005

Source: Authors.
Note: Pearson correlation of observed and simulated values: R^2=0.7 p≤0.01.

a_{ice} and a_{snow} without considering a validation period. The optimized parameters obtained were 1.45°C for T_0, 380 mm.month^{-1}.°C^{-1} for a_{snow} and 600 mm.month^{-1}.°C^{-1} for a_{ice}. The agreement between simulated and observed data is good (the Pearson correlation's coefficient is R^2=0.7 with p≤0.01) and the seasonal cycle is well represented by the model. Some discrepancies occur, likely due to the fact that the conceptual monthly approach is not able to represent all physical processes involved in the hydrologic cycle of a glaciated area.

Model Calibration and Validation for the Historical Period (1970–1998) for the Santa River Watershed

For the entire Santa River watershed, the calibration strategy was to calibrate the standard WEAP rainfall-runoff parameters for the Tablachaca and Corongo subwatersheds because these lack glacier coverage (Table A7.3). The parameters obtained for nonglaciated subwatersheds were applied uniformly to the entire basin. Next, the calibrated glacier parameters obtained for Artesoncocha (see 3.1) were used to run the model for a calibration period and a validation period. Monthly time series of precipitation and temperature were available for the 1968–1999 period. The 1970–1984 period was set as the calibration period and the 1985–1999 period was used for validation (in some watersheds several years of data were missing, so the calibration and validation periods change accordingly). During the calibration period, small adjustments of the Artesoncocha glacier parameters were allowed to capture and improve the calibration across the basin. The efficiency criteria results for *RMSE*, *Bias* and *Ef* for all subwatersheds are presented in Table A7.4.

Table A7.3. Land use parameters for the nonglaciated part and parameter values for the glacier module

Land use parameters (part without glacier)		
Parameter	**unit**	**Value**
Crop coefficient		1.1
Root zone capacity	mm	80
Root zone conductivity	mm/mes	500
Deep water capacity	mm	500
Deep water conductivity	mm/mes	50
Runoff Resistance Factor		
Cultivos		4
Matorral		3.2
Tundra		0.8
Planicie Costera		0.8
Flow Direction	% horizontal	0.68
Z1	%	35
Z2	%	35
Glacier parameters		
Parameter	**unit**	**Value**
T0	°	1.45
a_{snow}	mm.month^{-1}.°C^{-1}	380
a_{ice}	mm.month^{-1}.°C^{-1}	600

Source: Authors.

Table A7.4. Criteria for the calibration and validation periods

	Calibration					Validation				
Sub-watershed	Period	n	RMSE	BIAS	Ef	Period	n	RMSE	BIAS	Ef
1 - La Recreta	1969-1979	120	0.77	39%	0.63	1979-1989	120	0.87	44%	0.50
2 - Pachacoto	1969-1979	120	0.43	-9%	0.64	1979-1989	120	0.43	-13%	0.55
3 - Querococha	1969-1979	120	0.39	1%	0.72	1979-1989	120	0.36	-20%	0.74
4 - Olleros	1969-1979	120	0.48	12%	0.53	1979-1989	120	0.38	-4%	0.63
5 - Quillcay	1969-1979	120	0.31	9%	0.66	1979-1989	120	0.31	-2%	0.64
6 - Chancos	1969-1979	120	0.44	21%	0.28	1979-1989	120	0.29	-4%	0.63
7 - Llanganuco	1969-1979	120	0.46	36%	0.64	1979-1989	120	0.92	-15%	0.13
8 - Paron	1969-1979	120	1.70	6%	0.25	1979-1989	120	0.33	-16%	0.10
9 - Artesoncocha	*	*	*	*	*	*	*	*	*	*
10 - Colcas	1969-1979	120	0.47	25%	0.19	1979-1989	120	0.44	4%	0.23
11 - Los Cedros	1969-1979	120	0.29	4%	0.33	1979-1989	120	0.38	-18%	0.19
12 - Quitaracsa	1969-1979	120	0.32	-8%	0.65	1979-1989	120	0.42	-24%	0.19
13 - La Balsa	1969-1979	120	0.41	3%	0.70	1979-1989	120	0.39	1%	0.72
14 - Corongo (Manta)	1969-1979	120	0.56	-13%	0.53	1979-1989	120	0.63	-10%	0.41
15 Chuquicara	1969-1979	120	0.47	5%	0.69	1979-1989	120	0.40	1%	0.77
16 - Tablachaca (Condorcerro)	1969-1979	120	0.79	28%	0.56	1979-1989	120	0.67	16%	0.61
17 - Puente Carretera	1969-1979	120	0.62	2%	0.62	1979-1989	120	0.89	-46%	0.11

Source: The results are given for the principal subwatersheds.

Figure A7.3a shows the correspondence between simulated (continuous thick line) and observed (broken thick line) streamflow at the La Balsa gauge station between September 1969 and August 1997. The La Balsa gauge station includes the aggregated response of most glaciated subwatersheds in the Santa River system and it represents a critical water management time series because it lies at the point of diversion to the Cañón del Pato hydroelectric facility. The performance of the model in capturing the structure of the observed hydrograph at La Balsa is notable.

In order to see if the model captures the interannual variations in flow, we plotted simulated and observed annual flows for the La Balsa gauge station during 1969–1997. Comparing simulated and observed values (Figure A7.3b), one can be confident of the model's ability to represent the interannual variations. The long-term trend is well represented and the magnitude is captured. In Figure A7.3b, El Niño events are plotted in gray (Smith et al. 2000). It can be noted that El Niño years are generally associated with high flows, for example 1970–1971 or 1982–1983, but more average flows can also be observed during these climate events (1990–1991). One point should be mentioned: for the extremely high flows (for example, during 1982–1983 or 1993–1994), the observed


Figure A7.3a. Correspondence between simulated (continuous think line) and observed (broken thick line) streamflow at La Balsa gauge station between September 1969 and August 1997
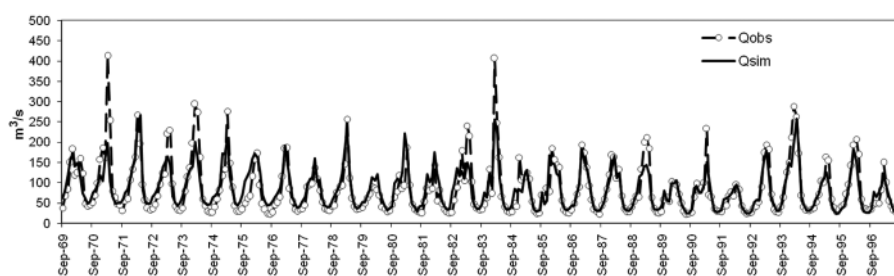
Source: Authors.
Note: This is the lowest pour point before the Cañón del Pato hydroelectric facility, which includes the aggregated response of most glaciated subwatersheds in the Santa River Basin. Pearson correlation of observed and simulated values: R^2=0.74 $p \le 0.01$.

Figure A7.3b Interannual variability of simulated and observed streamflow at La Balsa gauge station between hydrologic years 1969–1970 and 1996–1997
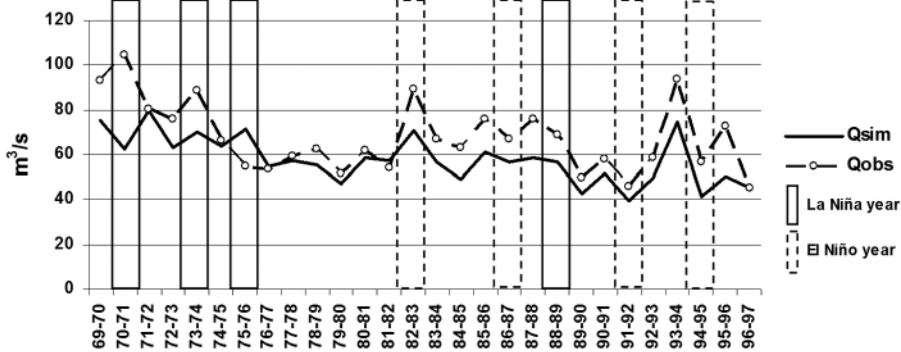

Source: Smith et al. 2000.
Note: Distribution of El Niño and La Niña events.

data are very highly influenced by extreme daily events that are inherently difficult to measure because of the precision of the calibration curve.

Figure A7.4 shows that good agreement between observed and simulated outflows was achieved for the Chuquicara, Quillcay and La Balsa subwatersheds. Nevertheless,

Figure A7.4. Mid-monthly calculated and simulated streamflows of three sub-watersheds (La Balsa, Quillcay, and Chuquicara) during the 1969–1998 period
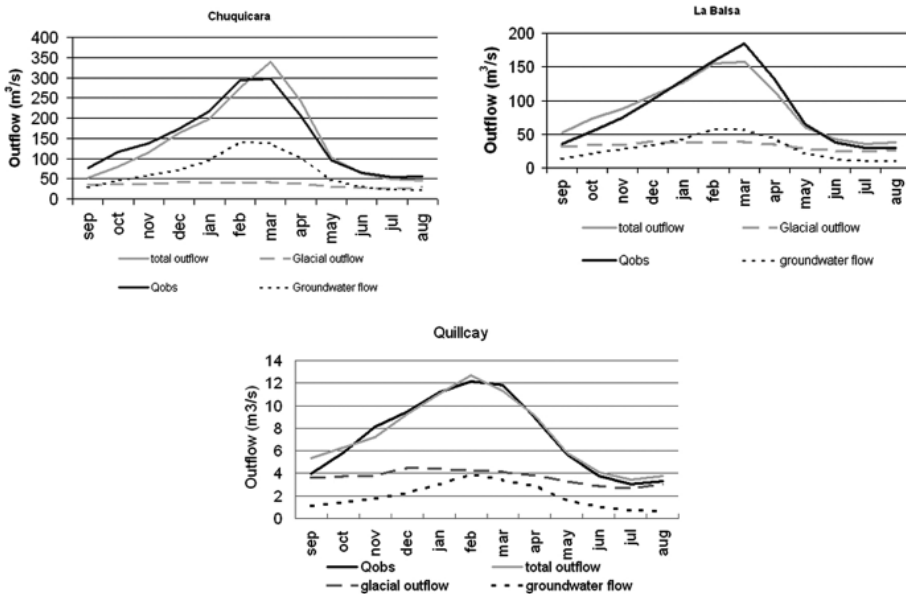
Source: Authors.
Note: For each calculated subwatershed streamflow, the total streamflow (continuous gray line), the glacial part (dashed line) and the groundwater part (black dashed lines) are indicated.

some discrepancies exist for the Parón watershed and Puente Carretera subwatershed (see Table A7.4). For Parón, the historical operation of the regulated glacier lake was probably not fully captured in the model. For Puente Carretera, the observed hydrologic response likely includes changes in the river geomorphology at this meandering, gravel-dominated, lower-slope reach that are not present at higher-elevation subwatersheds. Further effort could have been made to develop subwatershed-specific model parameters to improve the calibration on a subwatershed-by-subwatershed basis, but this would by necessity be done in an ad hoc manner that would potentially limit the robustness of the calibration. Again, because the management focus of the study was on potential impacts at the Cañón del Pato diversion, no effort was made to correct these smaller-scale local discrepancies at this time.

Another important test of model performance is the differentiation of the simulated amount of streamflow that comes from glaciated and nonglaciated portions of the watershed. An analysis of the total simulated water passing through La Balsa for the 1969–1999 modeling period indicates that on an annual basis, 38 percent of the flow comes from melting glaciers (Table A7.5). This value is similar to the 37 percent value presented by Vergara et al. (2007) based on an analysis of observed climate and hydrologic data. Seasonally, the model suggests that melting glaciers contribute 30 percent of streamflow at La Balsa during the wet season (December, January, February) and 67 percent during the dry season. This result provides insight into the importance of glaciers as water reservoirs during the dry season and the implications of their accelerated melting on water resources management in the region.

The model allows the computation of interflow and baseflow for each elevation band and each subwatershed. Table A7.5 shows the total outflow as well as the proportions of water from melting glaciers and from groundwater accretions for each subwatershed and for each season (wet and dry). The total outflow is always higher during the wet season. If we consider only the subwatersheds where the ice area covers more than 20 percent of the total area, we note that the proportion of glacier meltwater is higher during the dry season. For groundwater, the seasonal importance varies depending on the conditions in each subwatershed. If we consider the mean proportion of groundwater accretions in the total outflow, we find 32 percent during the wet season and 35 percent during the dry season.

The model allows for an estimation of the proportion of river flow originating as glacier runoff (snow and ice meltwater) and groundwater accretions. The results are compiled in Table A7.5. For groundwater, the subwatersheds with the lowest aquifer contributions are Llanganuco and Parón, with 11 percent during the 1969–1999 period. These lower values can be explained by the high altitude of these subwatersheds where the aquifers are of small lateral extent. At the scale of the entire Santa River watershed, the mean proportion of groundwater accretions is 30 percent of total annual discharge volume (1969–1999). The glacier meltwater of annual discharge volume is directly linked to the ice area of the subwatershed.

The proportion of glacier runoff in the total runoff is between 77 percent for Llanganuco and 0 percent for Tablachaca (see Table A7.5). At the La Balsa gauge station and during the 1969–1999 period, the glacier meltwater was equal to 38 percent of the total annual discharge volume. For the Querococha subwatershed, the value is 15 percent, which is in accordance with the 10 percent that was calculated in a previous study (Mark

Table A7.5. Results for simulated and observed runoff, groundwater part, and glacier part for the calibration and the validation periods

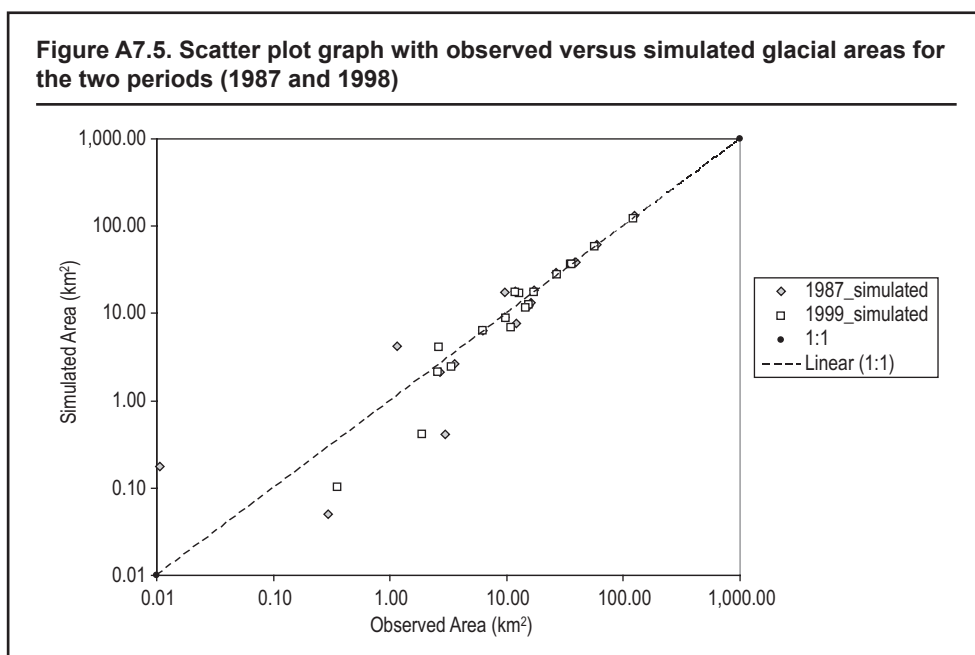| Sub-watershed	Area (km2)	Ice Area (km2)	% area ice in 1970	DJF total Outflow (1969-1999) (m3/s)	JJA total Outflow (1969-1999) (m3/s)	DJF ice Outflow (1969-1999) (% of total)	JJA ice Outflow (1969-1999) (% of total)	DJF groundwater Outflow (1969-1999) (% of total)	JJA groundwater Outflow (1969-1999) (% of total)	Glacier meltwater (snow+ice) of annual discharge volume (1969-1999) (% of total)	Groundwater part of annual discharge volume (1969-1999) (% of total)
1 - La Recreta	231	0.12	0.05	7.39	0.83	0.04	0.05	30.41	57.44	0.01	34
2 - Pachacoto	203	21.76	10.72	5.83	1.64	27.97	67.31	29.51	27.88	35	30
3 - Querococha	58	3.55	6.12	2.62	0.57	10.64	36.26	34.24	49.56	15	37
4 - Olleros	175	18.91	10.79	7.70	2.05	24.98	60.77	30.18	32.01	32	31
5 - Quillcay	245	46.17	18.84	10.98	3.76	40.93	76.47	28.03	21.13	50	27
6 - Chancos	265	71.15	26.87	13.04	5.41	53.21	83.79	21.98	14.27	61	20
7 - Llanganuco	83	35.80	43.03	4.21	2.25	70.73	93.16	13.27	6.28	77	11
8 - Paron	31	20.00	64.02	1.95	1.00	73.89	93.42	10.37	5.60	79	11
9 - Artesoncocha	9	6.27	71.41	*	*	*	*	*	*	*	*
10 - Colcas	234	45.89	19.60	9.27	3.58	46.17	79.86	25.11	17.63	53	23
11 - Los Cedros	106	23.00	21.65	4.24	1.74	45.79	74.92	22.79	15.76	52	21
12 - Quitaracsa	310	14.13	4.56	12.51	3.58	11.92	30.15	25.22	25.21	15	25
13 - La Balsa	4696	420.77	8.96	129.69	38.70	30.76	67.99	33.91	28.31	38	33
14 - Corongo (Manta)	562	5.03	0.89	13.40	2.10	3.52	16.21	51.62	76.01	5	55
15 Chuquicara	9540	442.65	4.64	228.47	57.98	18.82	48.58	44.09	42.64	23	44
16 - Tablachaca (Condorcerro)	3179	1.66	0.05	56.61	9.09	0.05	0.08	66.77	97.55	0	71
17 - Puente Carretera	10776	443.00	4.11	247.30	70.04	17.82	45.74	44.62	43.23	25	40

Source: Authors.
Note: Stations on the Santa River are shaded in gray. DJF (December, January, February)–wet season; JJA (June, July, August)–dry season. Groundwater outflow is the sum of simulated interflow and baseflow.

and Seltzer 2003). At the scale of total watersheds, the results of this study are also in agreement with those presented by Mark and Seltzer in 2003, who estimated that more than 20 percent of the annual discharge volume to the Santa River in the Callejón de Huaylas comes from the glacier meltwater. Based on all of this information, one can consider that the model captures the hydrological setting in the Santa River system reasonably well.

Simulation of the Glacial Area Evolution Since the 1970s

In addition to simulating river flows, one can be rather confident that the glacier module captures observed changes in glaciated area in the Cordillera Blanca. An analysis of the trends in glacial area evolution for the Santa River watershed indicates good correspondence between simulated and observed data (Figure A7.5 and Table A7.6). The model captures the overall change in area between both the 1970–1987 period (characterized by rapid glacier retreat) and the 1987–1999 period (characterized by less pronounced retreat). Note that the 1970 glaciated areas are the same for observed and simulated cases since these values were used as the initial conditions for the model runs.

Figure A7.5. Scatter plot graph with observed versus simulated glacial areas for the two periods (1987 and 1998)

Source: Authors.

Table A7.6. Simulated and observed data of glacier evolution between 1970 and 1999

Total Areas (km²)	1970*	1987	1999	% Change 70-87	87-99	70-99
Simulated	507	411	391	-19%	-5%	-23%
Observed	507	396	387	-22%	-2%	-24%

* Observed data error +– 25 km²

Source: Authors.

When one looks at the glacial area evolution of individual subwatersheds, the model provides good correspondence with observed data (1970–1987 and 1987–1999), particularly for the subwatersheds with larger initial glacial area cover (Figure A7.5). When one looks at some of the smaller subwatersheds, such as Colca, Pachacoto and Quitaracsa, the correspondence between observed and simulated data is reduced. One explanation for the lower correspondence for small glaciers is the fact that the observed data have an intrinsic error on the order of ± 5 percent of the total glacial area. In addition, the glacier model, which is based on empirically derived relationships, may not represent particular physical characteristics of small glaciers, such as slope and aspect, which will tend to have more average aggregate characteristics for larger glaciers.

This observation is evident in Figure A7.5, in which the evolving observed and simulated glacial areas in subwatersheds with glacier cover >10 km^2 tend to align well with the 1:1 line, while the glacial area of subwatersheds with glacier cover <10 km^2 tends to diverge from the 1:1 line, sometimes under-predicting and other times over-predicting.

Conclusion and Discussion

Understanding hydrology and having the capacity to model it are crucial in Andean tropical mountains as part of efforts to plan and manage water resources. The main challenge in this region is to be able to simulate the hydrology with a scarce availability of meteorological and hydrological data that have high spatial variability, similar to the temperature and precipitation gradients observed in the Santa River watershed. Several assumptions need to be made and interpolation methods need to be implemented in order to obtain continuous climate time series that can feed hydrologic models. This paper makes an attempt to respond to these challenges, but more research is certainly needed to define the best approach for developing continuous climate fields in the Andes.

However, the originality in this work goes beyond the preparation of usable climate input data and rests on the successful linkage of transient climate time series, a model of glacier evolution within a rainfall-runoff modeling framework, to simulate the hydrology of glaciated watersheds and the water management implications. In this paper, glacial meltwater and groundwater flows were computed, taking into account the spatio-temporal variations in climate at the scale of a fairly large river basin.

This is critical because, in addition to the hydrologic dimension of the model, the WEAP software provides the ability to represent and simulate different water uses and water system elements. Further steps into this modeling exercise should focus on detailing the implications of hydrologic change on water demands, including hydropower and agriculture, and the consequent economic implications. Having developed the basic analytical framework, future research will focus more heavily on the water management impact and adaptation aspects of potential climate change projections. To accomplish this, the next step will be to simulate the implications of climate change on glaciated watersheds in the tropical Andes, using future scenarios derived from global climate models.

Assessment of the Impacts of Climate Change on Mountain Hydrology is part of the World Bank Studies series. These studies are published to communicate the results of the Bank's ongoing research and to stimulate public discussion.

Climate change is beginning to have effects on climate, weather, and resource availability in ways that need to be anticipated when planning for the future. In particular, changes in rainfall patterns and temperature may impact the intensity or schedule of water availability. In addition, the retreat of tropical glaciers, the drying of unique Andean wetland ecosystems, as well as increased weather variability and weather extremes will affect water regulation. These changes have the potential to impact the energy, agriculture, and other sectors and could have broader economic effects.

Anticipating the impacts of climate change is a new frontier. There are few examples of predictions of the impact of climate change on resource availability and even fewer examples of the applications of such predictions to planning for sustainable economic development. However, having access to an effective methodology would allow planners and policy makers to better plan for adaptation measures to address the consequences of climate change on the power and water sectors.

This report presents a summary of the efforts to develop methodological tools for the assessment of climate impacts on surface hydrology in the Peruvian Andes. It is targeted to decision makers in Peru and in other countries to give them guidance on how to choose available and suitable tools and make an assessment of climate impacts on water regulation.

The Energy Sector Management Assistance Program (ESMAP) is a global technical assistance program administered by the World Bank that assists low- and middle-income countries to acquire know-how and to increase institutional capability to secure clean, reliable, and affordable energy services for sustainable economic development. ESMAP was established in 1983 under the joint sponsorship of the World Bank and the United Nations Development Programme as a partnership in response to global energy crises. Since its creation, ESMAP has operated in over 100 different countries through more than 500 activities covering a broad range of energy issues.

The World Bank's Global Expert Team on Climate Change Adaptation seeks to disseminate knowledge and support the application of best practices in the adaptation field.

World Bank Studies are available individually or on standing order. This World Bank Studies series is also available online through the World Bank e-library (www.worldbank.org/elibrary).

THE WORLD BANK

ESMAP
Energy Sector Management Assistance Program